NUMERICAL SIMULATION OF IMPLANT-BONE INTERACTION FOLLOWING CEMENTLESS JOINT REPLACEMENT

G R Starke, B.Sc. (Mech.) Eng.

April, 1996

Submitted in fulfilment of the requirements for a Doctorate in Philosophy

---

Department of Mechanical Engineering
University of Cape Town
Rondebosch
7700
South Africa

ABSTRACT

The advent of cemented joint replacements has revolutionised the management of patients suffering from chronic arthritis. However, establishing a durable bond between the prosthesis and the surrounding bone remains a considerable problem. As a result, cementless implants have been developed. These components rely on the ingrowth of bone into a porous coating, which covers a portion of the component surface, to achieve the required mechanical interlock. Once mineralised bone tissue has formed within the porous surface, a stable bond results which will be maintained by the normal bone turnover processes, thereby providing long term attachment. However, one of the problems associated with the use of cementless implants is the unpredictability of the extent of bone ingrowth. The process of osseo-integration is greatly influenced by the magnitude of the micro-motion between the implant and the surrounding bone. Large movements inhibit ingrowth, and may result in the formation of an interfacial fibrous tissue layer. In addition, interface strains will influence the early repair process and guide long term bone remodelling within this region.

A numerical model for the prediction of bone formation within the porous surface has been developed. The evolution laws consider the early repair activity, possible fibrous tissue formation, and long term remodelling, as a function of the history of inelastic relative displacements and elastic interface strains. The model is based on the development of an isoparametric interface element, which is suitable for implementation into a non-linear finite element code. In the unbonded condition, the contact is governed by a Coulomb friction formulation. The position and shape of the Coulomb yield surface is altered according to the evolution equations, which govern the development of mineralised tissue within the surface porosity. The strain history and post-operative time are then used to develop a stimulus coefficient, which determines the course of the interface tissue development. If bone tissue is predicted, the subsequent interfacial material will be governed by a remodelling algorithm for the prediction of the long term response. If the bond strength is exceeded, fracture occurs and the joint may open or slide, thus returning to its original, unbonded, state. In the event of large micro-motions, the yield surface and material formulation are altered to include fibrous tissue.

The model is used to predict the development of interfacial tissues at the porous surface of a tibial tray component, with a central peg and a *PCA* (Howmedica, Inc.) femoral stem. Although many factors influence interfacial tissue development, mechanical loads are assumed to be dominant. In the short term, the relationship between micro-motion and interface tissue response has been shown. However, long term remodelling of interfacial tissues has not been widely demonstrated and, therefore, additional experimental data is required to validate the current long term remodelling predictions.

ACKNOWLEDGEMENTS

I would like to express my enormous gratitude to the following people and organisations:

My Supervisors, Professor John Martin and Mr. Thanos Spirakis for their continual encouragement, technical assistance and effort in reading through the various drafts.

Colleagues at CERECAM, in particularly Greg Mitchell and Hellmut Bowles for their constant assistance over the last few years.

Kathrine van Vuuren for painstakingly reading through the final draft.

The Centre for Research in Computational and Applied Mechanics (CERECAM) and the Foundation for Research Development (FRD) for financial assistance.

DECLARATION

I, Gregory Starke, declare that the work set out in this thesis is essentially my own work and that no part has been submitted for a degree at any academic institution.

Signed by candidate

.....

Gregory Starke

April, 1996

TABLE OF CONTENTS

RELEVANT MEDICAL TERMILOGY

acetabulum	socket portion of the hip joint
adjuvant therapy	drug treatment aimed at destroying secondary tumours
anterior	towards the front of the body
arthritis	disease of the joints
arthroplasty	reconstruction of a joint using artificial components
callus	mass of blood and granulation tissue, containing bone forming cells. Callus formation is an essential part of bone fracture repair
cancellous bone	spongy bone type found at the joints
chondroblast	cell responsible for cartilage formation
contralateral	the side which is not being used
cortical bone	dense bone making up the shell of the long bones
diaphysis	the shaft of a long bone
distal	lower part of a joint
endosteal	internal bone surface
epiphysis	the end of a long bone which, in early life, is separated from the shaft
femur	thigh bone
fibroblast	cell that forms fibrous tissue
fibrocyte	dormant fibroblast
hydroxyapatite	bone-like material often used to coat an implant surface
inferior	towards the lower part of the body
lateral	away from the mid-line of the body
medial	towards the mid-line of the body
mesenchyme	primitive tissue from which bone producing cells can form
modelling	adjusting the bone structure to meet new mechanical demands
osseo-integration	bone growth into a porous region or roughened surface
osteoblast	cell responsible for bone production

osteoclast	cell responsible for bone removal
osteocyte	dormant osteoblast that has become buried in bone matrix
osteoprogenitor cells	pluripotential cells derived from mesenchyme. Under appropriate conditions these cells can proliferate and differentiate into chondroblasts or osteoblasts
osteotomy	removal of bone by surgery
periosteal	external bone surface
posterior	towards the back of the body
proximal	upper part of a joint
remodelling	maintaining the bone structure to meet mechanical demands
superior	towards the upper part of the body
tibia	bone below the knee joint

NOMENCLATURE

The following is a list of the symbols used in the main text of this thesis

Special Symbols

$\dot{}$	(accent) differential with respect to a time scale
$\hat{}$	(accent) peak value during cycle
$\tilde{}$	(accent) constant value of
$\bar{}$	(accent) equivalent value
T	(superscript) transpose of a vector or a matrix
d	differentiation with respect to
δ	virtual quantity
∂	partial differentiation with respect to
Δ	increment in

Operators

:	double contraction of two tensors
sgn(x)	-1 if $x < 0$ or 1 if $x > 0$

Lowercase Symbols

a	thickness of the porous coating
b	number of influential days in load history
c	cohesion
d	number of load cases for day k
e	remodelling error function
f	yield surface in stress space
g	non-linear elastic stress-strain relation
h	thickness of interface material
j	load case number
k	day counter
l	length of interface element
m	constant defined in text
p	constant defined in text
s	half the width factor of the lazy zone
t	time scale in days
u	nodal displacement in the x direction
v	nodal displacement in the y direction

x	first co-ordinate direction
y	second co-ordinate direction
$\mathbf{f}$	nodal force vectors
$\mathbf{r}$	traction vector
$\mathbf{i}$	element unit normal vector
$\mathbf{j}$	element unit tangential vector
$\mathbf{n}$	element normal vector
$\mathbf{s}$	element tangential vector
$\mathbf{t}$	applied surface traction

Uppercase Symbols

B	normalising parameter
C	constant defined in the text
E	Young's modulus
G	shear modulus
H	fibrous tissue stiffening parameter
J	element Jacobian
K	constant defined in the text
N	shape function
N	number of cycles for load case j
Q	position of mineralised tissue surface
S	memory function
T	current time
U	strain energy density
$\mathbf{B}$	compatibility matrix
$\mathbf{D}$	constitutive matrix
$\mathbf{K}$	stiffness matrix
$\mathbf{T}$	transformation matrix

Lowercase Greek Symbols

α	time constant
χ	stimulus parameter
δ	relative displacement
ε	normal strain
ϕ	friction angle
γ	shear strain
η	first natural co-ordinate
φ	arbitrary rotation angle
κ	yield surface tensile angle
λ	inelastic strain multiplier

λ	ratio of cohesion to adhesion bond strength
μ	remodelling response measure
ν	Poisson's ratio
θ	tensile angle in state diagram
ρ	density
σ	normal stress
τ	shear stress
υ	volume fraction of porous bead structure
ω	measure of inelastic shear strain
ξ	second natural co-ordinate
ψ	friction angle in strain space
ε	strain vector
σ	stress vector

Uppercase Greek Symbols

Ψ	flow rule function
X	distance normal to surface
Ψ	applied load vector

Superscripts

A	apex of the yield surface
e	elastic component
e	element
i	iteration number
p	inelastic component

Subscripts

n	general increment number
m	remodelling
r	repair
p	increment denoting days

CHAPTER ONE

INTRODUCTION

Total hip arthroplasty (THA), as developed by Sir John Charnley, has revolutionised the management of patients suffering from arthritis of the hip. However, aseptic loosening is the most frequent cause of failure (Beckenbaugh and Ilstrup, 1978; Sutherland *et al.*, 1982; Stauffer, 1982). Sarmiento *et al.* (1988) have reported an incidence of radiological component loosening, cement fracture and radiolucency around the cement of 32-58% at 10-20 year follow-up. Chandler *et al.* (1990) reported similar complication rates after five years in patients younger than 30 years old. However, more recently, improved cementing techniques have resulted in a drop in implant failure rate to less than 10% after follow-up periods of up to eleven years (Oishi *et al.*, 1994; Ballard *et al.*, 1994; Raut *et al.*, 1995).

Femoral component loosening is primarily a mechanical problem, and many factors have been implicated into its initiation. These include: the strength of the polymethylmethacrylate (PMMA) bone cement; failure of mechanical interlocking of the cement as a result of large stress gradients at the interfaces; the design of the component and the thickness of the cement mantle. Harris (1992) suggested that loosening starts with debonding between the cement and the implant, which subsequently results in fractures within the cement mantle. As a result of the problems associated with cemented hip arthroplasties, a cementless method of implant stabilisation has been introduced. The cementless arthroplasties rely on bone ingrowth into a porous coating, which covers a portion of the implant surface, to achieve the interlock between the component and bone. It is hoped that once the bond has been established it will be continually maintained during the normal bone turnover processes and, subsequently, provide a indefinite life span for the joint. However, the difficulty in the design of these implants lies in determining whether or not a bond will form.

The ongoing interest, over the last two decades, in using porous coating as a method of implant stabilisation has resulted in extensive animal experimentation into this method of attachment (Galante *et al.*, 1971; Cameron *et al.*, 1973; Cameron *et al.*, 1976; Ducheyne *et al.*, 1977 Spector *et al.*, 1978; Bobyn *et al.*, 1982; Hedley *et al.*, 1982; Hedley *et al.*, 1983; Engh *et al.*, 1987). This experimental work has aimed at defining the criteria for the design and use of the cementless implants. Investigations have shown that, under the right circumstances, mineralised bone tissue will form within the porous surface, resulting in a stable prosthesis attachment, that will be maintained by the normal bone turnover processes, to provide long term support. Although it is believed that cementless implantation is a viable and reproducible method of skeletal attachment, and could replace cemented fixation for active patients, retrieval studies (Engh *et al.* 1987; Cook *et*

al., 1988; Collier *et al.*, 1992) have shown many instances of minimal ingrowth, even in successful joint replacements. The response of the interface tissue will be influenced by hormonal, metabolic and medicinal factors (Ling, 1986). However, it is believed that the dominant influence will be the mechanical environment between the implant and the surrounding bone.

Cameron *et al.* (1973) found that the magnitude of the implant displacement relative to the surrounding bone, directly influenced the formation of the bond, and concluded that "ingrowth can take place in the presence of micro-movement but not macro-movement." They and others (Ling, 1986) emphasised the importance of the press-fit obtained during implantation to reduce component movement. Subsequently, other investigators (Ducheyne *et al.*, 1977 and Bobyn *et al.*, 1982) have confirmed that penetration of bone will not take place in the presence of displacements greater than approximately 150μm. Pilliar *et al.* (1986), investigating dental implants, found that calcified tissue formed in the presence of movement of approximately 30μm. Spector (1988) argued that increased implant movement damaged the layer, within which the osseous tissue was regenerating, resulting in the formation of fibrous (scar) tissue. He found that if the movements were not too large, the ingrowth tended to take the form of a fibrous tissue attachment, while relative displacements above 150μm prohibited the formation of a bond and resulted in the implant being encapsulated in scar tissue. Although an implant coated in fibrous tissue may be stable, fibrous tissue has a low Young's modulus and very little ability to transmit shear and tensile stresses (Hori and Lewis, 1982; Weinans *et al.*, 1990).

While relative displacements may inhibit the formation of a bond, cell activity is necessary to promote tissue formation, which will result in osseo-integration. Two processes are important in the formation of an osseous bond, and are broadly termed "repair" and "remodelling" (Spector, 1988). During the surgical procedure, bone is broached and reamed so as to accommodate the implant, which stimulates a wound healing response, initiating the formation of new bone tissue. This healing process continues for approximately 4 to 6 weeks post-operatively (Hollister *et al.*, 1994). Once the repair process is complete, the interface region will be governed by the normal remodelling activity.

The remodelling response, due to loading, will be affected by the presence or the absence of mechanical load. Bone is continually in a process of growth and renewal as old bone is removed and replaced by new tissue (Parffit, 1984). There exists an optimal combination of load magnitude and the number of load cycles for which there is no net remodelling (Carter, 1984), resulting simply in the replacement of existing tissue. In the case of under-loading (such as bed rest), the process is quickly shifted to the side of bone loss with the recruitment and activation of osteoclasts, the cells responsible for bone removal. Conversely, in the case of over-loading, the osteoclasts still remain active, but following bone removal the subsequent deposition exceeds the amount removed, resulting in a net gain of tissue. Remodelling can be divided into internal and surface remodelling (Frost, 1964). Internal remodelling is the alteration of the density and structure of bone, while surface remodelling is the removal or apposition of bone on the periosteal and endosteal surfaces. The changes that take place at the interface between bone and porous beads constitutes surface remodelling.

Numerical modelling of the interaction of porous coated implants and bone has largely been limited to examining the influence of various ingrowth scenarios, without considering the surface evolution (Carter *et al.*, 1984; Tensi *et al.*, 1990; Weinans *et al.*, 1990; Pedersen *et al.*, 1991). However, Sadegh *et al.* (1993) used the boundary element method on a micro-model of a beaded surface to examine the advancement of the bone tissue surface into the beads. Following from the work of Cowin and Hegedus (1976), Hegedus and Cowin (1976) and Cowin (1978), they assumed that the rate of advancement or retardation of the surface was proportional to the difference between the actual surface strain and an optimal value. Starting with a bonded interface, Weinans *et al.* (1993) used a thin element formulation to examine the development of a fibrous tissue layer as a result of cyclic loading.

The objective of this work is to develop a numerical model for the prediction of implant-bone interaction, following cementless joint arthroplasty. The development of the model was undertaken by initially identifying the important mechanical factors governing the evolution of the implant-bone interface tissue. The mechanical parameters were then used to formulate equations for the prediction of bone growth into the porous surface of the implant, as well as the formation of fibrous tissue. The model is based on the development of an isoparametric interface element, which is suitable for implementation into a standard finite element code. In the initial post-operative condition, the contact is governed by a Coulomb yield criterion. As a result of ingrowth the Coulomb model is altered, by adding cohesion and adhesion, according to the evolution equations. If the bond surface fractures the interface is once more governed by the initial Coulomb model.

This thesis begins in Chapter Two by describing the composition and structure of bone, and the processes of formation. Included in this, is a discussion of constitutive modelling of bone and fibrous tissue. In this chapter, a description of bone remodelling physiology is presented, which is followed by a discussion of numerical modelling of bone remodelling processes. Chapter Three outlines the concepts, procedures and problems facing joint replacement. Cementless hip joints are discussed in some detail, with particular attention being given to aspects of the implant-bone interface. The discussion includes a review of numerical modelling of bone growth and remodelling of interfacial tissues. Chapters Four, Five, and Six describe the development of the interface element. Chapter Four sets out the constitutive formulation for two interacting bodies. In Chapter Five, the development of the evolution equations for the interface are described. Then, in Chapter Six, the development of the interface element is presented. This is followed by the implementation of the element and evolution equations into the finite element program. The verification of the element and the examples which demonstrate the element capabilities are shown in Chapter Seven. Finally, this chapter is followed by a discussion of the overall modelling approach and the results which have been presented.

CHAPTER TWO

BONE MORPHOLOGY AND REMODELLING

2.1 Introduction

The material presented in this chapter is intended to provide a background to the concepts that follow later. Here the composition, structure and formation of bone are discussed. Included in this discussion are the mechanics of bone and fibrous tissue. This is followed by a discussion of bone remodelling, which includes remodelling physiology, the mechanical factors which influence remodelling, as well as rate equations for the simulation of this process.

2.2 Bone Morphology

The role of the bones is to provide the structural and protective components of the skeleton. They support the body and the limbs, protect internal organs and secure the skeletal muscles for movement and locomotion. Apart from the structural function, bone fulfils an important biochemical role by providing a reservoir for calcium, phosphorus and other components

Bone is a highly specialised, hard connective tissue with a complex structure consisting of very distinct solid and fluid phases. Although the material is classified as a connective tissue, its hardness makes it unique amongst other tissues. The reason for this is that the extracellular collageneous matrix, the main organic component of all connective tissue, is impregnated with a mineral phase, which is similar to *hydroxyapatite* (Ca_{10} $(PO_4)_6 \cdot OH_2$), which is made up primarily of calcium and phosphate (Cowin, 1981). The collagen fibres account for 90% of the tissue volume and, being fibres, only have strength in tension, and simply buckle under compression. In mineralised or calcified bone, it is the presence of the mineral phase which provides the compressive strength.

The bones comprising the skeleton are organised into two distinct structural forms: cortical and cancellous bone. Cortical, or compact, bone makes up the outer shell of long bones, while the less dense cancellous, or spongy, bone exists within the cortical shell, particularly in the region of the joints. Most bones exhibit both types, with the area around the joints being made up primarily of cancellous bone, and the long bones supporting the joints consisting of a tubular structure of cortical bone. The volume fraction of the bone structure broadly classifies the tissue into the two types. Human cortical bone in young healthy individuals has a minimum porosity of between 5 and 10%, while cancellous bone has a solid volume fraction of between 5 and 30% (Carter

and Hayes, 1977; Gibson, 1985). A typical bone organ can be seen in Figure 2.1. The geometry of the bone can be divided into three distinct regions. The central region with the tubular cortical structure is the diaphysis, while the areas at either end, near the joints, are called the epiphysis. The hollow core in the diaphysial region, which is called the medullary canal, holds the bone marrow that is in direct contact with the cancellous bone at either end. The surface of the inner marrow cavity and outer bone surface, are called the endosteum and the periosteum, respectively. The periosteum is a very tough specialised connective tissue. This term often refers not to the tissue, but to the outer bone surface.

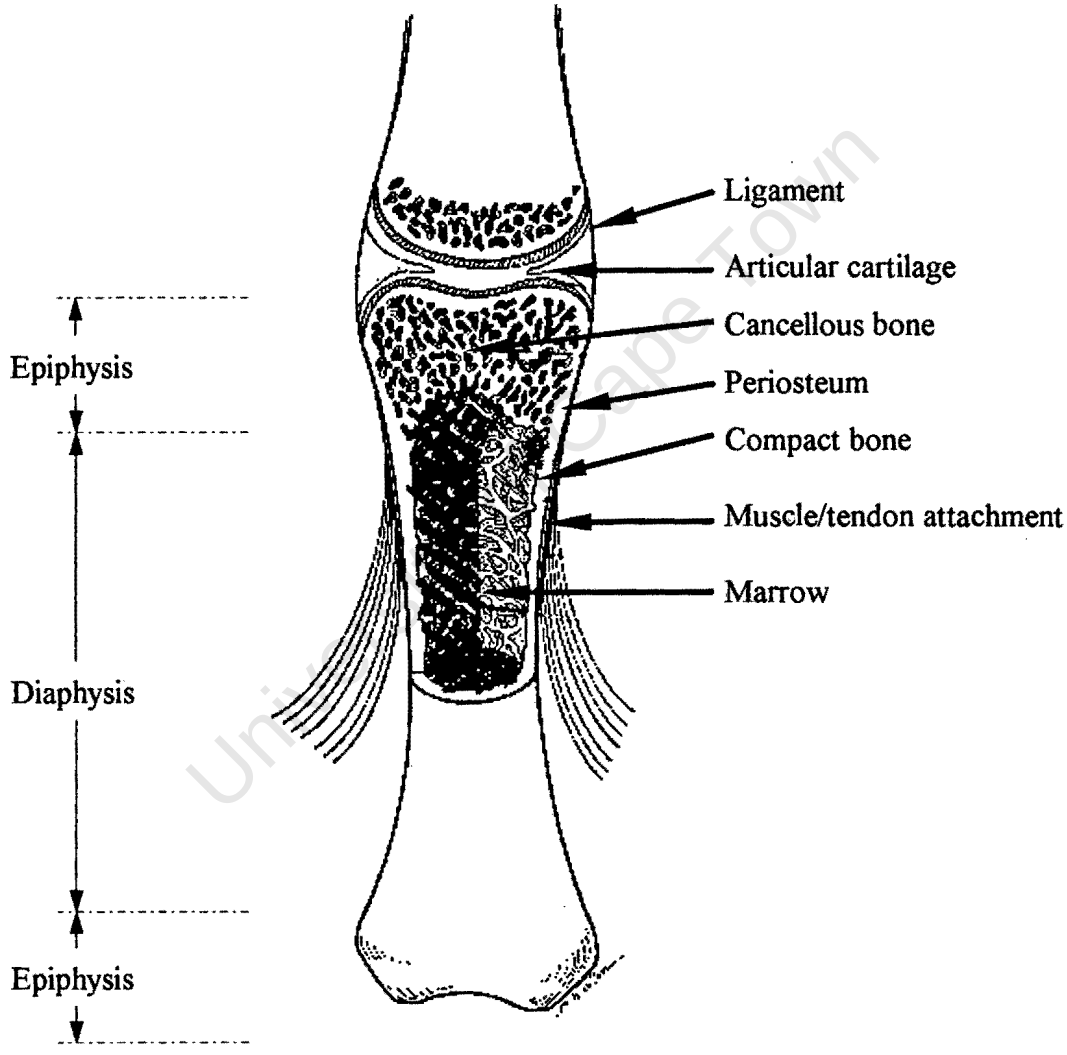

Figure 2.1 A typical bone organ (adapted from *Functional Histology*, 1980).

The organisation and structure of trabeculae bone has been extensively examined by Whitehouse and Dysan (1974), whose microscopy studies of healthy bone in the

proximal femur revealed several distinct forms of trabeculae structure. In the relatively small area of the proximal femur, they were able to show a large variation in structural geometry and apparent density, thereby clearly indicating that bone is not homogeneous. Examination of certain planes of the resected specimens revealed noticeable symmetries, indicating isotropic structure; however, in many instances the out-of-plane surface was clearly anisotropic, which led to the conclusion that, in general, bone is anisotropic.

Based on the work of Whitehouse and Dysan (1974), Gibson (1985) characterised the many structural forms of trabeculae architecture into three categories (shown in Figure 2.2) which broadly describe the structural forms of bone within the human body. In areas where the stress pattern is complex and no preferred direction of loading can be found, the trabeculae structure is also complex and asymmetric. Depending on the stress magnitudes, the cellular structure may form open or closed cells. The cell structure is described in terms of relative density, which is defined as the density of the cellular

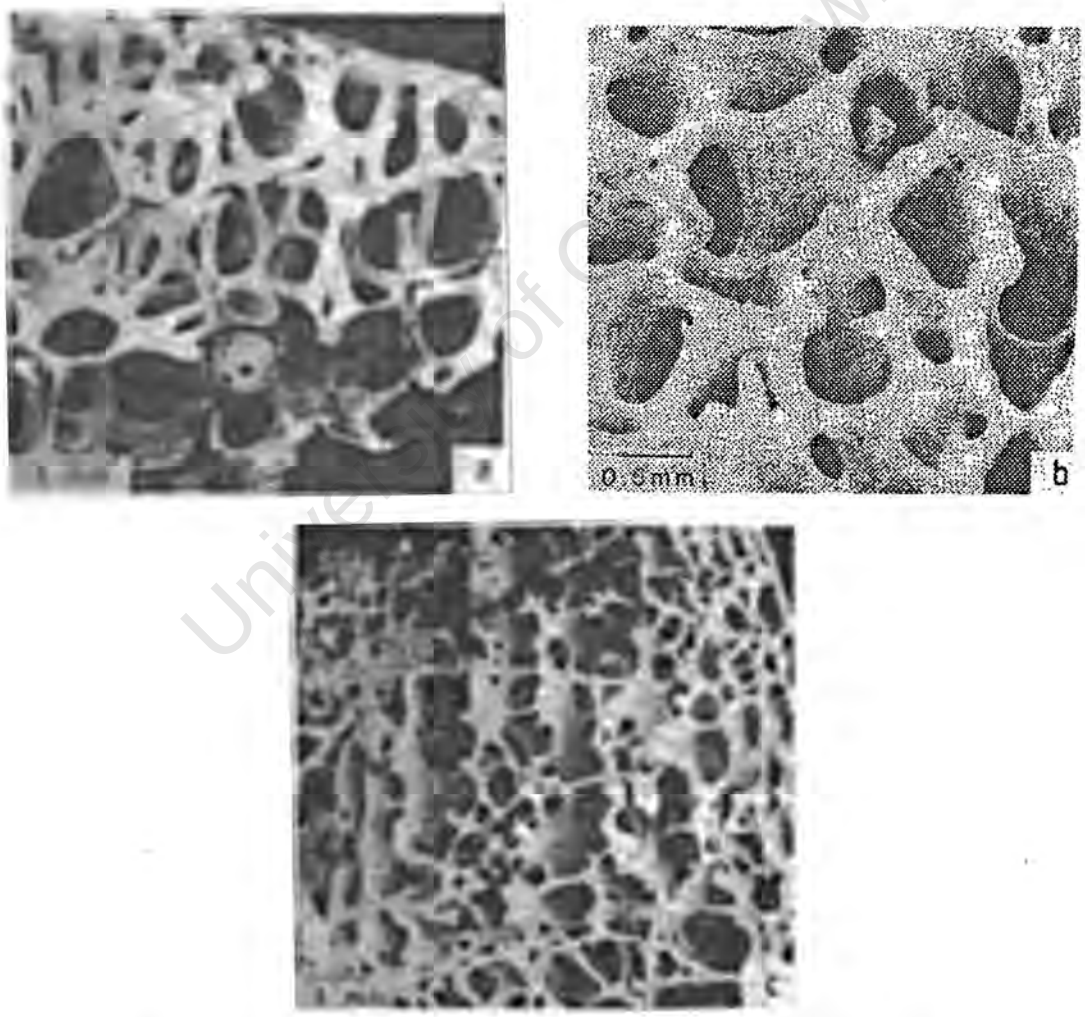

Figure 2.2 Bone Structure (a) Open cells (b) Closed cells (c) Plates (Gibson, 1985).

material ρ^* divided by the bone tissue density ρ_s. Open cells have relative densities of less than 0.13 (Figure 2.2 (a)), while the closed cell structures will have relative densities of over 0.2 (Figure 2.2(b)). Where there is a definite direction of loading, such as the area directly beneath the femoral head, through which the reaction force is transmitted, the trabeculae develop a plate-like, columnar, structure with cylindrical symmetry, which is shown in Figure 2.2(c).

2.3 Bone Formation

Before discussing the process of bone development and remodelling, the four primary cells involved in bone production and maintenance will be discussed (Jee, 1980). *Osteogenic* cells, which are derived from mesenchyme, will differentiate into chrondroblasts or osteoblasts. Subsequently, osteoblasts secrete a bone matrix that ossifies into bone tissue. These cells are involved not only in the development of bone tissue, but also in fracture repair. *Osteoblasts* differentiate from osteogenic stem cells. They secrete the organic component of the bone matrix as well as indirectly contributing to the subsequent calcification. Once osteoblasts have completed their task they become isolated within the matrix they created. Subsequently, a small fraction of the osteoblasts (in the region of 4%) become osteocytes (Martin and Burr, 1989). *Osteocytes* are the principal cells of bone tissue and are interconnected by a complex network that, it has been suggested (Cowin, 1995), allows for the transfer of information. These cells are responsible for the maintenance rather than the formation of bone, and are less active than osteoblasts. *Fibroblasts* are widely distributed among the connective tissues and are particularly active during wound healing when they produce collagen fibres. Although several cell types produce collagen, fibroblasts are by far the most active and widespread. *Osteoclasts* are responsible for the degrading of bone matrix in areas where bone will be remodelled. During remodelling old bone is removed and subsequently replaced with new tissue. During growth there is a net excess of bone deposited by osteoblasts, while with increasing age osteoclastic resorption outpaces deposition. As these cells remove surface tissue, they are most often found on bone surfaces. Osteoclastic resorption proceeds by initially dissolving the minerals and subsequently degrading collagen (Parfitt, 1984).

The complex process of bone formation or *osteogenesis* is characterised by cellular migration, differentiation and modulation. A distinction is drawn between the formation of bone tissue and the formation of bone organs. As the current work is focused on the development of bone during adult life, only the formation of bone tissue is discussed. The origin of bone tissue is mesenchyme - which is an undifferentiated, loosely organised tissue, whose individual cells can migrate to various parts of the body. Bone forms in one of two ways: by apposition onto pre-existing surfaces through the action of osteoblasts or by endochondral ossification. During the first phase, osteoblasts secrete an organic intercellular material called pre-osseouss tissue or osteoid (ground substance and collagen) through the cell walls. Subsequently the collagen is calcified or mineralised with mineral salts (Torzilli *et al.*, 1981).

When bone forms on an existing surface, mesenchymal cells, called osteoprogenitor cells, gather to provide a covering of the surface onto which the new bone is to form. These cells possess the ability to synthesise protein and, at this stage, are called osteoblasts. During formation the cells produce a ground substance and lay down collagen fibrils which are orientated with respect to the existing surface. The mineralisation results in the entrapment of the osteoblasts. By modulation of the osteoprogenitor cells, the new surface is replenished with osteoblasts and the process continues. This process means that interstitial growth is not possible, and therefore the growth of all bone tissue takes place by apposition onto an existing surface. As a result of the formation process bony spicules develop which, when they become larger, are known as trabeculae which partially fuse to form spongy or cancellous bone. Compact or cortical bone is formed by further apposition onto the trabeculae resulting in the near filling of the intervening spaces.

As a result of improper fracture healing and in the presence of foreign bodies, bone will often form a scar tissue known as fibrous tissue. This material is often found at the interface between grouting cement, used for joint replacements, and the surrounding bone, and also in regions where metal-alloy implants come directly into contact with bone. The tissue consists of collagen fibres with fibrocytes interspersed throughout the tissue matrix. Depending on the local mechanical conditions, the tissue fibres are either organised roughly parallel to the interface, or they are randomly distributed and woven in a manner similarly to a mat. The individual fibres are well linked to those around them and even after severe trauma do not become separated.

2.4 Tissue Mechanics

Bone is a highly complex, inhomogeneous and anisotropic material and therefore careful consideration needs to be given to the development of suitable material models, if accurate structural predictions are to be made. Experimental evidence has shown that in the normal physiological range of loading, bone obeys the laws of linear elasticity where the stress is related to the elastic strain by

$$\boldsymbol{\sigma} = \mathbf{D}\boldsymbol{\varepsilon}^{e} \tag{3.1}$$

where $\boldsymbol{\sigma} = (\sigma, \tau)$ and $\boldsymbol{\varepsilon}^{e} = (\varepsilon^{e}, \gamma^{e})$ are the stress and elastic strain vectors, respectively, and $\mathbf{D}$ is the elasticity matrix, which is a function of the Young's modulus of the bone. The form and components of $\mathbf{D}$ will depend on the approximations regarding the material structure, which is then treated as a continuum. The structure of bone will be a function of the loading it experiences and therefore orientated specimens with material symmetries will exist. In general bone can be regarded as orthotropic (Turner *et al.*, 1990); however, transversely isotropic (Reilly and Burnstein, 1975; Lappi *et al.*, 1979) or isotropic (Rohlmann *et al.*, 1983; Vichnin and Batterman, 1986; Huiskes and Boeklagen, 1989; Weinans *et al.*, 1990) assumptions have been frequently used. As bone is a structure and not a continuum, the stresses and strain calculated are the continuum or *apparent* values, and not the magnitudes experienced by the bone tissue. Tissue level stresses can be

calculated using, amongst other methods, the theory of homogenisation (Hollister, 1991), in which the microstructural and continuum level analyses are undertaken separately and subsequently combined in a systematic way to calculate tissue level strains and stresses.

2.4.1 Mineralised Bone Tissue

The tissue making up the structure of cortical and cancellous bone is essentially very similar in composition and form (Carter and Hayes, 1977). Cortical bone has a density of approximately 1800kg/m^3, which is very similar to the density of the individual trabeculae which make up the structure of cancellous bone (Gibson, 1985). Despite some controversy (Rice *et al.*, 1988), the similarity in the materials has lead to the conclusion that the differing properties of the various bone types is essentially a function of their structures. The stiffness and ultimate strength of bone is therefore a function of apparent density, structural arrangement and properties of the bone tissue (Carter and Hayes, 1977; Ashman *et al.*,1988; Linde *et al.*, 1991; Lotz *et al.*, 1991 Goulet *et al.*,1994).

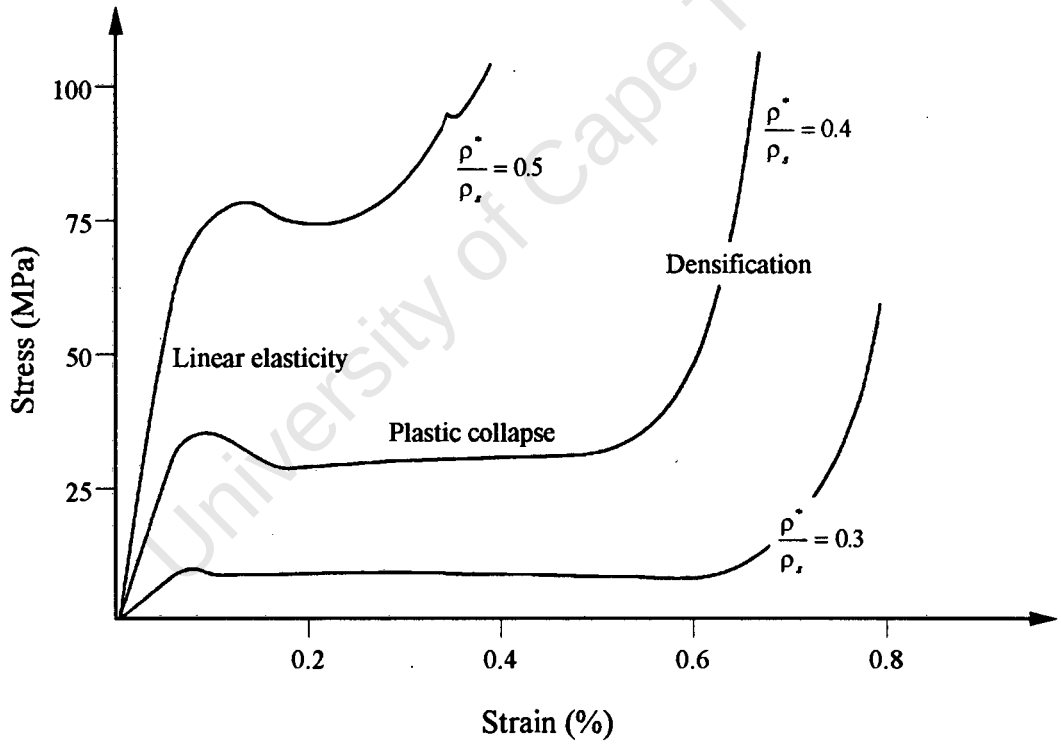

Figure 2.3 Compressive behaviour of cancellous bone for various relative densities (adapted from Gibson, 1985).

Compressive behaviour of cancellous bone is characterised by three distinct phases of deformation. The stress - strain curves for three relative densities are shown in Figure 2.3, with compressive strains being taken as positive. Initially, the deformation of the structure is characterised by bending of the trabeculae, which results in a linear elastic region of the stress - strain curve. With increased straining, the trabeculae begin to

buckle and collapse as they yield, which results in a plateau of stress as the strain increases during plastic collapse. Finally, the trabeculae come into contact with one another resulting in a densification and subsequent stiffening of the material, which is seen by the sudden increase in slope of the curves. In tension a linear elastic region is seen, which is as a result of the elongation of the trabeculae. Before fracture, the trabeculae will yield, resulting in non-linear behaviour.

The mechanical characteristics of bone have been shown to be very similar to open-celled rigid plastic foams (Gibson, 1985). As a cellular solid, the mechanical properties of the material can be primarily related to the apparent density and, to a lesser extent, the structural geometry. The initial mode of deformation of bone structure is linear-elastic and, in this region, the Young's modulus E is a function of the density (Carter and Hayes, 1977; Rice *et al.*, 1988; Linde *et al.*, 1991), material orientation and the strain rate. The Young's modulus can be related to the apparent density by

$$E = A\left(\dot{\varepsilon}^{e}\right)^{B} \rho^{C} \tag{2.2}$$

where $\dot{\varepsilon}^{e}$ is the elastic strain rate and A, B and C are constants. The value of C will depend on the density, and on whether the specimen is loaded in the "longitudinal" or "transverse" direction of an orientated specimen. In the longitudinal direction $C = 2$, while in the transverse direction a high degree of non-linearity is introduced and $C = 3$. In specimens where there is no preferred orientation, C is found is also found to be approximately two at low densities and three a higher densities (Carter and Hayes, 1977). This relation can be modified to include a fabric tensor F_i which carries information about the local material orientation (Cowin, 1985; Turner *et al.*, 1990; Cowin and Turner, 1992), so Equation (2.2) can be written as

$$E_i = P F_i \dot{\varepsilon}^{Q} \rho^{R} \tag{2.3}$$

where $i = 1, 2, 3$ refers to the three co-ordinate directions and P, Q and R are constants. Using this approximation, the value of R is independent of material orientation.

In compression, cancellous bone fails as a result of the either elastic buckling of the trabeculae or plastic yielding. The mode of failure will depend on the slenderness ratio of the trabeculae, which in turn will be a function of the density. At low densities, and subsequently high slenderness ratios, elastic buckling will dominate, while at higher densities, where the slenderness ratios will be lower, plastic collapse will be prevalent. Compressive tests undertaken with asymmetric specimens for a wide range of data (collated by Gibson, 1985) showed that compressive strength was a function of density squared. However, Williams and Lewis (1982) reported that for specimens with a preferred orientation, the transverse strength will be a function of the density squared, while the longitudinal strength will be a linear function of density.

Multiaxial and compressive strength tests of bovine trabeculae bone were undertaken by Stone *et al.* (1983) to investigate ultimate normal and shear strength. The multiaxial specimens came from the transverse plane, perpendicular to the bone axis, while the

compression specimens had their longitudinal axis parallel to the bone axis. The yield data, plotted on a normal stress (σ) versus shear stress (τ) stress axis, resulted in an elliptical yield surface, as shown in Figure 2.4. The material was found to have its greatest strength in compression, with the values being in the range of 8.29 ± 1.82MPa. Shear strength is slightly lower than compressive strength (6.60 ± 1.66MPa), but larger than the tensile strength, which was calculated from the shear data to be approximately 2.63MPa. In contrast to these findings, Rice *et al.* (1988) and Røhl *et al.* (1991) found, by direct measurement, cancellous bone tensile strength to be significantly greater than the compressive value. It would seem likely that the more recent data of tensile strength, which has been taken from direct measurement, would produce more realistic results.

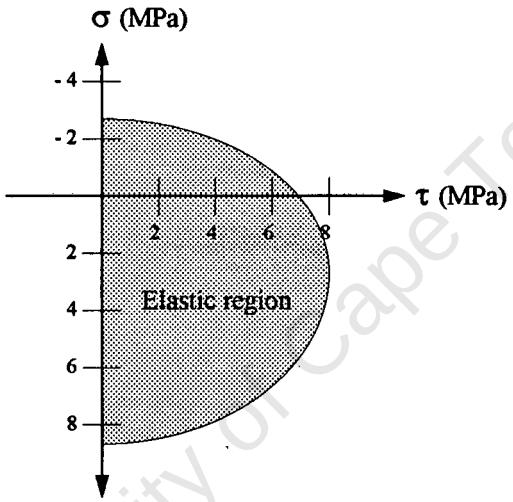

Figure 2.4 Cancellous bone yield surface (adapted from Stone *et al.*, 1983).

2.4.2 Fibrous Tissue

One common consequence of bone fracture or joint reconstruction, is the formation of a fibrous tissue layer adjacent to the fracture site or, in the case of reconstruction, adjacent to the foreign material. The fibrous or scar tissue layer forms as a result of improper healing or as a result of mineralised tissue resorption, which is primarily caused by a combination of high shear and tensile stresses as a result of relative displacements between two surfaces. In the case of fracture, this could be as a result of improper union of the bone, or as a result of movement between the two sides of the fracture. Fibrous tissue is characterised as having densely packed parallel-fibered collagen bundles, with the fibres distributed in a mat-like structure (Hori and Lewis, 1982; Goldring *et al.*, 1983). The mechanical properties of this material are completely different to those of mineralised bone, and will therefore play an important role in determining the load transfer characteristics of the affected region.

Despite the importance of fibrous tissue, there has been little work reported on the mechanical properties of the material. Hori and Lewis (1982) undertook compressive tests on specimens taken from the cement-bone interface and under the tibial plateau of the reconstructed canine proximal tibia The *sub-plate* tissue was taken from beneath the tibial plateau, which sat proud of the resected surface, due to the support of the central post. The *cavity* tissue was taken from beneath the central post in a cementless tibial implant. The compressive tests of the cavity and sub-plate tissue are shown in Figure 2.5(a) and Figure 2.5(b), respectively, where compressive strains are assumed to be positive. Compared to mineralised bone, fibrous tissue is weak in tension and shear, while in compression it is compliant, exhibiting highly non-linear behaviour. The compressive tests showed the fibrous tissue to be very compliant and able to undergo large deformations at low loads. The material exhibited a non-linear stiffening behaviour and had a tangent modulus of approximately 2MPa at strain levels of 50%, with a corresponding compressive stress of 0.5MPa. While at zero strain the modulus was found to be approximately 0.17MPa, which is orders of magnitude lower than the modulus of trabeculae bone.

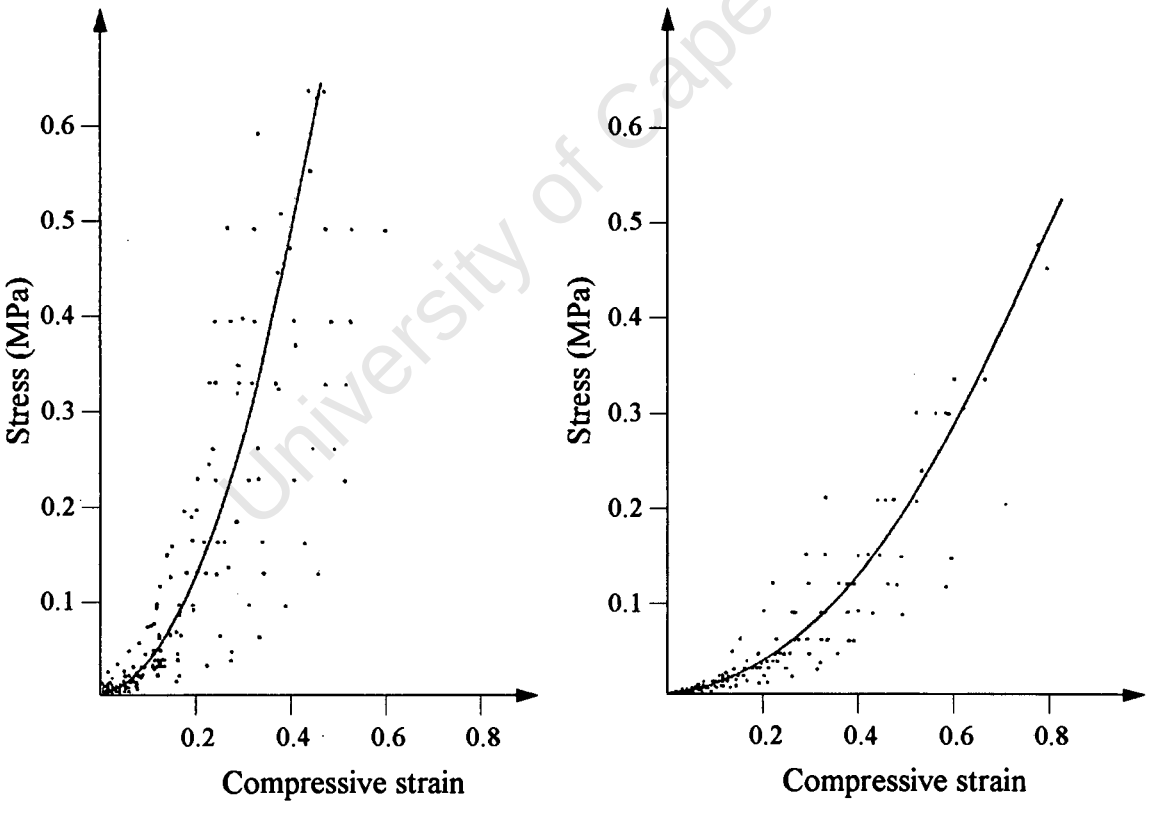

Figure 2.5 Compressive behaviour of fibrous tissue (a) cavity tissue (b) sub-plate tissue (Hori and Lewis, 1982).

The non-linear compressive behaviour recorded by Hori and Lewis (1982) was quantified by Weinans *et al.* (1990) as

$$\sigma = \frac{E_0}{H}\left\{\frac{1}{(1-\varepsilon)^H} - 1\right\} \quad \text{for } \varepsilon \geq 0 \tag{2.4}$$

where E_0 is the modulus at zero strain, and H is a constant which will determine the stiffening rule. It is known that fibrous tissue is weak in tension and has little ability to transmit shear stresses; however, there are no mathematical expressions in the literature relating to the shear or tensile behaviour. When modelling fibrous tissue, Weinans *et al.* (1990) assumed the material to have no strength in shear or tension. The normal stress - strain relations, for E_0 values of 0.17, 1.00 and 2.00MPa, are shown in Figure 2.6. The compressive tangent modulus can simply be found by taking the derivative with respect to strain of the stress - strain relation, and is given by

$$\frac{\partial \sigma}{\partial \varepsilon} = E = \frac{E_0}{(1-\varepsilon)^{H+1}}. \tag{2.5}$$

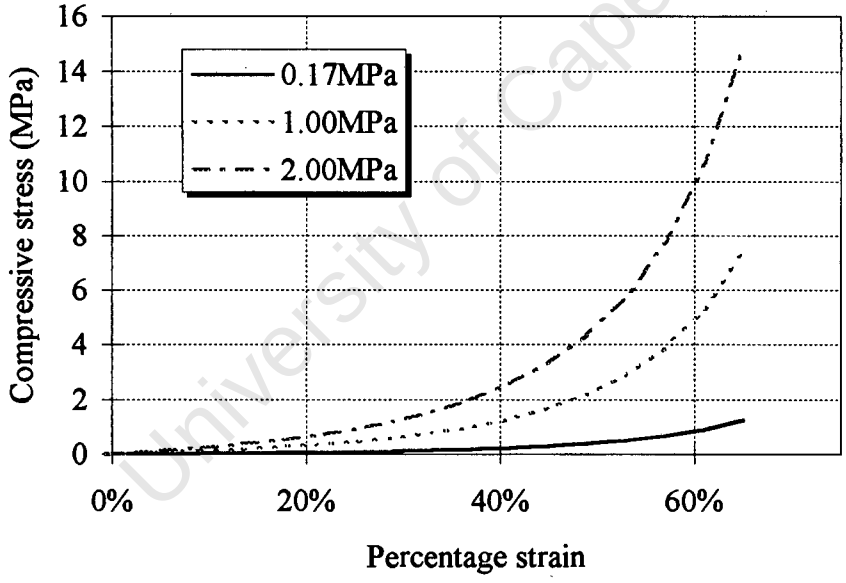

Figure 2.6 Fibrous tissue compressive behaviour for E_0 values of 0.17, 1.00 and 2.00MPa.

2.5 Bone Remodelling

During growth and adult life, bones are under a continual process of growth and renewal which, guided by mechanical demands, maintains a homeostatic condition. This ongoing process provides the body with a structure which is continually able to meet the

mechanical demands placed upon it. It has been suggested that with time and loading the bone structure becomes weakened by dehydration of the hydroxyapatite crystals (Neuman and Neuman, 1958), which necessitates the replacement of effected osteons. Furthermore, it is believed that cyclic loading results in fatigue micro cracks (damage) of the trabeculae, which therefore need to be continually repaired (Carter *et al.*, 1983; Burr, 1984; Martin, 1992). Subsequently, to maintain the physiological function, the renewal process replaces the dehydrated bone and repairs the damaged trabeculae (Carter and Caler, 1983; Martin and Burr, 1989; Jee, 1980).

Apart from maintaining a reliable structure for load bearing, the composition of human bone is believed to be formed and maintained so as to provide optimal load carrying capacity, with the greatest economy of materials. Pauwels (1980) concluded, following the ideas of Roux (cited in Pauwels, 1980), that not only were the individual bones optimal with respect to their task within the locomotor apparatus, but the stress in each of the bones is kept as low as possible by the overall architecture of the skeleton. Furthermore, the internal structure and external geometry of bones are able to adjust to meet new mechanical demands. To achieve this, the density, structural orientation and surface geometry of load bearing bones are developed and maintained so as to provide optimal fitness for purpose. The structural orientation and density can be altered by adding or removing bone on the endosteal surfaces, while the external geometry is altered by periosteal remodelling (Jee, 1980; Martin and Burr, 1989).

2.5.1 Remodelling Physiology

Commonly, the term remodelling refers to all the processes of growth and renewal, whether it be the addition or resorption of bone as a result of new mechanical demands, or whether it is simply the process of renewing existing tissue. Parfitt (1984) distinguishes between this process of maintenance (remodelling) and bone modelling, which is the formation or removal of bone for extended periods of time without interruption. Bone modelling would be responsible for adjusting the density, structure and surface geometry as a result of some altered biomechanical demands on the bone tissue. Remodelling physiology was described by Frost (1964), who proposed that the organisation of cells responsible for the process be grouped into units called Bone Remodelling Units (BMUs). These groups of cells operate on the free surfaces of cancellous and cortical bone, as well as within cortical bone. The bone remodelling units travel through the cortex or across the trabecular surface. Each BMU replaces approximately the same volume of old bone material with new.

Parfitt (1984) and Burger (1995) identify five stages in the processes of remodelling, which are graphically represented in Figure 2.7. The first phase, *activation*, is characterised by the recruitment of osteoclasts. This is followed by *resorption* which, after approximately 12 days, results in a cavity. During the resorption phase, the newly formed osteoclasts arrange into a so called *cutting cone*, which moves forward longitudinally at a rate of approximately 2μm/day. Processes of remodelling and modelling possibly always begin with the resorption of existing tissue. The third stage, *reversal*, results in the ceasing of the osteoclastic activity and the lining of the newly formed cavity, resulting in the formation of a "cement line". It is not known how the size

and shape of the resorbed cavity is controlled. The reversal phase is characterised by the arrival of osteoblasts at the base of the resorbed cavity. The arrival of osteoblasts could be stimulated by mechanical or biochemical factors. However, Parfitt (1984) argues that "to account for the spatial specificity of the new bone formation, the ostoegenic stimulus must be related to resorption or activation."

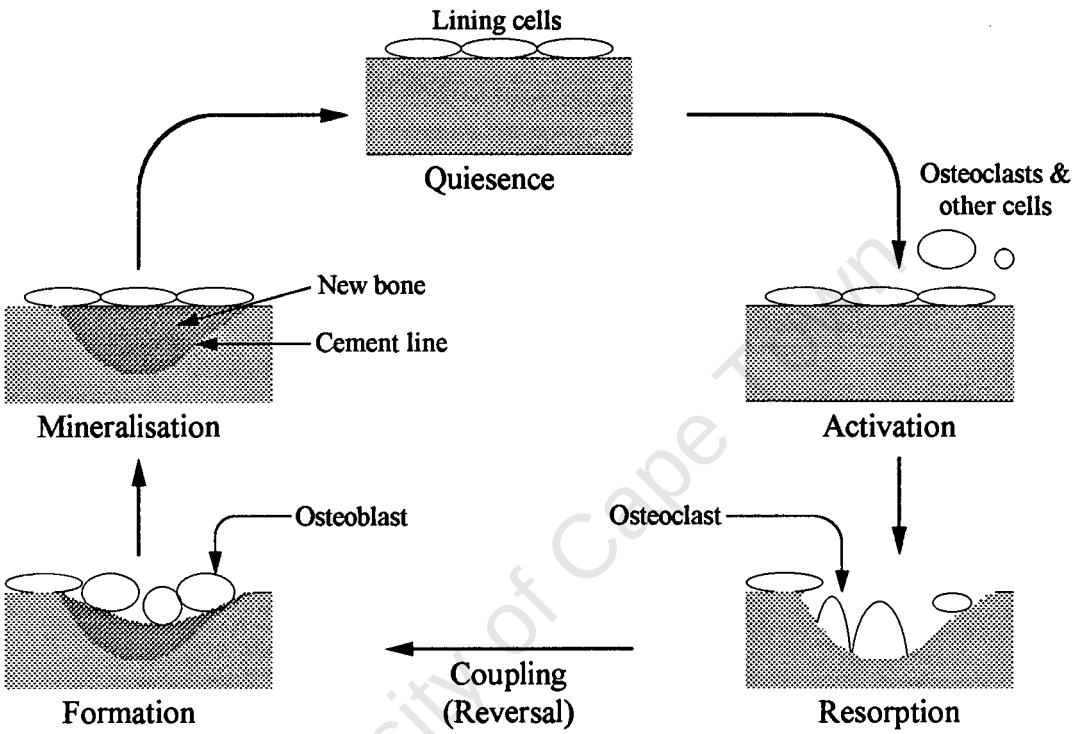

Figure 2.7 The five stages of bone remodelling (adapted from Parfitt, 1984 and Burger, 1995).

The presence of osteoblasts results in the *formation* stage, during which bone is added. The total time from when the osteoclasts first began the erosion of bone to the beginning of formation is about 30 days. Under normal circumstances, the extent of resorption and formation are coupled and are, therefore, equal. However, the nature of this coupling may change as a result of mechanical or chemical influences. Whether the cavity created by the osteoclasts is under-filled or over-filled, will determine whether there is a net loss or gain of bone tissue. Formation includes the secondary stage of tissue mineralisation, which may also be influenced by mechanical factors. It is unclear whether the number of osteoblasts recruited or the degree of cell activity is responsible for the extent of cavity filling. Parfitt (1984) argues that only a single generation of cells is required to complete the process of bone formation. However, Martin and Burr (1989) suggest that several generations of cells would be required to complete this process. They argue that as the osteoblasts are less mobile than the osteoclasts, they remain stationary while the bone filling progresses at a rate of approximately 40μm/day. As the cells are stationary, they get left behind and become embedded in the bone matrix. Therefore, to continue the

filling process, new osteoblasts must be produced each day. The embedded osteoblasts become known as osteocytes, while those on the surface become lining cells. Whether or not several generations of cells is required to complete the filling process is important when examining the influence of mechanical loading on bone adaptation, as it is likely that the mechanical and hormonal influences will effect the number of cells recruited. However, this issue is complex and remains to be resolved.

The final stage in the remodelling process is a return to *quiesence* which, under normal circumstances, is the state of 80% of the free bone surfaces in the adult skeleton. The total time from activation to quiesence in human cortical bone is approximately 120 days (Martin and Burr, 1989). This is in contrast to young, developing, bones which are always in a state of apposition or resorption.

Although bone is largely influenced by mechanical loading, the form and architecture of bones may also be a product of genetic coding and hormonal influences, which will exist whether or not the bones are loaded. However, in bones whose function is primarily load bearing, such as the femur and tibia, the structural form will be profoundly affected by the daily mechanical demands. Bones which have been functionally isolated during growth do not necessarily posses normal morphology. On the other hand, bones whose function is mostly protective, such as the skull, will not be greatly influenced by these factors. This difference points to the possible existence of a basic bone structure, which may exist in some bones.

2.5.2 Mechanical Influences on Bone Remodelling

The first observations of the relation between bone structure and the loading it experiences were made by Galileo in 1638 (Ascenzi, 1993). However, it was only in the nineteenth century that Cullman and von Meyer (cited in Cowin, 1986) discussed the organisation of the bone trabeculae, with respect to the stress trajectories due to normal loading. The obvious relation between trabeculae architecture and the principal stress directions is often attributed to Wolff (from the translation, 1986), and it has become known as Wolff's law. No experimental confirmation of Wolff's law was undertaken until this century, when Thompson (1917) suggested that strain might be the stimulus for bone adaptation. Subsequently, experimental work undertaken by Glucksmann (1938) showed that cellular events could be stimulated in tissue cultures by applying deformations. More recently, Frost (1964) and Pauwels (1965, from the translation, 1980) have attempted to write explicit mathematical relations between structural loading and bone architecture; these are discussed later.

The relation between load and bone adaptation has been the subject of numerous research efforts (Lanyon *et al.*, 1982; Lanyon, 1984; Meade *et al.*, 1984; Rubin and Lanyon, 1984; Brown *et al.*, 1990; Rubin *et al.*, 1990; Sumner *et al.*, 1992). In humans, exercise provides a simple means of relating loading to bone adaptation. Jones *et al.*, (1977) examined the cortical thickness in the dominant arm of tennis players, and found an increase of between 28 and 35% when compared to the contralateral side. However, animal experimentation provides a means of relating load magnitude, the number of load cycles and the type of loading, to tissue response. Churches and Howlett (1981) applied

compressive loading of between 2 and 8MPa to the metacarpal bone in young adult sheep, and found an increase in cross-sectional area of up to 8%. More dramatic results were demonstrated in pigs which were subjected to overloading as a result of an ulna osteotomy (Goodship *et al.*, 1979). The subsequent increase in strain resulted in a 50% enlargement of the cross-sectional area of the overloaded radius.

While the experimental models show that loading (over or under-loading) can alter bone structure, there has been much controversy as to which loading parameter will influence remodelling (Cowin, 1993). Initially, researchers (Frost, 1964; Cowin and Hegedus, 1976) proposed that bone will be influenced by strain magnitude, based on intuitive arguments that ".. the reason bone senses strain or stretch and not stress, is that strain is a primary, directly measurable, physical quantity, whereas stress is not." (Cowin, 1984). Subsequently, strain energy density (Huiskes *et al.*, 1987) and equivalent stress magnitudes (Fyhrie *et al.*, 1986; Carter *et al.*, 1987; Beaupré *et al.*, 1990; Levenston *et al.*, 1994), have been assumed to drive the remodelling processes.

Apart from the intuitive arguments presented by Cowin and his co-workers, there exists an overwhelming amount of experimental evidence (Lanyon, 1984; Rubin and Lanyon, 1984; Turner, 1992) in support of strain magnitude being the driving force behind adaptive bone remodelling. The most likely cells to respond to mechanical loading are the osteocytes - which are dormant osteoblasts that have become embedded in the extracellular matrix. Duncan *et al.*, (1989) reported both stretch and voltage sensors in osteocytes. Although the cells are well distributed in the extracellular matrix, each osteocyte is connected to other osteocytes and osteoblasts on all adjacent bone matrix surfaces. Therefore, these cells can communicate the stimulus to other cells over a distance which is thought to be in the range of 150 to 200μm (Cowin, 1993). The fact that cells are capable of sensing stretch (strain), and communicating this to other cells suggests that strain, and not stress, due to loading is the most likely candidate for the remodelling stimulus.

While it is clear that strain magnitude will influence the formation or removal of bone, there is much controversy as to exactly how different strain signals will effect the process. Although a considerable amount of experimental work has focused on resolving these issues, an exact understanding of the influence of the straining mode remains illusive. Lanyon (1984) examined and summarised the influences of the number of strain cycles, the peak strain magnitude, the rate of straining and the strain distribution, on tissue response. The effects of these parameters, as well as the influences of compressive and tensile strains, are set out follows:

Number of cycles

In an experimental model using an adult rooster, Lanyon (1984) demonstrated that at a fixed peak strain magnitude (2000×10^{-6}), the number of load cycles strongly influenced the bone response. As few as 36 cycles per day resulted in a 33% increase in the midshaft mineral content. However, increasing the number of cycles above this value did not have any further influence. At this load magnitude, only 4 cycles per

day were necessary to maintain the current level. This extremely low number of cycles led to the conclusion that

> "... the remarkably few strain cycles required to produce these reactions suggest a specific response induced within a receptive cell population, rather than an indirect effect such as tissue damage or increased perfusion."

Strain magnitude

The same model was used to investigate the influence of peak strain magnitude, while keeping the number of cycles and strain rate constant at 100 cycles and 0.01 sec^{-1} respectively. With no load, extensive bone loss resulted, which was not prevented when the strain magnitude was increased to 500μstrain. Bone cross-sectional area was maintained with strain magnitudes of 1000μstrain, however, increasing the strain magnitude above this value, resulted in area increases approximately proportional to the strain magnitude increase.

Lanyon *et al.*, (1982) collated measurements of the peak functional compressive strain magnitudes for several species, including humans, from the work of Rubin, Lanyon and others. The data showed a remarkable similarity amongst the values of peak strain magnitudes, which where found to be in the range of 2100 to 3200μstrain. Lanyon (1975) reported the first *in vivo* measurements of strain in the human tibia during locomotion. He found that the strain magnitudes were similar to the values found in the animals previously measured. Functional compressive strains are in general larger than tensile strains. This is because the combined bending and axial load to which the long bones are subjected results in the bending strain being superimposed on the compressive (or axial) strains. Therefore, the tensile strains are

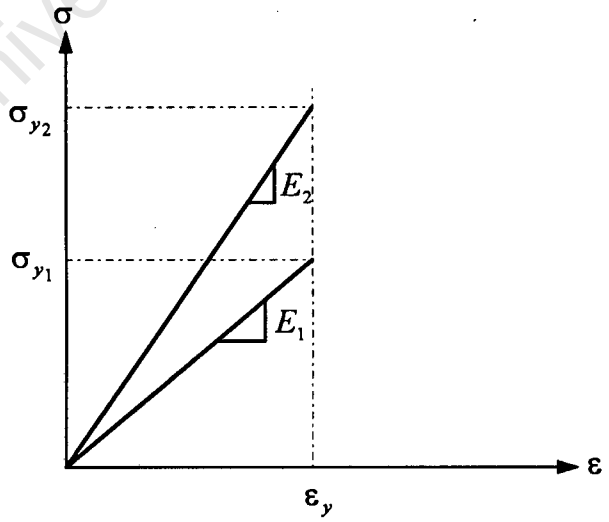

Figure 2.8 Constant yield strain theory for bone remodelling (adapted from Turner, 1992).

reduced, and the compressive strains increased. Rubin (1984) examined several species (dog, horse, turkey, buffalo and elephant) and found the ratio of compressive to tensile strains to be 1.54.

Turner (1989) measured the compressive yield strain of 61 specimens of bovine trabeculae bone. He found that the variation in yield strain was small (yield strain = 0.915 ± 0.169%), and independent of specimen orientation. These findings lead to the hypothesis (Turner, 1992) that cancellous bone will evolve so that the yield strain is fairly uniform in a specific area of the skeleton. This theory may also help to explain tissue anisotropy in bone, as it is proposed that bone will adjust its structure so that yield strain in orthogonal directions will be constant. Therefore, density and structure, and subsequently Young's modulus, may vary, but the yield strain remains constant, as shown in Figure 2.8. The two material responses shown in the figure have Young's modulus values of E_1 and E_2, and corresponding yield stresses of σ_{y_1} and σ_{y_2}. However, for both materials, the yield strain has a constant value of ε_y. This hypothesis supports the existence of an optimal value of peak strain during normal loading. If there exists a constant loading safety factor (yield strain/peak strain), then the experimental findings suggest that bones will adapt so as to keep peak strain uniform and isotropic.

Tension or compression?

Early observations (Martin and Burr, 1989) of bone fractures that had healed in a bent configuration and which were found to later straighten themselves, led experimentalists to attribute this change to bone remodelling. In order for this to occur, the compressive strains on the concave side must have resulted in bone formation, while the tensile stresses on the convex side must have caused bone loss, for the bone to straighten. However, this hypothesis implies that intact long bones which are angular would tend to straighten, which is not the case. This problem was investigated by Frost (1964), who suggested that increased surface convexity would result in osteoclastic activity, while decreased surface convexity would result in osteoblastic activity.

Rate of straining

Several researchers (Hert *et al.*, 1971; Rubin and Lanyon, 1984) have demonstrated that cyclic strains will stimulate bone response, while static strains will have no influence. This is shown by the fact that no difference was found when applying a static load to a functionally isolated bone, and comparing the response to a similar, but unloaded, bone. Furthermore, O'Connor *et al.* (1982) demonstrated that peak strain applied at higher strain rates, was associated with greater amounts of new bone formation.

Strain distribution

Lanyon *et al.* (1982) found that altering the strain distribution in the radius of sheep, by removing the supporting ulna (resulting in only a 20% increase in strain), caused new bone to form in order to compensate for the loss. After a one year period, the

strains were actually lower than they had been before removing the ulna. The experiment showed that the remodelling process is very sensitive to small changes in the typical strain value - possibly a deviation from the normal value is more important than the actual magnitude.

The observations discussed above, suggests that there exists a set of conditions under which bone attains an equilibrium state. Further, the alterations in loading that are required to produce noticeable changes in bone geometry and structure, suggest the existence of a so-called *lazy* or *dead* zone (Carter, 1984 and Huiskes *et al.*, 1987) in which bone is fairly unresponsive. In this equilibrium state, the remodelling processes will continue for the purpose of structural maintenance, without the net apposition or removal of bone. Carter (1984) proposed a "working hypothesis" regarding the response of bone to mechanical loading, in which he set out a qualitative relation between bone apposition, or removal, and mechanical stimulus. The stimulus may depend on one or more of several parameters, such as the load magnitude and the number of load cycles. His hypothesis incorporated the concept of an equilibrium region, in which the structure could be said to be in remodelling equilibrium. If the stimuli were increased such that they lay outside of this equilibrium region, bone tissue would be added. Similarly, if loading were decreased beyond the equilibrium, tissue would be removed, as shown in Figure 2.9. Carter does not make a distinction between the rate of bone production and the rate of bone loss. Whether or not these rates are different remains to be determined.

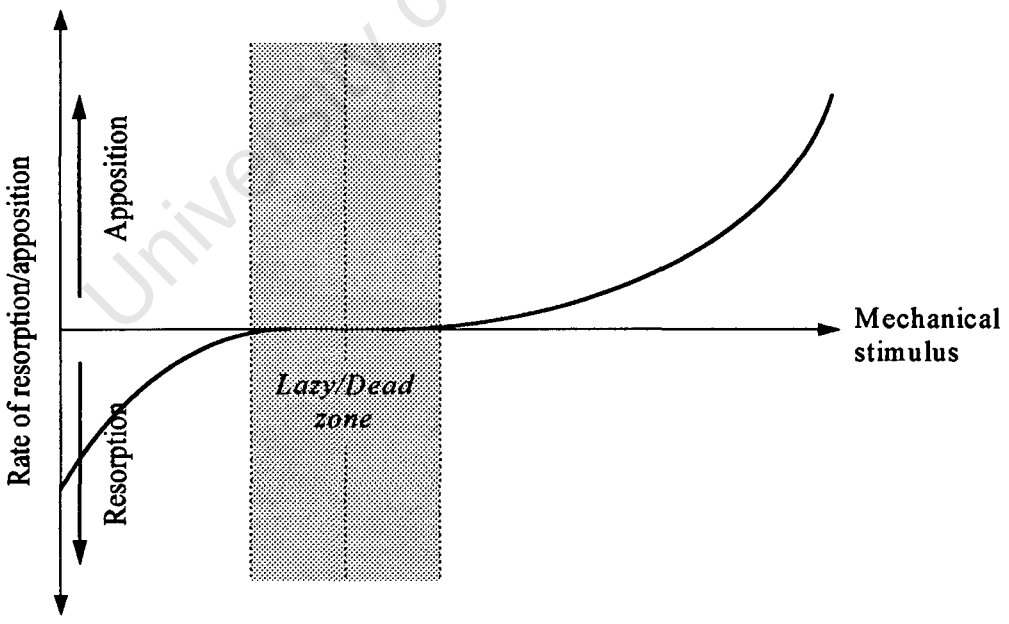

Figure 2.9 The influence of mechanically induced stimuli on bone resorption and apposition (adapted from Carter, 1984).

In addition, Carter's model does not examine the influence of a stimulus saturation level which, when exceeded, will not cause further alteration. The existence of a saturation level on the number of load cycles was demonstrated by Lanyon's avian ulna experiment, in which it was shown that, at a fixed load magnitude, increasing the number of cycles from 36 to 1800 cycles per day did not increase the amount of new bone formed.

This point was later raised by Beaupré *et al.* (1990), who proposed a series of responses for different anatomical regions. Of particular interest, are bones which are subjected to extremely small loads when compared to, say, the femur. However, because of their importance as protection, bone mass and structural integrity need to be maintained, and therefore irrespective of load, the bone in this region will not be resorbed. It is quite possible that in these areas, the mechanisms for remodelling are different to those in the load carrying members. This has important implications when studying bone adaptation, as the theory that is accepted and used may only be appropriate for that anatomical region.

2.5.3 Remodelling Rate Equations

Numerous research groups have given considerable attention to developing numerical models for the purpose of simulating the adaptive remodelling processes observed by Wolff (1892). Initial work in this field was conducted by Frost (1964), who proposed the division of bone remodelling into *internal* and *external* remodelling. Although all changes to bone structure are as a result of the addition or removal of bone tissue from an existing surface, internal adaptation is achieved by osteonal remodelling, whereas external remodelling is achieved by endosteal and periosteal remodelling. Frost proposed that the alteration of density and trabeculae alignment be classified as *internal* remodelling, while the alteration of the external geometry be referred to as *external* remodelling. Subsequently, remodelling rate equations have been developed for the purpose of separately simulating internal and external remodelling, based on some load induced stimulus.

Motivated by the work of Frost (1964), Cowin and Hegedus (1976) and Hegedus and Cowin (1976), developed a thermo-mechanical continuum theory to simulate the process of bone remodelling. A surface remodelling rate was later introduced to address the problem of adaptation caused by the introduction of a medullary pin (Cowin and Van Buskirk, 1979). In this and other work (Firoozbakhsh and Cowin, 1980; Cowin and Firoozbakhsh, 1981) they proposed that the rate of surface bone deposition or removal was proportional to the difference between the actual strain magnitude and an assumed optimal value. Therefore, the rate of bone apposition $\dot{X}$ normal to the surface is given by

$$\dot{X} = \mathbf{C}:(\varepsilon - \varepsilon_0) \tag{3.2}$$

where ε and ε_0 are the actual and optimal strain tensors respectively, while $\mathbf{C}$ is a matrix containing the remodelling rate coefficients, which are assumed to be independent of strain and position. The superscript dot implies a derivative with respect to time, and the : implies a double contraction. If compressive strains are taken as being positive, the relations described above will only result in bone formation in a state of compression. In

contrast, bone will be removed under tensile loading. This formulation is limited as a result of the difficulty in determining the nine rate coefficients, which have to be derived from experimentation. Various groups (Hart *et al.* 1984; Hart and Davy, 1984; Firoozbakhsh *et al.*, 1989) have extended the model of Cowin and Van Buskirk (1979) to include surface remodelling, in order to predict load induced adaptation using the finite element method.

Although strong arguments (Cowin, 1984; Martin and Burr, 1989; Cowin 1993) have been put forward that strain and not stress will determine the remodelling response, the difficulty in determining the necessary coefficients for the tensor valued function remains a considerable obstacle. To overcome this problem, phenomenological models have been developed where it has been assumed that energy and stress based quantities are responsible for adaptation. Huiskes *et al.* (1987), simulated internal and surface remodelling, by assuming that the out-of-balance of the current and optimal values of strain energy density ($2U = \sigma : \varepsilon$) would be the stimulus for bone formation and removal. Their model incorporated the "working hypothesis" proposed by Frost (1964) and Carter (1984), that there exists a region of loading in which bone will be fairly unresponsive. They assumed that, in the *dead zone*, the remodelling rate will be zero, and it would be linearly related to strain energy density on either side of this region. A relation of the same form was written for the rate of change of the external geometry of the bone surface. Carter (1984) believed that a greater deviation from the *dead zone* was required to initiate new bone formation, compared to the deviation required to cause bone loss. However, possibly because of the lack of experimental data, the slope of the rate equation was assumed to be the same for both bone loss and gain.

The use of strain energy density has an advantage in that it is a scalar quantity, so fewer constants are needed. However, its use is limited in that, as a scalar, it will carry no information about strain orientation and, as bone trabeculae will orientate according to the applied load, information about this will not be captured. A further limitation is that the magnitude of strain energy density will always be positive, so no distinction can be made between compressive and tensile loading. Furthermore, strain is directly measurable, and therefore meaningful experimental values can be obtained for the optimal and out of balance strain magnitudes. Notwithstanding the above limitations, excellent results were obtained using strain energy as a remodelling stimulus, when predicting the density distribution in the intact (Huiskes *et al.*, 1987) and reconstructed (Van Rietbergen *et al.*, 1993) proximal femur.

Carter *et al.* (1987) proposed that the density of the bone tissue will be a function of an equivalent stress measure $\bar{\sigma}$, which is defined as $\bar{\sigma} = \sqrt{2EU}$. In one dimension, the equivalent stress is equal to the actual stress. Their remodelling equation incorporated multiple load cases, where each load case was weighted according to the number of load cycles for which it was assumed to act. This work was later extended (Carter *et al.*, 1989) in order to include trabeculae orientations for the purpose of predicting the density and anisotropy of the intact proximal femur. From the analysis, they concluded that multiple load cases were necessary in order to more accurately predict density and

orientation patterns. They also found that the orientation of the trabeculae are not perpendicular, in contrast to the observations and hypothesis of Wolff (1986).

Many of the time dependent formulations developed to simulate the process of remodelling have included the idea that bone will respond to some time averaged value of a strain or stress based stimulus. This concept stems from the fact that bone does not respond instantaneously to load, but reacts over a period of time to a history of events. However, events that have happened some time previously will not influence the current response. Whereas events in the recent past will have an influence on the response, but not to the same extent as a current event. Furthermore, as there is an inherent lag in the response of bone to loading, it takes some time after a loading event for the response to get under way. Levenston *et al.*, (1994) included the idea of an exponentially decaying memory of past events into the stimulus functions of several previous researchers. The fading memory formulation was used to address the problem of the density distribution in the proximal femur, with memory time constant of 5, 20 and 100 days. The concept of a lag time for cellular events to reach their maximum influence was not included in this formulation (although the possibility was suggested), as the emphasis of the study was on the influence of the decay function.

It is well known that fatigue micro-cracking is common in cortical and cancellous bone (Carter *et al.*, 1983; Burr *et al.*, 1984; Martin, 1992). The body is continually repairing cracks as they develop and become potentially hazardous. It has been observed in individuals who have been sedentary and suddenly become very active (such as joining the army), that if the rate of cracking out-paces the rate of repair, a stress fracture can occur at normal stress levels. Prendagast and Taylor (1994) developed this idea, by proposing that there exists an equilibrium level of damage (and hence a homeostatic strength level), and that the remodelling stimulus will be the deviation from this level. Based on this, they proposed that the rate of bone resorption or deposition will be given by the difference between the equilibrium and the actual damage rates. Although their model was not used in conjunction with the finite element method to address classical biomechanics problems, this formulation represents an important change from the traditional approach to the remodelling problem.

More recently Cowin *et al.* (1991) have begun exploring the way in which bone cells sense mechanical loading, by examining the mechanics on a cellular level. Subsequently, Harrigan *et al.* (1993) and Weinbaum *et al.* (1994) have developed numerical remodelling simulations based on osteocyte deformations. These models are distinguished from phenomenological models in which the remodelling physiology is not explicitly considered, but simply assumed to exist based on observation. In these models, it has been proposed that the deformation of the osteocytes is a result of fluid shearing on their membranes, rather than fluid pressure.

CHAPTER THREE

JOINT RECONSTRUCTION

3.1 Introduction

This chapter forms the second part to the introduction and review of the literature. Here joint reconstruction and implant-bone interaction are discussed in detail. Particular attention is given to the evolution of interface tissues in cementless joint arthroplasties. This is followed by a discussion of constitutive and numerical modelling of the interaction of two deformable bodies, both in general terms and in orthopaedic applications.

The reconstruction of human joints using artificial implants, as a result of fracture and pathological changes, is one of the most frequent procedures in locomotive apparatus

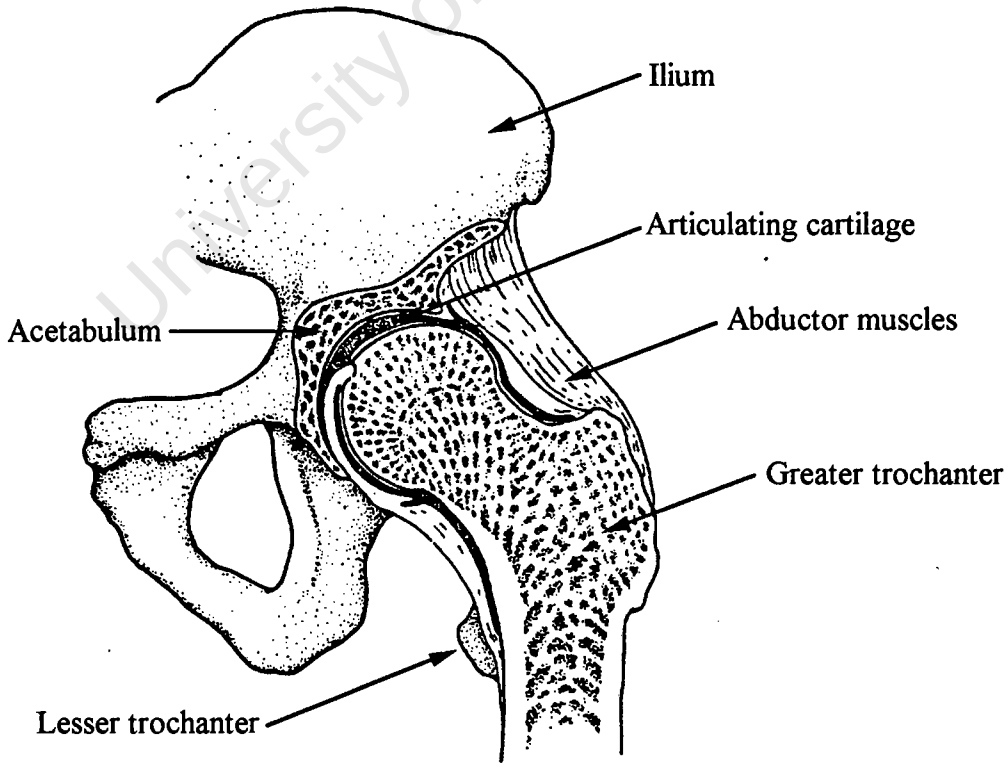

Figure 3.1 The articulation mechanism of the normal hip.

surgery today. In this work, attention has been given to the hip joint and, to a lesser extent, the knee. The choice of the hip is based on the high failure rate of these joints and the resulting large amount of research that has been undertaken in studying the mechanics of the joint and its replacement. However, the formulations presented in this thesis should, in general, apply to other joints.

3.2 Reasons for Joint Replacement

The two primary reasons for joint replacement are osteoarthritis and rheumatoid arthritis. Osteoarthritis is a degenerative bone disease of the joint cartilage which is associated with secondary changes in the underlying bone. This results in inflammation and subsequent mechanical failure of the articulating surfaces of the joint (Figure 3.1). During the progression of osteoarthritis, the lining cartilage of the joint wears down to the point that the underlying bone is exposed. As a result of this, a grinding, vibrating and jarring sensation is felt during walking, as the joint sticks and then slips. Subsequently the underlying bone is destroyed which, in the case of the hip, will lead to a shortening of the affected leg. The articulation cannot be repaired and it therefore becomes necessary to reconstruct the joint using artificial components.

3.3 Replacement Concepts and Procedures

Total joint reconstruction, as introduced by Sir John Charnley in the early 1960's, has revolutionised the management of patients suffering from chronic arthritis of the hip: by restoring pain free mobility to the affected joint. The approach pioneered by Charnley, which has become known as "low friction arthroplasty", relies on creating a new ball and socket joint. The concept of low friction came from the use of a highly polished steel femoral head, in contact with a ultra high molecular weight polyethylene (UHMWPE) acetabular cup or socket. Charnley aimed at finding the optimal head size which was sufficiently small to minimise frictional torque, while being sufficiently large to minimise contact pressure and prevent dislocation. A head size of 22mm was found to be the best compromise between the two.

The femoral component consists of a stainless steel, titanium, or cobalt-chromium stem, on the end of which is the articulating head. Between the stem and head are the shoulder and neck of the implant. Some designs incorporate a collar at the shoulder level to provide additional support. The joint reconstruction is achieved by securing the femoral stem within the medullary canal of the proximal femur. The femur is prepared for the stem by resecting the existing femoral head at the base of the neck, and broaching the medullary canal so as to accommodate the shaft. On the side of the pelvis, the natural acetabulum is replaced by an high density polyethylene acetabular component (cup). The worn natural acetabulum is prepared by reaming the cavity so as to locate the new polyethylene cup. The many designs of acetabular component include various thickness' of UHMWPE and metal backing to provide rigidity.

The most common and traditional method of securing the stem within the medullary canal, and the acetabular component within the pelvis, is by the use of a bone cement.

The cement is used as a grouting material between the stem and the bone, as well as between the cup and the pelvis. However, more recently a cementless method of implant fixation has been introduced. This method relies on bone ingrowth into a porous coating which covers a portion of the stem or cup surface, so as to achieve a bond to the surrounding bone. This method, known as cementless joint arthroplasty, has the potential advantage of providing an indefinite bond which is continually maintained during the normal bone turnover process.

3.3.1 Cemented Joint Arthroplasty

To secure the femoral component in position, the medullary cavity is broached to a size larger than the implant stem. The resulting gap is filled with Polymethylmethacrylate (PMMA), which is a grouting material used to support the implant (Figure 3.2). The cement is merely a space filler which does not bond securely to the steel implant, however, it is intended to form a bond to the surrounding bone by infiltrating into the pores of the bone structure. To create this bond, it is common practice for surgeons to pressurise the cement into the cavity so as to facilitate the penetration of the grout into the bone structure. If interdigitation is successful, the cement will penetrate the bone and subsequently relative displacement at this interface will be eliminated.

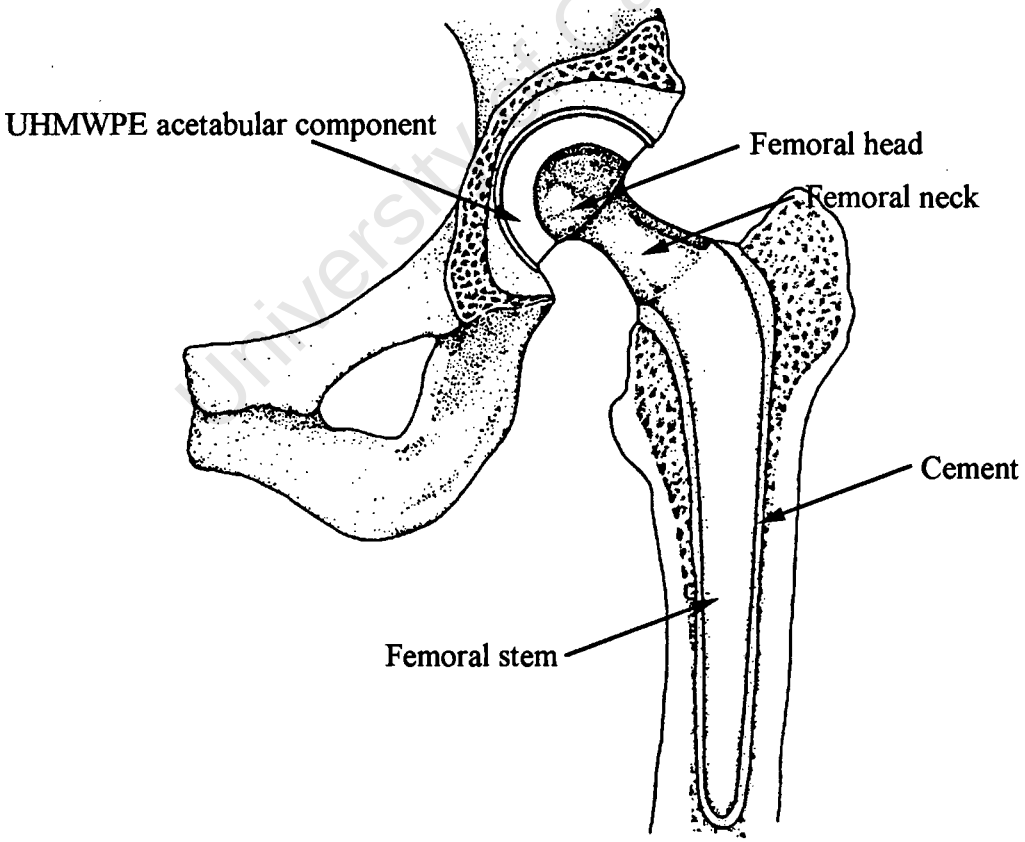

Figure 3.2 Cemented hip joint replacement.

implant surface will be well loaded, which may aid ingrowth and prevent subsequent resorption. Certain designs incorporate a collar below the neck of the femoral stem which will transfer some of the load from the implant to the underlying bone. An advantage of a collar is that it will restrict relative movement of the implant and bone. Also, as some of the load is transferred through the underside of the collar, overloading of the bond between the beads and the bone is prevented. However, the collar does not allow subsidence and subsequent anchoring of the implant. The use of a collar is controversial and remains unresolved.

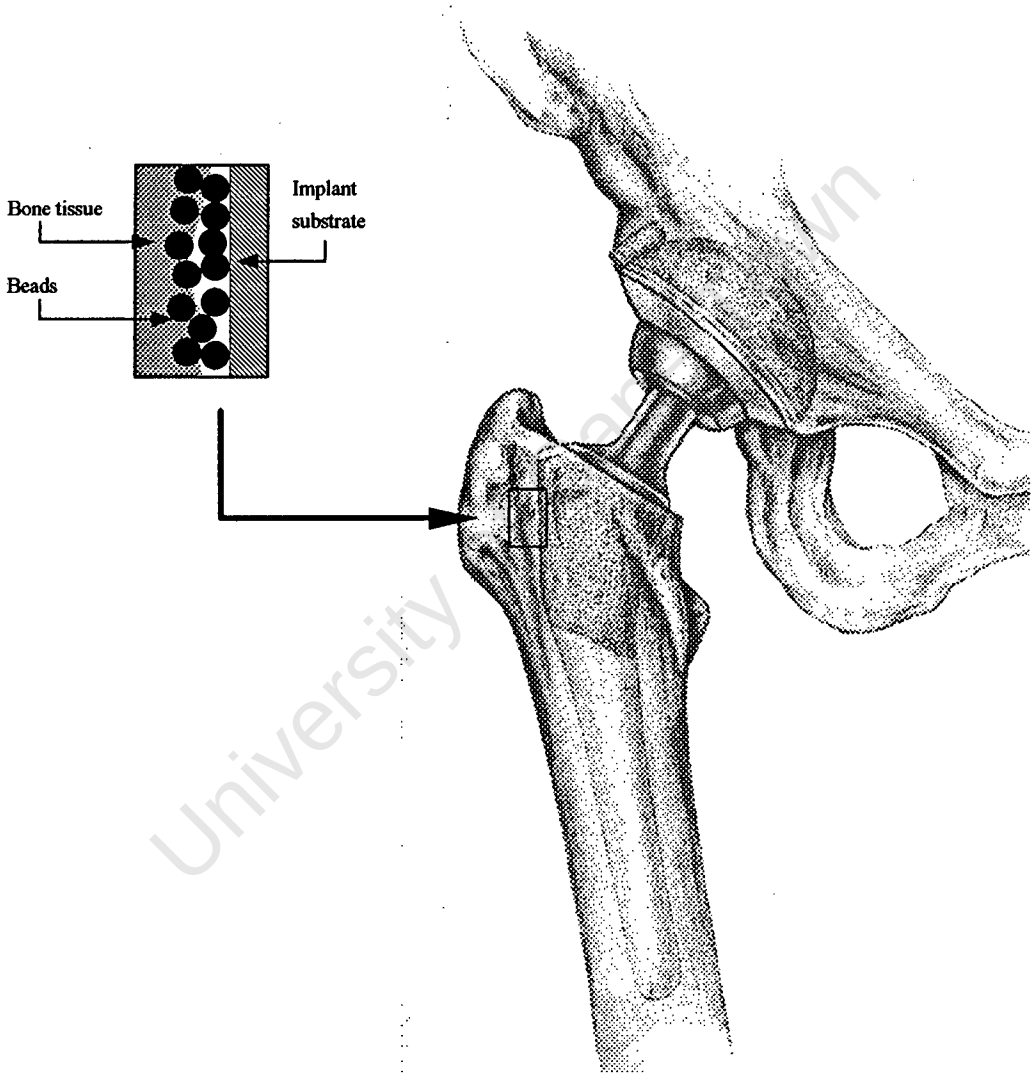

Figure 3.3 Cementless total hip reconstruction, showing a detail of the porous surface.

There are many types of porous coatings, the two most common being: fibre mesh and metal alloy beads. Fibre mesh consists of interwoven sheets of wire which are diffusely bonded onto the implant surface. Typically, a few layers are used which are laid orthogonal to each other on the implant surface. A second method of creating a porous coating is by sintering metal alloy beads onto the implant surface. The beads range in

diameter from 50 to 200μm and the application process results in relative porosities of approximately 0.4. An important aspect of the bead design is the pore size, which needs to be over 100μm to enable mineralised tissue ingrowth.

Although cementless arthroplasty offers a viable alternative to the traditional cemented method (Lawrence *et al.*, 1994), the problems of bone resorption, implant loosening (Cooke *et al.*, 1988; Havelin *et al.*, 1995) and thigh pain (Whiteside, 1989; Bourne *et al.*, 1994) still remain to be solved. At present, there is no documented evidence directly linking bone resorption to implant failure. However, the extensive loss of bone that is evident in radiographic follow-ups has been implicated in aseptic implant loosening. Initially designers of cementless implants coated the entire stem with porous material in the hope of maximising the bonded surface area. While this approach resulted in an excellent interlock to the surrounding bone, most of the load was transferred from the implant to the bone in the distal regions and subsequently large scale bone loss was found proximally. Based on experimental findings (Ducheyne *et al.*, 1977; Turner *et al.*, 1986), the extent of porous coating on current designs ranges from approximately 10%, for systems that use isolated porous coated pads, to 60-70% for stems that are said to be extensively coated (Sumner and Turner, 1992). Despite limiting the coated area, reduction of bone mineral density with these implants continues to be a major problem.

The problem of achieving bone ingrowth is coupled to that of resorption. To achieve a stable environment which will encourage ingrowth of mineralised bone, stabilisation is required along the length of the stem. This need has resulted in the use of a press fit. However, even if there is no porous coating in the distal regions, the press fit will result in the load being transferred distally, which may result in proximal resorption. In addition to this, reducing the amount of surface coating will mean that the stresses transferred through the coating will be increased. High interface shear stresses can discourage interface tissue mineralisation and result in fibrous tissue formation, which in turn can lead to implant instability.

Bone Ingrowth

Bone is unique amongst tissues in that it has the ability to regenerate and thus can heal with additional bone rather than with scar tissue (White *et al.*, 1977; Numamaker and Perren, 1979; Perren, 1979). This capacity makes bony ingrowth into porous surfaces a feasible method of implant attachment (Hulbert *et al.*, 1973; Engh, 1983; Hungerford *et al.*, 1983; Pilliar, 1983; Spector *et al.*, 1983; Brooker *et al.*, 1984; Bobyn and Engh, 1988). In addition to this, the structural integrity of skeletal tissues is maintained through remodelling, thus providing the potential for an indefinite bond between the implant and the bone.

The ongoing interest, over the last two decades, in using porous coating as a method of implant stabilisation has resulted in extensive animal investigations into this method of attachment (Galante *et al.*, 1971; Cameron *et al.*, 1973; Cameron *et al.*, 1976; Ducheyne *et al.*, 1977 Spector *et al.*, 1978; Bobyn *et al.*, 1982; Hedley *et al.*, 1982; Hedley *et al.*, 1983; Chen and Turner, 1983; Engh *et al.*, 1987). This experimental work has aimed at defining the criteria for the design and use of cementless implants. Investigations have

shown that, under the right circumstances, mineralised bone tissue will form within the porous surface. Although it is believed that cementless implantation is a viable and reproducible method of skeletal attachment, and could replace cemented fixation for active patients, retrieval studies (Harris *et al.*, 1983; Engh *et al.*, 1987; Collier *et al.*, 1988; Cook *et al.*, 1988) have shown many instances of minimal ingrowth, even in successful joint replacements.

Cameron *et al.* (1976) investigated the rate of ingrowth and resulting rate of bond shear strength development, for porous coated screws with pore sizes of less than 100μm. The 4.5mm diameter screws were inserted into holes of the same diameter in the femurs of adult dogs. Although the animals were allowed free movement there was no direct loading on the screws. After two weeks, they noted the presence of soft tissue within the beads, but no measurable shear strength. The maximum shear strength of the interface bond was reached in the third and fourth weeks, with no further increase in strength in the period up to 12 weeks.

Further experiments were conducted by Cameron *et al.* (1976) to investigate the ability of bone to bridge the gap between existing bone and a porous implant. To achieve this, screws were inserted into oversize holes which had gaps of 1.5mm, 1.0mm and 0.5mm. Within two weeks the gaps were filled with soft bone tissue only. However, at three weeks all but the largest gap was filled with woven bone. After a further week, the porous coating was being infiltrated and lamellar bone had formed in the gap. By twelve weeks there was no evidence of the gap, and the porous surface was completely penetrated with mineralised bone. This experiment illustrated the two processes involved in the formation of lamella bone. The first being the rapid formation of soft tissue, with the mineralisation process proceeding at a slower rate. These findings correspond with those of Homsy *et al.* (1972), who found that 100% of the 3000μm thick porous layer was filled with loose, immature collagen within the first five weeks. However, the rate of mineralisation was somewhat slower (between 40 and 120μm per week), and could be seen lagging behind the soft tissue front.

Insufficient or no stem fixation, due to lack of ingrowth, results in movement of the prosthesis relative to the adjacent bone, which can lead to bone resorption and replacement with fibrous tissue, resulting in migration or mechanical failure. Engh and Bobyn (1987) conducted clinical trials using AML prostheses with average pore sizes of 200 to 250μm. Their 6½ year follow-up of 100 cases examined the influence of ingrowth

Interface condition	Number of patients	Pain	Pain and Limp
Bone ingrowth	65	11%	3%
No Bone ingrowth	35	35%	23%

Table 3.1 The influence of bone ingrowth on the incidence of pain (Engh and Bobyn, 1987).

on the incidence of pain, and the influence of implant fit on bone ingrowth and pain. The resulting data for the ingrowth and implant fit analyses are summarised in Table 3.1 and Table 3.2, respectively. The follow-up results led to the conclusion that successful ingrowth considerably reduces the incidence of pain, and that a good implant fit is more likely to result in ingrowth, than an undersized stem. However, even in cases where successful ingrowth has been reported, pain and limping remain a problem. This problem may be attributable to incorrect implant positioning or incorrect implant size for the particular patient.

Implant fit	Number of patients	Appearance of ingrowth	Incidence of pain
Canal filling	35	91%	9%
Undersized	65	57%	25%

Table 3.2 The influence of stem fit on ingrowth and the incidence of pain (Engh and Bobyn, 1987).

A more recent study undertaken by Galante and Jacobs (1992) of retrieved porous acetabular and femoral components, which were removed for reasons other than implant loosening, showed highly varying degrees of bone ingrowth. Of the 19 primary THAs, 84% demonstrated ingrowth, while this figure was 71% for the 7 cases retrieved after revision surgery. The mean extent of ingrowth was found to be 29.9%, which came from a range of data from 0 to 84.5%. Examining the volume fraction of bone ingrowth, they found the range to be 0 to 35.2%, with a mean value of 8.9%. In a similar study, 14 porous coated femoral components were retrieved. Twelve of the retrieved implants were from primary replacements. All of the implants demonstrated some ingrowth, with a mean extent of 44.9% (range 19.6 to 92.6%). The range of volume fraction of ingrowth was somewhat lower (6.8 to 64.8%), with a mean value of 17.2%.

Interface Bonding

Parameters pertaining to the design of the porous coating, such as bead size, porosity, thickness of the bead layer and the bead material, will influence the mechanical strength of the bone-implant interface. Initial studies to examine the feasibility of using sintered fiber metal composites, as a basis for the attachment of an implant, were performed by Galante *et al.* (1971) and Hulbert *et al.* (1973). They investigated the bond strength when using a titanium fibre mesh on a cylindrical implant surface, implanted into the trochanteric areas of rabbit femora. The cylindrical implants were pulled out of the cortex into which they were implanted to ascertain shear limits. Approximately 80% of the ultimate values were reached within the first two weeks, with the ultimate value of 23.76MPa being reached at three weeks. No increase in strength was observed at six and twelve weeks.

Nilles *et al.* (1973) investigated the influence of time and material type on the shear strength of the interface bone, by undertaking push out tests on porous coated cylinders inserted in the cortex. They found that the shear strengths and apparent moduli of the bond approximately doubled between 2½ and 6 weeks, after which they remained fairly constant at approximately 15MPa, confirming the trends found by Galante *et al.* (1971). Typical shear stress-elongation curves for 2½, 6 and 12 weeks can be seen in Figure 3.4.

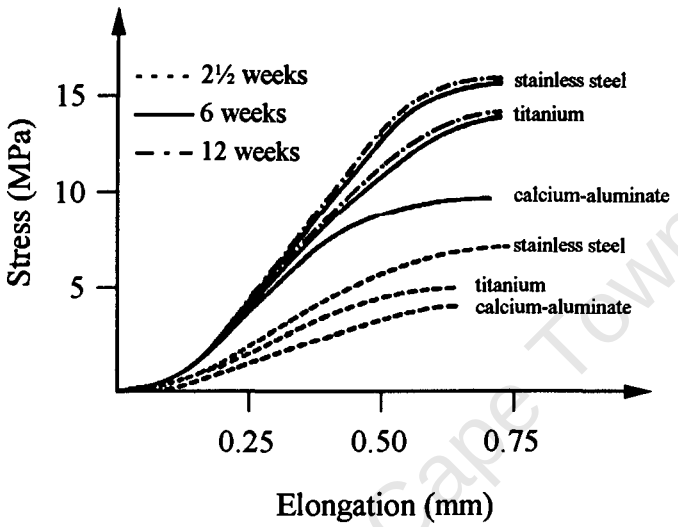

Figure 3.4 Shear stress-elongation curves for porous material at 2½, 6 and 12 weeks (adapted from Nilles *et al.*, 1973).

It is interesting to note, that although the modulus of stainless steel is almost twice that of titanium, they are both so stiff when compared to bone, that there is almost no difference in the apparent (interface) stiffness between the two. A further interesting observation of this study is that the shear failure strength of the bond is very similar to that of trabeculae bone, indicating that it is the material that fails, rather than the attachment of the bone to the beads. This was confirmed when examining the interface after failure. Figure 3.5 shows that the bone has failed at the implant surface leaving bone tissue within the bead structure.

The design of the beaded surface plays an important role in determining the mechanical, and interrelated biological, response of the interface. Although there are several designs of porous coating, this work is focused on the porous surface created using a layer of sintered beads. Experimental work with cementless implants has aimed at finding optimal values of the bead size, surface porosity, apparent modulus and depth of the layer. Examining cementless acetabular components, Harris *et al.* (1983) reported 55% ingrowth over the porous surface, with the tissue penetrating 3 layers of beads. The ingrowth was most prolific at the periphery of the acetabulum. The surface consisted of 4 layers of beads with a mean diameter of 300μm and a pore size range of 150 to 250μm. Cameron and MacNab (1976) found that even with a pore size of less than 100μm and a gap of 1.5mm between the implant and the surrounding bone, a bond strength of 13MPa

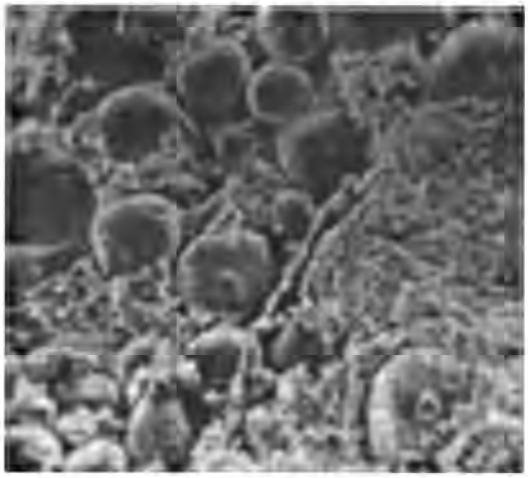

Figure 3.5 Scanning electron micrograph of the implant-bone interface fracture surface, magnified by 200 times (Bobyn, 1980).

was reached with 4 weeks post-operatively. Bobyn *et al.* (1980) inserted porous coated plugs into canine femurs in order to find the optimum pore size. They fabricated four porous surfaces with varying bead and pore sizes, which are set out in Table 3.3.

Design	Bead size (μm)	Pore size (μm)
A	25 - 45	20 - 50
B	45 - 150	20 - 200
C	150 - 300	200 - 400
D	300 - 850	400 - 800

Table 3.3 Particle and pore sizes of the four porous surfaces.

As shown in the graph of the bond shear strength against implant time (Figure 3.6), the intermediate designs, B and C produce the greatest shear strength in the shortest time. The pore size used in design A was found to be too small to allow uniform tissue calcification and therefore never reached full bond strength. When comparing small to large pore sizes, the smaller sizes have the advantage that bone tissue fills the pores more quickly. Further, smaller pores mean a greater amount of contact between implant and bone, which will aid in implant stability because of frictional forces. Bobyn *et al.* (1980) concluded that the optimal pore size was between 50 and 400μm. However, this is in contradiction to the findings of Hulbert *et al.* (1973) who concluded that pore sizes of over 100μm were necessary for ingrowth and over 150μm for osteon formation.

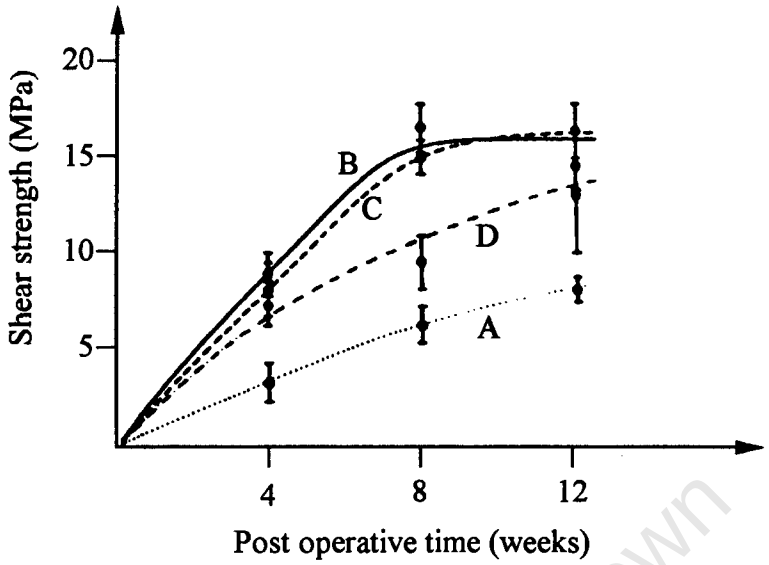

Figure 3.6 Shear strength shown at 4, 8 and 12 weeks for different porous coatings (adapted from Bobyn *et al.*, 1980).

While several research groups have investigated the strength of the bond formed by bone ingrowth, little work has been reported on the strength of a fibrous tissue attachment. Peel strength tests were undertaken by Bobyn *et al.* (1982) to gain some understanding of the mechanics of fibrous tissue when attached to porous beads on a cementless implant. The mechanism of failure at the interface was a combination of tensile failure and shear rupture, with the fibres pulling out of the bead structure. They found that the attachment strength was a function of the ingrowth time, as well as of the size and porosity of the bead structure. At 16 weeks, with a bead size and porosity of 90μm and 38%, respectively, the greatest peel strength of 27.5 g/mm (0.27MPa) was found. For this same bead structure, at four weeks the peel strength was 11.4g/mm (0.11MPa). An interesting observation of this study was that the strength of attachment was very similar to the tensile strength of the tissue, indicating that the failure at the interface was dominated by failure of the tissue, and not failure of the bond. This finding was confirmed by histological observations.

Mechanical Adaptation

The ability of bone tissue to adapt to a new mechanical environment will mean that, with the altered strain patterns which will follow joint replacement, a structural reaction to the surgery can be expected within the bone architecture. The structural adaptation following joint replacement can either be beneficial or detrimental to the reconstructed joint. If new bone is formed in highly stressed areas, this can contribute to the long term stability of the joint. However, as is often the case, in areas were stresses are reduced, particularly in the proxi-medial region in the case of hip joints, insufficient loading in this area results in extensive bone loss. This may be tolerable under normal loading conditions; however, in the event of some unexpected load, the lack of bone in a crucial region could lead to failure of the replacement. Further, revision surgery is then jeopardised because of

insufficient bone stock. Extensive bone loss is most prevalent in cementless arthroplasties (Engh and Bobyn, 1987; Galante, 1988), in the form of cortical thinning and increased porosity. This thinning takes place where the extreme mismatch of implant and bone moduli results in regions of the bone being "protected" from stress by the implant. Five year follow-ups using dual x-ray absorptiometry have shown bone losses of between 40 and 60%.

Bone loss is generally attributed to the change is strain patterns that occur as a result of the load transfer characteristics of the extremely stiff femoral implant. This has prompted researchers to develop more flexible stems, in an effort to recreate the normal stress distribution. Clinical results with these stems (Homsy, 1972; Bobyn *et al.*, 1992) have shown that after a three year period, bone mineral content with the flexible stems decreased by approximately 20% compared to the control femur. After the same period, the mineral content decreased by 40% when using the stiffer stems. These clinical findings were confirmed by numerical modelling (Huiskes *et al.*, 1992), which showed that while increased stem flexibility reduced stress shielding and subsequent bone resorption, this was at the expense of increased interface stresses in the proximal region. These stems however, have not gained in popularity as a result of the low strengths associated with the flexible designs.

In order to predict the changes in bone density associated with the use of cementless joint arthroplasties, several researchers (Huiskes and Numamaker, 1984; Cheal *et al.*, 1985; Huiskes *et al.*, 1992) have used bone remodelling algorithms, in conjunction with the finite element method, to predict the evolution of bone densities following total joint replacement and other surgical procedures. The complex geometry and loading on the proximal femur makes the finite element method a powerful tool for the design of prosthetic implants (Huiskes and Chao, 1983; Markele, 1992; Markele, 1994). This method, in conjunction with remodelling algorithms may enable designers in the future to make predictions of the long term success of implants, with an acceptable level of accuracy (Van Rietbergen *et al.*, 1993). However, the finite element models developed for bone density prediction do not include the evolution of the implant-bone interface. In general, it is assumed that the implant is perfectly bonded to the surrounding bone, which is not necessarily the case.

3.4 The Implant-Bone Interface

The response of the interface tissue will be influenced by blood supply, hormonal, metabolic and medicinal factors, as well as by the prosthesis design (Ling, 1986). However, it is believed that the dominant influence on the short and long term development of the interface tissues will be the mechanical environment between the implant and the surrounding bone. The long term success of any cementless arthroplasty will be directly determined by the type of interface tissue, and the extent of ingrowth. It is therefore crucial to understand the relation between interface mechanics and the resulting tissue formation.

3.4.1 Definition of the Interface

In a cementless arthroplasty, the implant-bone interface can be defined as the region between the implant material and the bone that is anatomically typical of the adjacent site. The interface is not simply a boundary line between the two materials, but rather a "region of interaction" (Howie, 1988). This region comprises debris material, an array of cells, coagulation products, fluids and tissue matrix

3.4.2 Categories of Interface

The post-operative interface of a cementless arthroplasty generally falls into one of two categories: osseo-integration or fibrous tissue encapsulation. In an osseo-integrated interface, there is intimate contact between the implant material and the underlying bone. As shown in Figure 3.7(a), the cancellous bone structure has penetrated the porous surface. The tissue integration results in an interlocking of the bone and beads producing a lasting bond between the prosthesis and the surrounding bone. A detail of tissue penetration into the bead surface can be seen in Figure 3.7(b).

Fibrous tissue encapsulation is primarily a result of large movements at the interface and is often associated with implant loosening. Under such circumstances, bone resorption

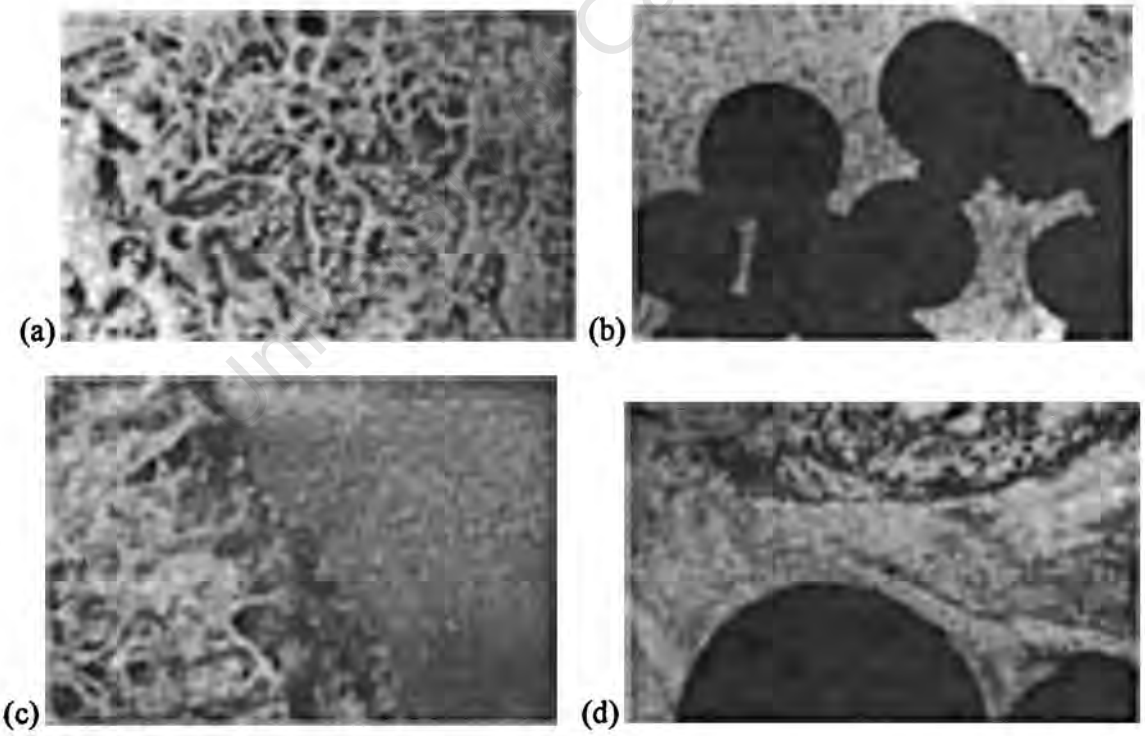

Figure 3.7 Implant-bone interface following arthroplasty (Collier, 1988) (a) Bone ingrowth into cobalt alloy implant. (b) Detail of bone ingrowth into porous beads. (c) Fibrous tissue formation around smooth implant surface. (d) Detail of fibrous tissue interposed between bone tissue and beads.

and subsequent fibrous tissue formation may proceed until a layer of up to a few millimetres is formed (Boehler *et al.*, 1994). Figure 3.7(c) shows the formation of fibrous tissue against the smooth steel surface of an implant (the implant material is on the left of the figure). Although no preferred orientation can be seen here, the fibrous tissue is normally orientated parallel to the foreign surface. The tissue layer may or may not penetrate the beaded structure. A detail of the bone tissue separated from the beads by a layer of fibrous tissue can be seen in Figure 3.7(d). In gross cases of implant loosening, there may also be damage and inflammation of the underlying bone.

3.4.3 Bone Ingrowth: The Biological Response

The process of bone ingrowth into the porous surface of an implant is a variation of normal fracture healing (Spector, 1988; Søballe *et al.*, 1992). During the surgical procedure, the bone cavity is prepared by broaching and reaming the medullary cavity to accommodate the implant, and this results in cuts and fractures of the bone trabeculae. The resulting interface region will vary in thickness depending on the surgical procedure, as well as the quality and type of the surrounding bone. During the healing process, the interface layer and voids of the porous coating will be infiltrated with mesenchymal osteoprogenitor cells, as a result of the flow of blood and marrow. Other cells will also migrate to the area, stimulating a healing response. If there is sufficient blood supply, the osseous precursor cells will undergo mitosis and differentiation to form osteoblasts and/or fibroblasts (Spector, 1988; Friedlander, 1988). The resultant callus tissue may mature to form osseous bone, and hence osseo-integration. The formation process will result in new woven bone forming within one week. After two weeks, new trabeculae will bridge the gap between the new woven bone and the existing tissue. This healing response dominates the implant-bone interface for 4 to 6 weeks post-operatively (Hollister *et al.*, 1994). Subsequently, the evolution of the interface and the resultant

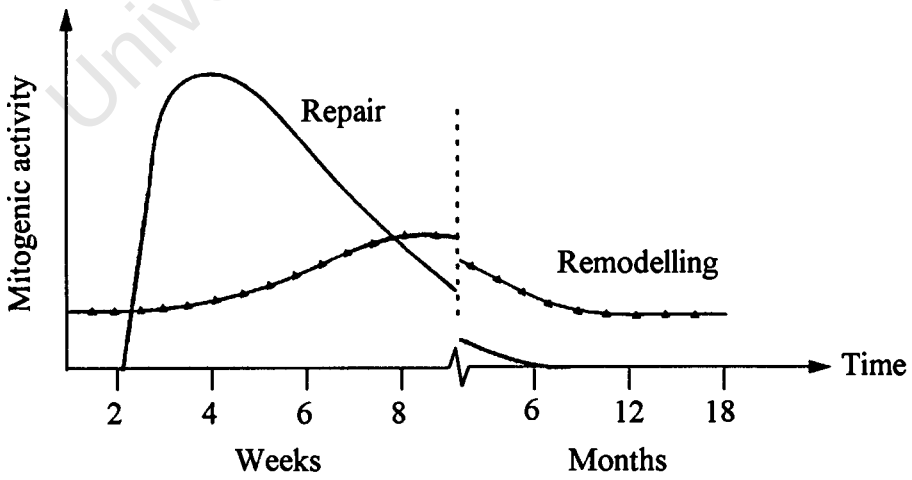

Figure 3.8 Interface repair and remodelling activity levels following surgery (adapted from Spector, 1988).

biological fixation will be controlled by remodelling as a result of stimulus due to loading. A schematic representation of the time scales for repair and remodelling are shown in Figure 3.8.

The dominance of repair activity in the early post-operative period was demonstrated by Hollister *et al.* (1994), who used a canine model with implanted surgical platens to investigate the influence of post-operative repair. Two groups of animals were examined. In the first group, the implants were subjected a load of 35N/platen for 1800cycles/day, and in the second group the platens were unloaded. After a five week period, they found no significant difference in the extent of new tissue formation between the two groups. From this they concluded that "accelerated bone turnover in response to surgical trauma may supersede mechanical stimulus effects in early bone response to a porous coated implant".

However, there is some controversy as to the influence of the repair activity. Rubin and Lanyon (1984) argued that the formation of woven bone in their turkey model was not a function of repair, as groups that underwent identical surgery showed no bone apposition when loaded with only 4 cycles per day. However, these findings are certainly not conclusive as loading devices were placed at the ends of the bones, while the mid-shaft was examined for remodelling. Part of the reaction may have been due to a regional acceleration of bone turnover in response to surgery. The activity due to wound healing implies that an unloaded implant will only have ingrowth as a result of repair activity, which is in contrast to the findings of Hulbert *et al.* (1970) - cited in Ducheyne *et al.* (1977) - who observed that no growth took place into an unloaded implanted plug.

3.4.4 Mechanical Factors Affecting Interface Development

It is clear that the short and long term response of the interface will be influenced by local mechanics, and it now remains to examine how the mechanical factors will influence the development of the initial interface tissue.

Relative motion

Relative displacement at the implant-bone interface is regarded as the key factor in determining the post-operative development of the interface tissue (Ducheyne *et al.*, 1977, 1978). In the short term, displacements can result in damage of the tissue produced by the repair activity and, subsequently, fibrous tissue will form. While in the long term, if there is fracturing at the interface and subsequent relative displacement, the mineralised bone adjacent to the surface will be resorbed and replaced with fibrous tissue. Cameron *et al.* (1973) found that the magnitude of the displacements of the implant relative to the surrounding bone directly influenced the formation of the bond, and concluded that "...ingrowth can take place in the presence of micro-movement but not macro-movement." This finding was confirmed by Ducheyne *et al.* (1977) and Pilliar *et al.* (1981), who found that relative displacements resulted in a fibrous tissue attachment, which had a considerably lower attachment strength when compared to osseous tissue. They concluded that if the current designs of cemented implants were to be used for cementless attachment, fundamental design changes would be required.

Subsequently, Bobyn *et al.* (1982) have confirmed that ingrowth will not take place in the presence of displacements greater than approximately 150μm as this magnitude of displacement resulted in the implant being encapsulated in scar tissue. Pilliar *et al.* (1986) investigated the influence of movement on the attachment strength of dental implants, and found that calcified tissue only formed in the presence of movement less than approximately 28μm. Most of the experimental studies which have examined the influence of movement on the interface tissue response have not controlled the magnitudes of the relative displacements. Søballe *et al.* (1992) developed an implant device which exactly controlled the relative displacement magnitude between the implant and the surrounding bone. The implants were set into the weight bearing condyles of dogs, with the movement set to 500μm. With this magnitude of relative displacement, they found a well developed layer of fibrous tissue, with islands of fibrocartilage at the interface, while in the stable implants, bone ingrowth was observed. Interface development can be compared to the process of fracture healing. Stable fractures will heal with direct bone attachment, while unstable fractures will tend to form fibrocartilage, which may later be replaced by bone as a result of endochondral ossification (Aro *et al.*, 1993). Whether or not later ossification of the fibrocartilage observed in this study will take place was not investigated.

The relation between applied loading and the interference-fit created during surgery will have a great influence on the development of the interface tissue (Ling, 1986). If the fit of the implant is good, and the early post-operative applied loading is low, osseo-integration will take place (Jasty and Harris, 1988), as shown in the upper left region of Figure 3.9. At the other extreme, if a poor fit is created at surgery, and subsequent loading is high, gross displacements of the implant will occur. This response, which may lead to *cutting out*, is shown in the lower right region of the figure. Between these two extremes, the formation of fibrous tissue will be evident. Where a reasonable interlock is

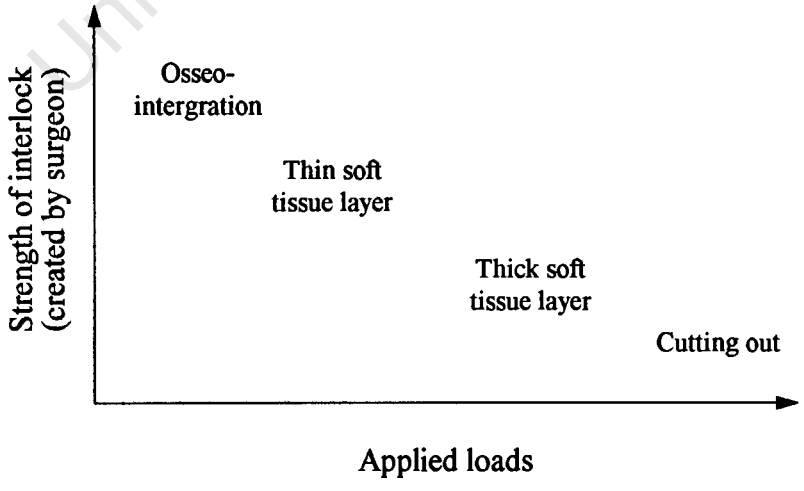

Figure 3.9 The influence of implant press fit on the evolution of interface tissues (adapted from Ling, 1986).

created during surgery, and loading is not too high, a thin fibrous layer will develop. While, with decreased interlock, and increased applied loading, a thicker fibrous layer will form.

During the initial period, the nature of the wound healing will depend on the mitogenic potential of the constituent cells, as well as the local mechanical conditions (Spector, 1988). Under mechanically stable conditions, differentiation will result in the formation of osteoblasts, which will generate new woven bone trabeculae inside the porous surfaces. However, if during this period there is relative displacement between the two interacting surfaces, the cellular differentiation will result in the formation of fibroblasts which will lay down fibrous tissue (Ling, 1986; Muschler *et al.*, 1988). Although the exact histological development of how the movement will influence the cellular response is not well characterised, Spector (1988) argues that the movement will "...destroy the stroma within which the osseous tissue is regenerating ...".

The experimental findings of many researchers seem to clearly indicate that excessive cyclic relative displacement will stimulate the formation of fibrous tissue. However, the exact characterisation of the stress and strain state in these reports is not clear. The term "relative displacement" may refer to elastic (recoverable) movement of the interface tissues or too inelastic slip of the two surfaces. It is quite likely that if the displacements are sufficiently large to be observed experimentally, they are inelastic. Furthermore, it is not relative movement *per se* which will prevent ossification and cause resorption, but the high shear strains and/or damage to the surroundings tissues, which are a combination of inelastic relative displacement and normal interface pressure.

Stress and Strain

It is generally thought that bone growth and the differentiation of mesenchymal cells following fracture, will be strongly influenced by the stress or strain state (Perren, 1979; Pauwels, 1980; Carter *et al.*, 1987; Carter, 1988). The initial thoughts regarding the influence of different stress or strain states on the development of tissues were put forward by Roux (cited in Carter *et al.*, 1988). Roux believed that compressive stresses resulted in the formation of bone tissue, while tensile stresses caused fibrous tissue formation. If shearing was combined with tension or compression, cartilage formation would result. While the influence of the stress magnitude and state on the development response have become a subject of much debate, Roberts *et al.* (1981) demonstrated, by subjecting rats to a weightless environment, that the transition of osteoproginator cells to pre-osteoblasts requires normal levels of tissue stress. Pauwels (1980) separated the stress components into hydrostatic and octahedral stress states, in order to examine the influence of mechanical parameters on early bone development and fracture repair. He believed that shear and tensile stresses specifically stimulated the formation of fibrous tissue, while hydrostatic pressure stimulated the formation of cartilage. He believed that there was no specific stimulus for mineralised bone tissue formation.

Perren (1979) suggested that bone will only be successfully formed in the interfragmentory region, if the tissue tolerates the local strain. Therefore, once differentiation has taken place, the new tissue will contribute to the stability of the site,

which in turn will make possible the next stage of differentiation. Following the ideas of Perren (1979), DiGioia *et al.* (1986) proposed that tissue differentiation would be controlled by the ratio of the local strain level to the maximum allowable strain for a particular tissue type. Limiting strains for undifferentiated granulation tissue would be in the region of 100%, while for cartilage and mineralised bone these values would decrease to approximately 10 and 2%, respectively. Local deformation can interrupt the blood supply, and hence disrupt the process of revascularisation. However, as in the case of remodelling, strains may directly elicit a cellular response, which may enhance and accelerate the repair process. Goodship (1995) found that applied dynamisation of 500 cycles at 0.5Hz on an ovine tibial osteotomy increased the rate of healing in terms of mineralisation and fracture stiffness index. Despite the encouraging findings that a mechanical signal may influence the cellular processes during repair, the controlling factors of the cellular events have not been established. Furthermore, whether the mechanical signals which were found to stimulate osteotomy repair are appropriate to bone ingrowth in cementless athroplasties is unclear.

Although mechanical factors may guide the healing process, tissue differentiation is sensitive to oxygen tension and the degree of vascularisation. Following from the ideas of previous researchers, for a well vascularised system Carter (1988) suggested regions in stress space in which the formation of various tissue types would proceed. Carter (1988) proposed that hydrostatic and octahedral shear stress will be responsible for bone, cartilage and fibrous tissue formation. He hypothesised that for a well vascularised system, high tensile and shear stresses would result in fibrous tissue formation, while low tensile and low compressive stresses would result in bone tissue formation (Figure 3.10(a)). Increased hydrostatic pressure inhibited the formation of bone tissue, and resulted in cartilage production (Carter *et al.*, 1988). Subsequent endochondral ossification will be promoted by shear stresses, while this process will be inhibited by

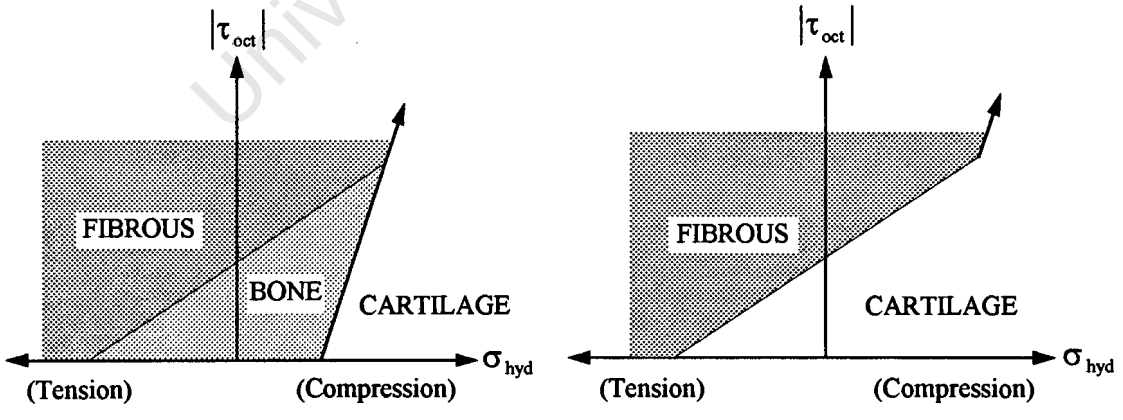

Figure 3.10 Influence of the stress state on the differentiation of immature tissue for good vascularity and poor vascularity (adapted from Carter, 1988).

hydrostatic stresses. However, if the system is poorly vascularised (Figure 3.10(b)), bone formation will be inhibited and, under the conditions normally suited to bone formation, cartilage formation would dominate. The overall response of the tissues will depend on the history of loading. Carter *et al.* (1988) believed that only a few cycles of high tensile or shear strains would be sufficient to alter the course of tissue differentiation from osteogenesis to fibrosis.

Carter *et al.* (1988) proposed a numerical model for endochondral ossification in which they introduced the concept of an ossification index, which was assumed to be a function of hydrostatic and octahedral shear stress. The form of the index followed from the ideas that octahedral shear stress would encourage, whereas compressive hydrostatic stress would inhibit, endochondral ossification. They proposed a linear model in which the ossification index was only affected by stress magnitude (in which case tensile hydrostatic stresses reduced the index value), and a bilinear model in which tensile stresses were excluded.

Ling (1986) examined the influence of stress and strain on cellular differentiation of interface tissues. He proposed that where tissue stress and strain are low, osteogenesis and subsequent osseo-integration would take place, as shown in Figure 3.11. Increased strain and stress will result in damage to the junctional tissues, causing bone resorption (osteoclasis) and, with further increase in loading, fibrous tissue will form (fibrosis). The extent of the area between osteogenesis and osteoclasis suggests a large tolerance of load before interface damage begins to take place. However, the exact point at which tissue will stop forming and be withdrawn, to be replaced with fibrous tissue, is not well defined.

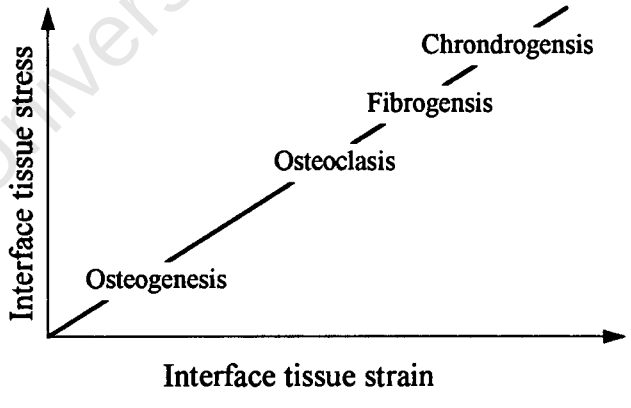

Figure 3.11 The influence of strain on the subsequent development of interfacial tissue (adapted from Ling, 1986).

The hypotheses of the various researchers as to the influence of stress and strain on tissue differentiation, provide only a qualitative basis for modelling tissue development. While it seems reasonable that normal stress will encourage bone and cartilage formation, and shear will be responsible for the creation of fibrous tissue, the magnitudes of the stresses have not been quantified.

3.4.5 Bone Remodelling

It is widely accepted that mechanical loading will affect bone physiology. Therefore, the initial interface repair response is soon followed by remodelling activity. Osteocytes, which some researchers (Cowin, 1995) believe to be the cells responsible for the control of the remodelling response, have been observed very close to the interface of osseo-integrated regions, some time after implantation (Linder, 1991). The remodelling process will be influenced by the amount of bone ingrowth, the design of the implant, and the nature of the loading (Spector, 1988). In combination with these influences, host factors, adjuvant therapies and metabolic factors will determine the remodelling response (Figure 3.12).

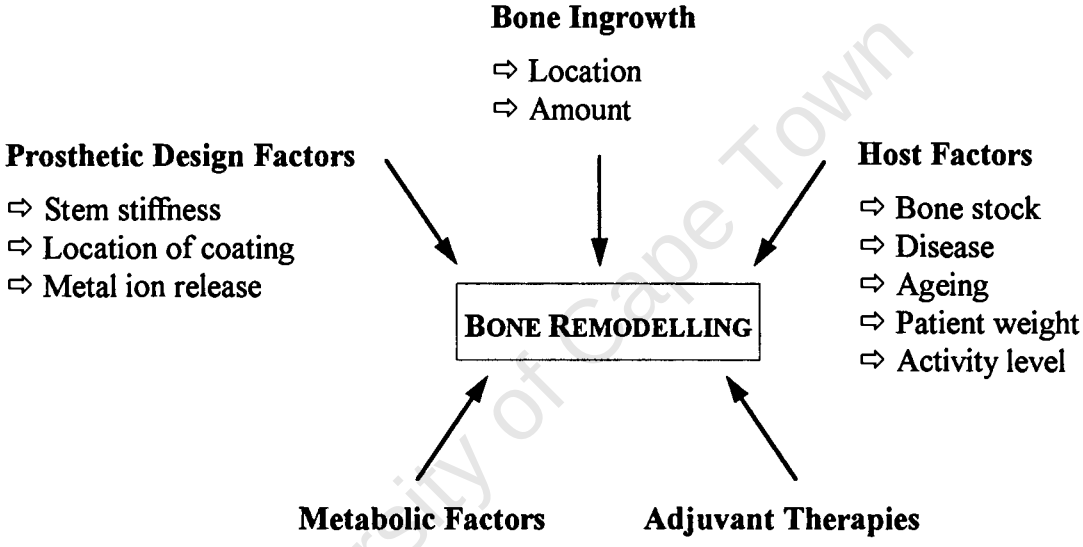

Figure 3.12 Factors affecting the bone remodelling response (adapted from Spector, 1988).

The remodelling processes will influence the bone within the surface porosity, the bone at the implant-bone interface, as well as the surrounding cortical and cancellous bone. The location and the amount of bone ingrowth will determine the strain distribution, both within the porosity (Pedersen *et al.*, 1991) and in the surrounding material (Fyhrie *et al.*, 1988). As the amount of bone ingrowth increases, so too does the stiffness of the implant bone composite. Subsequently, a greater amount of load is transmitted to the cortex in areas of bone ingrowth, which will influence the remodelling response. The extent of this response will, however, depend on the stiffness of the implant and the location of the porous coating.

Brunski *et al.* (1985) inserted screw-like implants into the mandibular of mature dogs to examine interface remodelling. Two groups were analysed: one in which the implants were loaded with cyclic loads of 50 and 110N, and one in which no additional loading was applied. Before loading, the implants were allowed to "heal" for 4 to 7 months. Three weeks after the start of loading, histological examination showed that there was no

appreciable difference in the amount of bone apposition between the two groups. These results suggest that either the additional applied load was not sufficient to induce a remodelling response in the interfacial tissues, or the three week time period was insufficient to cause a histologically observable response.

As most long term follow-ups of cementless arthroplasties have been concerned with the remodelling of the cancellous and cortical bone surrounding the implant, few studies have examined the remodelling response of the interface tissue. Naturally, the remodelling of the surrounding bone and interface material will be coupled, in that adaptation changes which take place in one region will result in an alteration of the stress state in another region, which in turn will affect the remodelling response. Where bone tissue has been removed due to stress shielding, this would normally be associated with a removal of the adjacent interface tissue. Therefore to fully understand and characterise the remodelling in the surrounding bone, it is essential to gain an understanding of the interface remodelling response.

3.5 Numerical Modelling of Interface and Implant Mechanics

Numerical modelling of the interaction of an implant and the surrounding bone can be undertaken by making use of well accepted contact formulations. The classical Coulomb friction law is the most widely used constitutive model for simulating the friction interaction of two deformable bodies and has been extensively used to model implant-cement and implant-bone interaction. However, the difficulty in modelling cementless arthroplasties lies in deciding what assumption to make regarding the implant-bone contact. As a result of the unpredictability of bone ingrowth and subsequent bonding it is not clear whether the porous coated region should be assumed to be bonded or unbonded (Beaupré *et al.*, 1985; Fyhrie *et al.*, 1985; Orr *et al.*, 1985; Rohlmann *et al.*, 1988; Van Rietbergen *et al.*, 1993).

3.5.1 Constitutive Models of Contact Problems

The Mohr-Coulomb model can be formulated using the theory of elasto-plasticity (Beer, 1985; Snyman *et al.*, 1991). For a planar interface, the elastic behaviour is represented by the normal and shear stiffness terms K_n and K_s, respectively, which relate the elastic normal and shear relative displacements δ_n and δ_s, to the respective conjugate forces by

$$\begin{bmatrix} N \\ S \end{bmatrix} = \begin{bmatrix} K_n & 0 \\ 0 & K_s \end{bmatrix} \begin{bmatrix} \delta_n \\ \delta_s \end{bmatrix} \tag{3.1}$$

The peak strength and dilation is represented by a yield criterion and a flow rule respectively, and the plasticity behaviour is governed by a hardening or a softening rule. In implant-bone interface problems, the dilation is normally assumed to be zero. The yield criterion proposed by Coulomb relates the shearing resistance S to a friction angle ϕ and a cohesion term c. The shearing limit is reached when the yield function

$$f = |S| - N \tan\phi - c \tag{3.2}$$

is equal to zero. The friction angle and cohesion are assumed to be functions of the material comprising the interface and remain constant. In the case of cementless joint arthroplasty the cohesion term will be a function of the extent of tissue penetration into the porous surface of the implant. By assuming an associated flow rule the rates of inelastic normal and shear deformation $\dot{\delta}_n^p$ and $\dot{\delta}_s^p$ are obtained

$$\dot{\delta}_n^p = \dot{\delta}_s^p \tan\phi \tag{3.3}$$

As the friction angle is constant, the shear deformation is accompanied by dilation and a change in relative displacement in the normal direction

3.5.2 Numerical Implementation

To implement the interface constitutive behaviour in models employing the finite element method, isoparametric finite element formulations are typically used. The element formulation must fulfil the function of compatibility between the two interacting surfaces. Therefore, a scheme for checking whether the two bodies are in a state of contact or separation, needs to be used. Furthermore, if the two bodies are in contact, sticking and frictional sliding must be catered for.

The most commonly used approach to solving contact problems is the "penalty method". Using this approach, the interface between the two interacting bodies is essentially treated like a continuum finite element, with a zero thickness in the normal contact direction. The element formulation produces a stiffness matrix and a load vector, which are assembled into the global finite element equations by the normal method. The penalty method enforces the contact constraints approximately, by introducing a penalty stiffness term in the normal direction. Since the contact conditions do not hold exactly, material overlapping can occur. A larger penalty term will reduce the amount of overlapping resulting in a more accurate solution. However, this method can introduce ill conditioning of the stiffness matrix, as the large penalty terms will tend to overshadow the surrounding terms. The value of the penalty term needs to be chosen carefully.

In general, the relation between shear force and displacement is determined from experimental data. From this data the shear stiffness, friction angle and cohesion term can be determined. However, for a zero-thickness element, the choice of K_n is more difficult. Assuming that the two interacting materials do not overlap at the interface, this value must be chosen to be as high as possible without introducing numerical problems. To overcome the problems associated with the penalty formulation, Desai *et al.* (1984) formulated a continuum element with a small thickness. The element is referred to as a thin-layer element, as it essentially models a thin layer of material between the two bodies. The element has a uniform thickness, and the strain in the thickness direction is assumed to be constant. As the layer has a finite thickness, the through thickness stiffness term is not required purely to enforce the contact constraint, but can be chosen instead from experimental data. This term may be constant, or may vary as a function of normal strain.

The opening, closing and sliding of the joint can be modelled by using elasto - plasticity. Opening can be modelled by means of a failure criterion, and when the interface is open, the behaviour is considered inelastic and, therefore, the stiffness term is set to zero. Sticking and frictional sliding are modelled in a similar way, where the frictional response is assumed to be elasto-plastic. Sticking of the joint is governed by linear elastic behaviour. One difficulty in implementing an interface element, lies in deciding which contact conditions to apply. Snyman *et al.* (1991) suggested an approach to overcome this by setting up regions in relative displacement space. Each region accounts for different contact conditions; opening, closed but sticking and sliding.

3.6 Numerical Modelling of Interface Tissue Evolution

The development of interface tissues can be simulated by formulating evolution laws based on the local mechanics and other factors. These formulations will need to be compatible with the contact equations for the interface interaction. Constitutive equations have been developed for the formation of fibrous tissue, following an interface disruption, as well as for the prediction of bone ingrowth into a slot or cavity of an implant.

3.6.1 Bone Resorption and Fibrous Tissue Formation

Finite element modelling of the presence of a soft interfacial layer between an implant and bone has not been extensively examined, despite the dramatic influence the presence of such a layer will have on the stress transfer. In an experimental model of cemented implants, Markolf *et al.* (1980) found that implant subsidence was increased by up the twenty times with the presence of a silastic liner between the cement and bone. This result was confirmed by Weinans *et al.* (1990), who used a two dimensional finite element model to examine the influence of a fibrous tissue layer at the cement-bone interface. The presence of a compliant layer resulted in a considerable increase in bone stresses, particularly on the medial side. Subsequently, this finding was confirmed in a study of a proximal femur that had been reconstructed with a cemented femoral stem, using a fully three dimensional finite element model.

The studies previously discussed have examined the overall influence of fibrous tissue on a reconstructed joint. In order to study the local interface mechanics, Ko *et al.* (1992) developed finite element models of threaded and unthreaded dental implants. By using a homogenisation procedure, they were able to examine the influence of a 10μm fibrous tissue layer on the stresses at the implant-bone interface. The homogenisation method offers the advantage of being able to model the whole implant-bone composite, without losing the details of the interfacial architecture. This is achieved by separately creating a unit cell model of a single screw thread and the adjacent bone, in addition to the global model. The cell is used to calculate equivalent unit cell material constants and matrices which relate the local strain to the global strain. In addition to the homogenisation models, standard models of a threaded implant, both with and without a fibrous tissue interface layer, were developed.

The results from the standard models showed that the fibrous tissue layer, which had a thickness of 100μm, resulted in a ten fold increase in bone stresses in the middle third of the screw length. This stress increase occurred due to a complete alteration in the load transfer mechanisms. The homogenisation results showed that the effective elastic constants of the implant-tissue composite are sensitive to the microstructure of the screw threads and interface layer. Ko *et al.* concluded that the homogenisation method provides an advantage of being able to accurately consider the local geometry, without having to construct complex finite models.

Huiskes (1988) proposed a hypothetical model for the evolution of the implant-bone interface, which is set out in Figure 3.13. This model was later implemented into a finite element formulation and tested on various simple models. The original conceptual model considered the influences of bone remodelling on the interface, while the later model, which was implemented, did not incorporate adaptive bone remodelling (Weinans *et al.*, 1993). There are essentially two possibilities of interface development. If the relative displacements are small, bone ingrowth will progress, resulting in the development of a bond between the implant and bone. However, if there is an interface disruption (fracture), and large subsequent relative displacements, the tissue surrounding the implant will be resorbed and replaced with fibrous tissue. The amount of ingrowth and type of tissue formed will determine the interface geometry and material properties.

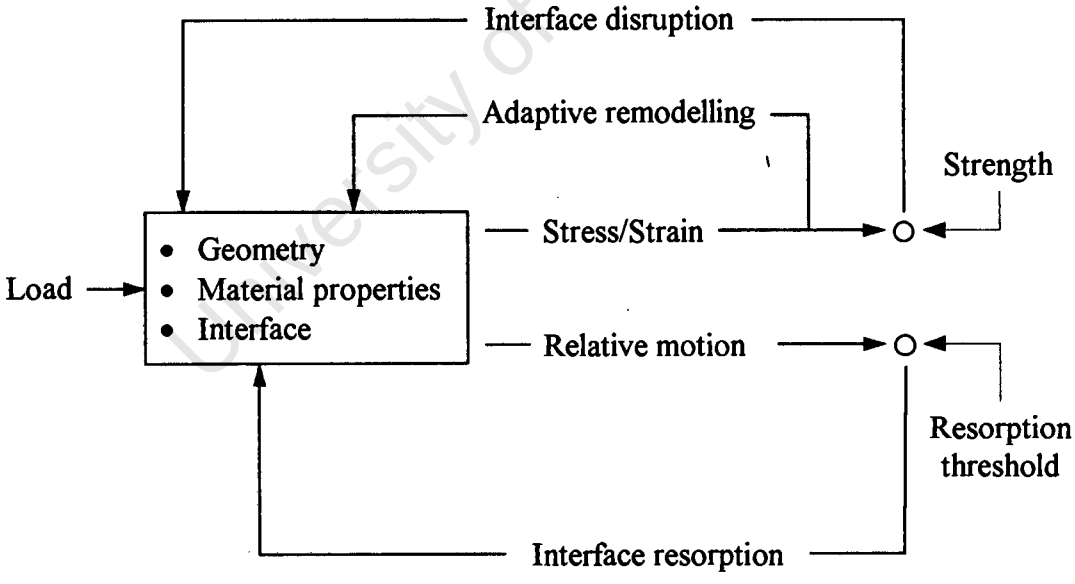

Figure 3.13 Hypothetical scheme of the processes involved in bone remodelling within the interface tissues (adapted from Huiskes, 1988).

Weinans *et al.* (1993) modelled the gradual loosening of cementless implants associated with fibrous tissue formation, based on the initial work by Huiskes (1988). They used a thin element to model the contact between the implant and the surrounding bone. When

modelling the interaction of an implant and bone, the thin element formulation would appear to be most suitable, as in reality a thin layer of material can be found at this interface. In their approach they assumed that complete calcified tissue ingrowth had been achieved in all areas, and therefore a rigid attachment had occurred. The joint reconstruction model was then loaded by a periodic loading, and interface rupturing was monitored. They then hypothesised that (in the event of an interface fracture) the rate of resorption of mineralised tissue and subsequent replacement with fibrous tissue, would be proportional to the magnitude of the slip experienced during the cyclic loading. In reality, fibrous tissue offers some interface bonding, and indeed a prosthesis may be considered stable on a long term basis with fibrous tissue bonding. However, because of the weakness of this bond, they assumed that once fracture had taken place, and fibrous tissue had formed, any subsequent bond would have no strength in shear or in tension. The compressive behaviour of the layer was considered to be highly compliant, exhibiting a very non-linear stiffening behaviour, as described by Hori and Lewis (1982). The yield surface used to describe the bonded interface was based on the function proposed by Stone *et al.* (1983), for the yielding of cancellous bone. The usefulness of this criterion for the interface needs to be examined in the light of the fact that compressive yielding of the trabeculae structure is governed by the buckling of the members, while the interface constitutes solid tissue, whose yield in compression is not well defined.

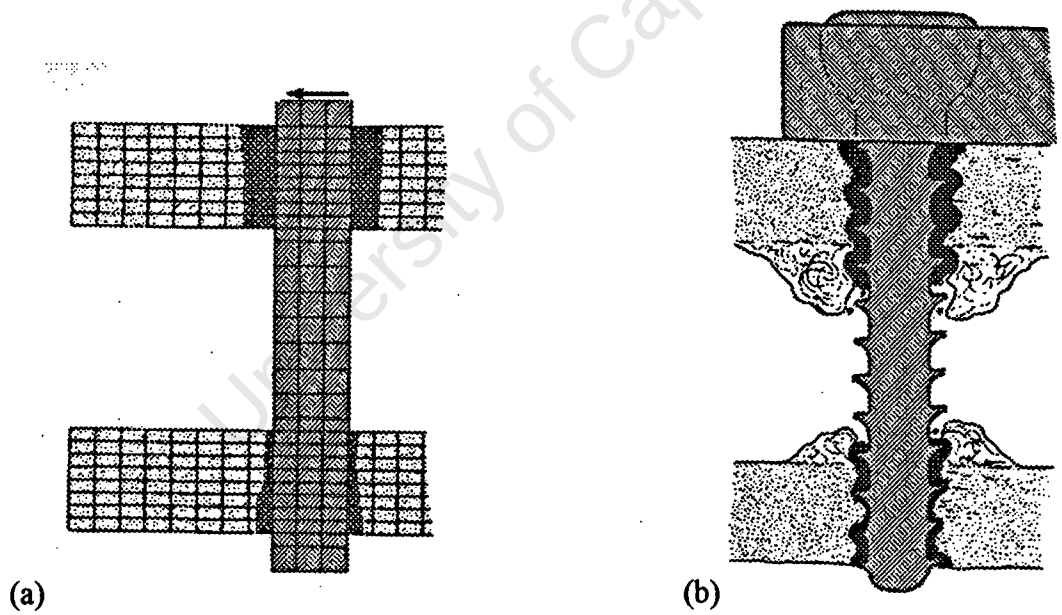

Figure 3.14 Numerical simulation of bone resorption around a cortical bone screw. (a) The dark regions indicate predicted fibrous tissue formation. (b) Schematic diagram of observed resorption patterns (Weinans *et al.*, 1993).

The model was used to predict bone resorption and fibrous tissue formation in the femoral head, following a surface replacement, as well as the formation of fibrous tissue which is often observed around cortical bone screws. Figure 3.14(a) shows the finite

element mesh, with the dark areas indicating the predicted extent of fibrous tissue. The schematic diagram (Figure 3.14(b)) of the clinically observed fibrous tissue formation was based on the work of Perren *et al.* (1979). The reasonable correlation with the clinically observed patterns, for both the femoral head surface replacement and the cortical bone screw suggests that their initial qualitative analysis has provided the first step towards the prediction of fibrous tissue formation around threaded and porous coated implants.

3.6.2 Bone Ingrowth

Although there have been many numerical investigations concerning the influence of bone remodelling on cortical and cancellous bone, few have concentrated on the interface tissues. Sadegh *et al.* (1993) implemented an evolution law for bone growth, using the boundary element method, to predict the advancement of the bone surface into the threads of an implanted screw, and the penetration of bone into a slot. They made use of surface remodelling theory, in which they assumed that the velocity of the bone surface was proportional to the difference between an optimal and the actual value of surface strain

$$\dot{X} = C(\gamma - \gamma_0) \tag{3.4}$$

where γ and γ_o are the optimal and actual values of tangential surface strain respectively, and C is the rate constant. The total amount of bone ingrowth as a result of biaxial loading can be seen in Figure 3.15. The approach followed in this model predicts ingrowth as a result of the load induced remodelling response, without considering the inherent repair activity or the possible resorption due to relative displacement between the bone and the implant surface.

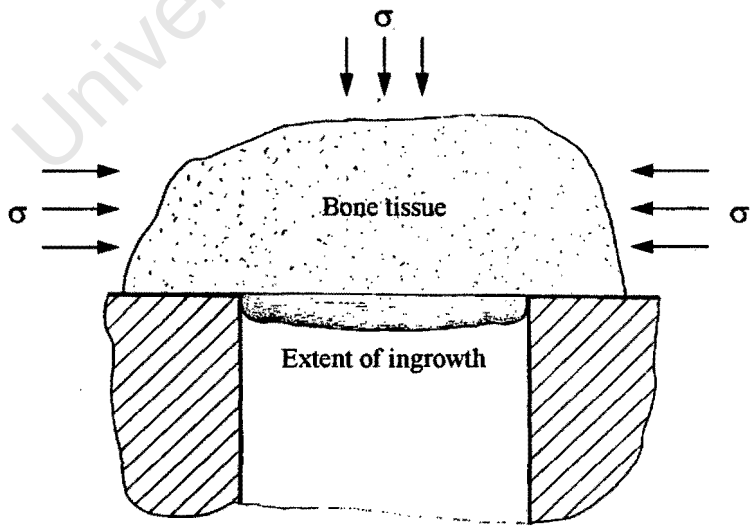

Figure 3.15 Bone ingrowth into an implant slot using the boundary element method (adapted from Sadegh *et al.*, 1993).

Hollister *et al.* (1993) hypothesised that bone ingrowth produced a structure which is globally optimised so as to minimise strain energy density. To test this hypothesis, they used a topology optimisation program, which predicted the material layout (ingrowth) around a porous coated tibial component with support cones. Bone apposition occurred consistently at the cone tips, providing good agreement with experimental observations. However, they predicted that the depth of ingrowth would not exceed the first row of beads, which indicates that tissue ingrowth deeper than this level does not significantly contribute to the stiffness of the interface. This discrepancy with the experimental observations may be due to the exclusion of repair activity, which produces bone ingrowth that does not result purely from mechanical demands. This approach differs to that of Sadegh *et al.* (1993), where a local interface model was developed which examined the rate of bone ingrowth, rather than addressing global optimality.

3.7 Summary

The importance of gaining further understanding of the mechanics and evolution of the implant-bone interface has been highlighted by several researchers (Howie, 1988; Brunski, 1988; Lewis, 1988; Linder, 1991) at symposia on cementless arthroplasties. The important issues which were raised included: the timing and degree of load application during the stabilisation period following surgery. The understanding of the biomechanical factors acting at the bone-implant interface, in order to understand both successful and failing bone-implant interfaces. The need to explore the biological side of the interface as "... the successful component design is one that considers not only the structural demands to which it will be subjected, but also the sensitivity of the bone tissue to its local mechanical milieu." (Rubin, 1988).

It appears from the literature that no numerical model currently exists for the prediction of bone ingrowth and fibrous tissue formation, taking as the starting point the unbonded post-operative condition and considering the adaptive bone remodelling and loosening processes that exist from the early post-operatively stages. The remainder of this thesis is concerned with the development of a model which will consider the possible development of the interface for some arbitrary loading history following joint replacement. It is the intention of this work to examine remodelling at the implant-bone interface with respect to bone ingrowth and fibrous tissue formation. An isoparametric interface element is developed for this purpose.

CHAPTER FOUR

CONSTITUTIVE MODELS FOR IMPLANT-BONE INTERACTION

4.1 Introduction

In this chapter, a material model for the interface layer between the prosthetic implant and the bone is formulated. The interface is modelled as a thin, but finite thickness, layer. The derivation is carried out within the framework of classical plasticity. Initially, a simple Coulomb friction model with no dilation and a non-associated flow-rule is presented. The model is then extended to include a layer of fibrous tissue at the interface. Finally, the Coulomb model is modified to include the cohesion and adhesion that develop as a result of bonding due to bone ingrowth.

4.2 Interface Modelling

Consider two bodies separated by a layer of interface material of thickness h, as shown in Figure 4.1. The interface normal and shear directions are denoted by the vectors **n** and **s**, respectively, and the corresponding strain components are denoted by ε and γ. The directions of the interface strains are such that compressive strains are assumed to be

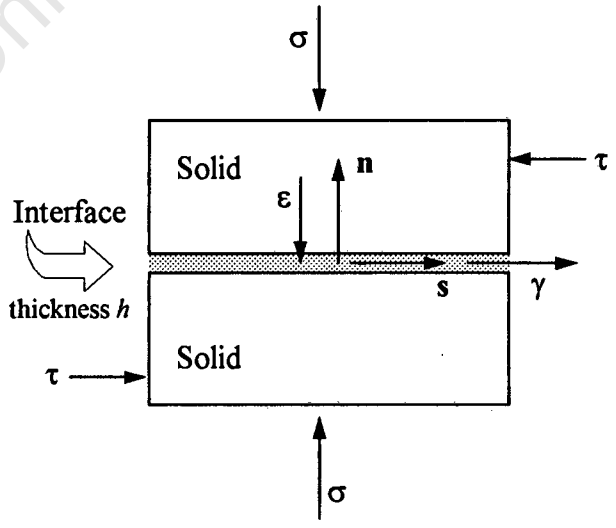

Figure 4.1 Plane implant-bone interface.

positive. Apart from the interface layer, compressive strains are always taken to be negative. The normal and shear stress components are denoted by the vectors σ and τ, respectively.

Relative displacement between the two bodies may occur as a result of slip and/or some reversible linear elasticity within the interface material. Therefore, the total strain rate vector is decomposed into the elastic and inelastic parts, denoted by superscripts *e* and *p* respectively

$$\dot{\boldsymbol{\varepsilon}} = \dot{\boldsymbol{\varepsilon}}^e + \dot{\boldsymbol{\varepsilon}}^p \tag{4.1}$$

The interface layer is assumed to be thin compared to the length scale. Subsequently, the strain is assumed to be uniform through the thickness and, therefore, the strain rate vector has components $\dot{\boldsymbol{\varepsilon}} = (\dot{\varepsilon}, \dot{\gamma})^T$. The stress rate vector $\dot{\boldsymbol{\sigma}} = (\dot{\sigma}, \dot{\tau})^T$ is related to the elastic strain rate vector by means of the symmetric elasticity matrix **D**

$$\dot{\boldsymbol{\sigma}} = \mathbf{D}\,\dot{\boldsymbol{\varepsilon}}^e \tag{4.2}$$

where, for a simple uncoupled relation, the components of **D** are given by

$$\mathbf{D} = \begin{pmatrix} E & 0 \\ 0 & G \end{pmatrix} \tag{4.3}$$

with E and G the Young's and shear moduli, respectively. If mineralised bone has formed then $\mathbf{D} = \mathbf{D}(Q)$, where Q is the extent of growth into the porous beads, while if a fibrous tissue layer has developed then $\mathbf{D} = \mathbf{D}(\boldsymbol{\varepsilon}^e)$.

The inelastic strain rates are written in terms of the flow function Ψ as

$$\dot{\boldsymbol{\varepsilon}}^p = \dot{\lambda}\frac{\partial \Psi}{\partial \boldsymbol{\sigma}} \tag{4.4}$$

in which $\dot{\lambda}$ is a scalar multiplier which denotes the magnitude of the inelastic strain rate.

The onset of inelastic sliding is defined by a convex yield function $f(\boldsymbol{\sigma}, Q, \phi)$ drawn in stress space, where ϕ is the friction angle. The constraints on the yield function, set out in the Kuhn - Tucker form, are given by

$$\begin{aligned} f &\le 0 \\ \dot{\lambda} &\ge 0 \\ f\dot{\lambda} &= 0 \end{aligned} \tag{4.5}$$

Combining Equations (4.1) to (4.4) leads - after some manipulation - to the general form of the stress - strain relation,

$$\dot{\sigma} = \mathbf{D}^* \dot{\varepsilon} \tag{4.6}$$

where $\mathbf{D}^*$ is the tangent modulus, which is dependent on the current state of the interface.

The interface formulation will be incorporated into a standard finite element program, which uses an incremental formulation, with a two-step Newton Raphson iterative solution procedure, to solve the non-linear incremental equations. The first step - the predictor - uses the tangent stiffness matrix and the out of balance force to predict the estimates in displacement. In the second step - the corrector - the stresses and internal forces are calculated, based on the displacement estimates. The internal forces are then used to calculate the out of balance forces for the next iteration. The essence of this approach is that the incremental inelastic problem is essentially broken into a series of non-linear elastic problems.

Using a backward difference method, the rate problem set out in Equations (4.1) to (4.4) can be recast in terms of an incremental problem by dividing the time domain into a sequence of intervals. The times at the start and the end of an arbitrary interval are given by t_n and t_{n+1}, respectively. Therefore, the problem posed is as follows: at time t_n, given the strain vector $\varepsilon_n = \varepsilon(t_n)$ and the corresponding stress vector $\sigma_n = \sigma(t_n)$ as well as strain increments $\Delta\varepsilon_{n+1}$, a solution is required for the inelastic strain increments. This can be found by solving the non-linear equation

$$\Delta\varepsilon^p_{n+1} = \Delta\lambda_{n+1} \left.\frac{\partial\Psi}{\partial\sigma}\right|_{n+1}, \tag{4.7}$$

at the end of the interval corresponding to time t_{n+1}. At each increment in the solution procedure, the elastic strains can then be calculated from

$$\Delta\varepsilon^e_{n+1} = \Delta\varepsilon_{n+1} - \Delta\varepsilon^p_{n+1} \tag{4.8}$$

and subsequently the updated stresses are given by

$$\sigma_{n+1} = \sigma_n + \mathbf{D}_{n+1}\,\Delta\varepsilon^e_{n+1} \tag{4.9}$$

The solution of these equations is considered for the Coulomb friction model, the friction model with the fibrous tissue interface, and the model of interface bonding and fracture.

4.3 Simple Coulomb Friction Model

It is assumed that the contact and sliding of the interface material is governed by a Coulomb yield surface *f*. The surface, which remains unchanged when drawn in stress

space, is completely defined by the friction angle ϕ, as shown in Figure 4.2. The interface state point is constrained to lie within, or on, the boundaries of the surface, as shown by the shaded area. The yield function is given by

$$f = |\tau| - \sigma \tan\phi \tag{4.10}$$

If the state point lies within the shaded area, $f < 0$, the interface behaviour will be elastic. However, if the state point lies on the boundary of the yield surface, $f = 0$, inelastic shear deformation (slip) may take place. Under this condition, the limiting value of shear stress is reached, and the inelastic strain rate is not necessarily zero.

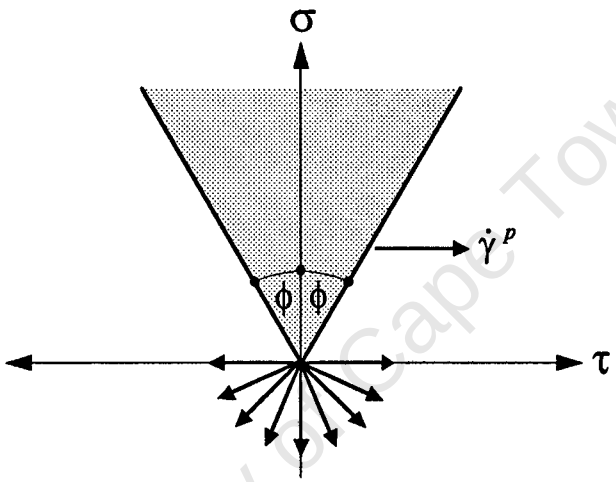

Figure 4.2 Coulomb yield surface and flow direction.

It is assumed that that there is no interface dilation and therefore the flow direction is parallel to the γ-axis as indicated in the figure. The flow function is therefore given by

$$\Psi = \begin{cases} |\tau| & \text{for } \sigma \geq 0 \\ 0 & \text{for } \sigma < 0 \end{cases} \tag{4.11}$$

and subsequently the rates of inelastic strain are

$$\dot{\varepsilon}^p = \dot{\lambda}\frac{\partial \Psi}{\partial \sigma} = 0 \tag{4.12}$$

$$\dot{\gamma}^p = \dot{\lambda}\frac{\partial \Psi}{\partial \tau} = \pm\dot{\lambda} \tag{4.13}$$

At the apex of the yield surface $\sigma = \tau = 0$, the inelastic strain rate vector is not defined, and therefore at this point the direction of the inelastic strain rate is constrained to lie within the fan of normals as indicated in Figure 4.2.

4.3.1 Application of Strain to the Virgin State

Consider the joint in the initial state with no previous strain or load history, so that $\varepsilon_0 = \gamma_0 = 0$ and $\sigma_0 = \tau_0 = 0$. If a set of finite strains $\Delta\varepsilon_1$ and $\Delta\gamma_1$ are imposed on the interface, a solution is sought for the resulting interface stresses σ_1 and τ_1. As the strains are imposed on the virgin state, the resulting interface strain components are $\varepsilon_1 = \Delta\varepsilon_1$ and $\gamma_1 = \Delta\gamma_1$. A backward difference assumption is adopted, which is equivalent to assuming that the change in interface stresses can be divided into two parts. In the first part, the stresses change from (σ_0, τ_0) to (σ_1, τ_1) along an elastic path within the yield surface. Therefore the stress components are given by

$$\begin{pmatrix}\sigma_1\\ \tau_1\end{pmatrix} = \begin{pmatrix}E & 0\\ 0 & G\end{pmatrix}\begin{pmatrix}\varepsilon_1^e\\ \gamma_1^e\end{pmatrix} \tag{4.14}$$

During the second part, the stresses are held constant while the inelastic strains develop in the direction of the inelastic strain rate vector.

The response of the interface (sticking, sliding or opening) can be determined by constructing a state diagram in strain space (Snyman *et al.*, 1991), as shown in Figure 4.3. If E and G are assumed to be equal, then the elastic region, defined as Region 1, can be determined by drawing lines A-X and A-Z from the origin, each at an angle ϕ, on either side of the ε-axis.

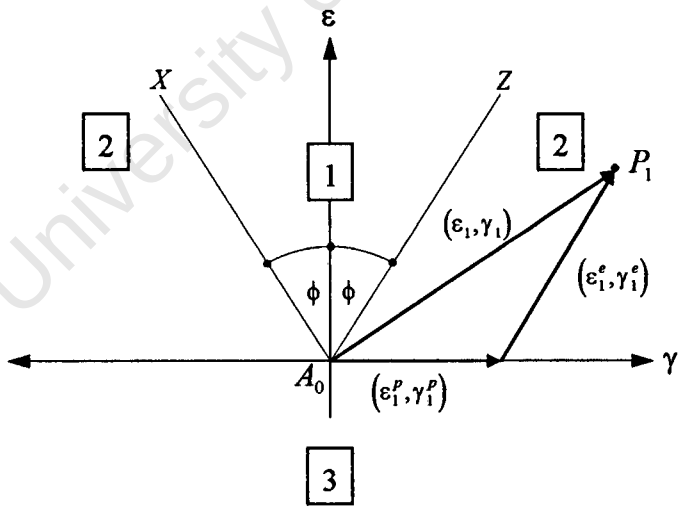

Figure 4.3 Regions in strain space.

Therefore, if $\varepsilon_1 \geq |\gamma_1| \cot\phi$ the state point P_1, resulting from the imposed strain $(\varepsilon_1, \gamma_1)$, lies within Region 1, the response of the interface will be elastic. The strain components are therefore given by

$$\begin{aligned} \varepsilon_1^e &= \varepsilon_1 & \gamma_1^e &= \gamma_1 \\ \varepsilon_1^p &= 0 & \gamma_1^p &= 0 \end{aligned} \tag{4.15}$$

If the interface is in contact and sliding, the state point P_1 will lie in Region 2. This region is given by areas on either side of the lines A-X and A-Z, above the γ-axis. In this region, the strain components are geometrically separated into their elastic and inelastic portions. As there is no dilation, the elastic component of the normal strain is simply the total component of this strain. Therefore, if $0 < \varepsilon_1 < |\gamma_1| \cot\phi$, after straightforward manipulation

$$\begin{aligned} \varepsilon_1^e &= \varepsilon_1 & \gamma_1^e &= \varepsilon_1^e \tan\phi \operatorname{sgn}(\gamma_1) \\ \varepsilon_1^p &= 0 & \gamma_1^p &= \left(|\gamma_1| - \varepsilon_1^e \tan\phi\right) \operatorname{sgn}(\gamma_1) \end{aligned} \tag{4.16}$$

If the point P_1 is within Region 3, which lies below and including the γ-axis, then the interface is open and contact is lost. In this region the elastic components of the normal and shear strain are zero, subsequently the total strain components comprise the inelastic portions. Therefore, if $\varepsilon_1 \leq 0$, the strain components are given by

$$\begin{aligned} \varepsilon_1^e &= 0 & \gamma_1^e &= 0 \\ \varepsilon_1^p &= \varepsilon_1 & \gamma_1^p &= \gamma_1 \end{aligned} \tag{4.17}$$

4.3.2 Updating the State Diagram

The yield surface in stress space remains unchanged at the start of the second increment. However, the state diagram will have changed as a result of the imposed strains. Thus an updating scheme for the state diagram needs to be formulated. As there is no dilation, the updating of the state diagram is simple. If the imposed strains result in the state point $(\varepsilon_1, \gamma_1)$ lying in Region 2 (as shown in the example of Figure 4.3), then the lines joining the apex position A_0 to X and Z will simply translate, without rotating, along the γ-axis, to the position A_1. This position is defined by the point $(\varepsilon_1^A, \gamma_1^A)$, as indicated in Figure 4.4.

If the state point $(\varepsilon_1, \gamma_1)$ lies in Region 1, then the response of the interface is elastic, in which case the lines A-X and A-Z remain unchanged, and the apex position is given by $A_1 = A_0$.

Finally, if the point $(\varepsilon_1, \gamma_1)$ lies in Region 3, then contact has been lost and the interface is open. In this case, there is no elastic strain and, therefore, the apex position A_0 will translate along the γ-axis by the distance of the total shear strain. Therefore $\varepsilon_1^A = 0$ and $\gamma_1^A = \gamma_1 = \gamma_1^p$.

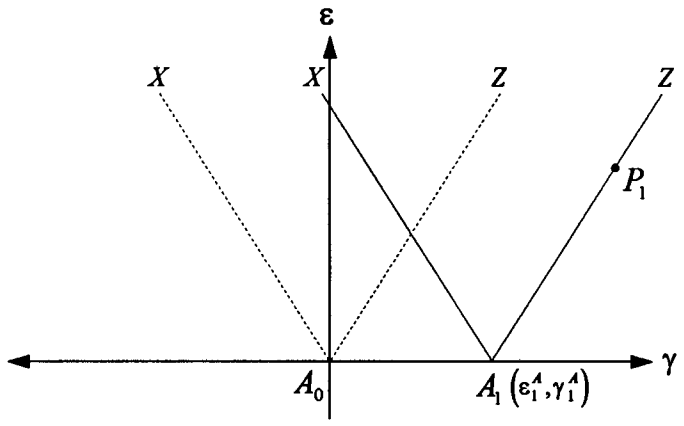

Figure 4.4 Updated state diagram.

4.3.3 Constitutive Equations

With the simple updating rule set out in the previous section, the Equations (4.14) to (4.17) are generalised for an arbitrary increment $(n+1)$. The assumption that the Young's and shear modulus are equal, is now relaxed. Therefore the elastic region is constructed by drawing lines *A-X* and *A-Z* at an angle ψ to the ε-axis, where

$$\tan\psi = \frac{E}{G}\tan\phi . \tag{4.18}$$

At time t_n, the total strain $(\varepsilon_n, \gamma_n)$, defining the state point P_n, the inelastic strain $(\varepsilon_n^p, \gamma_n^p)$, apex position $(\varepsilon_n^A, \gamma_n^A)$, as well as the interface stresses (σ_n, τ_n) are known. Given an increment in strain $(\Delta\varepsilon_{n+1}, \Delta\gamma_{n+1})$ and hence the total strains $(\varepsilon_{n+1} = \varepsilon_n + \Delta\varepsilon_{n+1}, \gamma_{n+1} = \gamma_n + \Delta\gamma_{n+1})$, which defines a state point P_{n+1}, the full incremental equations for the $(n+1)^{th}$ increment are as follows:

If $\varepsilon_{n+1} \geq \varepsilon_n^A + \left|\gamma_{n+1} - \gamma_n^A\right| \cot\psi$ the state point P_{n+1} lies in Region 1. In this region the interface response will be elastic, and the updated strain and stress components are therefore given by

$$\begin{aligned}
\varepsilon_{n+1}^e &= \varepsilon_{n+1} - \varepsilon_n^A & \gamma_{n+1}^e &= \gamma_{n+1} - \gamma_n^A \\
\varepsilon_{n+1}^p &= \varepsilon_n^A & \gamma_{n+1}^p &= \gamma_n^A \\
\varepsilon_{n+1}^A &= \varepsilon_n^A & \gamma_{n+1}^A &= \gamma_n^A \\
\sigma_{n+1} &= E\,\varepsilon_{n+1}^e & \tau_{n+1} &= G\,\gamma_{n+1}^e
\end{aligned} \tag{4.19}$$

If $\varepsilon_n^A < \varepsilon_{n+1} < \varepsilon_n^A + |\gamma_{n+1} - \gamma_n^A| \cot\psi$, the state point P_{n+1} will lie in Region 2, as shown in Figure 4.5. In this region, the interface is in contact and sliding and therefore, after straight forward manipulation, the updated components are given by

$$\begin{aligned}
\varepsilon_{n+1}^e &= \varepsilon_{n+1} - \varepsilon_n^A & \gamma_{n+1}^e &= \varepsilon_{n+1}^e \tan\psi \, \mathrm{sgn}\left(\gamma_{n+1} - \gamma_n^A\right) \\
\varepsilon_{n+1}^p &= \varepsilon_n^A & \gamma_{n+1}^p &= \gamma_n^A + \left\{|\gamma_{n+1} - \gamma_n^A| - \varepsilon_{n+1}^e \tan\psi\right\} \mathrm{sgn}\left(\gamma_{n+1} - \gamma_n^A\right) \\
\varepsilon_{n+1}^A &= \varepsilon_n^A & \gamma_{n+1}^A &= \gamma_{n+1}^p \\
\sigma_{n+1} &= E\,\varepsilon_{n+1}^e & \tau_{n+1} &= G\,\gamma_{n+1}^e
\end{aligned} \tag{4.20}$$

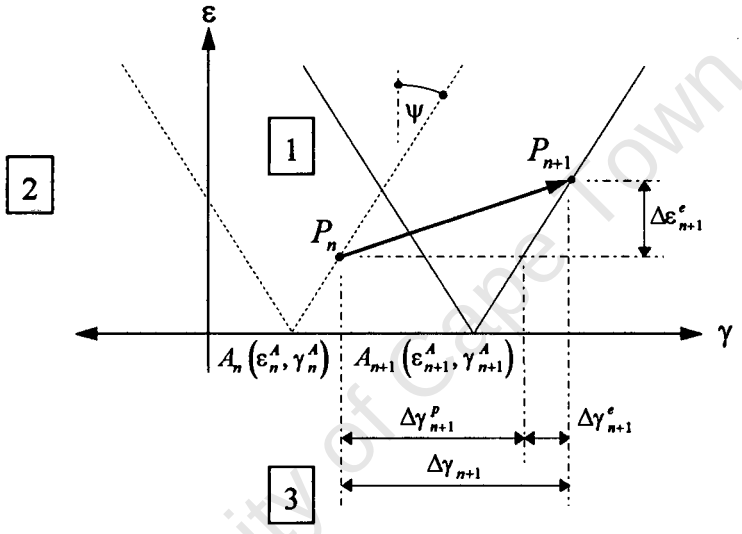

Figure 4.5 Incremental strains for closed and sliding interface.

Finally, if $\varepsilon_{n+1} \le \varepsilon_n^A$, the state point P_{n+1} will lie in Region 3, as shown in Figure 4.6. In this region, contact will be lost and the interface stresses will be zero. The updated components are given by

$$\begin{aligned}
\varepsilon_{n+1}^e &= 0 & \gamma_{n+1}^e &= 0 \\
\varepsilon_{n+1}^p &= \varepsilon_{n+1} & \gamma_{n+1}^p &= \gamma_{n+1} \\
\varepsilon_{n+1}^A &= \varepsilon_n^A & \gamma_{n+1}^A &= \gamma_{n+1} \\
\sigma_{n+1} &= 0 & \tau_{n+1} &= 0
\end{aligned} \tag{4.21}$$

The formulation presented above, describes a simple model where contact stresses and sliding is governed by a classical Coulomb formulation. The contact state is determined by examining regions in strain space, where each region determines different contact behaviour. In the following section, the Coulomb model is extended to include the interface response, following the formation of a fibrous tissue layer at the implant-bone interface.

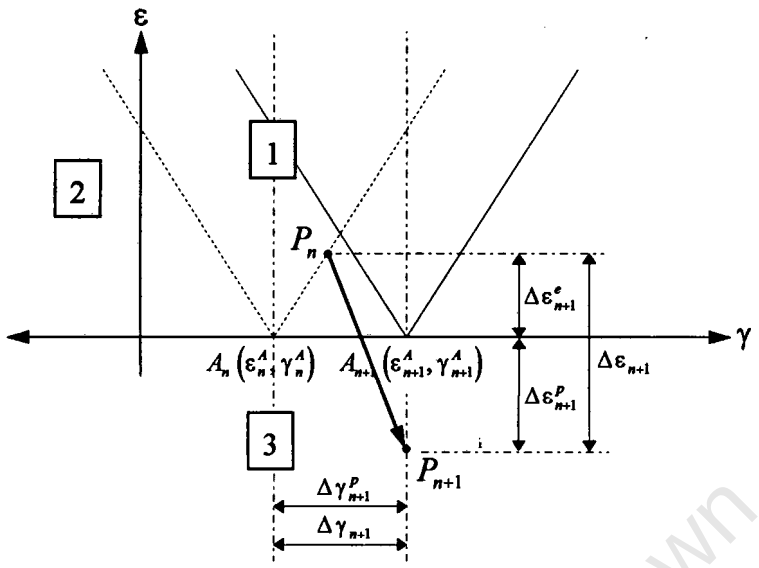

Figure 4.6 Incremental Strains for open interface.

4.4 Extension of the Coulomb model

The Coulomb model formulated in the previous section is extended to include a layer of fibrous tissue at the interface. The initial shape of the yield surface, in stress space, is unaltered by the new material. However, fibrous tissue exhibits non-linear compressive behaviour and as a result, the translation to strain space will now be a function of compressive strain. The construction and updating of the state diagram for this case is considered in the following section.

4.4.1 Construction of the State Diagram

To construct the state diagram in strain space, consider the joint in the initial state with no previous strain or load history, so that $\varepsilon_0 = \gamma_0 = 0$ and $\sigma_0 = \tau_0 = 0$. A set of finite strains, $\Delta\varepsilon_1$ and $\Delta\gamma_1$, are imposed on the virgin interface and the resulting interface strain components are $\varepsilon_1 = \Delta\varepsilon_1$ and $\gamma_1 = \Delta\gamma_1$, which defines the point P_1 as shown in Figure 4.7.

In the initial Coulomb model, the state diagram is constructed by drawing lines *A-X* and *A-Z* at an angle ψ on either side of the ε-axis. However, the Young's modulus of the interface material is no longer constant, but is a function of the normal elastic strain. As there is no interface dilation, the total compression strain is elastic and therefore, $\varepsilon_1^e = \varepsilon_1$. The new state diagram is constructed, based on the compressive strain, by drawing lines *A-X* and *A-Z* at an angle ψ_1 on either side of the ε-axis, where

$$\tan\psi_1 = \frac{E_1\left(\varepsilon_1^e\right)}{G}\tan\phi \qquad (4.22)$$

If the compressive strain is zero $\left(\varepsilon_1^e = 0\right)$, the Young's modulus is given by $E = E_0$ and therefore $\psi = \psi_0$, so that Region 1 is bounded by the dashed lines, as shown in Figure 4.7. The relative size of the regions defining the interface response will change as a function of normal strain, and thus the state diagram can only be constructed once the normal strain is known.

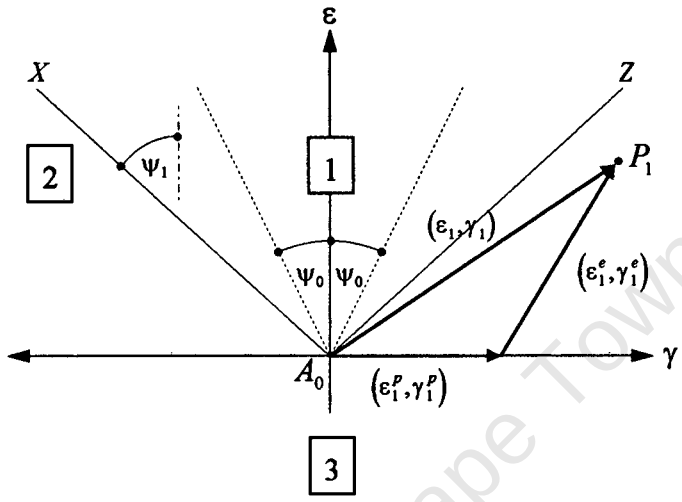

Figure 4.7 State diagram for fibrous tissue interface.

4.4.2 Updating in Strain Space

The updating of the state diagram for the fibrous tissue interface follows the same simple procedure used in the initial Coulomb model. If the imposed strains result in the state point P_1 lying in Region 2 (as shown in the example of Figure 4.7), then the lines joining the apex position A_0 to X and Z will simply translate, without rotating, along the γ-axis, to the position A_1. The new apex position is defined by the point $\left(\varepsilon_1^A, \gamma_1^A\right)$, as indicated in Figure 4.8.

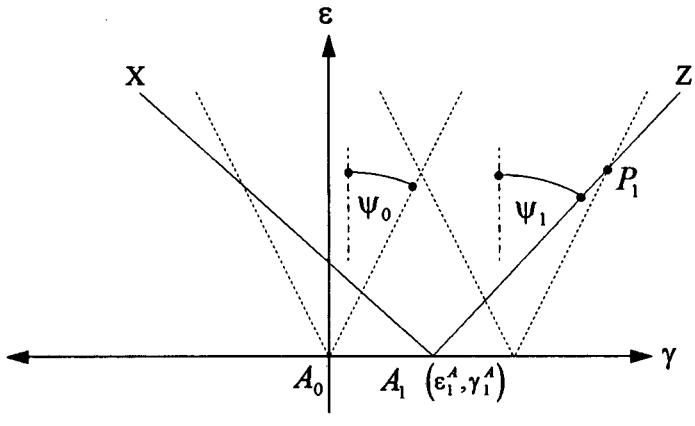

Figure 4.8 Updated state diagram for fibrous tissue layer.

If the state point lies in the elastic region (Region 3), or if the interface is open and the state point lies in Region 1, the rule for updating the state diagram is the same as that used in the initial Coulomb model.

4.4.3 Constitutive Equations

Following a similar approach to that used in the initial Coulomb model, given the interface conditions at increment (n), as well as an increment in strain $(\Delta\varepsilon_{n+1}, \Delta\gamma_{n+1})$ and hence the total strain $(\varepsilon_{n+1} = \varepsilon_n + \Delta\varepsilon_{n+1}, \gamma_{n+1} = \gamma_n + \Delta\gamma_{n+1})$, constitutive equations are formulated for increment $(n+1)$. As there is no interface dilation, the elastic component of compressive strain is equal to the total compressive strain. Subsequently, the angle ψ_{n+1} is explicitly known, and the constitutive equations are given as follows:

If $\varepsilon_{n+1} \geq \varepsilon_n^A + \left|\gamma_{n+1} - \gamma_n^A\right| \cot\psi_{n+1}$, then the interface is in the elastic region, and the updated components are given by

$$\begin{aligned} \varepsilon_{n+1}^e &= \varepsilon_{n+1} - \varepsilon_n^A & \gamma_{n+1}^e &= \gamma_{n+1} - \gamma_n^A \\ \varepsilon_{n+1}^p &= \varepsilon_n^A & \gamma_{n+1}^p &= \gamma_n^A \\ \varepsilon_{n+1}^A &= \varepsilon_n^A & \gamma_{n+1}^A &= \gamma_n^A \\ \sigma_{n+1} &= g\left(\varepsilon_{n+1}^e\right) & \tau_{n+1} &= G\,\gamma_{n+1}^e \end{aligned} \tag{4.23}$$

If $\varepsilon_n^A < \varepsilon_{n+1} < \varepsilon_n^A + \left|\gamma_{n+1} - \gamma_n^A\right| \cot\psi_{n+1}$, then the interface is in contact and sliding, and the updated components are

$$\begin{aligned} \varepsilon_{n+1}^e &= \varepsilon_{n+1} - \varepsilon_n^A & \gamma_{n+1}^e &= \varepsilon_{n+1}^e \tan\psi_{n+1}\,\mathrm{sgn}\left(\gamma_{n+1} - \gamma_n^A\right) \\ \varepsilon_{n+1}^p &= \varepsilon_n^A & \gamma_{n+1}^p &= \gamma_n^A + \left(\left|\gamma_{n+1} - \gamma_n^A\right| - \delta_{n+1}^e \tan\psi_{n+1}\right)\mathrm{sgn}\left(\gamma_{n+1} - \gamma_n^A\right) \\ \varepsilon_{n+1}^A &= \varepsilon_n^A & \gamma_{n+1}^A &= \gamma_{n+1}^p \\ \sigma_{n+1} &= g\left(\varepsilon_{n+1}^e\right) & \tau_{n+1} &= G\,\gamma_{n+1}^e \end{aligned} \tag{4.24}$$

where the function g is determined from experimental data of compressive tests (Hori and Lewis, 1982).

If $\varepsilon_{n+1} \leq \varepsilon_n^A$, then the interface is open, and so the components are given by

$$\begin{aligned} \varepsilon_{n+1}^e &= 0 & \gamma_{n+1}^e &= 0 \\ \varepsilon_{n+1}^p &= \varepsilon_{n+1} & \gamma_{n+1}^p &= \gamma_{n+1} \\ \varepsilon_{n+1}^A &= \varepsilon_n^A & \gamma_{n+1}^A &= \gamma_{n+1} \\ \sigma_{n+1} &= 0 & \tau_{n+1} &= 0 \end{aligned} \tag{4.25}$$

The formulation presented above, describes an extension of the simple Coulomb model to include a fibrous tissue layer at the implant-bone interface. The initial Coulomb model is now extended to include cohesion and adhesion, simulating the bonding which takes place when mineralised bone grows into the porous bead structure. The formulation will allow fracture, and a return to the initial Coulomb model.

4.5 Interface Bonding

To model the adhesion and cohesion that develops when mineralised bone tissue grows into the porous beads, a new yield surface is needed, which is assumed to be convex. The new surface needs to be compatible with the Coulomb surface, in the sense that the bonded surface must evolve from the Coulomb surface and, in the event of interface fracture, the new surface must return to its original shape. Most research involving the failure modes of cancellous bone (Carter and Hayes, 1977, Stone *et al.*, 1983) has been concerned with the overall bone structure, and not the actual tissue making up the structure or the bonding of this tissue to porous coatings. Thus the elliptical yield surfaces found for cancellous bone can not necessarily be used for bonding and failure of the implant-bone interface. A new interface yield surface is proposed, which considers the bonding due to bone ingrowth and the interaction of normal and shear stresses.

4.5.1 The Yield Surface

The simulation of interface bonding is accomplished by adjusting the Coulomb model to allow tensile stresses to be transmitted across the interface. Further, by the addition of a cohesion term, shear stresses can be transmitted in the absence of normal pressure. This is be accomplished simply by translating the Coulomb surface into the tensile region $(\sigma < 0)$. However, this translation over-predicts the tensile strength, so a modified Coulomb surface is defined, as shown in Figure 4.9. This surface is defined by adding a cohesion term c and a tensile angle κ to the Coulomb model, such that $c = c(Q)$ and $\tan\kappa = \lambda^{-1}$, where λ is the ratio of cohesive to adhesive bond strength.

In the compressive region $(\sigma \geq 0)$, the yield surface is defined by $f = |\tau| - (c + \sigma \tan\phi)$. The dependence of the ingrowth shear strength on the friction angle ϕ may over-predict the influence of interface compression on the bond's shear strength. However, no data on this influence could be found and therefore, in addition to the cohesion term, the interface shear strength will also be a function of the normal pressure in the same way as in the unbonded interface. The interface will now be elastic when

$$f \leq 0 \text{ such that } f = \begin{cases} |\tau| - (c + \sigma \tan\phi) & \text{for } \sigma \geq 0 \text{ and} \\ |\tau| - (c + \sigma \tan\kappa) & \text{for } 0 < \sigma \leq -c\cot\kappa \end{cases} \tag{4.26}$$

If the state point lies on the boundary of the yield surface, inelastic shear deformation (slip) and fracture (debonding) may take place. Under this condition, the limiting value of shear stress

$$|\tau| = \begin{cases} c + \sigma \tan\phi & \text{for } \sigma \geq 0 \text{ and} \\ c + \sigma \tan\kappa & \text{for } 0 < \sigma \leq -c\cot\kappa \end{cases} \tag{4.27}$$

is reached, and the inelastic strain rate may be non-zero. If this limit is reached, the cohesion term c is reset to zero, and the interface is once more governed by the Coulomb model, which is shown by the dashed lines in Figure 4.9.

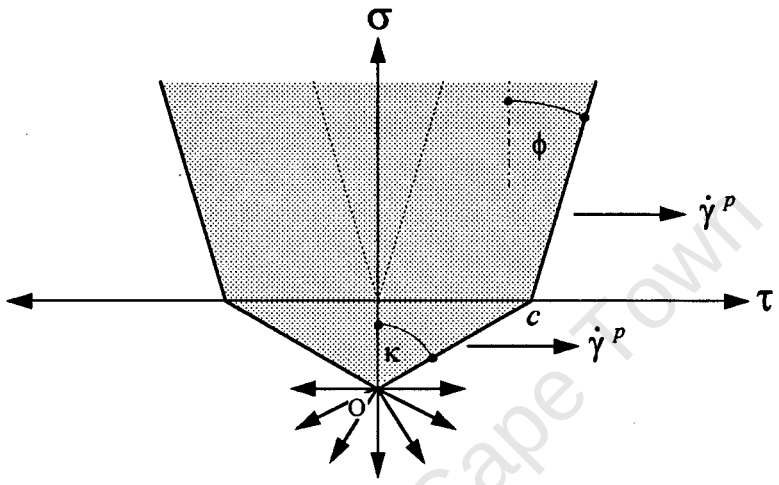

Figure 4.9 Bonded interface yield surface.

As in the Coulomb model, it is assumed that there is no interface dilation, and as a result, the flow direction is parallel to the γ-axis, as indicated in Figure 4.9. The flow function is given by

$$\Psi = \begin{cases} |\tau| & \text{for } \sigma \geq -c\cot\kappa \\ 0 & \text{for } \sigma < -c\cot\kappa \end{cases} \tag{4.28}$$

The rates of inelastic strain are, therefore, given by

$$\dot{\varepsilon}^p = \dot{\lambda}\frac{\partial\Psi}{\partial\sigma} = 0 \tag{4.29}$$

$$\dot{\gamma}^p = \dot{\lambda}\frac{\partial\Psi}{\partial\tau} = \pm\dot{\lambda} \tag{4.30}$$

Again, the flow direction of inelastic strain is not defined at the apex of the yield surface, which is indicated by point O on the diagram. At this point, the flow direction is defined by the fan of normals, which range from the positive to the negative τ-axis, as shown. In the tensile region $(\sigma < 0)$, the flow direction is consistent with the compressive region $(\sigma \geq 0)$, where flow is parallel to the γ-axis.

Under constant normal stress, the failing of the bond due to pure shear would result in the shear stress-strain relation shown in Figure 4.10. The slope of the elastic portion of the curve *I-J* is given by the shear modulus *G*. When the shear failure limit *J* is reached, the yield surface returns to its unbonded shape, and the shear limit reduces to the point *K*. After this point the shear limit remains constant, while interface relative displacement proceeds until the point *L* is reached.

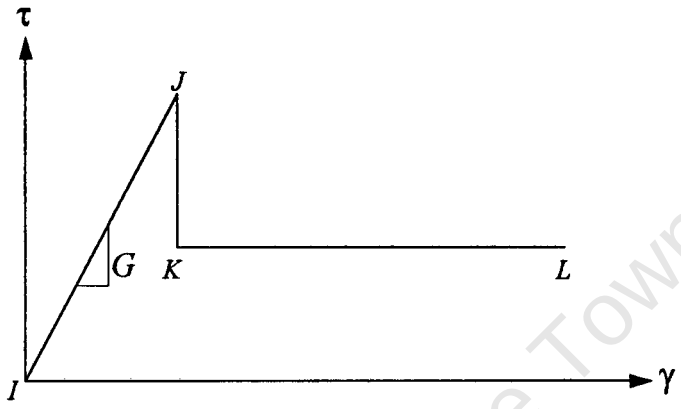

Figure 4.10 Shear stress-shear strain response.

4.5.2 Formulation of a State Diagram

A set of finite strains, $\Delta\varepsilon_1$ and $\Delta\gamma_1$, are imposed on the virgin interface and the resulting interface strain components are $\varepsilon_1 = \Delta\varepsilon_1$ and $\gamma_1 = \Delta\gamma_1$ which define point P_1, as shown in Figure 4.11.

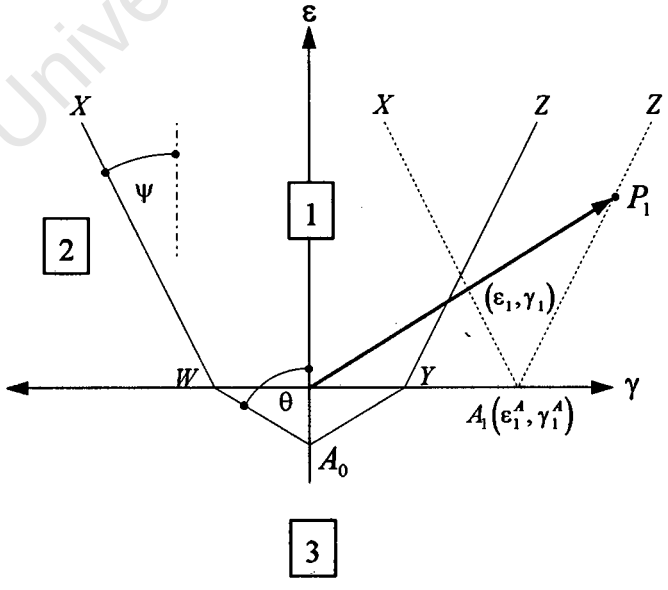

Figure 4.11 State diagram for the bonded interface.

A state diagram is constructed in strain space in order to determine the status of the contact for the bonded interface. Region 1 is again defined as the elastic region, which is constructed by drawing lines *W-X* and *Y-Z* from points *W* and *Y* respectively, each at an angle ψ to the ε-axis. Points *W* and *Y* are positioned at a distance $\frac{c}{G}$ along the γ-axis on either side of the origin. The apex position A_0 is determined by constructing lines *W-A* and *Y-A*, each at an angle θ to the ε-axis. If the state point lies in Region 1, the interface response will be elastic and the inelastic components of the strain vector will be zero. Therefore, if $\varepsilon_1 \geq |\gamma_1| \cot\theta$ and $\varepsilon_1 \geq |\gamma_1| \cot\psi$, the strain components will be given by

$$\begin{aligned} \varepsilon_1^e &= \varepsilon_1 & \gamma_1^e &= \gamma_1 \\ \varepsilon_1^p &= 0 & \gamma_1^p &= 0 \end{aligned} \tag{4.31}$$

If the interface is in contact and sliding (Region 2) as a result of fracture, the strain components can be separated into elastic and plastic components by considering the geometry of the state diagram. Therefore, if $0 < \varepsilon_1 < |\gamma_1| \cot\psi$, these components are given by

$$\begin{aligned} \varepsilon_1^e &= \varepsilon_1 & \gamma_1^e &= \varepsilon_1^e \tan\psi \, \mathrm{sgn}(\gamma_1) \\ \varepsilon_1^p &= 0 & \gamma_1^p &= \left(|\gamma_1| - \varepsilon_1^e \tan\psi\right) \mathrm{sgn}(\gamma_1) \end{aligned} \tag{4.32}$$

If the state point lies in Region 3, the interface has fractured in tension. Therefore, if $0 \leq \varepsilon_1 \leq |\gamma_1| \cot\theta$, the strain components will be given by

$$\begin{aligned} \varepsilon_1^e &= 0 & \gamma_1^e &= 0 \\ \varepsilon_1^p &= \varepsilon_1 & \gamma_1^p &= \gamma_1 \end{aligned} \tag{4.33}$$

4.5.3 Updating in Strain Space

The updating in strain space again follows the same simple updating rule used for the Coulomb model. If the state point $(\varepsilon_1, \gamma_1)$ lies in Region 1, then the response of the interface is elastic, in which case the lines *W-X* and *Y-Z* remain unchanged, and the apex position is given by $A_1 = A_0$.

If the imposed strains result in the state point $(\varepsilon_1, \gamma_1)$ lying in Region 2, as shown in the example of Figure 4.11, then the points *W* and *Y* of the lines *W-X* and *Y-Z* join at the origin, reforming the Coulomb state diagram. The resulting point is then translated along the γ-axis to the position A_1.

Finally, if the point $(\varepsilon_1, \gamma_1)$ lies in Region 3 then the interface has fractured and contact has been lost. In this case, there is no elastic strain and again lines *W-X* and *Y-Z* join at

the origin before translating along the γ-axis. The movement of the apex is given by the distance of the total shear strain and, therefore, $\varepsilon_1^A = 0$ and $\gamma_1^A = \gamma_1 = \gamma_1^p$.

4.5.4 Constitutive Equations

Equations (4.31), (4.32) and (4.33) are generalised for an arbitrary increment $(n+1)$. At time t_n, the total strain $(\varepsilon_n, \gamma_n)$, inelastic strain $(\varepsilon_n^p, \gamma_n^p)$, apex position $(\varepsilon_n^A, \gamma_n^A)$ as well as the interface stresses (σ_n, τ_n) are known. Given an increment in strain $(\Delta\varepsilon_{n+1}, \Delta\gamma_{n+1})$, and hence the total strains $(\varepsilon_{n+1} = \varepsilon_n + \Delta\varepsilon_{n+1}, \gamma_{n+1} = \gamma_n + \Delta\gamma_{n+1})$, the full incremental equations for the $(n+1)^{th}$ increment are set out as follows:

If $\varepsilon_{n+1} \geq \varepsilon_n^A + |\gamma_{n+1} - \gamma_n^A| \cot\psi$ and $\varepsilon_{n+1} \geq \cot\psi\left(\varepsilon_n^A \tan\psi + |\gamma_{n+1} - \gamma_n^A|\right)$ then the state point lies in the elastic region and

$$\begin{aligned} \varepsilon_{n+1}^e &= \varepsilon_{n+1} - \varepsilon_n^A & \gamma_{n+1}^e &= \gamma_{n+1} - \gamma_n^A \\ \varepsilon_{n+1}^p &= \varepsilon_n^A & \gamma_{n+1}^p &= \gamma_n^A \\ \varepsilon_{n+1}^A &= \varepsilon_n^A & \gamma_{n+1}^A &= \gamma_n^A \\ \sigma_{n+1} &= E\,\varepsilon_{n+1}^e & \tau_{n+1} &= G\,\gamma_{n+1}^e \end{aligned} \tag{4.34}$$

If $\varepsilon_n^A < \varepsilon_{n+1} < \cot\psi\left(\varepsilon_n^A \tan\theta + |\gamma_{n+1} - \gamma_n^A|\right)$, then the interface is closed, but shear fracture and subsequently sliding have occurred.

$$\begin{aligned} \varepsilon_{n+1}^e &= \varepsilon_{n+1} - \varepsilon_n^A & \gamma_{n+1}^e &= \varepsilon_{n+1}^e \tan\psi\,\mathrm{sgn}\left(\gamma_{n+1} - \gamma_n^A\right) \\ \varepsilon_{n+1}^p &= \varepsilon_n^A & \gamma_{n+1}^p &= \gamma_n^A + \left(|\gamma_{n+1} - \gamma_n^A| - \varepsilon_{n+1}^e \tan\psi\right)\mathrm{sgn}\left(\gamma_{n+1} - \gamma_n^A\right) \\ \varepsilon_{n+1}^A &= \varepsilon_n^A & \gamma_{n+1}^A &= \gamma_{n+1}^p \\ \sigma_{n+1} &= E\,\varepsilon_{n+1}^e & \tau_{n+1} &= G\,\gamma_{n+1}^e \end{aligned} \tag{4.35}$$

If $0 \leq \varepsilon_{n+1} \leq \varepsilon_n^A + |\gamma_{n+1} - \gamma_n^A| \cot\theta$ then the interface has fractured in tension and opened. The updated values are then given by

$$\begin{aligned} \varepsilon_{n+1}^e &= 0 & \gamma_{n+1}^e &= 0 \\ \varepsilon_{n+1}^p &= \varepsilon_{n+1} & \gamma_{n+1}^p &= \gamma_{n+1} \\ \varepsilon_{n+1}^A &= \varepsilon_n^A & \gamma_{n+1}^A &= \gamma_{n+1} \\ \sigma_{n+1} &= 0 & \tau_{n+1} &= 0 \end{aligned} \tag{4.36}$$

CHAPTER FIVE

INTERFACE TISSUE DEVELOPMENT

5.1 Introduction

This chapter sets out the development of the equations for the evolution of the implant-bone interface material. The proposed material model combines three of the major influences on the implant-bone evolution: the repair activity as a result of surgical reaming and broaching; the interface material adaptation as a result of the remodelling processes; and the formation of fibrous tissue as a result of bone resorption due to implant-bone relative displacements. Once the evolution equations have been presented, the interface constitutive equations are written in terms of the evolution parameters.

The implant-bone interface can be defined as the region between the implant substrate and the bone material that is anatomically typical of the adjacent site. The interface is not simply a boundary line between the two materials, but rather a "region of interaction". (Howie, 1988). In the post-operative condition, this region comprises debris material, an array of cells, coagulation products, fluids and tissue matrix. The response of this interface material following prosthesis implantation is the focus of this chapter.

5.2 Types of Interface

Following an injury, such as reaming during reconstructive surgery, bone can heal with connective tissue (cartilaginous or fibrous), or with osseous (mineralised) tissue. In the initial post-operative condition, the underlying bone and the implant are separated by an interface region, as shown in Figure 5.1(a). The thickness of this region will vary, depending on the implant design and surgical procedure. The mechanics of this interface material is governed by a simple Coulomb model, which has been described in the previous chapter. During the healing process, the interface region and the voids of the porous coating will be infiltrated with mesenchymal osteoprogenitor cells, as a result of the flow of blood and marrow. Other cells will also migrate to the area and, subsequently, the osseous precursor cells will undergo mitosis and differentiation to form osteoblasts or fibroblasts.

The interface material may differentiate to form callus tissue and, subsequently, osseous bone and hence osseo-integration (Figure 5.1(b)). The mineralised tissue integration results in an interlocking of the bone and beads, producing a bond between the prosthesis and the surrounding bone. The resulting cohesive and adhesive bond will be governed by the bonded interface model set out in the preceding chapter. The undifferentiated tissues

may, however, differentiate into fibrous tissue. The formation of fibrous tissue may proceed further as a result of the resorption of the surrounding bone and the subsequent replacement by fibrous tissue, until a layer of up to a few millimetres is formed. The fibrous tissue material may or may not penetrate the beaded structure, as shown by the shaded region in Figure 5.1(c). This unmineralised tissue has considerably different properties to calcified tissue, as it is extremely compliant and may undergo large deformations, exhibiting highly non-linear behaviour in compression. A fibrous tissue interface can tolerate some shear loading, but is hardly capable of transmitting tensile stresses (Linder, 1991). The mechanics of this material is governed by the modified Coulomb model, which has been described in the previous chapter.

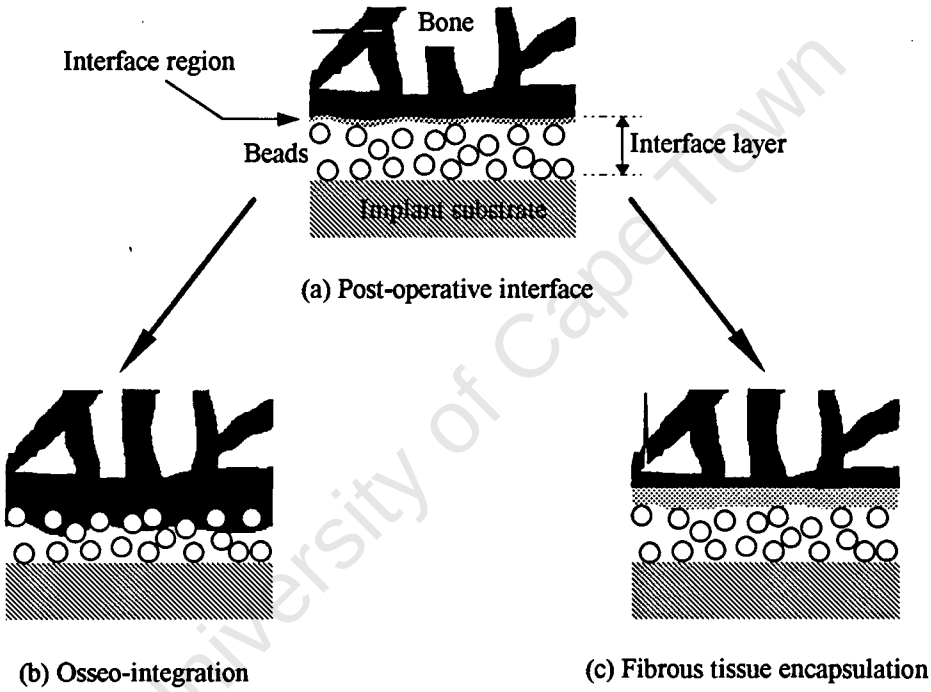

Figure 5.1 Possible pathways of tissue differentiation around porous coated implants (a) Post-operative interface. (b) Osseo-integration. (c) Fibrous tissue encapsulation.

There are many factors unrelated to the mechanics of the interface or the implant design, which will influence the extent and type of interface tissue which develops. These include the quality of the bone tissue into which the implant is inserted, the extent of bone disease, which will influence the degree of vascularisation, the number of osteoprogenitor cells, and the age of the patient. Adjuvant therapies, which are employed to stimulate bone growth, will influence osseo-integration to a greater or a lesser extent. While these factors are important, in this work it is assumed that their influence will be overshadowed by the parameters which will effect the interface mechanical loading history, such as the implant design, the location and design of the porous coating, the

surgical procedure, the weight of the patient and the extent of patient activity. Subsequently, the remainder of this chapter is concerned with the influence of the local mechanics on the evolution of the interfacial material. Starting with the Coulomb model, the position of the mineralised bone tissue surface, which is given by the internal variable Q, will determine whether the interface material will evolve to a bonded or fibrous tissue interface. The constitutive matrix, **D**, will be a function of the type of tissue development and the position of the mineralised bone tissue surface.

5.3 A Continuum Assumption

The purpose of the interface model is to simulate the evolution processes and subsequent interface mechanics of osseo-integration and fibrous tissue formation. The interaction and evolution of the bone and beaded surface of the implant is simulated without explicitly modelling the geometry of the beads and the movement of the bone tissue surface within them. The changes that take place at the implant-bone interface occur on a microstructural level, with the bone tissue advancing into the beaded surface which has a thickness of approximately 1500μm, beads size of 150μm and pore spaces of between 50 and 400μm. The intention of this model is to examine the implant-bone interaction on a global level and, therefore, it would be impractical to consider both bone ingrowth on a microstructural level and the overall mechanics of a reconstructed joint.

The possible paths of osseo-integration and fibrous tissue encapsulation are modelled by considering the mechanics of a thin region of material between the implant and bone surfaces (Figure 5.2). Using this approach, the amount and type (fibrous tissue or bone tissue) of tissue growth will be state variables, which will determine the properties of the interface region. The layer of beads is modelled as a continuum, where the properties of the continuum are the apparent properties of the beaded surface, which can be found by experimentation. It is assumed that these properties do not change during the interface evolution. This assumption is justified on the grounds that the stiffness of the beaded structure is of the order of 70GPa for a cobalt-cromium implant, while the stiffness of the bone tissue is of the order of 1GPa. Therefore, the ingrowth of bone or fibrous tissue (whose stiffness is considerably less then that of bone) will have little influence on the overall stiffness of the layer, and can thus be neglected. The strength of the interface bonding, due to bone growth, will be governed by the yield strength of the interface layer. This assumption is justified on the grounds that experimental work (Bobyn, 1980) has shown that failure (debonding) of the interface occurs as a result of the rupturing of the tissue adjacent to the beaded surface, while the bead structure itself, in general, remains intact.

Apart from the interface region, the cancellous and cortical bone surrounding the implant are porous materials, as illustrated by the bone structure figures in Chapter 2. The pores of the bone structure are generally filled with marrow, which is a viscous material that can flow under stress. However, in most work regarding the mechanics of bone, the marrow is ignored and the pore space is regarded as being empty. Therefore, the actual strain or stress at a point is that experienced by the individual trabeculae. In order to model the overall joint, it is assumed that the bone material can be regarded as a

continuum. The strains and stresses which are calculated or measured are, therefore, apparent values, as are the properties which are found by mechanical testing. This assumption holds so long as the specimens being tested are sufficiently large so that the continuum assumption holds (Harrigan *et al.*, 1988). The interface evolution and mechanics are considered at discrete points. In this, it is assumed that the evolution at a point will only be a function of the mechanics at that point, and the surrounding area will only influence that point in so much as it influences the mechanics of the point.

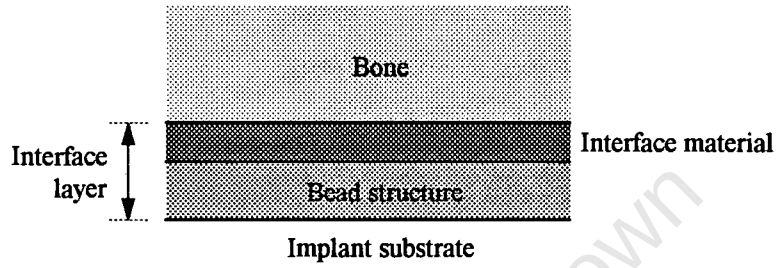

Figure 5.2 Model of interface layer and surrounding materials.

The extent of mineralised tissue formation is given by the state variable Q. Initially (immediately post-operatively), at time $t = 0$, the bone surface will be separated from the beads by the thickness of the interface material and therefore $Q_0 = -h_0$, as shown in Figure 5.3. If the repair process results in mineralisation, there will be an advancement of the bone tissue front from the initial position, and therefore $Q > -h_0$. Once the bone surface penetrates the porous structure ($Q > 0$) the bond cohesion and adhesion will develop. Under this condition, the thickness of the interface region will retain the initial value h_0, and the interface stiffness and yield strength will evolve as a function Q (Figure 5.4(a)).

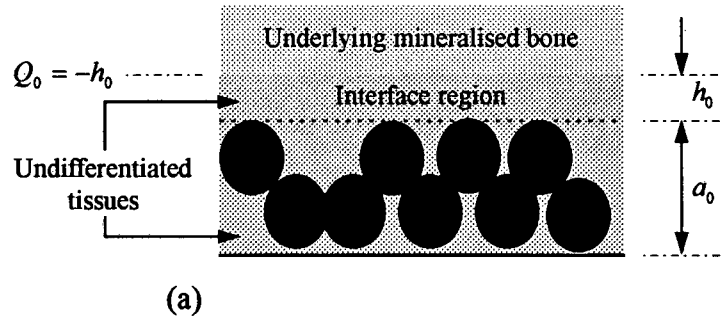

Figure 5.3 Position of the mineralised bone tissue surface in the initial post-operative condition ($t = 0$).

If there is excessive relative displacement, the repair process will take the path of fibrous tissue formation. As a result, there will not be an advancement of the underlying bone surface and therefore $Q = -h_0$. However, subsequent displacement may cause a withdrawal of the mineralised tissue and its replacement by fibrous tissue, therefore $Q < -h_0$, as shown in Figure 5.4(b). Under this condition, the thickness of the interface layer will be given by $h = |Q|$. The constitutive behaviour and bond strength will then remain constant, while the thickness of the layer evolves as a function of the extent of tissue withdrawal. As the tensile strength and cohesive properties of fibrous tissue are assumed to be negligible, it is unimportant whether or not fibrous tissue grows into the beaded surface.

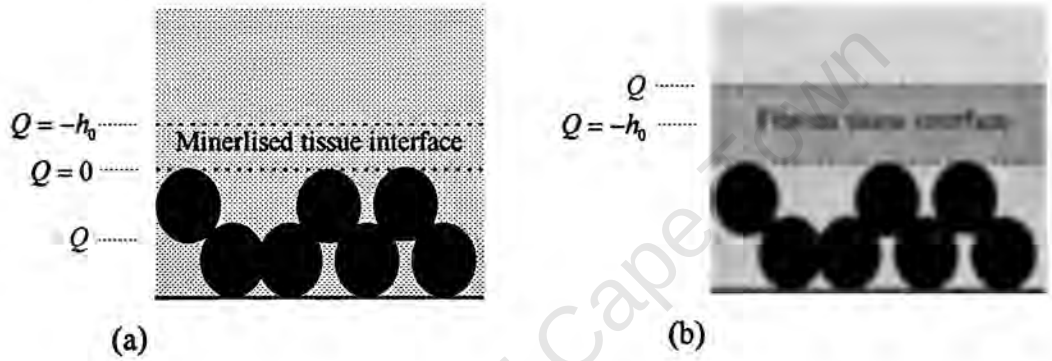

Figure 5.4 Position of the mineralised bone tissue surface Q for (a) mineralised bone ingrowth and (b) fibrous tissue formation.

5.4 Stimulus of Interface Cellular Responses

The driving force behind adaptive changes at the implant-bone interface is assumed to be the stimulus generated by cyclic elastic and inelastic strains. The importance of cyclic strains follows from the findings of numerous experimental investigations (Churches *et al.*, 1979; Lanyon and Rubin, 1984), which have shown that static loading will not induce a remodelling response. For the typical activity profile shown in Figure 5.5, the cyclic strain vector ε_c is given by the magnitude of strain which lies between the dashed lines. In the numerical model which follows, remodelling and the mineralisation of the immature tissues at the fracture site are assumed to be controlled by the cyclic elastic strain vector ε_c^e, while resorption and subsequent fibrous tissue formation will be governed by the cyclic inelastic strains ε_c^p. In the remaining part of this document, all strain magnitudes will refer to the cyclic values without special symbols or notation.

Typical cyclic loading events, such as walking, take place in the order of seconds, while the time scales of ingrowth and remodelling range from a few days - required for the initial bone repair - to months or years for remodelling. Therefore, the amount of activity time is very small, when compared to the time spend at rest. Typically, a person undergoes approximately 10^6 gait cycles per year. The frequency of gait is approximately

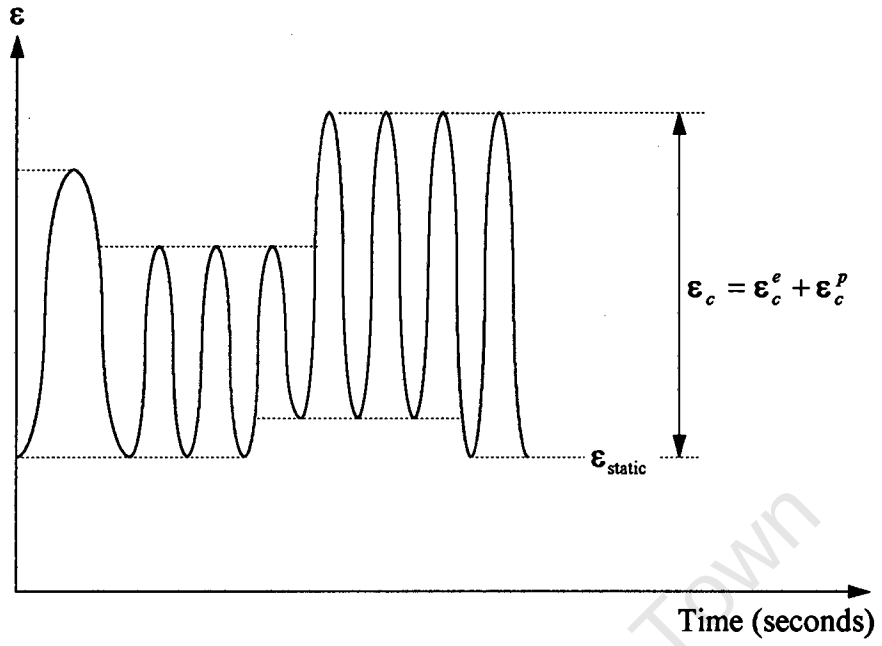

Figure 5.5 Cyclic strain due to normal loading.

1Hz and therefore, the time spent in gait is in the order of 3% of the total time. It can thus be assumed that the evolution of the interface takes place during the rest period as the amount of growth during loading is small enough to be neglected. Subsequently, the evolution equations are written in terms of variables which do not alter over the short period of loading. A practical time scale for growth and remodelling is days, and therefore the time scale t is given in days. Although the strain rate during loading is believed to have an influence on remodelling (Lanyon, 1984), for the present work, loading is written as a function of time t, which has no meaning during loading and unloading.

In the short and long term post-operative period, both repair and remodelling activity will be present. Repair may generate mineralised bone by the differentiation of interfacial tissues, while remodelling may add or remove mineralised tissue to meet mechanical demands. The rate of mineralised tissue production is given by the sum of the contributions due to repair and remodelling

$$\dot{Q} = \dot{Q}_r + \dot{Q}_m \tag{5.1}$$

where $\dot{Q}_r$ and $\dot{Q}_m$ are the rates of mineralised bone tissue formation due to repair and remodelling, respectively. Although these two processes may exist concurrently, the nature of the coupling is unclear. However, remodelling will only take place when mineralised tissue has been formed which subsequently requires maintenance, therefore $\dot{Q}_m$ may only be non-zero if $Q > 0$.

The form of these rate equations will depend on the magnitudes of elastic and inelastic strains within the interface layer. The processes of interface repair and long term mineralised tissue remodelling are considered separately. The two formulations are then combined to give the net mineralisation rate, which considers the current strain and history of interface loading.

5.4.1 Interface Repair

Fracture and surgical broaching initiate a complex series of biological events, which will be effected by the strain within the interface material. Elastic strains will influence the differentiation of the mesenchymal tissue, while inelastic strains may cause bone resorption and replacement with fibrous tissue. To capture the influence of the strain state on the repair process, a stimulus coefficient χ_r is introduced, which is a function of the strain history. The rate of mineralised bone formation, or resorption of the existing bone, is then assumed to be proportional to the stimulus coefficient, and is given by

$$\dot{Q}_r = K_r \chi_r(\varepsilon, t) \tag{5.2}$$

where χ_r will depend on the history of both the elastic and inelastic interface strains, and is normalised such that $-1 \le \chi_r \le 1$. A positive stimulus value will result in an advancement of the mineralised tissue front, simulating the progression of mesenchymal differentiation and subsequent mineralisation. And a negative stimulus value will cause a withdrawal of the surrounding bone, with a simultaneous replacement by fibrous tissue. To develop the history dependent stimulus coefficient χ_r, a parameter $\omega = \omega(\varepsilon)$ is introduced which is an instantaneous measure of the influence of the current strain state on the repair stimulus coefficient. This parameter can be regarded as an "input" to the receptor cells, which will influence and continue the repair process.

The value of the rate coefficient K_r will depend on whether the stimulus value is positive or negative. Under optimal conditions, the rate of mineralisation during the repair phase is approximately 50μm/day, which will mean that, if the interface layer is 2000μm thick (including the bead structure), interface repair will be complete within 40 days. However, interface resorption (which is considered to be a remodelling phenomenon) will not progress at the same rate as repair. Parfitt (1984) determined osteoclastic resorption to be at a rate of approximately 2μm/day. Therefore the rate coefficient is given such that $K_r = K_r(\chi_r)$.

Mineralisation

A simple rule for the differentiation of mesenchymal tissues is proposed, which will capture the fundamental concepts of bone fracture healing. The possibility of cartilage formation is not presently considered and therefore secondary healing due to endochondral ossification is excluded. Despite the numerous reports of the beneficial influences of compressive strains on the fracture healing process, the nature of this influence is unclear. For this reason, compressive strains are assumed not to aid the repair process. However, these strains are assumed not to inhibit repair either. Following

from the ideas of Perren (1979), it is assumed that mineralisation of pluripotential mesenchymal tissue will progress so long as the fracture site is stable. The interface can be regarded as sufficiently stable if the tissue is able to tolerate the local strain. The initial undifferentiated tissue is highly compliant and, therefore, can tolerate strains of up to 100%. However, as mineralisation progresses, the yield strain is reduced in a non-linear manner (Meroi and Natali, 1989) until, on completion, it has the yield value of mineralised tissue, which is in the region of 2%. Thus, the amount of strain which is permissible for the repair process to proceed, will depend on the extent of mineralised tissue, Q.

The proposed influence of elastic strain on the tissue mineralisation parameter ω is shown in Figure 5.6. The magnitude of ω is bounded, such that $0 \leq \omega \leq 1$. If the shear strain component is zero then $\omega = 1$, which will provide the maximum contribution to the repair stimulus coefficient. While if the current shear strain is equal to the shear yield of the material then $\omega = 0$, and there will be no contribution to χ_r.

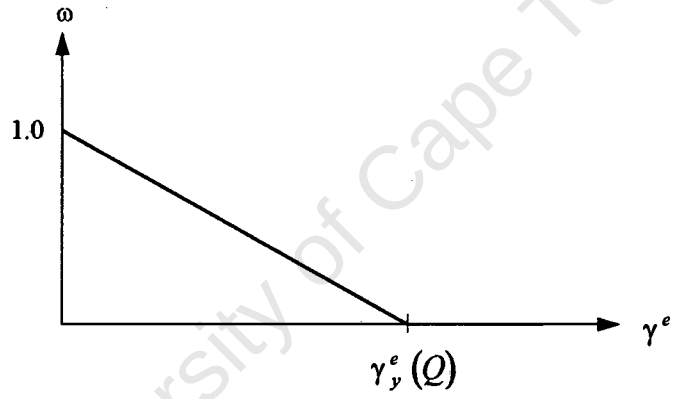

Figure 5.6 Influence of the elastic interface strain state on the repair stimulus parameter ω.

The assumed linear relation for the repair parameter ω, can therefore be expressed as

$$\omega = 1 - \frac{|\gamma^e|}{\gamma_y^e} \tag{5.3}$$

for $|\gamma^e| \leq \gamma_y^e$, where $\gamma_y^e(Q)$ is the yield strain, which is a function of the extent of mineralised tissue. The constitutive model of the interface material does not permit the transmission of tensile stresses until mineralised tissue has developed within the bead structure. Once this has happened, the tensile stresses will be taken up by the bone tissue. However, if before ingrowth has taken place, the interface loses contact during the loading, even although there are no tensile strains, it is assumed that repair will be inhibited by the displacement of the tissue and, therefore, $\omega = 0$.

If large inelastic shear strains are present, mineralisation may cease and be replaced by bone resorption, in which case, the repair coefficient is written in terms of inelastic relative displacements, which is set out as follows.

Resorption and Fibrous Tissue Formation

Resorption of mineralised bone will take place if a threshold value of inelastic strain γ^p_{th} has been overcome. If this value is exceeded, the repair parameter ω will be less than zero, and will decrease from 0 to -1 with increase in the inelastic strain magnitude. A saturation level of strain $\gamma^p_{\max}$ (approximately 150μm of relative displacement) exists, after which further increase in relative displacement will no longer contribute to the resorption parameter. The exact nature of this function is unclear, however the response can be approximated by a series of linear relations, which are shown in Figure 5.7, as

$$\omega = \begin{cases} 0 & \gamma^p \le \gamma^p_{th} \\ C_r\left(\left|\gamma^p_{th}\right| - \left|\gamma^p\right|\right) & \gamma^p > \gamma^p_{th} \end{cases} \tag{5.4}$$

where C_r is an empirical constant and ω is constrained by $-1 \le \omega \le 1$.

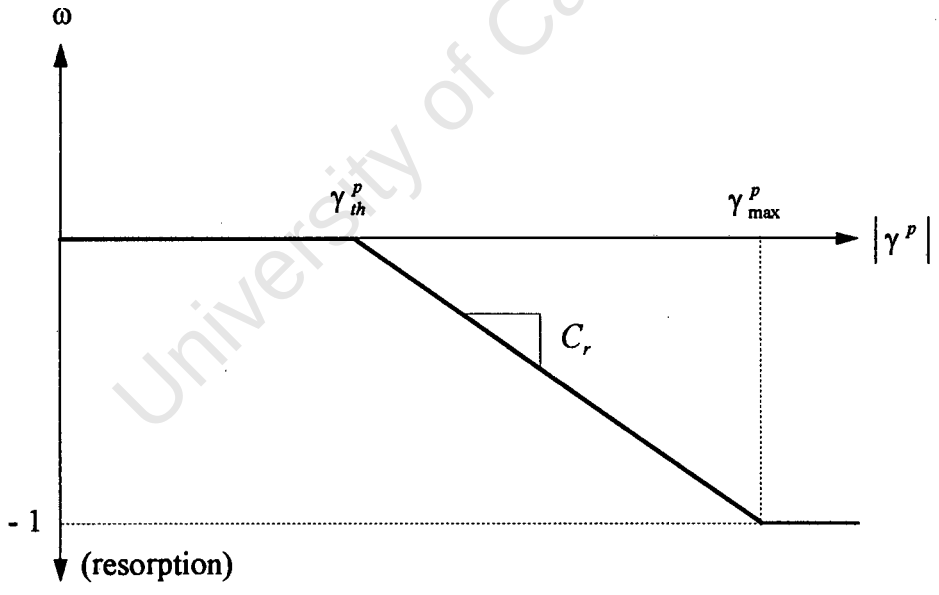

Figure 5.7 Influence of inelastic relative displacement on the repair stimulus parameter ω.

The optimal value of strain which is assumed to exist in mineralised bone represents a state of remodelling equilibrium, which has not been shown to exist in fibrous tissue. Clinical observations have shown that the fibrous layer tends to reach a constant thickness in the long term. However, it is unclear as to whether this is as a result of the

implant reaching a level of stability, or whether this is a biological consideration suggesting that sufficient fibrous tissue has been produced to protect the underlying bone from the harmful effects of relative displacements. The finding of Uhthoff and Germaine (1977), that once stable, with respect to loading, fibrous tissue will be replaced with mineralised tissue suggests that the formation of fibrous tissue occurs in an unstable situation which does not reach equilibrium. In the model presented here, the fibrous layer will continue to form until the relative displacements are reduced to below the threshold value, so that there is no longer any stimulus aiding resorption.

5.4.2 Remodelling of Mineralised Tissue

It is widely accepted that mechanical loading will affect bone physiology. Therefore, once mineralised tissue has formed at the interface and within the porous beads, it should be influenced by loading history in the some way as other regions of bone tissue. Central to the remodelling formulation, is the assumption that mineralised bone requires a certain amount of stimulus, due to loading, to maintain normal levels of bone mass. It is further assumed that the optimal value of stimulus is constant over the region investigated, even if it may vary over the body. If joint loading results in bone stimulus greater than the optimal value, additional cells are recruited and become active, resulting in net bone formation - which in the case of the interface would result in the advancement of the mineralised tissue surface. If there is insufficient stimulus, too few bone producing cells (osteoblasts) are recruited, and the remodelling process is dominated by the activity of osteoclasts, which are the cells responsible for bone removal. Osteoclastic activity is always present, but under optimal loading conditions there is sufficient osteoblastic activity to result in no net gain or loss of bone. The remodelling formulation assumes the existence of a homeostatic remodelling condition, which means that the local bone remodelling response will be a function of the amount by which the current strain induced stimulus χ is out of the homeostatic condition. The homeostatic condition will have been reached when

$$\chi = \chi_0 \tag{5.5}$$

Bone remodelling has two aspects: formation and resorption. Formation will result from loading, while resorption will occur as a result of under-loading. The number and type of cells recruited, and therefore the resultant remodelling activity, will depend on the amount of stimulus produced by loading. The proposed remodelling rate $\dot{Q}_m$ is simply assumed be proportional to the available stimulus χ_m

$$\dot{Q}_m = K_m \chi_m \tag{5.6}$$

where the stimulus parameter $\chi_m = \chi_m\left(\varepsilon^e, t\right)$ is normalised such that $-1 \le \chi_m \le 1$. A negative stimulus value will imply bone resorption, while a positive value will imply mineralised bone formation. The constant K_m is the rate of tissue apposition or removal. Although this parameter will depend on factors such as age and metabolic rate, it is assumed to be constant. The position of the mineralised tissue surface Q will determine the stiffness and strength of the interface bond.

To develop the form of the stimulus function, a scalar or tensor valued parameter $\mu(\varepsilon^e,\sigma)$ is introduced, which is a measure of the current elastic strain and stress state. The function is sought, such that its magnitude will determine the "error" between the current and optimal value. There are many possibilities for the form of μ, the most simple of which is that proposed by Cowin and Hegedus (1979), in which they assumed that the "stimulus" available for remodelling is given by the difference between the actual elastic strain tensor and an optimal tensor. However, this approach had the complexity of requiring many constants, which were difficult to determine. Huiskes *et al.*, (1987) used a similar approach. However, the error measure was assumed to be the difference between the actual strain energy density U, and an optimal value U_0

$$\mu = U - U_0 \tag{5.7}$$

Strain energy density has the advantage of being a scalar value, and therefore, only a single constant is required. Furthermore, the difficulty of determining the relative influence of compressive and tensile strains is eliminated, as both strain states will contribute equally to remodelling. There is still, however, much controversy as to whether or not tensile strains can lead to bone formation, which has been reviewed in Chapter Two. As there is no physical evidence supporting the concept of an optimal value of strain energy density, and equilibrium values are difficult to determine. In the present study, an equivalent strain magnitude is proposed for the remodelling stimulus. The equivalent strain is simply the resulting interface strain which is given by $\bar{\varepsilon}_0^e = |\varepsilon^e + \gamma^e|$. The resultant strain magnitude has the advantage of having physical meaning, while being a scalar value.

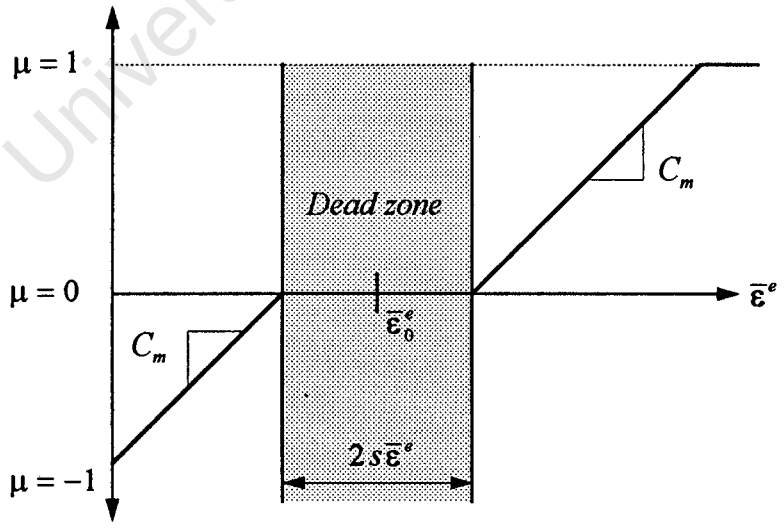

Figure 5.8 Influence of equivalent strain on the remodelling coefficient

To incorporate the idea of a *dead zone* on the cellular response, the tri-linear relation proposed by Huiskes *et al.* (1987) has been used. However, the error function is constrained, such that $-1 \le \mu \le 1$, as shown in Figure 5.8. The function is normalised for two reasons: firstly by normalising the error and stimulus functions, the rate coefficients can be chosen so as to have physical meaning. Secondly, in reality the amount of stimulus felt by the osteocytes does not fluctuate without bounds for increased and decreased values of strain. Experimental evidence (Lanyon, 1984) has shown that there exists definite saturation levels of strain in the case of overloading. Similar limits will also exist for under-loading

The tri-linear remodelling parameter can be expressed as

$$\mu = \begin{cases} C_m\left(\bar{\varepsilon}^e - (1+s)\bar{\varepsilon}_0^e\right), & \bar{\varepsilon}^e > (1+s)\bar{\varepsilon}_0^e \\ 0, & (1-s)\bar{\varepsilon}_0^e \le \bar{\varepsilon}^e \le (1+s)\bar{\varepsilon}_0^e, \\ C_m\left(\bar{\varepsilon}^e - (1-s)\bar{\varepsilon}_0^e\right), & \bar{\varepsilon}^e < (1-s)\bar{\varepsilon}_0^e \end{cases} \qquad (5.8)$$

where $2s$ will determine the width of the *dead zone*, and C_m will determine the slope of the curves. The centre of the *dead zone* is given by the optimal value of the equivalent strain $\bar{\varepsilon}_0^e$. As the same relation is used on either side of the optimal equivalent strain value, no distinction is made in the error function between the extent of under loading and over loading, as was suggested by Carter (1984).

Bone remodelling will take place within the layer of surface beads, although it is unclear how the remodelling process will be influenced by the profile of strain through this layer. Previous researchers (Cowin and Hegedus, 1979; Hart, 1984; Sadegh and Cowin, 1993) have simulated surface remodelling by considering the strain on the surface of the tissue, and relating the normal velocity of the surface (growth or resorption) to the magnitude of this strain. Many free surfaces will form within the bead structure as tissue ingrowth progresses, and thus an assumption is needed regarding how the overall strain distribution will influence remodelling. The magnitude of the equivalent strain within the porous beads will vary as a function of the design of porous coating, the depth of the bead layer, the amount of ingrowth, and the magnitude and type of loading in the adjacent material. To overcome these difficulties, it is assumed that the remodelling will be a function of the peak equivalent strain with the beads. For a given bead design, the peak strain is assumed to be a function of the host bone strain magnitude and the extent of ingrowth Q.

Pedersen *et al.* (1991) examined the stress distribution through a screen like prosthesis coating with a regular structure. The results from their two dimensional finite element models showed a considerable variation in stress, both around the titanium wire and through the depth (2 - 9 times the stress applied to the host bone). Their finding was consistent with that of Hollister *et al.* (1993), who observed that most of the strain energy was concentrated within the first row of beads. They also demonstrated a considerable variation in peak stress, depending on the extent of bone tissue ingrowth.

Their results showed that at the smallest ingrowth depths (bone in contact with the wire mesh), the peak stresses were approximately 30 times the host bone stress. With increased ingrowth, this value decreased asymptotically to a value of 2, when the ingrowth reached one wire diameter. Further ingrowth did not significantly alter the peak stress.

A similar study was undertaken (Steele, 1995) for a sintered bead coating in order to investigate the peak tissue strain magnitude within the surface porosity. The porous coating of a *PCA* (Howmedica, Inc.) femoral implant was sectioned and polished to examine the bead structure. Using an optical microscope, two distinct patterns of the bead geometry were found, as shown in Figure 5.9. The geometry of the two bead arrangements were generated using plane strain finite element models.

As a result of the large difference in stiffness between the beads and the bone tissue, it was assumed that the deformation of the individual beads could be considered negligible, when compared to the deformation of the surrounding bone. Therefore, the beads were modelled as rigid surfaces, which were interconnected by beam elements, to provide flexibility for the bead structure. The stiffness of the beam elements were calculated so as to provide the correct overall stiffness of the porous structure. The magnitude of this stiffness was assumed to the half that of the implant substrate material. The tissue surrounding the beads was assumed to be rigidly connected to the bead surface, which was consistent with the approach used by Pedersen *et al.* (1991). Combinations of unit shear and normal loads were applied to the bone that was adjacent to the tissue surrounding the bead surface. The magnitude of the resulting peak strain was determined for three levels of bone tissue ingrowth: one third, two thirds and full ingrowth.

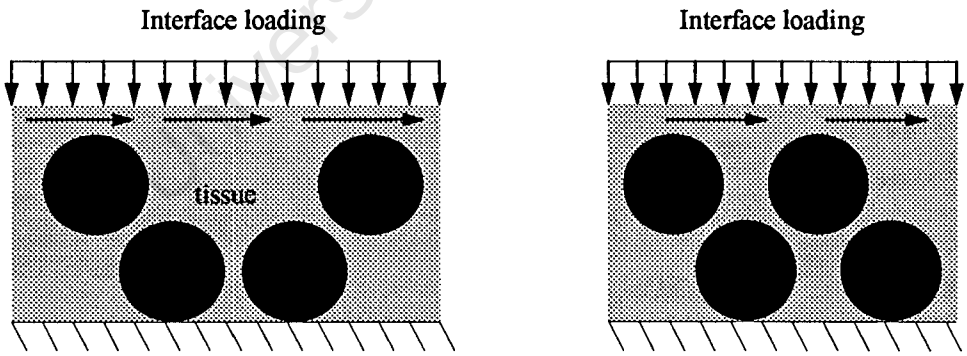

Figure 5.9 Two typical bead structures of the porous coating of the *PCA* femoral stem.

A peak strain of between two and four times the applied strain was found for both bead patterns when one third of the bead surface was filled with mineralised tissue. At two thirds ingrowth, the peak strain was approximately twice the applied strain. This value was not increased when bone tissue completely filled the porous coating. The results of this study were used to specify the peak strain within the beads, as a function of the interface strain and the extent of mineralised bone ingrowth.

5.4.3 The Influence of Load History

Biological processes, such as bone apposition and removal, will respond to loading events over a finite period of time. A significant loading event, acting for a short period of time, will result in cell recruitment, and subsequent activity which will span the lifetime of the cells recruited. Therefore, cellular activities can continue for some time after an influential loading event. This introduces the idea of a "memory" of past events (Skerry *et al.*, 1988). A recent event will have more influence on remodelling than one further in the past, while an event far in the past will have no affect as the cells recruited as a result of that event will have completed their life span. Also an event at the current time will require some time before the cells recruited, in response to that event, become fully active, thereby introducing a lag into the remodelling response.

The rate of mineralised tissue movement is assembled to include the contributions due to repair, resorption and remodelling

$$\dot{Q} = K_r(\chi_r)\chi_r + K_m\chi_m \tag{5.9}$$

The repair and remodelling stimulus at the current time T, from the start of loading (which would be the life of the individual), is given by

$$\chi_r = \int_T \omega(t)dt \quad \text{and} \quad \chi_m = \int_T \mu(t)dt \tag{5.10}$$

To account for cell recruitment and the finite life span of cell activity, a memory weighting function is introduced (Levenston *et al.*, 1994). Effectively the current value of stimulus is moderated by the function $S(t)$, to account for the "fading memory" and "lag" of cell activity. The above equations are therefore reformulated as

$$\chi_r = \int_T \omega(t)S_r(T-t)dt \quad \text{and} \quad \chi_m = \int_T \mu(t)S_m(T-t)dt, \tag{5.11}$$

Memory functions for mineralisation and remodelling may well be similar, and even if they are not, there is a lack of experimental data, therefore $S_r = S_m = S$, so the stimulus values are rewritten as

$$\chi_r = \int_T \omega(t)S(T-t)dt \quad \text{and} \quad \chi_m = \int_T \mu(t)S(T-t)dt, \tag{5.12}$$

The choice of $S(t)$ is somewhat arbitrary, due to the lack of exact data on the life span and activity levels of cellular events. In addition, different cellular activities (resorption and formation) have different activity functions which are not well defined. However, the function is required to introduce some lag to account for the time required for cell

recruitment, as well as to provide a exponential decay, to account for the gradual decline in cell activity. A function that fits both of these criteria is of the form

$$S(t) = t\, e^{-\frac{t}{\alpha}} \tag{5.13}$$

where α is a time constant. The lag period of $S(t)$ is given by α, while the decay period is approximately equal to 7α. As the function is intended to simulate the activity levels of osteoclasts and osteoblasts, the bandwidth of the function (8α) should approximate the life spans of the cell activities. The life span of an osteoclast is not well defined, as they appear (Martin and Burr, 1989) to evolve from and into other cell types. However, the activity time of these cells was recorded in dogs and found to be approximately 11 days. The activity times of osteoblasts is more difficult to determine, as these cells are less mobile than osteoclasts, and they can get left behind and become impregnated in the bone matrix. Thus, up to approximately 120 new cells are required each day to complete the filling process. However, this issue has many additional complications, and is presently not completely resolved. The choice of the same memory function for repair and remodelling (even though the time constants may be different), is based on the fact that both processes involve the recruitment and activation of bone producing cells. It would therefore seem feasible that the activity profile of both processes would be the same. Whether or not the time constants should be the same, still remains to be determined. Figure 5.10 shows the influence of past events, with α equal to 1, 4 and 7 days, when the present time T is equal to 60 days.

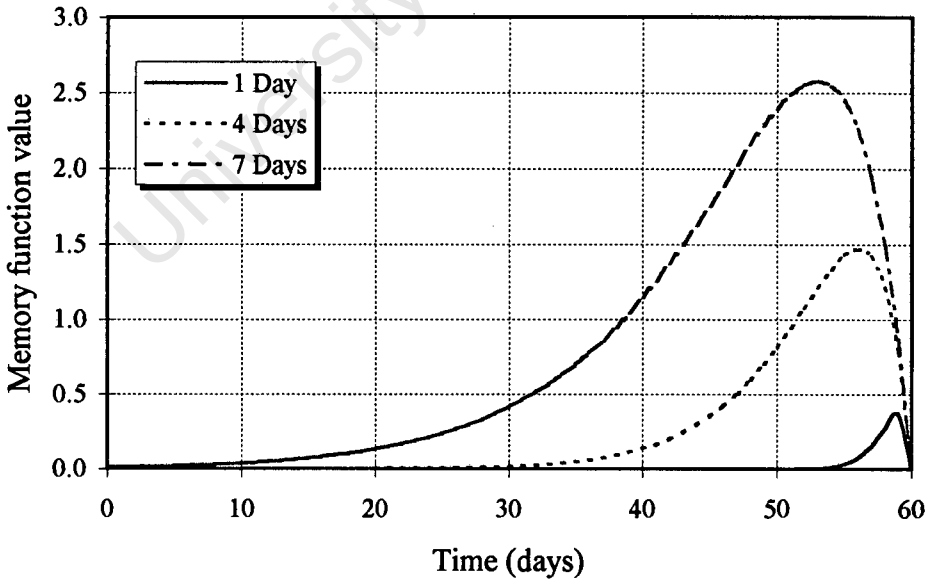

Figure 5.10 Memory function with time constant α = 1, 4 and 7 days and T equal to 60 days.

The stimulus values are normalised by introducing a constant B, such that

$$\lim_{T\to\infty} \int_0^T B\, S(t) = 1. \tag{5.14}$$

Therefore, the resultant mineralisation rate is written as

$$\dot{Q} = B\left\{K_r \int_T \omega(t) S(T-t)dt + K_m \int_T \mu(t) S(T-t)dt\right\}. \tag{5.15}$$

If the interface is at remodelling equilibrium ($\chi_m = 0$) at time $t \le t_0$, as shown in Figure 5.11(a), and additional loading is introduced at $t = t_0$ such that $\chi_m > 0$, the stimulus will accumulate with a lag in the manner shown in Figure 5.11(b). When the loading ceases at time $t = t_1$, the stimulus will decline exponentially as a result of the memory function. The resultant bone growth due the stimulus is shown in Figure 5.11(c). The growth will

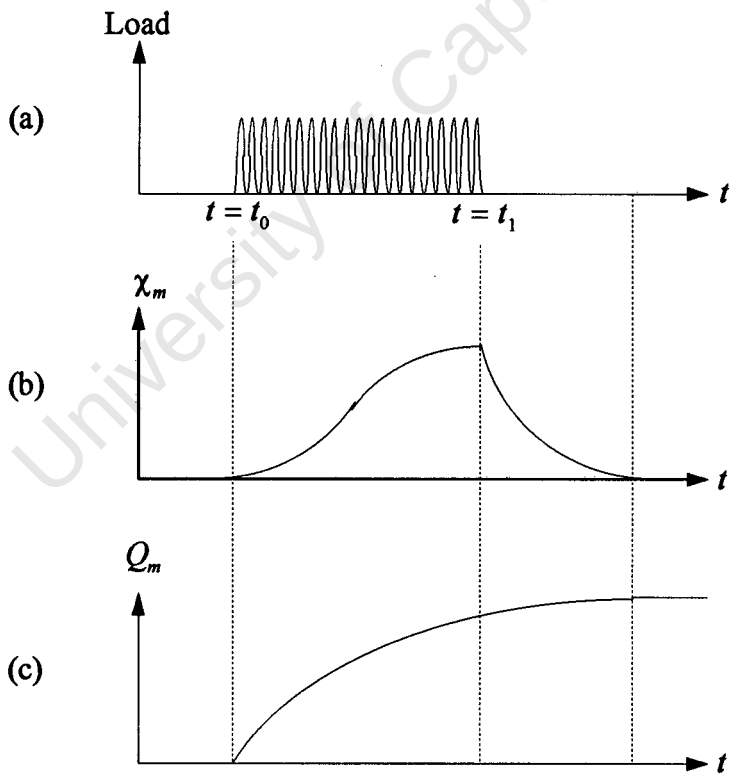

Figure 5.11 Load-Response of elastic cyclic loading. (a) Cyclic loading. (b) Resultant remodelling stimulus. (c) Extent of mineralised tissue formation.

proceed while $\chi_m > 0$, after which it will cease. Whether the new bone that was produced will later be resorbed, depends on subsequent loading. Remodelling equilibrium will not simply be reached by the removal of the load, as the new bone growth will have altered the strain state and, therefore, the remodelling equilibrium will have been altered.

A schematic representation of the proposed numerical model for the evolution of the interface tissue is shown in Figure 5.12. Given the interface geometry and material properties and bond strength, the cyclic loading will result in interface strain ε. The strain vector is then separated into the elastic and inelastic parts ε^e and ε^p, respectively. Mineralisation of the tissue at the fracture site and the remodelling of mineralised tissue

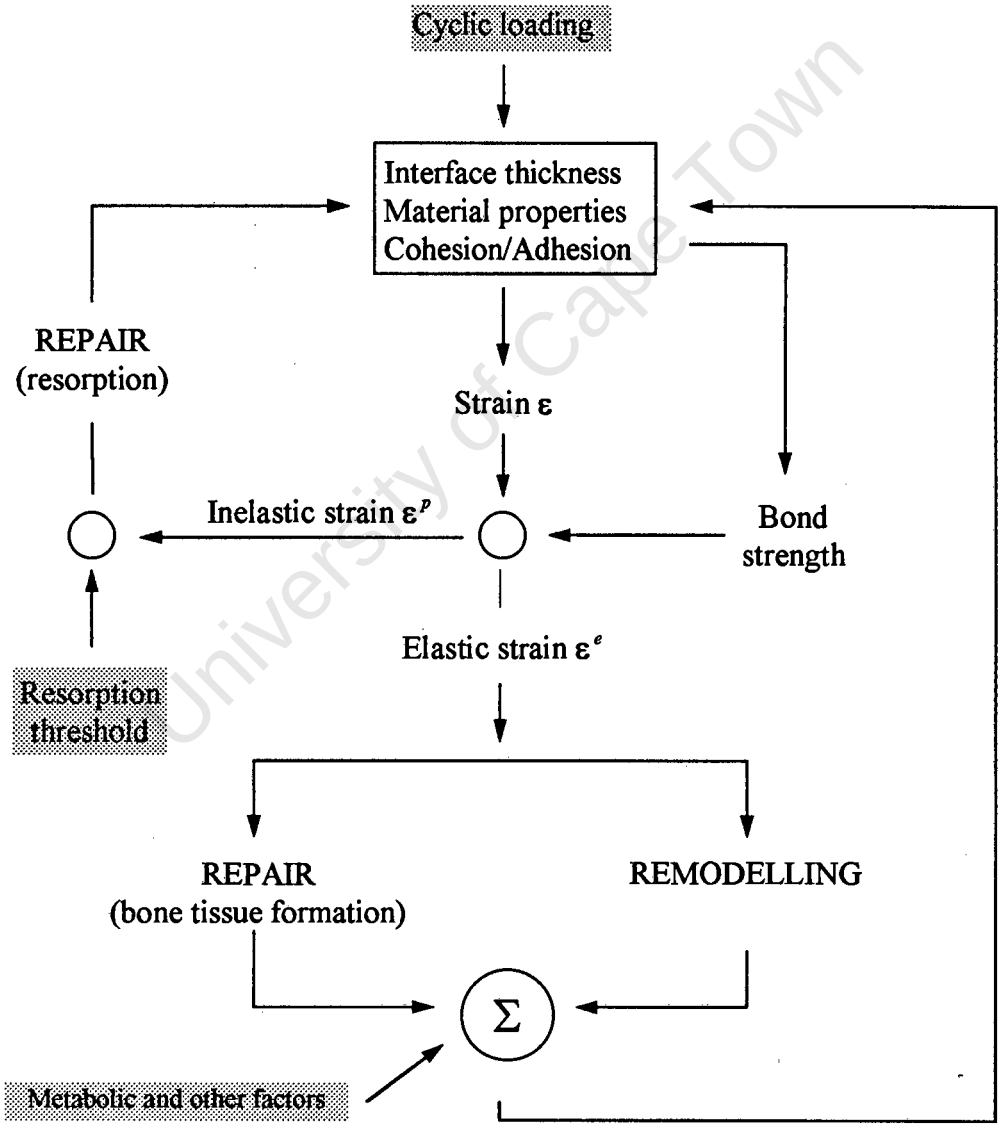

Figure 5.12 Proposed model for the evolution of the implant-bone interface.

will be a function elastic strain. Inelastic strain will determine whether or not resorption of the underlying mineralised tissue, and its replacement with fibrous tissue, will take place.

If there is contact and relative sliding of the two materials, the repair process will take the path of fibrous tissue formation, which is coupled with the resorption of the underlying bone. Once the resorption threshold has been exceeded, the rate of resorption of the surrounding bone will be a function of the magnitude of cyclic inelastic strain. If the threshold has not been overcome, the tissue will not be mineralised and it will persist as a thin fibrous layer at the interface. Once mineralisation has ceased, due to inelastic relative displacements, it will not begin again. Whether or not this is the best assumption still remains to be clarified, as it may be quite possible that, after a period of stability, the fibrous layer could be replaced with mineralised tissue, by the same fracture repair process which is present in the post operative condition (Uhthoff and Germaine, 1977).

Remodelling of the interface tissues will only take place if there is bone to remodel. Therefore, remodelling will begin if the mineralisation of the immature tissues is complete ($Q = a_0$). Before remodelling has started (and while it is progressing), the immature tissues in the interface region will develop as a consequence of a repair or remodelling. The resulting signal will influence the material properties in the interface region, as well as the bond strength of the possible bond between the implant and bone.

If the stimulus function is simplified so as to exclude past loading events, then it is equal to the error function $\chi = \mu\left(\bar{\varepsilon}^e\right)$, and if the repair activity is ignored $\dot{Q}_r = 0$ then the growth rate, Equation (5.1), is reduced to

$$\dot{Q}_m = K_m \, \mu\left(\varepsilon^e\right). \tag{5.16}$$

This is in a similar form to the internal remodelling rate equation developed by Cowin and Hegedus (1979) and Huiskes *et al.* (1987), except that in the present work, an equivalent strain measure is used, which does not consider the type of strain, but only the magnitude.

5.5 Interface Constitutive Relations

Initially (immediately post-operatively), the interface region will have the mechanical properties of undifferentiated tissue. Limited mechanical data is available for the material comprising the post-operative interface region (Bourgious and Burny, 1972; DiGioia III *et al.*, 1986; Carter *et al.*, 1998). However, it is clear that the modulus of this material, which may be highly variable, will be considerably lower than that of bone tissue. In addition, as a result of the more "rubber like" nature of the soft initial tissues, the Poisson's ratio will be greater than that of bone. The Young's modulus and Poisson's ratio of the undifferentiated tissue are given by E_s and ν_s, respectively. Associated with bone mineralisation will be an increase in interface stiffness, and the development of cohesion and adhesion. However, before the tissue within the beads becomes

mineralised, the adjacent interface tissue will differentiate and mineralise, resulting in an increase in Young's modulus with a corresponding decrease in Poisson's ratio. Apart from the amount of ingrowth, the stiffness and strength of the interface will be a function of the bead-layer geometry and material properties.

In the event of fracture and slipping, the initial stage of fibrous layer formation will be characterised by the changing of the thin layer properties to those of fibrous tissue. Following the change of material, the properties of the non-linear material will remain constant, while the thickness of the interface changes. The material properties of mineralised and fibrous tissue are presented separately.

5.5.1 Mineralised Tissue

Mineralised bone tissue exhibits linear-elastic behaviour during normal loading. In general, the material is anisotropic and inhomogeneous. However, the material anisotropy and inhomogeniuty are a result of the bone structure, and not the tissue from which the structure is made up. The implant-bone interface consists of bone tissue and does not have a structural form, and thus, in general, no preferred orientation exists, making an isotropic assumption acceptable. In addition, the interface material will have the properties of the bone tissue itself. Mineralised bone tissue has a Young's modulus of approximately 1.5Gpa, and the shear modulus can be related to the Young's modulus by

$$G = \frac{E}{2(1+\nu)} \tag{5.17}$$

where ν is the Poisson's ratio.

The Young's modulus, Poisson's ratio and cohesion of the interface depend on the extent of the mineralised tissue. Before bone ingrowth has started ($Q < 0$), the Young's modulus E and Poisson's ratio ν are assumed to be related to the normalised amount of mineralised tissue formation $\hat{Q}$, which is defined by Q/d_0, where d_0 is the thickness of the interface tissue. Once the mineralised tissue penetrates the porous surface and a bond begins to form, the stiffness of the interface is governed by the stiffness of the bone tissue and the geometric interaction with the beads. During the development of the bond, the Poisson's ratio is assumed to stay constant, while the Young's modulus and bond cohesion c depend on the depth of bone ingrowth, which is normalised with respect to the depth of the bead layer a by $\hat{Q} = Q/a$.

Therefore, if $-1 \le \hat{Q} \le 0$ then

$$E = E_c - \{E_c - E_s\}\left|\hat{Q}\right|^m, \tag{5.18}$$

$$\nu = \nu_c - \{\nu_c - \nu_s\}\left|\hat{Q}\right|^m \text{ and} \tag{5.19}$$

$$c = 0 \tag{5.20}$$

and if $0 < \hat{Q} \leq 1$ then

$$E = E_b - (E_b - E_c)\left(1 - \hat{Q}\right)^p, \tag{5.21}$$

$$\nu = \nu_c \quad \text{and} \tag{5.22}$$

$$c = c_b\left\{1 - \left(1 - \hat{Q}\right)^p\right\} \tag{5.23}$$

where E_s, E_c and E_b are the Young's moduli for an unmineralised, mineralised and bonded interface, respectively. The Poisson's ratio of the undifferentiated and mineralised tissue are given by ν_s and ν_c, respectively. The cohesive strength of the fully osseo-integrated interface is given by c_b. To account for the non-linear relation between tissue mineralisation and the subsequent Young's modulus, a constant m is introduced such that $m \geq 1$. Figure 5.13 shows the Young's modulus as a function of mineralisation, for m equal to 1, 2, 3 and 4, with a soft tissue modulus E_s of 10MPa and a mineralised tissue modulus E_c of 1GPa. When m is equal to 1, the relation is linear while, when m is equal to 4, the tissue reaches its final modulus after approximately 70% mineralisation. Most of the increase in interface stiffness and strength develops when the bone grows into the first row of beads, with little increase as bone develops deeper into the layer (Nilles *et al.*, 1973). The constant p accounts for the this non-linear evolution. With p equal to 1, full stiffness and bond strength is reached only when the integration of the mineralised tissue is completed, as shown in Figure 5.14 and 5.15, respectively. When p is equal to 5, the maximum stiffness and strength is reached when 60% of the tissue has been infiltrated with mineralised tissue.

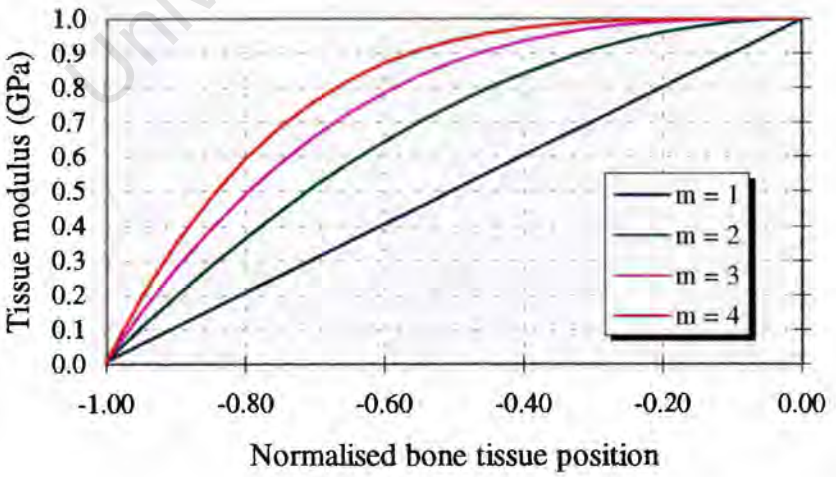

Figure 5.13 Interfacial tissue modulus as a function of the extent of mineralisation of the interfacial region.

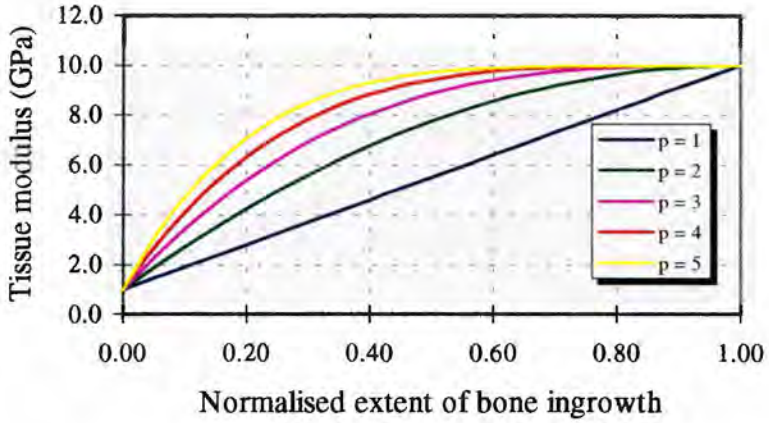

Figure 5.14 Interfacial tissue modulus as a function of the normalised extent of bone ingrowth.

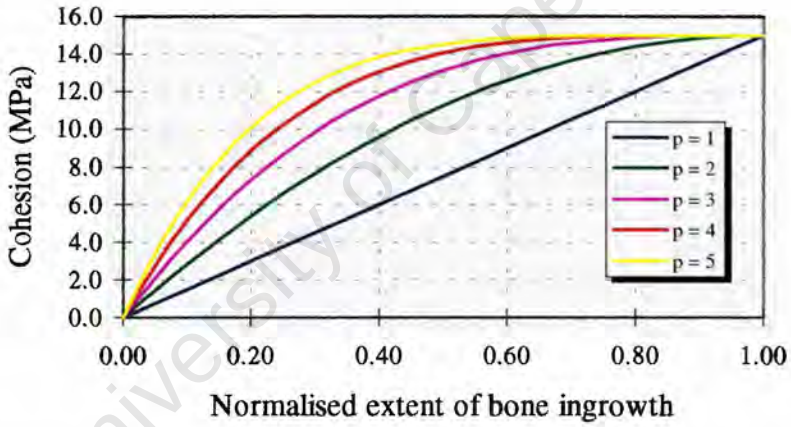

Figure 5.15 Interfacial tissue modulus as a function of the extent of bone ingrowth.

The experimental results relating the bond shear strength to the amount of ingrowth did not provide any information regarding the corresponding development of the tensile bond strength. The yield function described in Chapter Four assumes a fixed relation between the tensile and cohesion strengths of the bond. The ultimate tensile strength is assumed to be given by λc, where λ is the ratio between cohesion and adhesion. The tensile angle κ is therefore given by

$$\varphi = a \tan \lambda^{-1} \tag{5.24}$$

which is simply taken from the geometry of the bonded yield surface.

5.5.2 Fibrous Layer Formation

In compression, fibrous tissue exhibits non-linear stiffening with increased strain up to values of approximately 50%, as shown in Figure 2.6. At this strain level, the "short - term" tangent modulus is approximately 1.9MPa, with a stress magnitude of 0.5MPa. The material is characterised by having low shear and tensile moduli, as well as low strength. Weinans *et al.* (1990) proposed that the relation between compressive stress and strain could be modelled by

$$\sigma = \frac{E_0}{H}\left\{\frac{1}{\left(1-\varepsilon^e\right)^H} - 1\right\} \quad \text{for } \varepsilon^e > 0 \text{ and}$$
$$\tau = G_0\gamma^e \tag{5.25}$$

where H is a stiffening constant, and E_0 is the compressive modulus at zero strain. The tangent modulus can be found by differentiating the above with respect to the normal strain.

If $\chi_r \le 0$, fibrous tissue formation will proceed and, therefore, the Young's and Shear moduli are given by

$$E = \frac{E_0}{\left(1-\varepsilon^e\right)^{H+1}} \text{ for } \varepsilon^e > 0 \text{ and}$$
$$G = G_0 \tag{5.26}$$

respectively. There is little experimental data available on the shear characteristics of fibrous tissue, therefore, it is assumed that the shear modulus G will be related to the initial compressive modulus E_0 by Equation 5.17.

The thin region comprising the interface material initially has a thickness of h_0. If the interface is stable and bone ingrowth proceeds, the material thickness remains constant, while the mechanical properties evolve according to the extent of bone formation. If there is fibrous tissue formation, the increasing thickness of the fibrous layer is modelled by changing the thickness of the interface region. Therefore, if $\chi_r \le 0$, the layer thickness can be written as

$$h(T) = h_0 + \int_0^T \left|\dot{Q}\right| dt \quad \text{for} \quad |Q| > h_0. \tag{5.27}$$

As no fibrous tissue ingrowth is modelled, the interface will have no bond strength. Therefore the cohesion term $c = 0$, and so the tensile angle $\kappa = 0$.

CHAPTER SIX

NUMERICAL IMPLEMENTATION

6.1 Introduction

In this chapter the implementation of the interface element and the evolution equations, in the context of a finite element program, is outlined. First, the components of the tangent stiffness matrix are described. This is followed by a description of the element formulation, element stiffness matrix and residual vector. The numerical implementation of the evolution equations and the cyclic loading history is then presented. Finally, the implementation of the element equations into the finite element program is outlined.

6.2 The Newton-Raphson Algorithm

The interface formulation will be implemented into a general purpose, non-linear, finite element program which employs a Newton-Raphson solution algorithm. The constitutive model must, therefore, be consistent with the two step iterative solution procedure employed. The first step (the predictor) uses the consistent tangent and residual force vector at the beginning of an iteration, to predict the current increment in nodal displacements. Then, in the corrector step, the displacement increment is separated into the elastic and inelastic parts. These values are then used to update the consistent tangent and the internal nodal loads and hence, the residual force vector for the next iteration. The iterative process is repeated until the residual forces have converged to within a prescribed tolerance. Using this method, the elasto-plastic problem is essentially subdivided into a series of non-linear elastic increments.

Consider the equilibrium of an externally applied load vector $\mathbf{r}_n$ and an internal force vector $\mathbf{f}_n$, at the end of the increment n, in terms of the discretised nodal displacement vector $\mathbf{u}_n$

$$\Psi_n \equiv \mathbf{f}(\mathbf{u}_n) - \mathbf{r}_n = 0, \tag{6.1}$$

where Ψ_n is the *residual* or out-of-balance load vector. Since the internal nodal forces depend non-linearly on the nodal displacements, an iterative solution procedure is required for the solution of Equation (6.1). The iterative procedure starts from an equilibrium state where

$$\mathbf{u} = \mathbf{u}_n,\ \Psi_n = 0 \text{ and } \mathbf{f} = \mathbf{f}_n. \tag{6.2}$$

The out-of-balance force, in general, arises from an increment in the applied load vector, which is assumed to be independent of the nodal displacements

$$\mathbf{r}_{n+1} = \mathbf{r}_n + \Delta\mathbf{r}_{n+1} \tag{6.3}$$

such that

$$\Psi_{n+1}^{(i)} \equiv \Psi\left(\mathbf{u}_{n+1}^{(i)}\right) = \mathbf{f}\left(\mathbf{u}_n\right) - \mathbf{r}_{n+1}, \tag{6.4}$$

where i is the iteration counter. An improved solution is found by taking a first order approximation of Equation (6.4), which is given by

$$\Psi_{n+1}^{(i+1)} \approx \Psi\left(\mathbf{u}_{n+1}^{(i)}\right) + \left(\frac{\partial\Psi}{\partial\mathbf{u}}\right)_{n+1}^{(i)} \delta\mathbf{u}_n^{(i)} = 0, \tag{6.5}$$

and solving for the incremental nodal displacements $\delta\mathbf{u}_n^{(i)}$.

6.3 Tangent Modulus

The Newton-Raphson solution procedure requires the tangent modulus $\mathbf{D}_{n+1}^{*(i)}$, which relates the stress rate to the strain rate, to calculate the tangent stiffness matrix. The stress rate - strain rate relation (Equation 4.6) is written in the incremental form, and making a backward difference assumption, is given by

$$\begin{bmatrix} \Delta\sigma_{n+1}^{(i)} \\ \Delta\tau_{n+1}^{(i)} \end{bmatrix} = \mathbf{D}_{n+1}^{*(i)} \begin{bmatrix} \Delta\varepsilon_{n+1}^{(i)} \\ \Delta\gamma_{n+1}^{(i)} \end{bmatrix}, \tag{6.6}$$

where the components of $\mathbf{D}_{n+1}^{*(i)}$ are given by

$$\mathbf{D}_{n+1}^{*(i)} = \left[\begin{array}{cc} \dfrac{\partial\sigma}{\partial\varepsilon} & \dfrac{\partial\sigma}{\partial\gamma} \\ \dfrac{\partial\tau}{\partial\varepsilon} & \dfrac{\partial\tau}{\partial\gamma} \end{array}\right]\Bigg|_{\varepsilon_{n+1}^{(i)},\gamma_{n+1}^{(i)}}. \tag{6.7}$$

The components of $\mathbf{D}_{n+1}^{*(i)}$ will depend on the region in which the state point lies and the type of interface material.

If the state point lies in the elastic region (Region 3) then

$$\mathbf{D}_{n+1}^{*(i)} = \begin{bmatrix} \dfrac{\partial\sigma_{n+1}}{\partial\varepsilon_{n+1}} & 0 \\ 0 & G \end{bmatrix}. \tag{6.8}$$

If the interface is in contact and sliding, the state point will lie in Region 2 and therefore,

$$\mathbf{D}_{n+1}^{*(i)} = \begin{bmatrix} \dfrac{\partial \sigma_{n+1}}{\partial \varepsilon_{n+1}} & 0 \\ G \tan \psi_{n+1} \operatorname{sgn}\left(\gamma_{n+1} - \gamma_n^A\right) & 0 \end{bmatrix}. \tag{6.9}$$

If the interface is open (Region 1) and contact has been lost, there is no interface stiffness and therefore

$$\mathbf{D}_{n+1}^{*(i)} = \begin{bmatrix} 0 & 0 \\ 0 & 0 \end{bmatrix}. \tag{6.10}$$

The tangent stiffness matrix for the case of interface sliding, given in Equation (6.9), is non-symmetric, requiring the use of a non-symmetric equation solver.

If the material of the interface layer consists of mineralised bone tissue, which is linear elastic, then

$$\frac{\partial \sigma_{n+1}}{\partial \varepsilon_{n+1}} = E. \tag{6.11}$$

However, if the interface material is fibrous tissue, which is non-linear elastic, then it follows from Equation (5.25) that, for $\varepsilon_{n+1}^e \geq 0$,

$$\frac{\partial \sigma_{n+1}}{\partial \varepsilon_{n+1}} = \frac{E_0}{\left(1 - \varepsilon_{n+1}^e\right)^{H+1}}. \tag{6.12}$$

As there is no ingrowth associated with fibrous tissue formation, only compressive strains are possible and therefore $\varepsilon_{n+1}^e \geq 0$.

6.4 Interface Element

Consider two bodies which are separated by a thin layer of material with thickness *h*, as shown in Figure 6.1(a). The two bodies are free to move relative to each other or

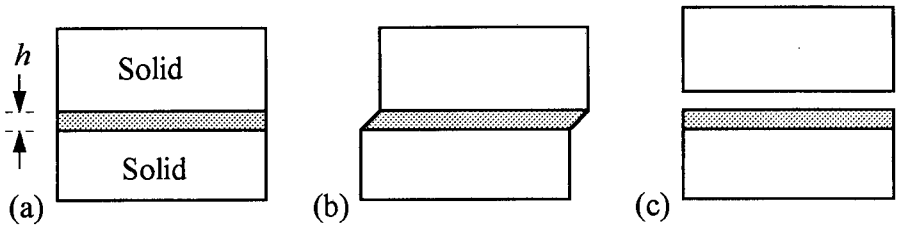

Figure 6.1 (a) Two bodies separated by a thin layer of material. (b) Shear relative displacement (c) Separation.

separate, as shown in Figure 6.1(b) and Figure 6.1(c), respectively. The interface layer is assumed to have physical properties in shear, compression and tension, in the case of the bonded interface. The layer is modelled as a modified joint/layer element. The element is assumed to be compatible with the elements which are used to model the interacting bodies.

The formulation of the isoparametric interface element essentially follows the approach proposed by Desai (1984). The parent element is formulated in the natural co-ordinates ξ-η, and is mapped to cartesian x-y space, as shown in Figure 6.2. The vectors **n** and **s** describe the normal and shear directions in the global co-ordinates, respectively. Nodal displacements in the cartesian x and y directions are given by u and v, respectively.

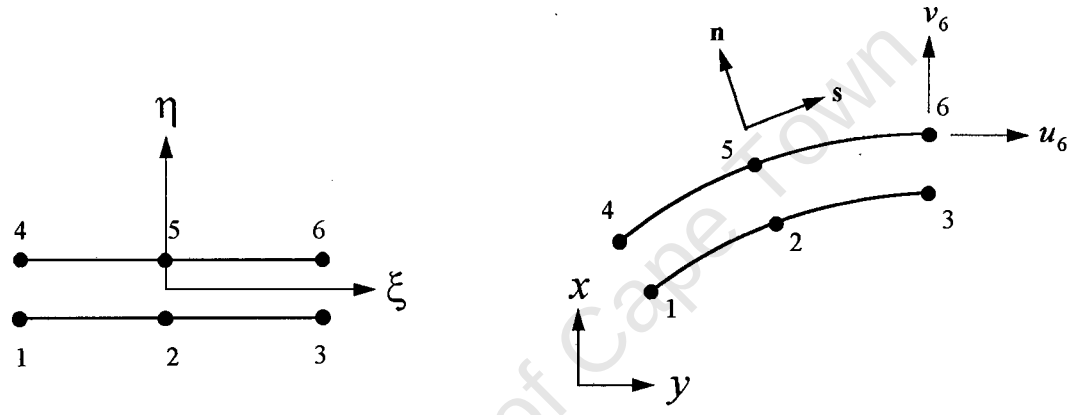

Figure 6.2 (a) Geometry of the reference element and (b) interface element.

The global co-ordinates on the element bottom face are written in terms of the nodal co-ordinates and the shape functions N_k, where $k = 1, 2$ for a linear element and $k = 1, 2, 3$ for a quadratic element. These are given by

$$x_b = \sum_{k=1} N_k x_k = \mathbf{N}_b x_b$$
$$y_b = \sum_{k=1} N_k y_k = \mathbf{N}_b y_b \qquad (6.13)$$

where the shape functions for linear elements are given by

$$N_1 = \frac{1}{2}(1-\xi), \quad N_2 = \frac{1}{2}(1+\xi), \qquad (6.14)$$

and for quadratic elements are given by

$$N_1 = \frac{1}{2}\xi(\xi - 1), \quad N_2 = 1 - \xi^2, \quad N_3 = \frac{1}{2}\xi(\xi + 1). \tag{6.15}$$

In a similar manner, the displacements on the bottom and top face can be written as

$$\begin{pmatrix} u_b \\ v_b \end{pmatrix} = \sum_{k=1} \begin{pmatrix} N_k & 0 \\ 0 & N_k \end{pmatrix} \begin{pmatrix} u_i \\ v_i \end{pmatrix} \tag{6.16}$$

and

$$\begin{pmatrix} u_t \\ v_t \end{pmatrix} = \sum_{k=1} \begin{pmatrix} N_k & 0 \\ 0 & N_k \end{pmatrix} \begin{pmatrix} u_i \\ v_i \end{pmatrix} \tag{6.17}$$

respectively. Since the displacements in the normal and tangential directions to the element surface are needed, a transformation of the nodal displacements is required. The tangential and normal directions are given by

$$\mathbf{s} = \frac{1}{J}\left\{\frac{\partial x_b}{\partial \xi}\mathbf{i} + \frac{\partial y_b}{\partial \xi}\mathbf{j}\right\} \text{ and } \mathbf{n} = \frac{1}{J}\left\{-\frac{\partial y_b}{\partial \xi}\mathbf{i} + \frac{\partial x_b}{\partial \xi}\mathbf{j}\right\} \tag{6.18}$$

respectively, where **i** and **j** are the unit vectors in the x and y directions, respectively, and J is the element Jacobian, which is given by

$$J = \left\{\left(\frac{\partial x}{\partial \xi}\right)^2 + \left(\frac{\partial y}{\partial \xi}\right)^2\right\}^{\frac{1}{2}}. \tag{6.19}$$

The appropriate transformation matrix for a rotation through an angle φ is given by

$$\mathbf{T} = \begin{pmatrix} \cos\varphi & \sin\varphi \\ \sin\varphi & \cos\varphi \end{pmatrix}, \tag{6.20}$$

which can be written in terms of the tangential and normal vectors by

$$\mathbf{T} = \begin{pmatrix} s_x & s_y \\ n_x & n_y \end{pmatrix}. \tag{6.21}$$

The displacements of the top and bottom face, in the transformed co-ordinate system, are then given by

$$\begin{pmatrix} \bar{u}_t \\ \bar{v}_t \end{pmatrix} = \mathbf{T}\begin{pmatrix} u_t \\ v_t \end{pmatrix} \text{ and } \begin{pmatrix} \bar{u}_b \\ \bar{v}_b \end{pmatrix} = \mathbf{T}\begin{pmatrix} u_b \\ v_b \end{pmatrix}, \tag{6.22}$$

respectively. The relative displacements that are normal and tangential to the interface, are calculated by subtracting the displacements of the nodes comprising the top face from those of the bottom face, as follows,

$$\begin{pmatrix}\delta_n\\ \delta_t\end{pmatrix} = \begin{pmatrix}\overline{v}_b\\ \overline{u}_b\end{pmatrix} - \begin{pmatrix}\overline{v}_t\\ \overline{u}_t\end{pmatrix} \tag{6.23}$$

The relative displacements can be written in terms of the cartesian displacements, using the transformation matrix **T** such that

$$\begin{aligned}\begin{pmatrix}\delta_n\\ \delta_t\end{pmatrix} &= \mathbf{T}\left\{\begin{pmatrix}v_b\\ u_b\end{pmatrix} - \begin{pmatrix}v_t\\ u_t\end{pmatrix}\right\}\\ &= \mathbf{T}\left\{\mathbf{N}_b\mathbf{u}_b - \mathbf{N}_t\mathbf{u}_t\right\}\end{aligned} \tag{6.24}$$

which, for a linear element, can be written as

$$\begin{pmatrix}\delta_n\\ \delta_t\end{pmatrix} = \mathbf{T}\begin{pmatrix}0 & N_1 & 0 & N_2 & 0 & -N_1 & 0 & -N_2\\ N_1 & 0 & N_2 & 0 & -N_1 & 0 & -N_2 & 0\end{pmatrix}\begin{pmatrix}u_1\\ v_1\\ \vdots\\ u_4\\ v_4\end{pmatrix}. \tag{6.25}$$

For small strains, and assuming that the strain through the element thickness is uniform, the components of the strain vector, $\varepsilon = (\varepsilon, \gamma)^T$, can be calculated from the relative displacements, such that

$$\varepsilon = \frac{\delta_n}{h} \text{ and } \gamma = \frac{\delta_t}{h}, \tag{6.26}$$

where h is the thickness of the element, as shown in Figure 6.3.

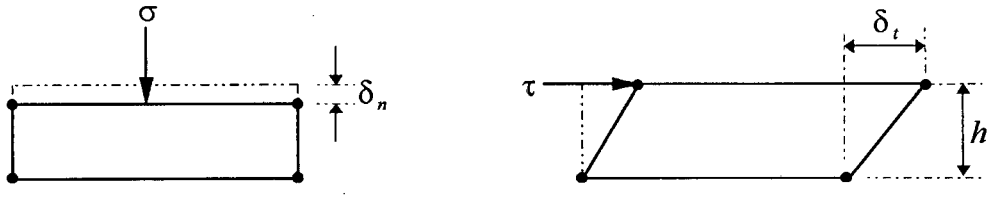

Figure 6.3 Geometric calculation of the normal and shear strain as a function of the relative displacement.

The element strains can now be written in terms of the nodal displacements by formulating the strain-displacement matrix **B,** which is given by

$$\mathbf{B} = \frac{1}{h}\mathbf{T}\left(\mathbf{N}_b - \mathbf{N}_t\right). \tag{6.27}$$

The element stiffness matrix,

$${}^{e}\mathbf{K} = \int_{\Omega} \mathbf{B}^{\mathrm{T}}\mathbf{D}_{n+1}^{*(i)}\,\mathbf{B}\,d\Omega, \tag{6.28}$$

is integrated over the element volume. Therefore, for a two dimensional element, this integration is performed over the element area. However, it has been assumed that the element is sufficiently thin so that the integration through the thickness can be undertaken directly. Therefore, the element is integrated over the length, as a result the stiffness matrix ${}^{e}\mathbf{K}$ is rewritten as

$${}^{e}\mathbf{K} = \int_{l} \mathbf{B}^{\mathrm{T}}\mathbf{D}_{n+1}^{*(i)}\,\mathbf{B}\,h\,ds = \int_{-1}^{1} \mathbf{B}^{\mathrm{T}}\mathbf{D}_{n+1}^{*(i)}\,\mathbf{B}\,J\,d\xi, \tag{6.29}$$

where l is the length of the element.

Similarly, the internal force vector ${}^{e}\mathbf{f}$ is now given by

$${}^{e}\mathbf{f} = \int_{l} \mathbf{B}\,\sigma_{n+1}^{(i)}\,ds = \int_{-1}^{1} \mathbf{B}\,\sigma_{n+1}^{(i)}\,J\,d\xi. \tag{6.30}$$

The integration is undertaken numerically using Gaussian quadrature, with a choice of either full or reduced integration, for both a four and a six noded element. The order of integration is important, and can dramatically effect the solution.

6.5 Evolution of the Interface

During normal daily activity, the articulating joints experience a large number of different loading events, which act over many cycles. Although the time scales of cellular activities are neither well known nor consistent across the population, the typical time scales of bone ingrowth and remodelling are in the order of months or years. During this period, the loading history results in a net remodelling signal (stimulus), which is responsible for the recruitment of osteoblasts to counteract the osteoclastic resorption. A typical life span of osteoblasts, in an adult, is in the order of one to ten weeks (Martin and Burr, 1989). The direct numerical simulation of a typical loading history, designed to capture the effects of bone ingrowth and remodelling, would be impractical, because of both the large number of cycles and the many different activities.

One way of overcoming this difficulty (Huiskes *et al.*, 1987; Carter *et al.*, 1989; Levenston *et al.*, 1994), is to group loading events together so as to produce a single

accumulative stimulus. The period over which the loads are grouped needs to be sufficiently large to incorporate enough loading cycles to be influential, whilst at the same time sufficiently small, so that the assumption of a single stimulus value holds. The period of one day fulfils both of these requirements. The slow response times and inertia in biological systems, permits such an assumption to be made. Therefore, the rate of advancement of mineralised tissue

$$\dot{Q} = B\left\{K_r \int_T \omega\, S(T-t)dt + K_m \int_T \mu\, S(T-t)dt\right\}, \tag{6.31}$$

can be written in a discrete form, by dividing the time interval into individual days, and integrating the loading function over a single day. Therefore, the growth rate is written as

$$\dot{Q}_p = B\left\{K_r \sum_{k=m}^{p}\left(\int_{day\,k} \omega(t)\,dt\right) S_k + K_m \sum_{k=m}^{p}\left(\int_{day\,k} \mu(t)\,dt\right) S_k\right\}, \tag{6.32}$$

where p is the current day, and $m = p - b$ such that b is the number of past days that will contribute towards the current stimulus value. The value of b is determined by the "bandwidth" of the fading memory function $S(T-t)$. The relation $S(T-t)$, which describes the relative contributions of past loading events, is now replaced by a non-dimensional memory weighting factor, S_k for the k^{th} day. The time dependent lag and memory function is given by

$$S(t) = \frac{1}{t} e^{-\frac{t}{\alpha}}. \tag{6.33}$$

The value of S_k must be chosen to satisfy Equation (6.33) and be consistent with the discrete Equation (6.32), so the above is rewritten as

$$S_k = \frac{1}{\Delta t_k (p-k)} e^{-\frac{\Delta t_k (p-k)}{\alpha}}. \tag{6.34}$$

The time scale is in days, and the time increment Δt is chosen to be one day, therefore $\Delta t = 1$. To satisfy the constraint of Equation (5.14), the constant B is evaluated using the discrete form, and is therefore given by

$$B = \left\{\lim_{k\to\infty} \sum_{k=m}^{p} \frac{1}{(p-k)} e^{-\frac{(p-k)}{\alpha}}\right\}^{-1}. \tag{6.35}$$

It is further assumed that the loading cycles are sufficiently closely spaced so that they can be represented by a single load cycle and a weighting factor, to account for the influence of the number of cycles for that load case. Therefore, the total load history for the k^{th} day is divided into d_k loading events, each acting for a number of cycles. In grouping the loading events, it is assumed that the order of application of the load cases does not influence the response. This assumption will hold if the grouping periods are sufficiently small: i.e. jogging is not implemented for six months, followed by walking for three months. The grouping during a day is meaningful, in that during normal activity, loads do tend to get grouped, as a person will naturally walk for some time and then sit and so on. However, in the approach followed, the exact details of the load history will be lost. The total accumulated stimulus value is, therefore, rewritten as

$$\dot{Q}_p = B\left\{K_r \sum_{k=m}^{p}\left(\sum_{j=1}^{d_k} \omega_j\, g(N_j)\right) S_k + K_m \sum_{k=m}^{p}\left(\sum_{j=1}^{d_k} \mu_j\, g(N_j)\right) S_k\right\}, \qquad (6.36)$$

where j refers to the j^{th} loading event, and N_j is the number of cycles of the j^{th} load case. The influence of the j^{th} loading event will depend on the number of cycles for which it acts. To account for this, a weighting factor $g(N_j)$ for each load case is introduced, such that

$$\sum_{j=1}^{d_k} g(N_j) = 1. \qquad (6.37)$$

For example, normal walking will most likely be the most commonly experienced activity, and will therefore carry the highest weighting. If it is assumed that 80% of loading is due to walking, then for this load case $g(N_j) = 0.8$. Activities such as stair climbing will carry lower weightings, such that the restriction of Equation (6.37) is maintained.

The implementation of the memory waiting factor requires that the stimulus values over a "window" period, of the previous b days, are stored as state variables.

The remodelling formulation presented in the previous chapter, assumes that bone formation and resorption will be a function of the peak elastic and inelastic strains experienced during cyclic loading. Therefore, the loading parameters μ_j and ω_j are evaluated at the peak of each loading cycle. This approach inherently includes the assumption that the effect of peak strain is remembered over a short term period of one day, possibly before cellular events have got underway.

The time incrementation is divided into two stages. In the first stage, the d_k load cases are applied incrementally and the inner summation of Equation (6.36) is evaluated. No time is accumulated during this period, as it is assumed that no growth takes place during

loading and unloading. The second stage consists of a growth increment, denoted by p, during which no cyclic load is applied, and the growth parameters are updated. The loading and growth incrementation for three load cases $(d_k = 3)$ is shown schematically in Figure 6.4.

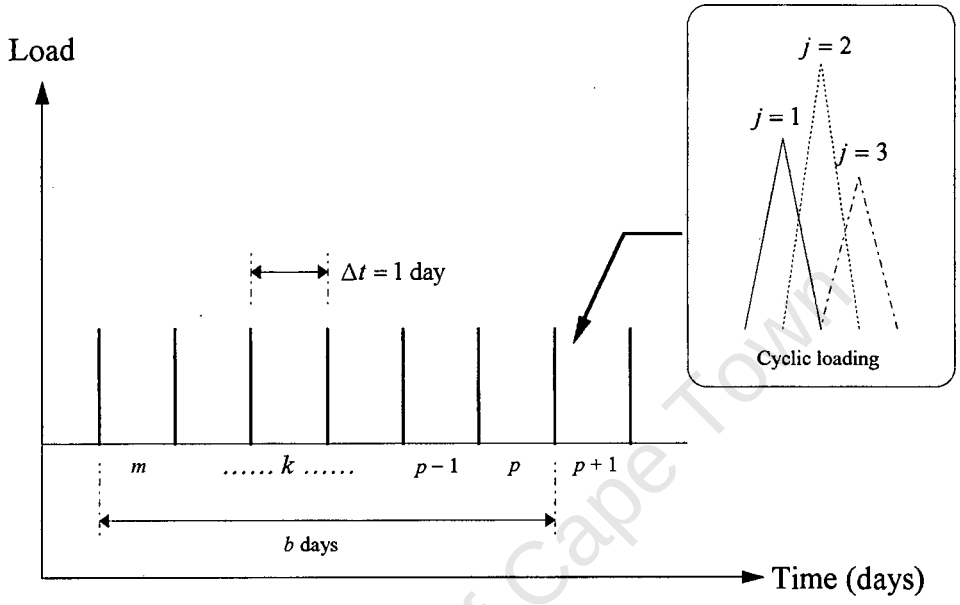

Figure 6.4 Time incrementation for loading and growth.

During a growth increment, the amount of bone ingrowth or resorption is updated, based on the rate formulations presented in the previous chapter. The integration of the bone formation rate, Equation (5.6), is undertaken incrementally using a forward difference method. Therefore, the position of the mineralised tissue surface at the end of the p^{th} day is given by

$$Q_p = Q_{p-1} + \Delta Q_p . \tag{6.38}$$

where

$$\Delta Q_p = \dot{Q}_p \, \Delta t_p . \tag{6.39}$$

The yield surface f, constitutive matrix $\mathbf{D}$, and element thickness h, which describe the interface, are a function of the position of the mineralised tissue surface as follows:

If $-1 \le \hat{Q}_p \le 0$, then the interface material will be undergoing mineralisation before bonding has taken place an therefore

$$\begin{aligned} f(c_p) &= f(c_p = 0) \\ \mathbf{D}_p &= \mathbf{D}_{p-1} + \Delta\mathbf{D}_p \\ h_p &= h_{p-1} \end{aligned} \quad . \tag{6.40}$$

If $0 \le \hat{Q}_p \le 1$, then bone ingrowth will be taking place, resulting in interface bonding, in which case

$$\begin{aligned} f(c_p) &= f(c_{p-1}) + f(\Delta c_p) \\ \mathbf{D}_p &= \mathbf{D}_{p-1} + \Delta\mathbf{D}_p \\ h_p &= h_{p-1} \end{aligned} \quad . \tag{6.41}$$

If $\chi_r < 0$ then there will be resorption of mineralised tissue and the interface region will take on the properties of fibrous tissue, and therefore

$$\begin{aligned} f(c_p) &= f(c_p = 0) \\ \mathbf{D}_p &= \mathbf{D}(\varepsilon^e) \\ h_p &= h_{p-1} + \Delta h_p \end{aligned} \quad , \tag{6.42}$$

where $\mathbf{D}(\varepsilon^e)$ is the constitutive matrix for fibrous tissue.

6.6 Implementation into ABAQUS

The interface element is implemented into the general purpose non-linear finite element program ABAQUS, Version 5.4 (Hibbitt, Karlsson and Sorensen, Inc.). It uses an incremental solution scheme, with a Newton-Raphson solution algorithm, for obtaining solutions at each increment. The program provides the user with a library of subroutines that can be coded by the user. One such subroutine is the user element routine, which allows for the coding of the local element equations.

6.6.1 Incremental Time Stepping

The interface element and material evolution equations are implemented into the generalised incrementation procedure, available in the finite element program. The incrementation is divided into two phases: loading and growth. The general increment n, is either a load/unload increment or a growth increment, in which case it is referred to as increment p. This separation stems from that fact that approximately 3% of time is spent loading, and thus the amount of growth during this time can be considered negligible. During loading and unloading, the time scale has no meaning and is not accumulated, while growth increments are accumulated in terms of days. The general incrementation procedure for $d = 3$ load cases is shown in Figure 6.5.

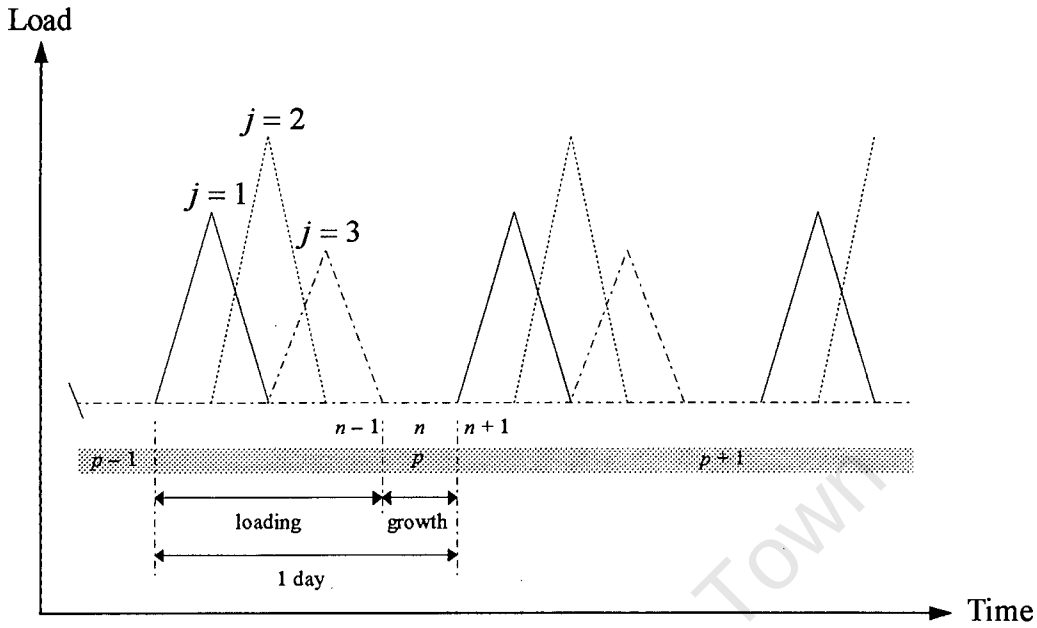

Figure 6.5 Time incrementation within ABAQUS.

6.6.2 Iterative Solution Procedure

For each increment, a Newton-Raphson iterative solution procedure is employed. Within each iteration, the user element routine "interface" provides the values of the nodal displacements at the previous increment $\mathbf{u}_n$ and the increments in nodal displacement at the current iteration $\Delta\mathbf{u}_{n+1}^{(i)}$, as well as the state point information at the end of the previous increment. The user is required to perform all the relevant element calculations for use by the program. These are the element stiffness matrix ${}^{e}\mathbf{K}_{n+1}^{(i)}$, and the residual force vector $\Psi_{n+1}^{(i)}$. The program carries out the assembly and equation solution operations. The state variables, which contain state point information (stresses, strains and evolution information), are recorded to be available. The calculations to update this information must also be carried out.

The stiffness matrix ${}^{e}\mathbf{K}_{n+1}^{(i)}$ and the internal force vector ${}^{e}\mathbf{f}_{n+1}^{(i)}$ are updated according to Equations (6.29) and (6.30), respectively and passed back to the program. These are then used to assemble the global stiffness matrix $\mathbf{K}_{n+1}^{(i)}$ and force vector $\mathbf{f}_{n+1}^{(i)}$, which are used to predict the next displacement increment vector by

$$\delta\mathbf{u}_{n+1}^{(i)} = \left[\mathbf{K}_{n+1}^{(i)}\right]^{-1}\left[\mathbf{r}_{n+1} - \mathbf{f}_{n+1}^{(i)}\right], \tag{6.43}$$

where the full increment in displacement and total displacements are given by

$$\Delta \mathbf{u}_{n+1}^{(i)} = \sum_{r=1}^{i} \delta \mathbf{u}_{n+1}^{(i)} \text{ and } \mathbf{u}_{n+1}^{(i)} = \mathbf{u}_n + \Delta \mathbf{u}_{n+1}^{(i)}, \tag{6.44}$$

respectively. This information is then passed back to the user element subroutine, and the process continues until the maximum component of the residual vector $\Psi_{n+1}^{(i)}$ is within a prescribed tolerance, after which the solution is regarded as converged and the next load increment begins.

CHAPTER SEVEN

EXAMPLE PROBLEMS

7.1 Introduction

In this chapter a series of applications of the interface element are examined. The objective of these applications is to illustrate the capabilities of the element formulation. The first example is that of a simple wedge being forced between two blocks. The purpose of this example is to compare the Coulomb model used in the thin element formulation with the mixed method used in ABAQUS. The normal and shear stress magnitudes along the interface have been compared, however, issues such as accuracy and convergence have not been addressed here. No interface remodelling or fracture is examined in this problem.

The first example serves primarily to verify the present interface element against the well accepted formulation used in ABAQUS. The subsequent two examples address problems in biomechanics. The first problem examines bone ingrowth and fibrous tissue formation around a cementless tibial tray component, used in a primary knee replacement. Only the tibial portion of the replaced joint is examined, as it is in this component where loosening is most common. In this analysis, two scenarios have been considered: in the first case a rest period is simulated and the slip threshold for fibrous tissue formation is included. In the second case, no rest period is included and the slip threshold is set to zero, simulating the "worst case" for fibrous tissue formation.

Subsequently, bone ingrowth and fibrous tissue formation around the *PCA* (Houwmedica, Inc.) femoral component are predicted. As in the previous example, two simulations have been undertaken: with and without a rest period, however, in both cases a slip threshold has been included. Before these two models are presented, a simple displacement history is implemented and the subsequent repair stimulus response is shown. This example illustrates the influence of the time constant on the memory formulation.

The interface evolution, and the finite element models of the reconstructed joints, contain a large number of parameters which will influence the load response of the joint, as well as the evolution of the interface tissues. The parameters which have been examined, and the results which have been presented in this chapter, are limited to only those aspects which are thought to be most important in understanding the evolution, and mechanics of the reconstructed joints.

7.2 Verification of Coulomb Model

By examining the displacement of a wedge embedded between two blocks, the thin interface element is compared to a standard interface element from the ABAQUS library. The ABAQUS element uses a mixed formulation, where the normal contact is explicitly enforced by using a method of Lagrange multipliers. The shear behaviour is governed by an elastic-plastic formulation. The base of the two blocks is fixed, while the interface between the two blocks, and the interface between the wedge and the blocks is modelled using the thin interface element. The geometry of the wedge and the blocks are modelled with four noded plane strain elements, which can be seen in Figure 7.1. A pressure of 10MPa is applied to the two outer vertical sides of the blocks. The top face of the wedge is displaced downwards by a distance of 0.1mm. The through thickness of the thin element may have an influence on the stresses at the interface. Therefore, two element thickness values have been investigated: 1.0 and 0.5mm. In this example the thickness of the element has no meaning, however, in the later examples of joint replacement, the thickness is intended to represent a layer of interface material.

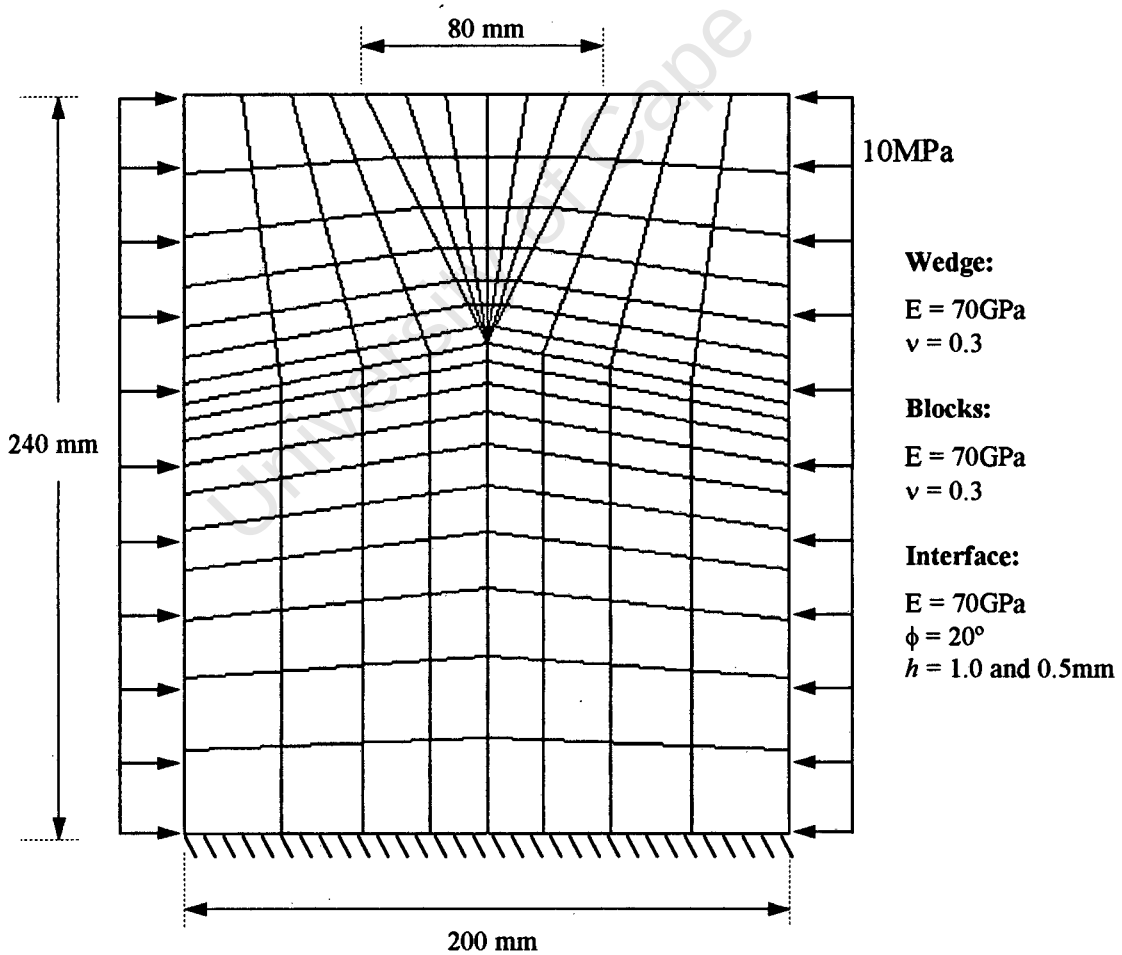

Figure 7.1 The displacement of a wedge between two blocks.

The normal and shear stresses along the length of the interface, using the two element formulations, are shown in Figures 7.2 and 7.3, respectively. The results are only shown for one side of the wedge, as the deformation is symmetric about the centre line. The boundary condition at the base of the blocks maintains the contact of the interface at this point. Above the boundary, the pressure reaches a peak of approximately 8MPa, however, in this region there is no elastic shear relative displacement at the interface, and *hence* no shear stress. Further up the interface has opened, as a result of the downward displacement of the wedge, and therefore in this area there is no normal pressure and hence no shear stress. A peak value of normal pressure occurs at the tip of the wedge. At this point the ABAQUS element produces a peak pressure of approximately 58MPa, while for both thickness values of the thin element, the peak contact pressure is approximately 53MPa. The opposite trend is noted for the shear stresses, where the peak magnitude using the ABAQUS element is 14MPa, compared to 19MPa when using the thin element. The discrepancy in the stresses is attributed to the possible differences in the magnitude of the shear stiffness term. On the sides of the wedge the pressure is in the region of 20MPa, for both element formulations, and for each value of element thickness. However, at the top of the wedge, the peak pressures for the ABAQUS and the thin element formulation are 30 and 36MPa, respectively. At this point the peak shear stress when using the thin element is 13MPa compared to 11MPa obtained using the ABAQUS element.

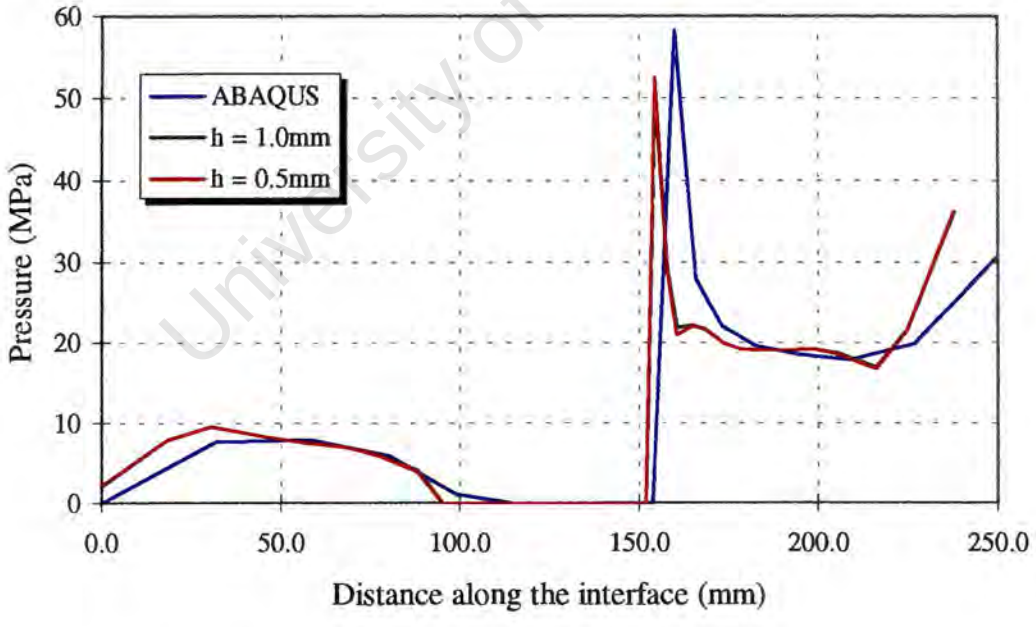

Figure 7.2 Interface pressure comparing an ABAQUS element to the current formulation, for different values of element thickness.

For the two values which have been examined, the thickness of the interface element has had little influence on the normal and shear stress magnitudes or distribution, along the

length of the interface. However, a larger variation of the element thickness may have a more dramatic effect on the solution.

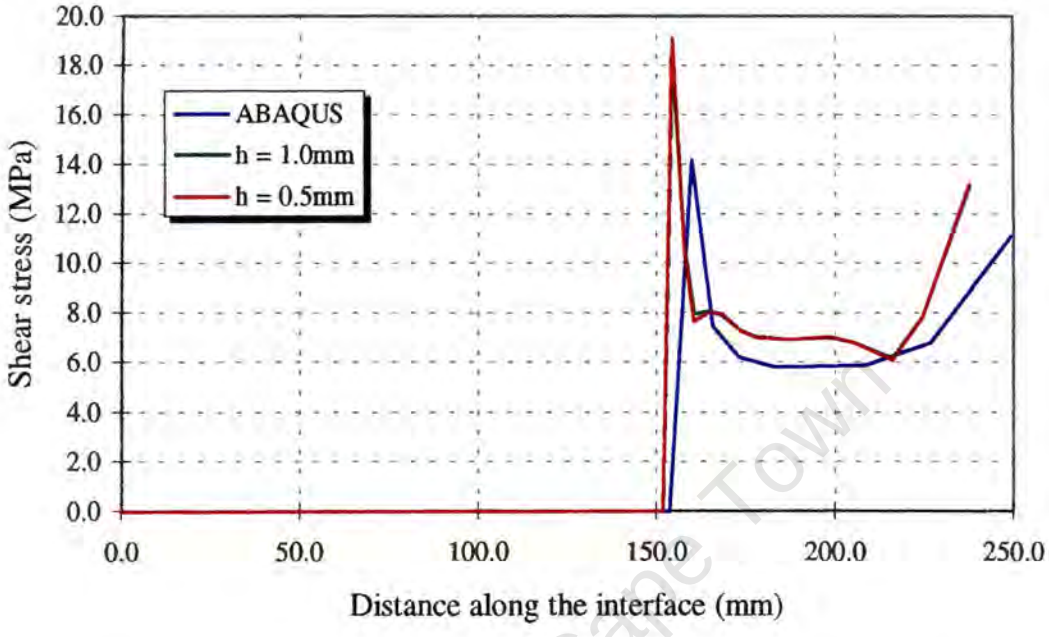

Figure 7.3 Interface shear stress comparing an ABAQUS element to the current formulation, for different values of element thickness.

7.3 Stimulus History

The influence of the memory function on the repair stimulus parameter, χ_r, is illustrated by a simple three element model, which is shown in Figure 7.4. The positions of the two integration points of the interface element (shaded) are shown by the crosses (+). The stimulus for bone and fibrous tissue formation is demonstrated by applying cyclic displacements to the bead element of the model. Bone tissue formation is simulated when the displacement magnitude is set to 25μm, while bone withdrawal and fibrous tissue formation is simulated by applying a displacement of 250μm, as shown in the figure. In the second test, the displacement magnitude is returned to 25μm after 80 days in order to demonstrate the decay of the function. For both displacement magnitudes, a pressure of 0.5MPa is applied to the surface of the bone element to simulate implant press-fit. The memory function is examined for time constants of $\alpha = 1$, 4 and 7 days. The total period for which a loading event will have an influence on the stimulus is approximately 8α, and therefore the corresponding memory times are 8, 32 and 56 days.

Figure 7.5 shows the value of the repair stimulus coefficient, χ_r, as a function of the growth time, at the first integration point. As a result of the boundary conditions, the elastic strain and inelastic relative displacements at the first point are considerably less

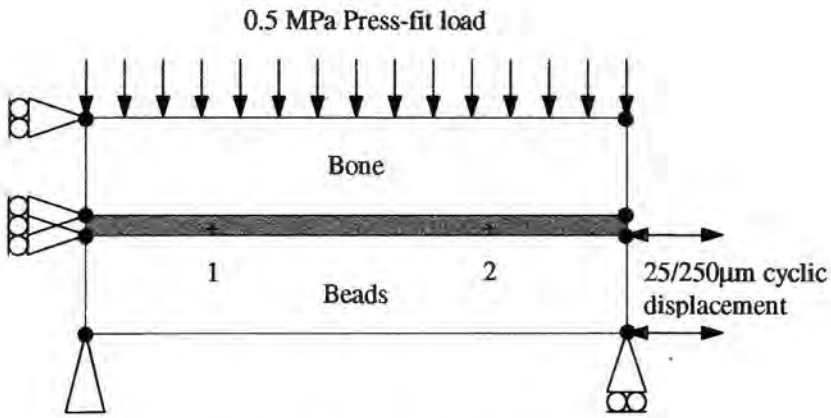

Figure 7.4 Simple model for bone ingrowth and fibrous tissue formation.

than those at the second. The smaller displacements at this point enable the repair process to continue. For each magnitude of the time constant α, the stimulus coefficient reaches a value slightly less than one. When the time constant is 1 day, the peak stimulus value is reached after approximately 14 days, while this value is reached at approximately 40 and 60 days, respectively, when the time constant is 4 and 7 days. This result illustrates the importance of the time constant in the short time, but with constant loading over a longer period, the memory function has no influence on the value of the stimulus coefficient. The value of the time constant may therefore be important in determining the path of interface repair.

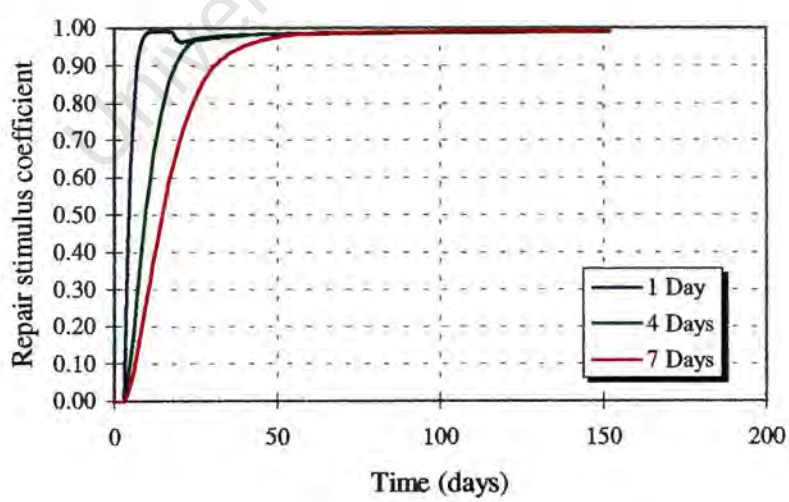

Figure 7.5 Repair stimulus coefficient, χ_r, for small cyclic displacements (25μm), with the time constant α equal to 1, 4 and 7 days.

In the second analysis, the displacement of the bead elements is increased to 250μm when $t < 80$ days and 25μm when $t \geq 80$ days. The bigger displacement results in large inelastic displacements at both integration points. The resultant repair stimulus coefficient at the second integration point is shown in Figure 7.6. As a result of the large displacements, the repair process does not result in the mineralisation of the interfacial tissue, but rather causes a withdrawal of the surrounding bone tissue, which is replaced with fibrous tissue. The value of the stimulus coefficient is therefore negative. As in the previous example, in the long term, the stimulus reaches a constant value of -1.0. However, the time constant influences the time required to reach this magnitude. When the displacement is reduced, a time constant of one day results in an immediate reduction in the stimulus value. However, with a larger time constant the reduction in stimulus is not experienced immediately and hence the response time is again increased. Again, the importance of the memory function and time constant has been shown for fluctuating loading conditions.

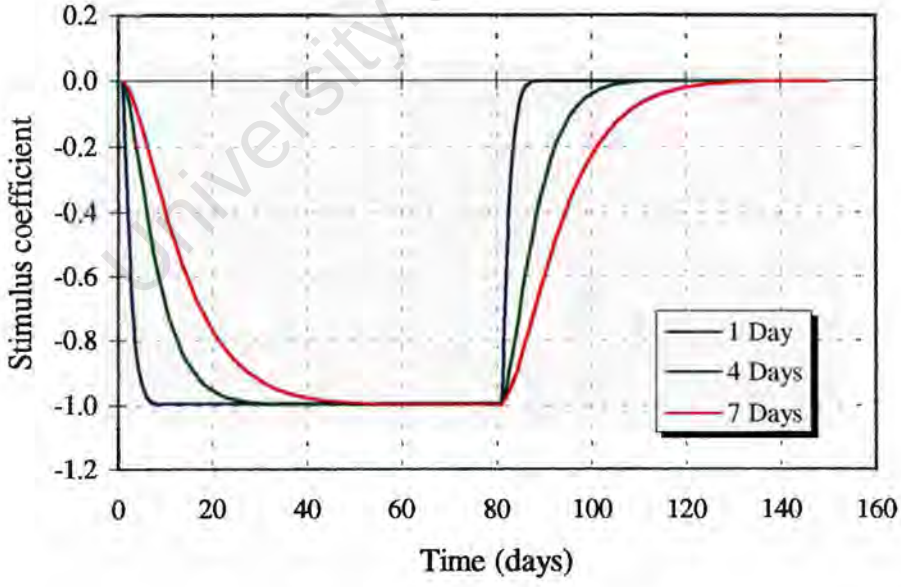

Figure 7.6 Repair stimulus coefficient, χ_r, for cyclic displacements of 250μm when $t < 80$ days and 25μm when $t \geq 80$ days. The time constant α is equal to 1, 4 and 7 days.

7.4 Examples of Interface Evolution

The numerical model of the interface evolution incorporates many empirical constants, whose values are not known exactly. The formulation has been kept as simple as possible in order not to introduce unnecessary constants, for which approximate values may not be available. In the example problems presented, the initial thickness of the interface material h_0 has been set to 0.1mm. The depth of the porous coating was measured from a sectioned and polished specimen of the *PCA* (Houwmedica, Inc.) femoral stem, and found to be approximately 1.5mm. Therefore, the porous coating thickness, a_0, is kept constant at the measured value. Rancourt *et al.* (1990) experimentally measured the friction coefficient ($\tan\phi$) between cancellous bone and a porous coating, which they found to range between 0.4 and 0.8. The influence of friction angle is examined by analysing values of 21.80° (0.4), 30.96° (0.6) and 38.66° (0.8). Once bone tissue begins to form within the surface porosity, a cohesive and adhesive bond will develop. The ratio of the cohesive to the adhesive bond strength is given by the *tan* of the tensile angle κ. While this ratio may be a function of the extent of bone ingrowth Q, as a result of the lack of experimental data, it is assumed to be constant. Therefore, the tensile strength of the bond, as a result of bone ingrowth, will always be half the developed shear strength, and subsequently $\tan\kappa = 2$.

Empirical values are required for the rates of repair mineralisation, fibrous tissue formation, and remodelling. In the present formulation, the daily and total stimulus values have been normalised, so that the rate constants of bone growth or removal can be taken from experimental data. The required rate constants are: the rate of tissue mineralisation due to repair activity K_r^+, the rate of fibrous tissue formation, K_r^- (corresponding to the removal of mineralised tissue) and the rate of bone formation, or removal, as a result of bone remodelling K_m. In addition to the rate constants, the level to which interface strains will influence tissue development will be determined by the parameters used in the formulation of the repair and the remodelling equations.

The optimal equivalent strain value, and the width of the *dead zone*, have been based of the experimental finding of Lanyon and Rubin (1984) and Rubin and Lanyon (1985) and therefore $\bar{\varepsilon}_0$ = 2000μstrain and S is assumed to be 0.5, which means that bone loss will take place if the equivalent strain value drops below 1000μstrain, and bone addition will proceed if the equivalent strain increases to above 3000μstrain. Experimental evidence (Pilliar *et al.*, 1986 and others) suggests that fibrous tissue formation will proceed when shear relative displacements are in excessive of approximately 20μm, which corresponds to an inelastic threshold strain value of $\gamma_{th}^{p} = 20/h$. However, fibrous tissue formation may proceed with smaller values of relative displacement, therefore, the knee example has been used to examine the influence of this threshold value on the subsequent extent of fibrous tissue formation. While the choice of this value will influence when fibrous tissue will begin to form, the magnitude of the constants C_r and K_r^-, which will determine the rate of fibrous tissue formation, are held constant for both example problems.

7.4.1 Total Knee Replacement

The forces in the knee joint reach a peak at approximately 50% of the gait cycle; where the cycle is initiated at heal strike. At this point – which is known as the *single-legged-stance* phase of the gait cycle – the body is momentarily in an equilibrium position where the line of action of the ground reaction force is shifted over to the side of the swinging leg. Estimates of the joint reaction loads at this moment range from two to seven times body weight (*BW*), during normal walking (Morrison, 1970; Harrington, 1976; Paul, 1976). However, Rydell (1966) indicated that loading across a reconstructed joint can be expected to be lower than normal. There is some conflicting evidence as to whether, in this loading condition, more load is applied to the larger medial condyle, or whether the load is shared equally between the condyles. Maquet (1976) concluded that the knee joint force was evenly distributed between both medial and lateral tibial plateaux; however, this conclusion has not been validated either theoretically or experimentally. From the analyses by Morrison (1970) and Kettlekamp and Chao (1972) it is evident that most of the knee joint force would pass through the medial compartment during walking.

A plane strain finite element model of the mid-frontal plane of the reconstructed knee joint has been developed, and is shown in Figure 7.7. At the mid-stance of the gait cycle the greatest forces in the joint are the reactions on the condyles. The mid-frontal plane is chosen in order to consider each of the condyle reactions. For this reason, most two dimensional models have been analysed by considering this section (Askew and Lewis, 1981; Shrivastava *et al.*, 1982; Murase *et al.*, 1983; Vasu *et al.*, 1986). Only the tibial component has been modelled, as it is in this half of the joint that mechanical loosening is most commonly reported. As the forces in the reconstructed joint are expected to be lower than in the intact joint, a total load value of 2100N ($3XBW \approx 2100N$), which is near the lower end of the experimentally observed range, was chosen. To overcome the controversy regarding the distribution of the load on the lateral and medial condyles, two load cases have been considered: one in which this load is shared equally between the condyles, and one in which two thirds of the force is transmitted through the medial compartment. Furthermore, it is assumed that the two load cases act for the same number of cycles, and therefore carry equal weighting. No muscle or ligament forces have been considered. There are other important load cases on the knee which occur during flexion of the joint, but these have not been examined in the present model. The boundary conditions at the distal end of the model constrain the tibia from movement in the vertical direction, while allowing expansion and contraction of the cortex.

Isotropic material properties have been assumed for the cortical and cancellous bone, with the mechanical constants taken from the literature (Williams and Lewis, 1982; Lewis *et al.*, 1982). The implant is assumed to be made of a steel alloy, which will have a modulus of approximately 200GPa, and subsequently the modulus of the porous coating will be in the region of 100GPa. The orange and green shading on the figure indicate the areas of cancellous and cortical bone, respectively, while the tibial implant is shaded in grey. The porous coating is indicated in red. The material and interface properties of the various regions, as well as some of the evolution constants, are shown adjacent to the figure.

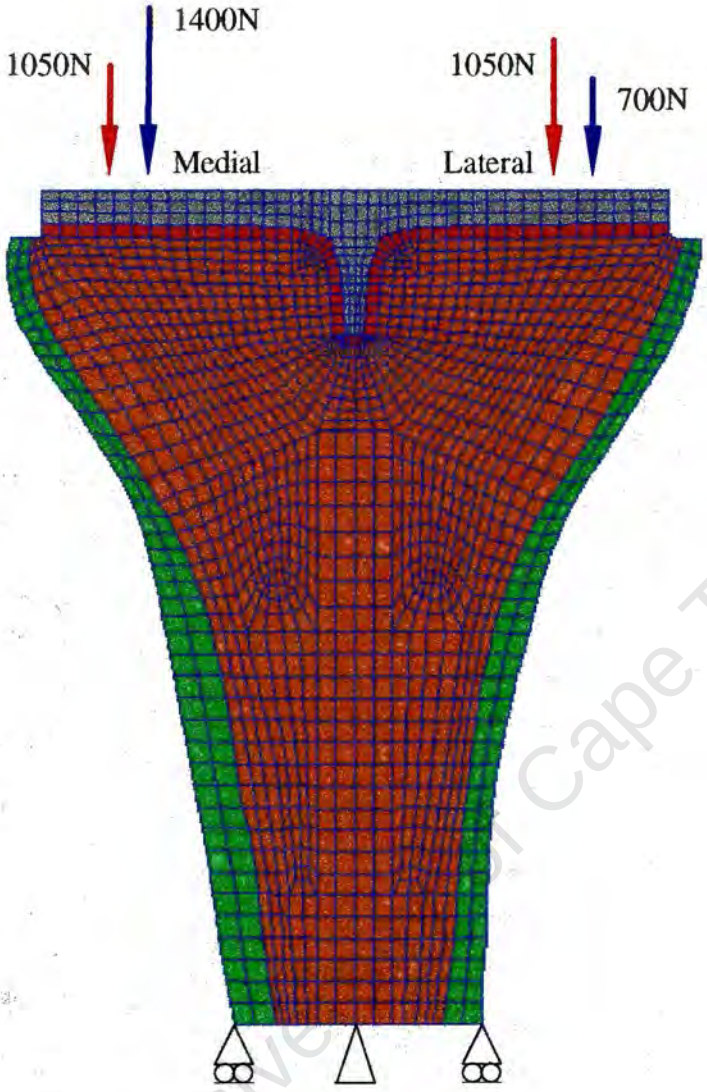

Material Properties:

$E_{implant}$ = 200GPa
E_{beads} = 100Gpa
$E_{cortical}$ = 15GPa
$E_{cancellous}$ = 1.5GPa
$\nu = 0.3$

Interface Properties:

h = 0.1mm
a_0 = 1.5mm
E_s = 100MPa
E_c = 1.5GPa
E_b = 15GPa
ν_s = 0.46
ν_c = 0.3
E_0 = 100MPa
H = 3
m = 3

Evolution Constants:

K_r^+ = 80μm/day
K_r^- = 40μm/day
K_m = 80μm/day
p = 3
α = 4

Figure 7.7 Finite element model of knee replacement showing the two load cases, boundary conditions and material regions.

The interface model was used to predict bone ingrowth and fibrous tissue formation on the porous coating which covers the underside of the tibial component. For the initial unbonded interface, Figure 7.8 and Figure 7.9 show comparisons of the normal and shear stress, respectively, with a standard ABAQUS interface element. The horizontal axis of the graphs denotes the distance (medial to lateral) along the interface. The knee is uniformly loaded, simulating the first load case. As the Lagrange multiplier method, used by ABAQUS, ensures that the contact is enforced exactly, the peak pressures (in the central region under the post) with the ABAQUS element are slightly greater than those predicted with the penalty method, used in the thin element. However, in regions of lower pressure, the results are very similar. The opposite trend is noted in the path plot of the shear stress. Here, the peak shear stresses predicted with the thin element are

slightly larger than those found with the ABAQUS element. This finding may be due to a greater stiffness term used in the thin element formulation.

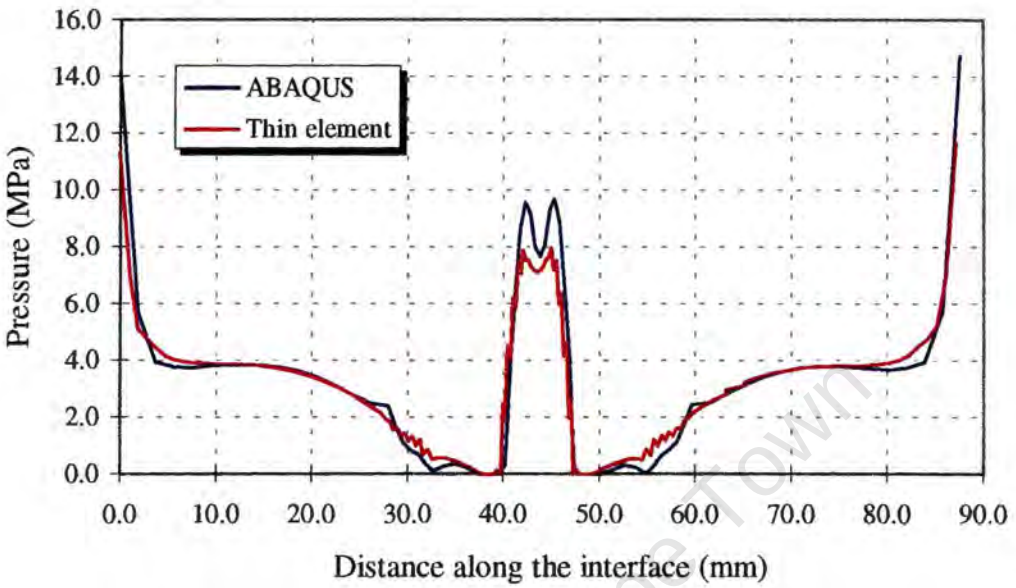

Figure 7.8 Comparison of the normal stress along the length of the interface using an ABAQUS element and the thin element.

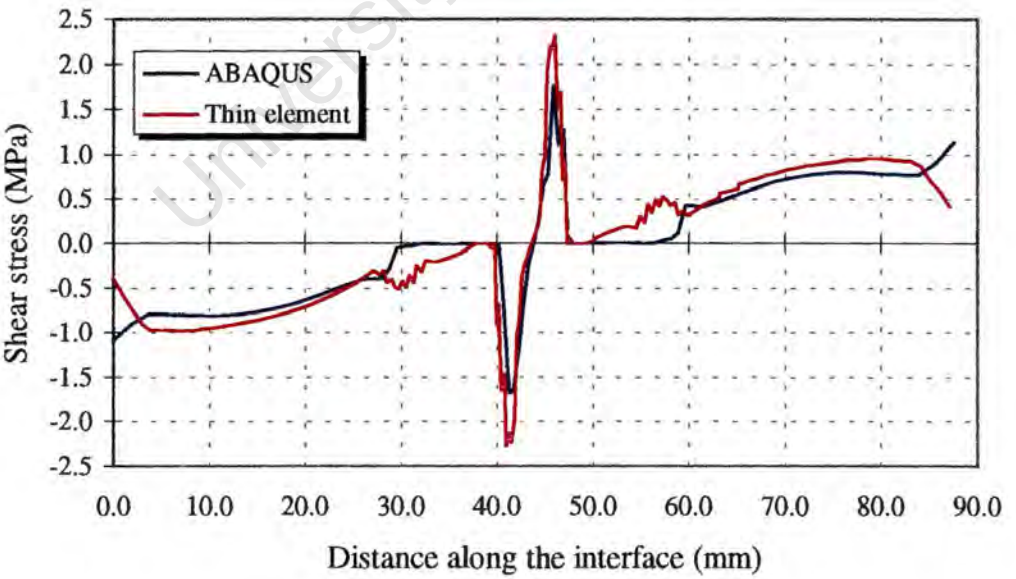

Figure 7.9 Comparison of the shear stress along the length of the interface using an ABAQUS element and the thin element.

The reconstructed knee example is used to examine the influence of certain of the parameters on the resultant interface tissue response. The parameters which have been examined are: the influence of the rest period, the friction angle and the value of the relative displacement threshold. The extent of the rest period may be crucial in determining the success of the reconstruction. No rest and a period of 14 days has been examined. When no rest period is simulated, the full load is applied immediately, simulating a "worst case" situation for fibrous tissue formation. Based on the experimental findings of Rancourt *et al.* (1990), friction coefficient values of 0.4, 0.6 and 0.8 (corresponding to ϕ equal to 21.80°, 30.96° and 38.66°, respectively) have been used in a parametric analysis. While it has been shown experimentally that relative displacement will result in fibrous tissue formation, the value of the threshold γ^{p}_{th} is unclear. Therefore, a value of zero and 20μm has been analysed.

Figure 7.10 shows the normalised position of the mineralised tissue surface ($\hat{Q}$) from left to right (medial to lateral) along the interface, after 40, 100, 150 and 200 days. The inserted figure shows five positions (A, B, C, D, E) on the surface of the tibial component, which are indicated on the distance axis of the graph. This representation has been included for all interface results of the knee model. In this analysis, the rest period has been set to 14 days and the slip threshold to 20μm. After 40 days, which is approximately the time when the repair activity ceases, the majority of the interface area has been fully ingrown. However, the growth pattern is not completely uniform as the long term growth configuration has already been established. The ingrowth predictions indicate that the strains, once loading began, where not sufficient to have a significant effect on the rate and extent of repair activity. However, once the repair activity ceased, and the interface was controlled by remodelling, the strains over the majority of the interface region were not sufficient to sustain the bone ingrowth pattern.

By 100 days the growth pattern had completely changed, with a large scale removal of bone tissue in all areas, except at the base of the post (position C). The extent of mineralised tissue after 200 days varies considerably along the length of the interface. At the outer edge of the medial condyle, the large elastic strains, and absence of inelastic displacement, have resulted in an almost fully integrated surface. It would appear that this growth region has protected the adjacent regions from elastic strains, causing a complete withdrawal of interface tissue by 200 days. However, under the medial condyle the large normal forces have provided sufficient stimulus to maintain approximately 30% ingrowth over the majority of the condyle area. As a result of the eccentric loading, there is less stimulus on the lateral condyle and therefore the remodelling activity has resulted in an almost complete withdrawal of bone in this area. Beneath the lateral condyle, after 100 days the extent of ingrowth was down to 20%, and subsequently to almost zero by 200 days. In a similar manner to the medial side, there is some ingrowth at the outer surface of the tibial tray. This growth in most likely maintained by the high normal pressure which is experienced at the outer edges during the two loading situations. This small amount of ingrowth may be an "edge effect" in the numerical model, and may not represent a realistic situation.

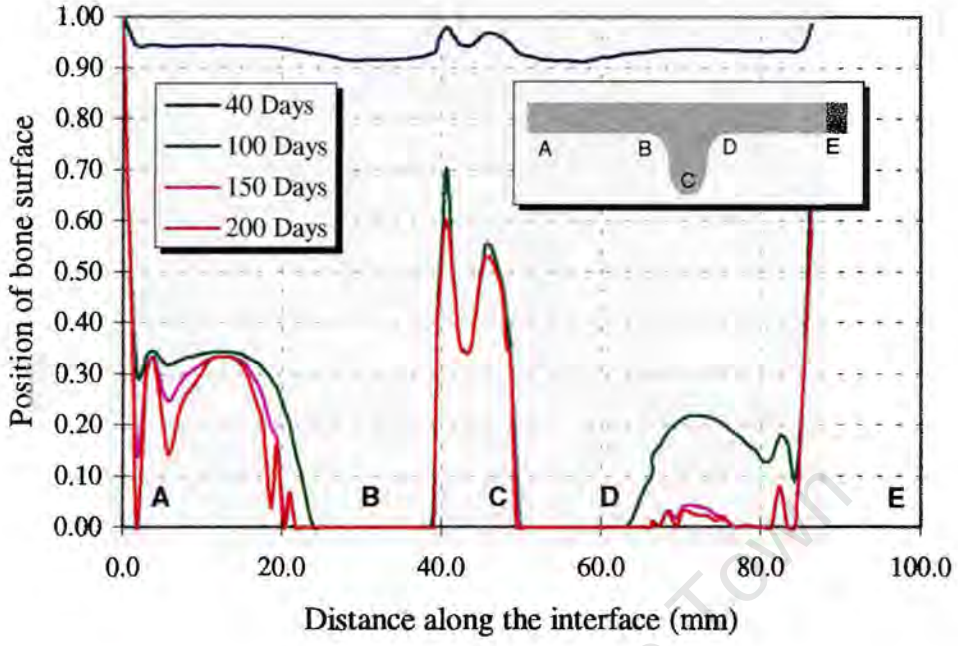

Figure 7.10 Resultant interface tissue formation after 40, 100, 150 and 200 days for γ_{th}^{p} equal to 20μm and a rest period of 14 days.

On the near vertical edges of the central post, the remodelling activity has caused a withdrawal of the mineralised tissue, resulting in a reduction of the bond strength. Subsequently, the shear forces have caused fracture of the tissue on these surfaces. Therefore, on either vertical side of the post there is no ingrowth by 100 days. At the base of the post, large forces are transmitted without any inelastic relative displacement. This has resulted in between 50 and 70% bone ingrowth in this area. It is interesting to note that growth has been predicted on the outer edges of the base of the post, with less tissue development towards the centre.

Figure 7.11 shows that the friction angle (21.80°, 30.96° and 38.66°, corresponding to friction coefficient values of 0.4, 0.6 and 0.8, respectively) has had little influence on the ingrowth pattern after 200 days. When the joint is loaded, and the entire interface region is not bonded, the friction angle will have a large influence on the amount of relative displacement. However, in this example where a rest period has been simulated, the friction angle can only influence the longer term solution, as by the time loading begins, the entire interface region has developed some bond strength. If, however, fracture occurred at the start of loading, the friction angle may influence subsequent fracture in other regions and hence the extent of ingrowth. In this solution, the fracture appears to have been limited to the sides of the post.

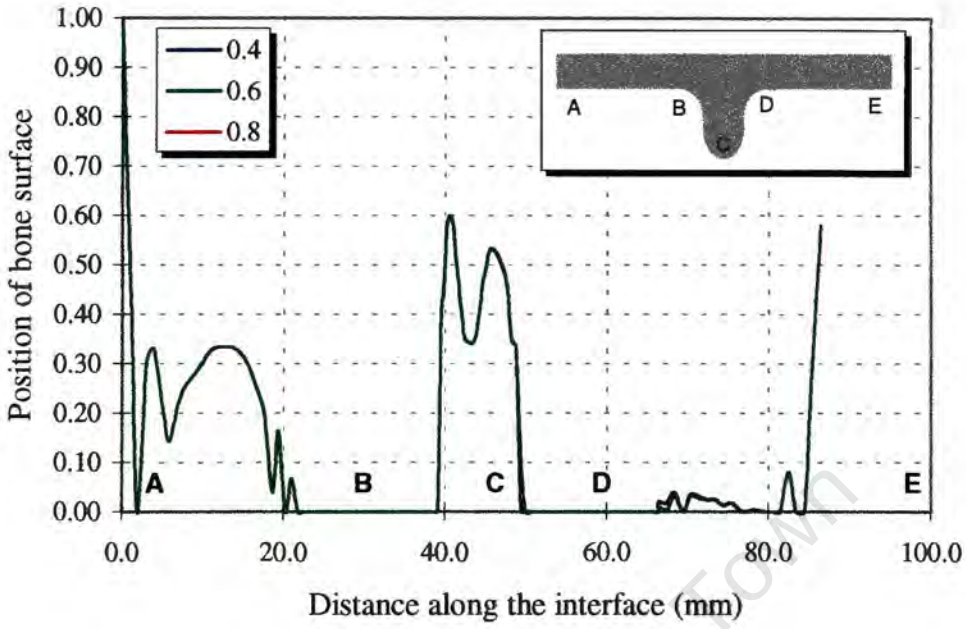

Figure 7.11 Resultant interface tissue formation after 200 days for friction angles of 21.80°, 30.96° and 38.66°.

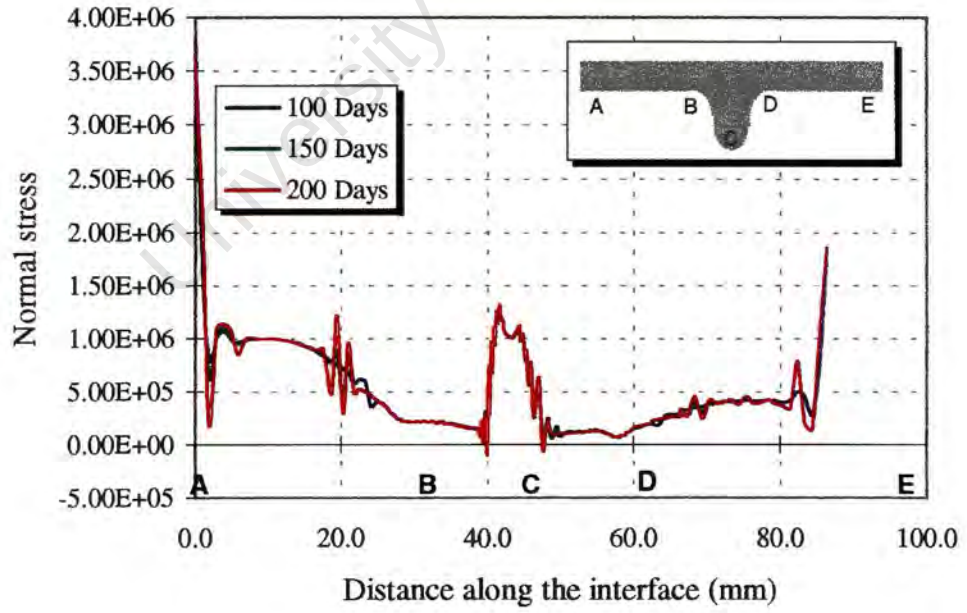

Figure 7.12 Interface normal pressure distribution after 100, 150 and 200 days for the eccentrically distributed load.

The normal and shear stress distributions along the interface, for the eccentric load case, are shown in Figure 7.12 and Figure 7.13, respectively, after 100, 150 and 200 days. The magnitude and distribution of the normal stress has been altered only marginally from the initial, unbonded, condition. Except that by 200 days, the oscillations which began to appear after 150 days have become more severe. After 200 days, the shear stress transfer has shifted so that a greater portion of the load is transferred through the central post. In the early period (less than 100 days) the load transfer is smooth. However, as the growth pattern becomes more erratic, so too does the transfer of shear stress; which is seen by the oscillations, which increase in magnitude after 150 and 200 days.

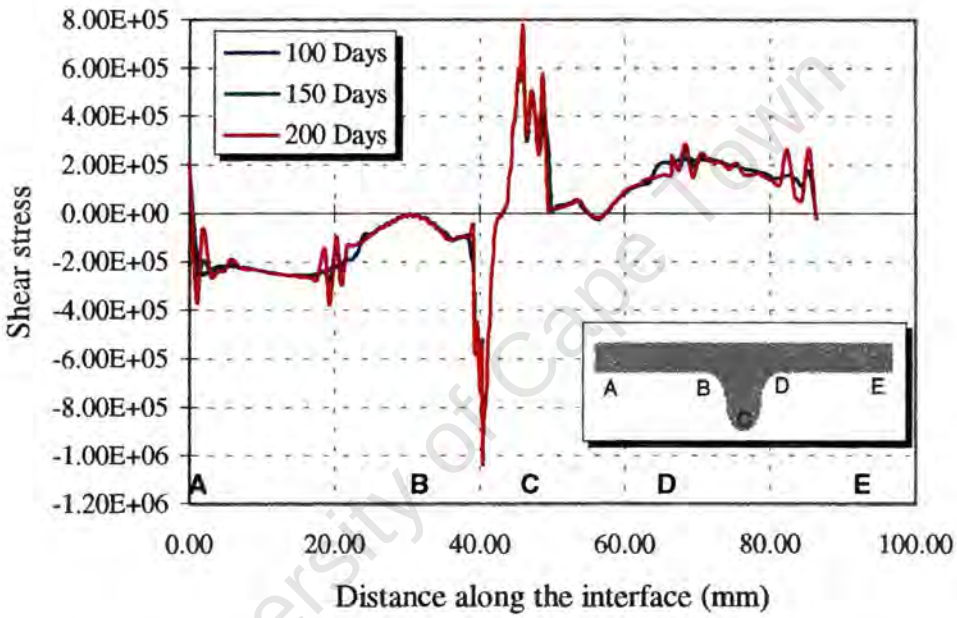

Figure 7.13 Interface shear stress distribution after 100, 150 and 200 days for the eccentrically distributed load.

The tissue evolution rate is shown at various positions along the interface, which are indicated in Figure 7.14. Although the tibial tray geometry is symmetrical, the asymmetrical loading and bone geometry necessitates the recording of positions on each side of the tray. Figure 7.15 shows the growth rate of mineralised tissue, plotted for the first 100 days, at 11 positions which are distributed along the interface region. Initially, the growth rate is positive and very similar for the 11 points, which occurs as a result of the repair activity, that takes place during the simulated bed rest. As soon as the repair growth has been completed, and the interface is governed by the remodelling processes, bone tissue is lost at all the positions recorded. The most rapid loss of bone occurs on the sides of the central post (3 - 5 and 7 - 9), and beneath the condyles (1 - 2 and 10 - 11). The lowest rates of bone loss occur at positions 5, 6 and 7, which are at the base of the post.

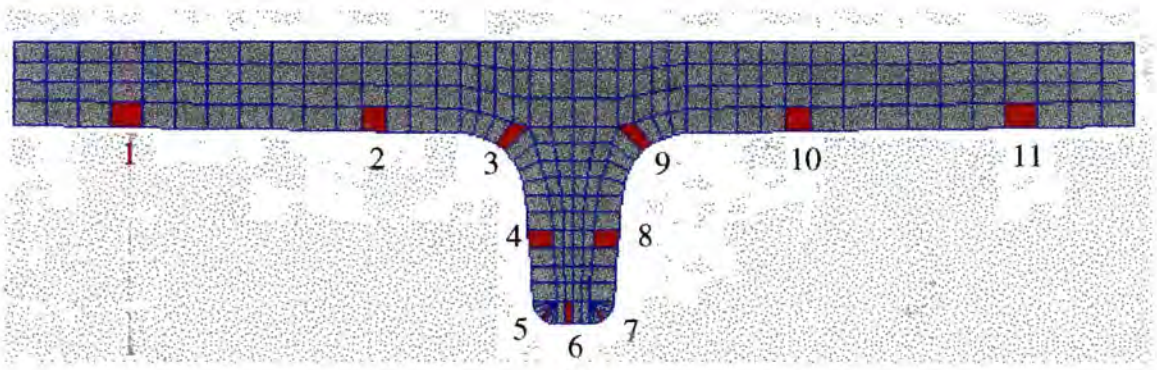

Figure 7.14 Positions (shown in red) along the interface at which tissue evolution variables are plotted.

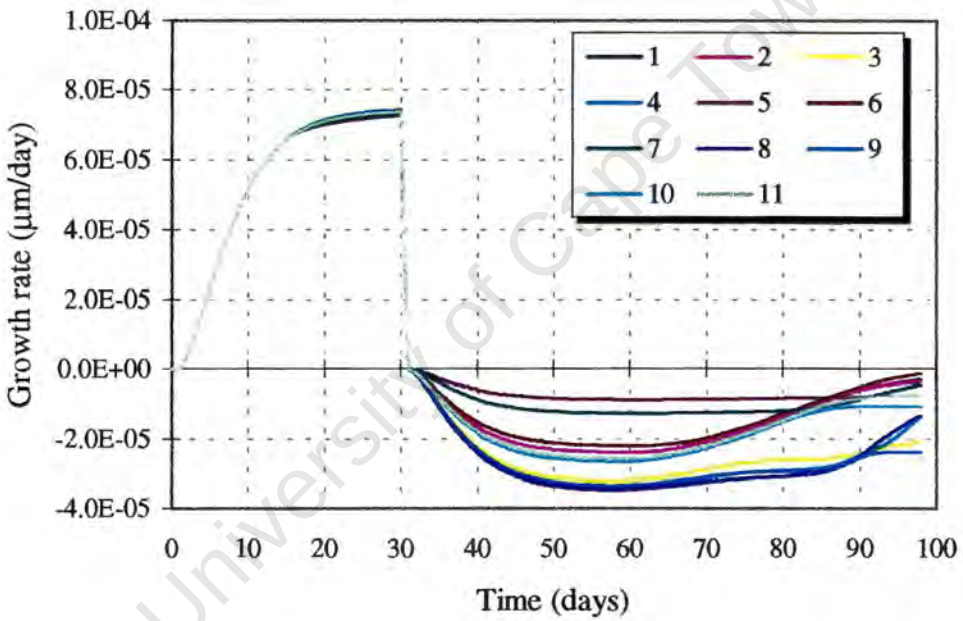

Figure 7.15 Mineralised tissue formation rate, $\dot{Q}$, at the 11 positions along the interface.

In the previous analyses, where a 14 day rest period was allowed, and the slip threshold was set to 20µm, no fibrous tissue has been predicted. However, some inelastic relative displacements where experienced once all the ingrown bone had been removed, and the bond lost. However, the magnitudes of these displacements, over the history of loading, were not sufficient to cause fibrous tissue formation. The worst case for fibrous tissue development will be simulated when the maximum amount of relative displacement is predicted. This will take place when the friction angle is at its smallest, the slip threshold is set to zero, and no rest period is allowed. Therefore this situation is analysed. The resultant extent of bone ingrowth and fibrous tissue formation ($\hat{Q}$) are shown in Figure

7.16. Negative values of $\hat{Q}$ indicate the thickness of the fibrous layer, while positive values denote the depth of bone ingrowth.

By 10 days a small amount of ingrowth is predicted beneath both condyles. While by 20 days, approximately half the depth of the porous coating is filled with mineralised tissue. In the long term (160 days), both condyles are completely penetrated by bone tissue. This result is in contrast to the previous analysis, where only in limited regions did the amount of ingrowth exceed 30%. However, previously ingrowth was only predicted at the base of the post, and in a limited region on the medial side. In this analysis, fibrous tissue formation has been predicted on the entire lateral surface of the post, and in a limited region on the medial side. The result on the medial side (and to a lesser extent on the lateral side) shows regions of ingrowth interspersed with regions of fibrous tissue. This development has resulted as a consequence of inelastic displacements in limited areas. The dip in the amount of ingrowth on the outer edges of each condyle appears to be either an "edge" effect, as a result of the numerical modelling, or has formed as result of uneven load sharing, where a greater portion of load is carried on the outer edges of the tibial tray.

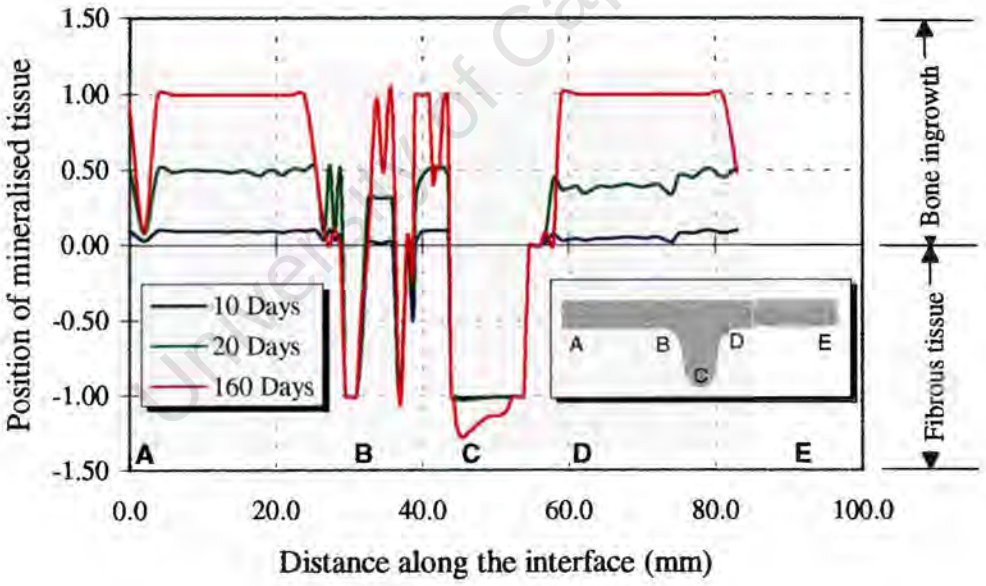

Figure 7.16 Resultant interface tissue formation for friction angles of 21.80° γ_{th}^{p} equal to 0μm and no rest period.

The areas in which bone ingrowth is predicted are shown on the implant mesh, by the green regions, in Figure 7.17. Although the figure does not indicate the extent of ingrowth, it shows the regions in which there is bonding, and where fibrous tissue has formed (indicated in red). On the under-side of both condyles, bone ingrowth and

subsequent bonding is evident. As in these regions the ingrowth has reached the full depth, a bond shear strength of approximately 15MPa will exist. The other areas of ingrowth are at the base, and on the medial side, of the central post. On both sides of the post fibrous tissue has formed, although the soft tissue region is smaller on the medial surface.

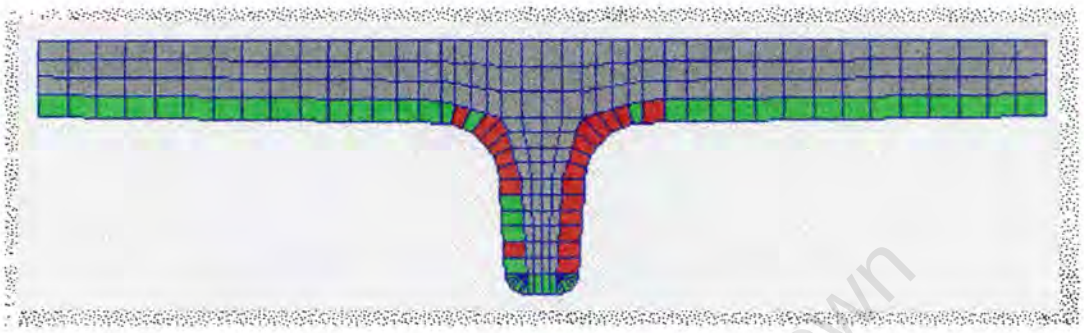

Figure 7.17 Mesh plot of the tibial tray, showing regions of bone ingrowth (green) and fibrous tissue formation (red).

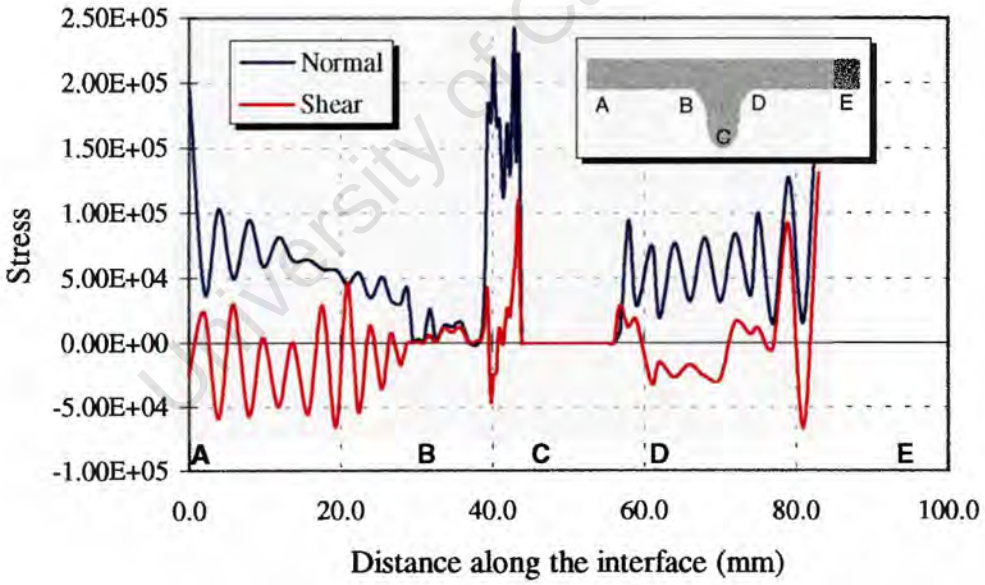

Figure 7.18 Normal and shear stress distribution along the implant-bone interface after 160 days.

Bone ingrowth, and the formation of soft tissue, have introduced oscillations into the normal and shear stress distribution along the length of the interface (Figure 7.18). Although reduced integration has been used, these oscillations have not been eradicated. As a result of the compliant nature of the fibrous material, in the regions where this tissue has developed, very little normal and shear stress have been transmitted.

Furthermore, the formation of fibrous tissue has resulted in an alteration of the manner in which the load is transferred during the eccentric load case. Subsequently, the normal stress magnitude beneath the two condyles is very similar. However, the shear stress is not equally distributed between the two load bearing surfaces, as it would appear that more shear stress is carried through the medial side. As a result of the extensive ingrowth beneath the condyles, there has been a reduction in the overall stress magnitudes along the length of the interface. The peak normal stress beneath the post is approximately 0.25MPa, with a corresponding shear stress of 0.1MPa.

7.4.2 Reconstructed Hip Joint

The constitutive model is applied to the problem of interface tissue formation, in the reconstructed proximal femur. Although the process of bone ingrowth and fibrous tissue formation is coupled to the processes of adaptive bone remodelling, in this analysis, only the interface evolution is considered, while the mechanical properties of cancellous and cortical bone are assumed to remain constant.

A plane stress finite element model, with a *side plate*, has been used to model the geometry of the reconstructed joint (Figure 7.19). The side plate is intended to simulate the stiffness provided by the cortex, which is lost as a result of the two dimensional approximation. This plate is simply a second plane of elements which share nodes with those making up the cancellous and cortical bone structure. The thickness of the cortex lessens towards the proximal end of the joint and therefore the stiffness of the bone will decrease. To capture this effect, the thickness of the side plate is reduced towards the proximal end. The side plate thickness is calculated so as to maintain the second moment of inertia of the three dimensional geometry. Huiskes *et al.* (1986) calculated the thickness profile of the plate and compared this approach to a three dimensional finite element model of the reconstructed proximal femur. They found excellent comparisons between the stress magnitudes and distribution in the two models. In many analyses of the proximal femur, a plane strain assumption is made; based on the fact that the outer cortex constrains the model from strain in the out of plane direction. However, in the present model, the choice of plane stress is based on the fact that element thickness has no meaning in plane strain and therefore in order to implement a varying thickness side plate, only a plane stress analysis is suitable.

The green and orange shading in the mesh indicate the regions of cortical and cancellous bone, respectively. The implant is shown in grey, while the porous coating is shaded in red. The inserted sectional view of the mesh shows the arrangement of the side plate, with respect to the remainder of the model. The material properties of the cortical and cancellous bone were the same as those used in the analysis of the knee joint (Martens *et al.*, 1983; Martin 1991). The side plate is assigned material properties pertaining to cortical bone.

The finite element mesh is constrained at the distal end of the cortical bone. The constraints permit contraction or expansion of the cortex, while eliminating the displacement in the axial direction of the femoral shaft.

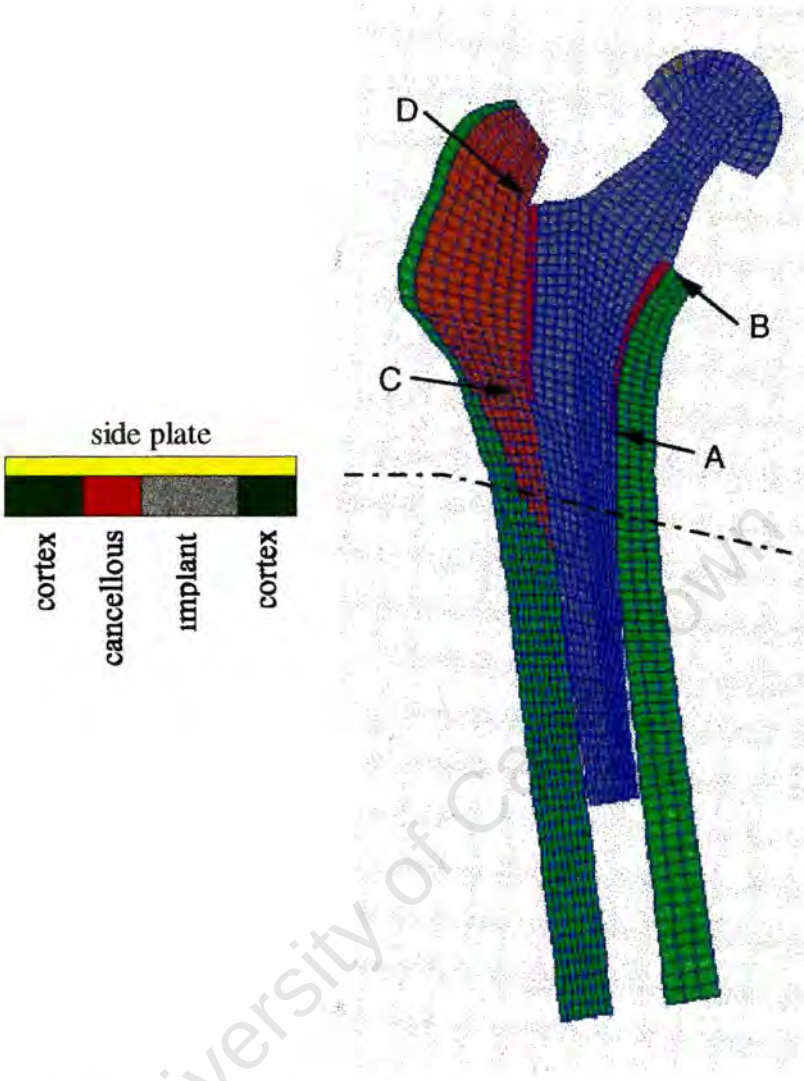

Figure 7.19 Finite element mesh of the proximal femur reconstructed with the *PCA* (Howmedica, Inc.) femoral component, showing the material regions. The inserted sectional view shows the side plate arrangement.

The loading on the proximal femur is extremely varied and complex, and comprises an array of muscles and ligaments, in addition to the contact forces between the femoral head and the acetabulum (Pauwels, 1980). Despite the many loading phases experienced during normal activity, several important load cases can be identified. The most important of which is the loading experienced during the *single-legged-stance* phase of gait. This is considered to be the "worst case" loading condition that occurs during normal activity, owing to the high loads that are transferred across the hip joint. During steady walking, the body is momentarily in an equilibrium position where the line of action of the ground reaction force is shifted over to the side of the swinging leg. In this position the femoral shaft is inclined at an angle of 9° to the vertical, in the frontal plane. The system of forces in the hip can be resolved into a reaction force on the femoral head and a tensile force in the abductor muscle group (Harrigan *et al.*, 1991). Subsequently,

for a person of average mass, this load case produces a femoral head reaction force of 2317N, acting at an angle of 15°, measured clockwise from the vertical axis, in the frontal plane. The abductor muscles have a resultant stabilising force magnitude of approximately 700N, acting at an angle of 19° to the vertical. The co-ordinate directions and muscle forces are shown in Figure 7.20. The force directions and magnitudes used in this analysis are consistent with those used by Crownshield *et al.* (1980).

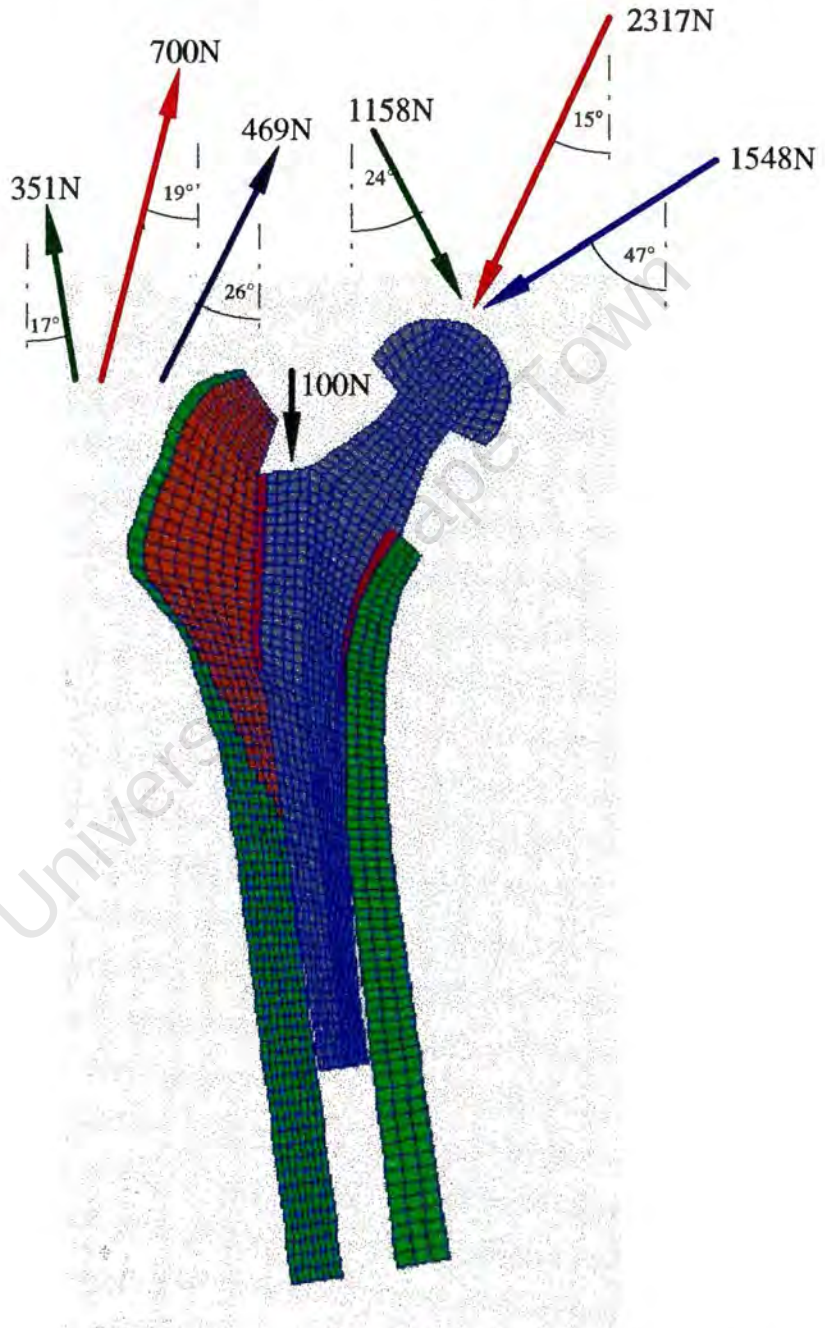

Figure 7.20 Three load cases on the proximal femur experienced during normal activity. The first, second and third load cases are shown in red, green and blue, respectively.

In addition to the loading experienced during the stance phase of the gait cycle, two other load cases are considered, which represent the set of forces on the joint at the extreme ranges of motion. These conditions are believed to be the extremes of normal activity (Carter *et al.*, 1989). In the second load case, the joint reaction force is 1158N acting at an angle of -24° to the vertical, while the abductor muscles produce a force of 351N acting at -17° to the vertical. The third load case considers a femoral head reaction force of 1548N acting at an angle of 47° to the vertical, and an abductor muscle force of 469N, acting at 26° to the vertical. The three load cases ($j = 1, 2, 3$) are shown in Figure 7.20, with load cases 1, 2 and 3, shown in red, blue and green, respectively.

Two analyses of the hip model have been undertaken. In the first analysis, the full load is applied after a 14 day rest period. In this analysis the slip threshold is set to 20 μm. In the second analysis no rest period is allowed. In both analyses the friction coefficient between the porous coating and the bone is assumed to be 0.6 (30.96°), while a value of 0.3 (16.70°) is used between the smooth portion of the stem and the bone. In addition, a press-fit load of 100N is applied to the implant at the start of each analysis, as shown in Figure 7.20. It has been assumed that the first load case acts for 50% of the total number of load cycles, while the other two load cases carry an equal weighting of 25%.

For the first analysis, the extent of mineralised tissue formation along the medial and lateral porous surfaces are shown in Figure 7.21 and Figure 7.22, respectively. Positions A and B lie at the distal and proximal ends of the porous coating on the medial side, while C and D are the corresponding positions on the lateral surface. As a result of the rest period, all regions have become bonded before the loading begins. In addition to this, the load magnitude has not been sufficient to cause fracture and subsequent inelastic relative displacement at any point on the coating. As a result, there is no fibrous tissue formation. In spite the choice of reduced integration, the growth profile on the medial surface has developed oscillations, which can be seen by 80 days. After 40 days the whole medial surface, with the exception of an isolated region towards distal end, is fully infiltrated with mineralised tissue. However by 80 days, the ingrowth in the distal region is reduced considerably and severe oscillations in the growth pattern have developed. These oscillations have possibly resulted due to the big change in load distribution with each load case, as the surface goes into both tension and compression. Towards the proximal end, less bone has been withdrawn and a firm attachment would be maintained. The amount of ingrowth increases towards the proximal end, however, the exact profile is difficult to discern as a result of the oscillations.

Along the lateral surface, the proximal half of the interface region is fully integrated. This region of osseo-integration is not affected by the subsequent remodelling. However, towards the distal part of the coating, the bone that was generated during the repair activity, has been withdrawn to approximately 30% of the coating depth. Despite the limited withdrawal of bone, the entire coating on the lateral side is bonded to the surrounding bone.

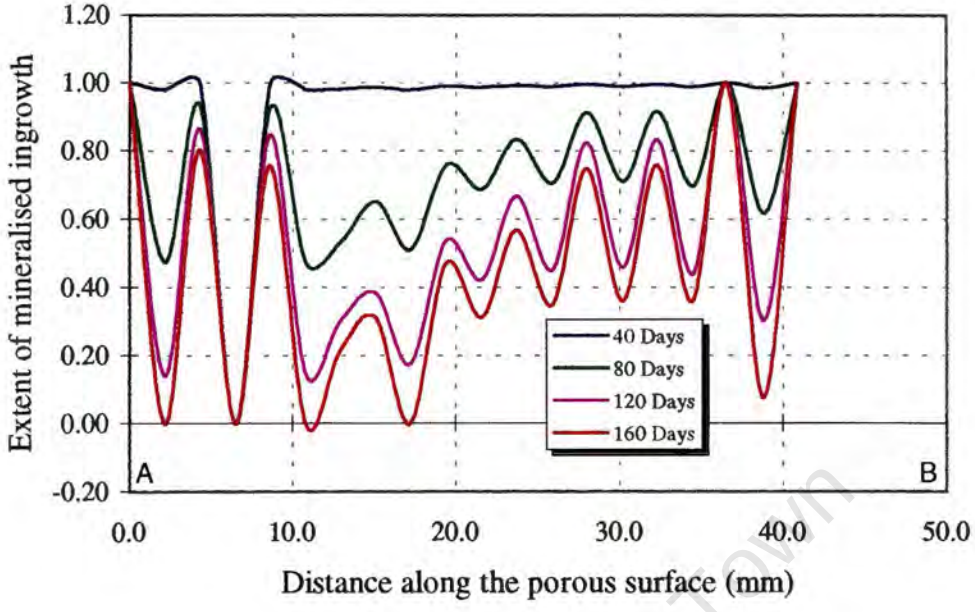

Figure 7.21 Extent of mineralised tissue along the medial porous surface after 40, 80, 120 and 160 days.

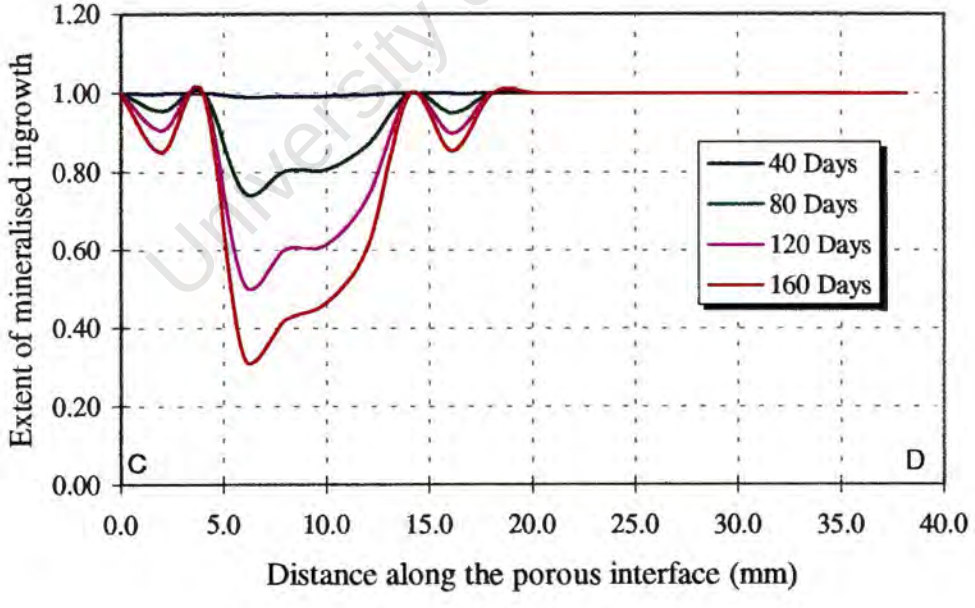

Figure 7.22 Extent of mineralised tissue along the lateral porous surface after 40, 80, 120 and 160 days.

The interface stresses after 40 days, for the first load case (single-legged-stance), along the medial and lateral surfaces, are shown in Figure 7.23 and Figure 7.24, respectively. At this point both surfaces are fully integrated, due to repair, and there has been no

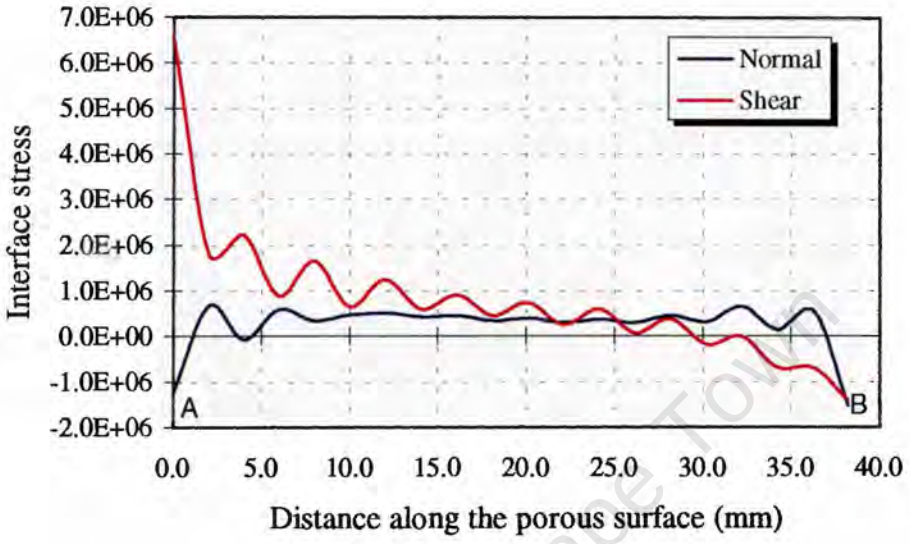

Figure 7.23 Interface normal and shear stress along the medial porous surface after 40 days. Stresses plotted for the first load case.

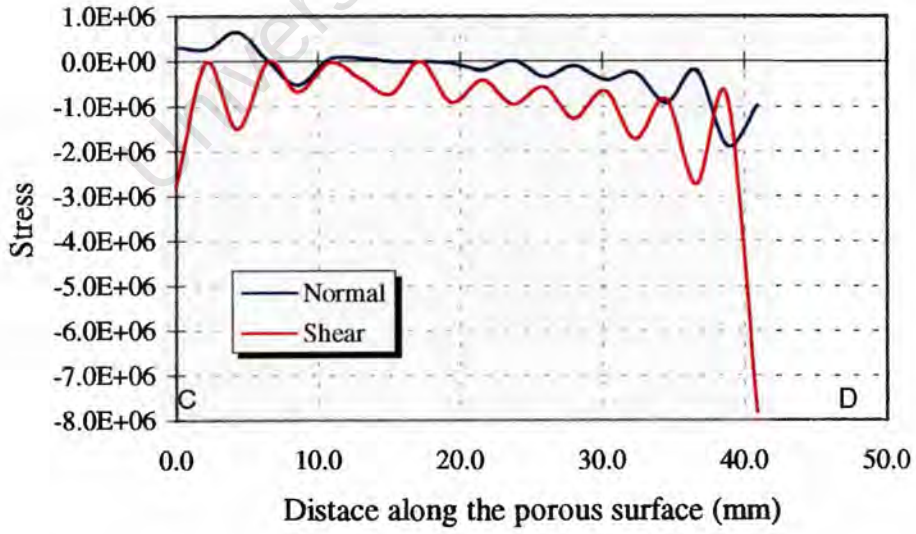

Figure 7.24 Interface normal and shear stress along the lateral porous surface after 40 days. Stresses plotted for the first load case.

fracture. Even at this early stage in the loading history, oscillations have developed. The pressure along the medial surface is evenly distributed, and has a value of approximately 0.5MPa. However, there are regions of tensile stress, with peaks of approximately 1.5MPa, at either end of the coating surface. On the lateral surface, the normal stress is compressive towards the distal part of the coating, and becomes tensile in the proximal region. This tensile stress is due to the large abductor muscle force which pulls the bone away from the implant. The tensile stress peak is approximately 2MPa. Large shear stresses have developed on both the medial and lateral surfaces, as a result of the wedge shape of the implant. At the distal end of the medial surface, the shear stress peak is in the region of 7MPa, which is approximately half the shear strength at full ingrowth. However this values decreases to less than 1MPa, towards the proximal end. Along the lateral surface, the shear stresses are evenly distributed, and are in the region of 1MPa. However, there is a peak of nearly 8MPa at the extreme proximal end.

In the second analysis, where no rest period is allowed, the loading on the joint has inhibited successful ingrowth on both the medial and lateral surfaces. The extent of bone tissue formation is examined after 40 days, at which point the interface evolution appears to have reached equilibrium. On the medial side (at the distal end) a region of bonding with a length of approximately 20mm has developed, while in the proximal third of the coating, mineralisation of the initial tissue has not taken place. The position of the bone tissue surface ($\hat{Q}$) is shown in Figure 7.27 and Figure 7.28, for the medial and lateral surfaces, respectively. The majority of the lateral surface has become osseo-integrated with the exception of a 10mm region at the distal end of the coating. The extent of ingrowth on the medial surface is very different to the previous analysis, where a rest

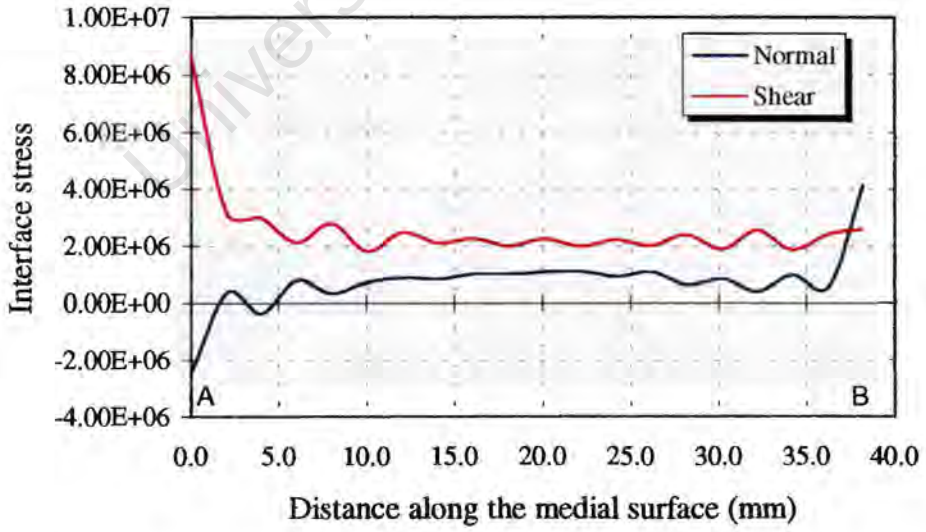

Figure 7.25 Interface normal and shear stress along the medial porous surface after 160 days. Stresses plotted for the first load case.

period was allowed. In this case ingrowth was predicted in the proximal region, while here the distal region has become osseo-integrated. However, along the lateral surface the ingrowth profile is very similar to the previous analysis, although here a complete absence of bone is predicted towards the distal region. In the previous example bone was removed due to remodelling, whereas here osseo-integration is lost as a result of fracture.

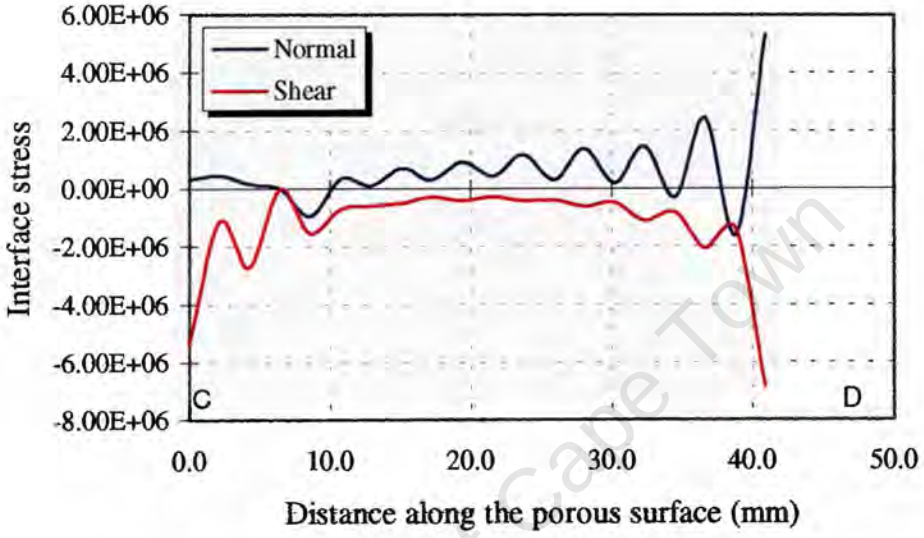

Figure 7.26 Interface normal and shear stress along the lateral porous surface after 160 days. Stresses plotted for the first load case.

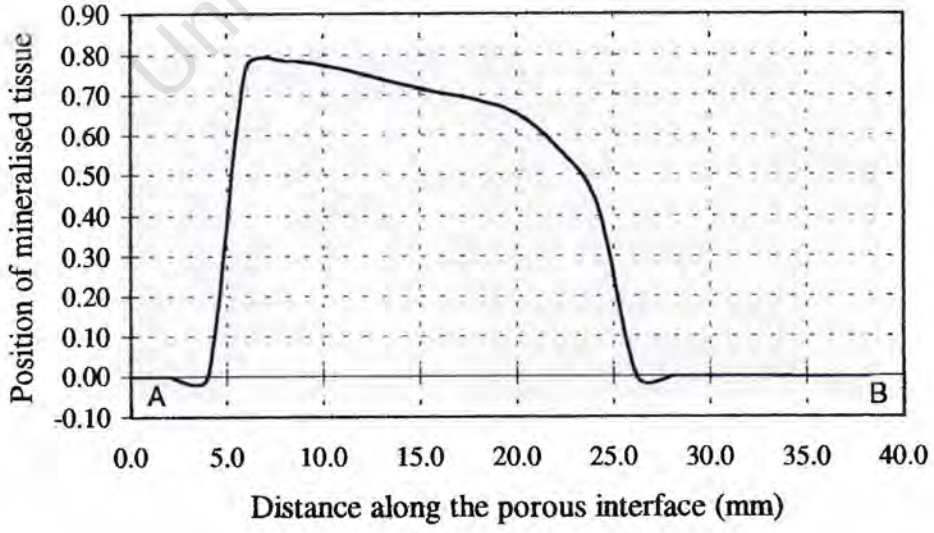

Figure 7.27 Extent of mineralised tissue along the medial porous surface after 40 days.

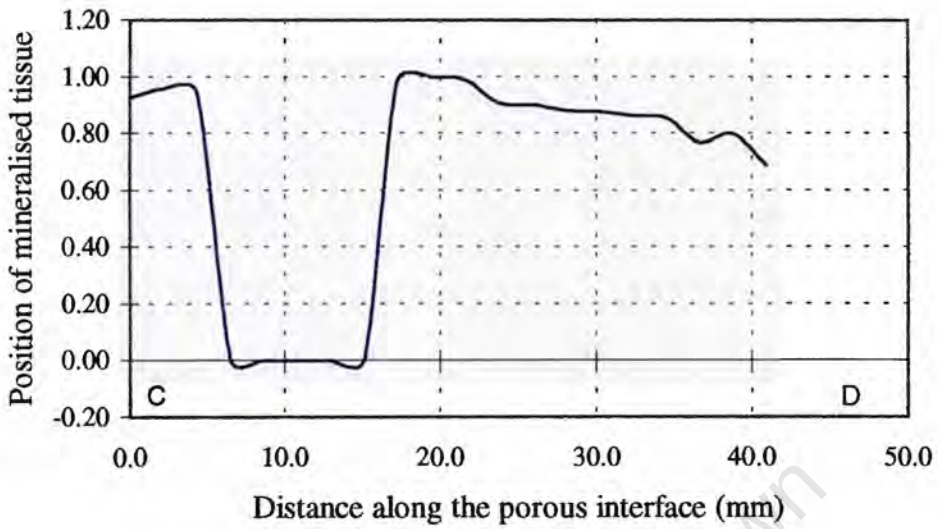

Figure 7.28 Extent of mineralised tissue along the medial porous surface after 40days.

The interface normal and shear stress along the medial and lateral porous surfaces are shown by Figure 7.29 and Figure 7.30, respectively. As a result of the limited region of bone ingrowth, the stress distribution is very different to the previous analysis. Along the medial surface the normal pressure has increased considerably, particularly in the central

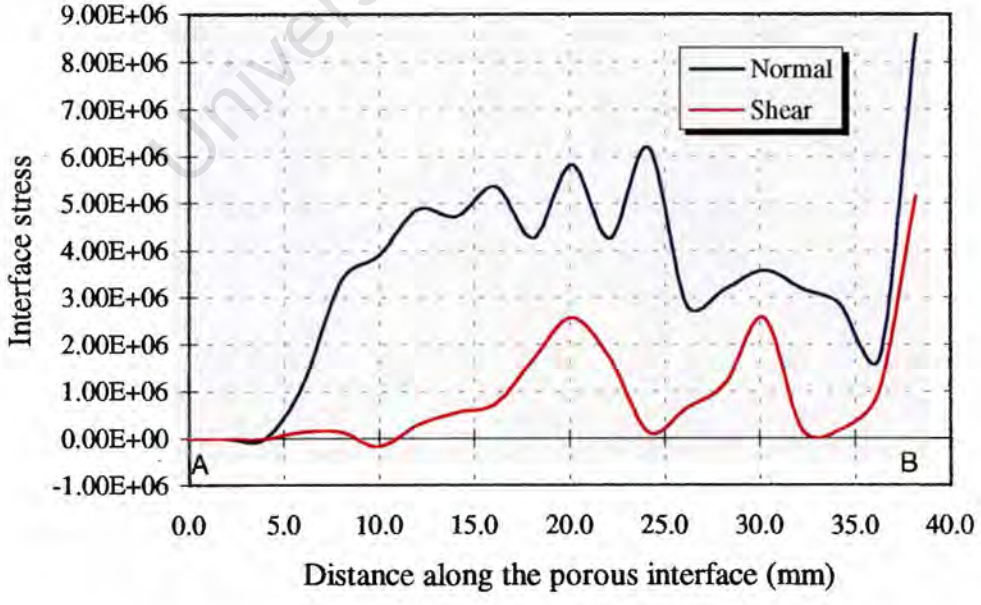

Figure 7.29 Interface normal and shear stress along the medial porous surface after 40 days, for the first load case.

region where pressures of up to 6MPa are experienced. In addition, a peak normal stress of approximately 10MPa has occurred in the extreme proximal region (B). The limited region of bone ingrowth has inhibited the transfer of shear stress. Interestingly, on the medial side most of the shear stress in transmitted in the proximal part of the coating where there is no bonding. In this region the peak shear stress is approximately 5MPa.

Along the lateral surface, the formation of fibrous tissue has resulted in a shift of the normal and shear stress transfer away from this region towards the distal, and to a lesser extent, the proximal region. This shift has resulted in a normal stress peak in the distal region of 13MPa, with a corresponding shear stress of 5MPa. Over the remainder of the lateral interface, the normal compressive stress is in the region of 2MPa, with an approximately 6MPa peak at the proximal extreme. The shear stress oscillates about the zero axis over the majority of the interface.

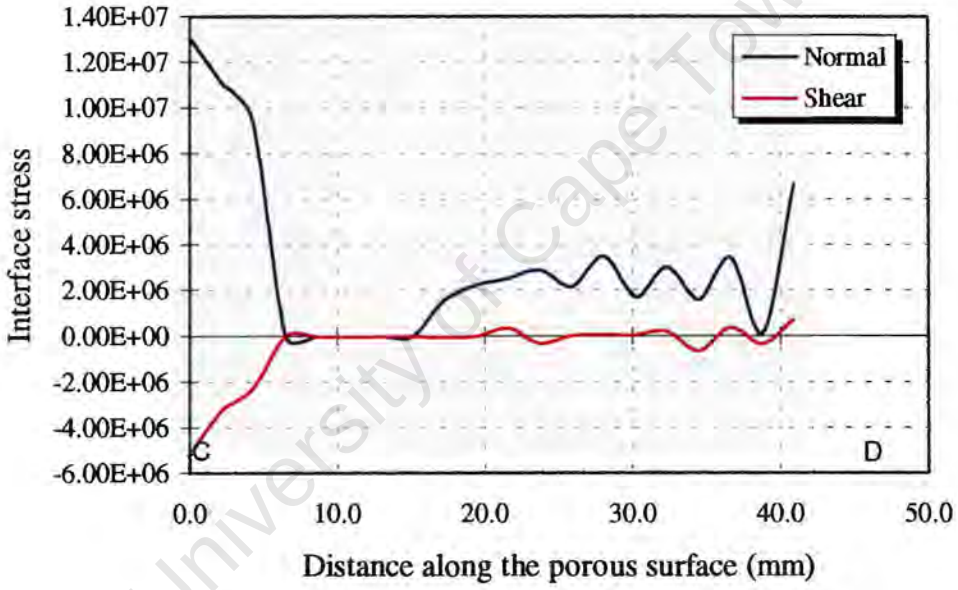

Figure 7.30 Interface normal and shear stress along the lateral porous surface after 40 days, for the first load case.

CHAPTER EIGHT

DISCUSSION

8.1 Introduction

This, the final chapter, sets out a discussion of the modelling approach in the light of the results presented. The interface model presented in this thesis considers the mechanics of the interaction between an implant and the surrounding bone. The interface element which has been developed, is fully compatible with the other planar elements in the finite element code. The isoparametric element forms the basis of the interface evolution for the simulation of the bond which develops due to bone ingrowth, and the formation of fibrous tissue as a result of implant-bone relative displacements.

8.2 Interface Mechanics

The purpose of the interface models is to simulate the mechanical interaction of the deformable bodies. This is accomplished by the development of a thin-layer interface element. For this application, the approach followed has an advantage over a zero thickness element, in that an actual material region is considered. In the initial state, the implant is separated from the bone by a layer of material, which primarily consists of dead and shattered bone trabeculae and other tissue debris. Although the thickness of the layer may be highly variable, the interface is a region and not a line of interaction, which therefore justifies the choice of a thin element. It is assumed that in the initial stage there is no cohesion between the bone and the implant and, therefore, shear stress can only be transmitted in the presence of normal pressure. In reality, there may be some cohesion as a result of the asperities of the bone surface and the roughness of the bead structure. As in the case of the initial tissues, the assumption of a thin interface layer for the formation of fibrous tissue is justified on the grounds that fibrous tissue does form a layer with a finite and measurable thickness.

The interface mechanics considers three possible states which may exist during the evolution of the implant-bone interface. Firstly, an initial unbonded interface, where the implant and bone are separated by a thin layer of undifferentiated tissue is considered. In this condition, the interaction between the two bodies is governed by a simple Coulomb friction model, with a non-associated flow rule. This model was then modified to include the possibility of fibrous tissue formation. Fibrous tissue exhibits highly non-linear compressive behaviour, and the interface mechanics has therefore been modified to include this behaviour. Finally, the bond which develops between the implant and the

bone, due to bone ingrowth, has been modelled by adding a cohesion and an adhesion term to the Coulomb yield surface. If the bond strength is exceeded, the interface formulation returns to the initial unbonded state.

The nature of the interaction between a cementless implant and the surrounding bone may be highly variable. The type of porous surface, as well as the type and quality of the surrounding bone, will determine the manner of the interaction. In the present model it has been assumed that the interaction can be modelled using a Coulomb friction law, which is consistent with the approach followed by numerous other research groups. Rancourt *et al.* (1990) experimentally determined the friction coefficient at the porous surface-bone interface to be between 0.4 and 0.8. In the model of the tibial tray, friction coefficient values of 0.4, 0.6 and 0.8 have been analysed. Although the friction coefficient influenced the magnitude of shear and normal strain, the coefficient had little influence on the extent of bone ingrowth. An additional complication is that the friction coefficient may well change as the initial tissue becomes mineralised. In the present analysis, the value remains constant because of the uncertainty in this evolution.

Experimental data for the mechanical properties of fibrous tissue is scarce, and therefore the numerical model of this layer must be seen in this context. However, it is clear from the experiments of Hori and Lewis (1982), that the material exhibits non-linear behaviour in compression. The expression for the compressive stress-strain relation proposed by Weinans *et al.* (1990) provides a suitable approximation for modelling this behaviour. However, choosing suitable values for the modulus at zero strain E_0 and the stiffening parameter H is difficult, as these values may be highly inhomogeneous and patient dependent. The experiments of Hori and Lewis showed that tissue taken from different regions, and formed under different conditions, will have different mechanical properties. The numerical model of Weinans *et al.* (1990) showed that the stress magnitudes around the fibrous layer were strongly influenced by the magnitude of the initial stiffness, but hardly influenced by the stiffening parameter. In addition to the difficulty in obtaining data on the compressive and tensile behaviour, no shear data could be found. For this reason, it was assumed that the shear modulus would simply be a function of Poisson's ratio and the modulus at zero strain. As the focus of the present study was on the interface evolution, the influence of the fibrous tissue parameters on the interface mechanics was not examined. A limitation of the fibrous tissue model (which is also the case with the mineralised tissue models) is the assumption that the relation between shear and normal stress will be uncoupled and therefore, transverse contraction and expansion, due to the Poisson effect, has not been accounted for. Again, the lack of material data meant that the nature of this coupling is not known. Secondly, it is assumed that there are no axial stresses in the fibrous layer as these stresses would be very small when compared to the normal and shear stresses and, therefore, could be neglected.

In order to model the bonded interface, the Coulomb yield surface was modified to include cohesion and adhesion. The shear limit of the resulting bond is a function of the cohesion and the normal pressure. To what extent the normal pressure will affect the bond strength, once cohesion has developed, is not clear. In the present model, it is assumed that the friction angle used for the Coulomb model remains unchanged once a

bond has developed. It is possible that this angle should decrease with increasing bond strength, in order to reduce the influence of the normal pressure, as the bone shear strength develops. Weinans *et al.* (1993) simulated the formation of fibrous tissue as a result of implant-bone relative displacements after interface fracture. To model the fracture, they used the elliptical yield surface for cancellous bone presented by Stone *et al.* (1983), in which the shape of the yield surface was not influenced by the normal pressure. Although this approach appeared to produce meaningful results, the applicability of a cancellous bone yield criterion to the implant-bone interface is doubtful.

The strength of the adhesive bond will be a function of the extent of bone ingrowth and the type of porous coating. The bond's shear strength will also depend on these factors. Therefore, there exists some coupling between adhesive and cohesive strength. The nature of this coupling is not clear, although adhesive strength will be lower than cohesion. Thus, to account for this unknown, it has simply been assumed that the adhesive strength will be proportional to the cohesive strength, which depends on the extent of osseo-integration.

8.3 Interface Evolution

The evolution of the interface includes the three dominant interface developments, which are strongly influenced by the local mechanics. Initially, repair due to surgical reaming and broaching will dominate growth within the porous surface of the implant. Once sufficient mineralised bone has formed, remodelling, as a result of the elastic strains, will govern the development and the long term maintenance of the bond. Finally, interface fracture and subsequent relative displacement of the two surfaces will result in an improper healing response, causing a withdrawal of the mineralised bone tissue and its replacement with fibrous tissue.

The interface evolution, which results in the changing mechanics of the interface, is governed by the local strains within that region. There are many factors, unrelated to mechanics, which will influence the development of interface tissues. These include: the quality of the bone stock, the extent of bone disease, the age and weight of the patient, as well as their activity level. While these factors will play an important role in bone tissue development, the belief that growth, repair and maintenance of bone is controlled by the mechanical environment has been widely demonstrated both clinically, experimentally (Pauwels, 1980) and analytically (Carter *et al.*, 1987; Carter 1988; Carter *et al.*, 1988; Huiskes *et al.*, 1987). Notwithstanding the above, the role that local interface mechanics will play in the development of junctional tissue has yet to be completely understood. Many experimental investigations (Cameron, 1973; Ducheyne, 1977 and Søballe *et al.*, 1992) have shown that relative displacements at the implant interface will result in a withdrawal of mineralised tissue, and the subsequent formation of fibrous tissue. However, the way in which elastic strains will influence tissue repair, following surgical preparation, and long term remodelling, is unclear. Søballe *et al.* (1992) points out that "the process of bone ingrowth can be compared to fracture healing ..." and therefore initial ingrowth should be affected by stress and strain in the same way as fracture repair in other areas. A premise which has been demonstrated by

many research groups (Pauwels, 1980; Perren, 1979; Goodship, 1995). In the context of bone growth into a porous coated implant, the way in which these quantities will influence development of the interfacial tissues is not yet completely understood.

8.3.1 Repair Mineralisation

Successful repair of the undifferentiated tissue will lead to mineralisation and subsequent osseo-integration. Implant press-fit is regarded as a key factor in determining the success of a cementless hip arthroplasty. It is believed that a good press-fit will ensure stability, provide a suitable environment for bone regeneration, and hence for ingrowth. However, implants which appear to be initially stable, due to press fitting, do not always achieve sufficient bone ingrowth. Ling (1986) discussed tissue regeneration as a consequence of the strength of the press-fit bond created during surgery. He suggested that with a good initial press-fit and low applied loads, osseo-integration would result. However, as press-fit strength decreased and applied loads increased, osteoclasis, fibrosis and chondrogenesis would result. It is difficult, from this work, to separate out the effects of stress and elastic strain from relative displacement, which may be responsible for osteoclasis and fibrosis. These ideas are consistent with those promulgated by Perren (1979) and DiGioia III *et al.* (1986), who believed that repair would continue as long as the fracture material was able to withstand the applied strains. Ling suggested that a rest period of no less than three months would facilitate the process of osseo-integration. He believed that during this period, if loading were required to stimulate tissue differentiation, the harmful effects due to excessive strains would outweigh the benefit achieved by the load induced repair stimulus. Although it is widely accepted (Goodship, 1995) that axial compression within the fracture site of a long bone may stimulate the repair activity, and hence reduce the time required for repair, the nature of this stimulus is not clear. Furthermore, strains which are too large, or which have a transverse component, may inhibit the repair of the fracture. In addition, it is not clear to what extent the influence of strain on fracture repair is appropriate to the repair of interface tissues in a cementless arthroplasty. For these reasons, in the present model it is assumed that strain will only have a negative influence on the repair stimulus. Therefore, the current work coincides with the ideas expressed by Ling (1986) and Perren (1979)

The importance of implant press-fit stems from the ideas put forward by Perren (1979), who suggested that mineralised tissue would form in the interfragmentory gap, if the interface tissue were able to withstand the local strain. The magnitudes of strains which can be tolerated will decrease during the healing process, as increased fracture site rigidity results in lower yield strains of the developing material. The structural properties of healing bone tend to follow a bi-phasic relationship, with an initially large increase in interface stiffness, decreasing gradually as the repair process comes to completion (Bourgois and Burny, 1972 and Meroi and Natali, 1989). Following the ideas of Perren, DiGioia III *et al.* (1986) suggested that there exists a critical relationship of applied strain to tolerable strain, which will determine the success of the repair process. The numerous investigations which have been conducted in order to examine ways in which fracture healing can be enhanced by mechanical loading, have shown that a small change to the local mechanical environment can have a considerable influence on the outcome of the healing process (Goodship, 1995). There is experimental evidence to support the

argument that interface strain will either inhibit or promote fracture repair. This highlights the sensitivity of fracture to local mechanics, and also points to the fact that the influence of mechanics on fracture repair will only be clarified when the controlling mechanisms of the repair processes are fully understood.

The numerical model presented for fracture healing process by Carter (1988) and Carter *et al.* (1988), considers the influence of hydrostatic and octahedral stresses on the process of endochondral ossification. Their model does not consider regeneration by direct bone union. Pauwels (1980) argued that there is no specific stimulus for bone formation. He believed that the formation of bone is a natural consequence of the repair process, which may be guided to form cartilage or fibrous tissue, depending on the stress state. The present model encompasses both of these ideas, in so far as the formation of fibrous tissue is considered in the presence of shear strain, which causes relative displacements. However, the possibility of cartilage formation was not considered, and therefore secondary fracture healing due to endochondral ossification has not been included.

It is quite clear that the short-term interface response will be governed by repair, whereas remodelling will govern the long term response. However, the nature of the coupling between the repair and remodelling processes is unclear. Spector (1988) loosely suggested that, based on the assumption that at the time of surgery the bone tissue is in a state of remodelling equilibrium, remodelling of interfacial tissues will begin approximately 4 to 6 weeks after surgery. However, this proposal also suggested that after this period there would be sufficient mineralised tissue requiring maintenance. This may not be the case. For this reason, it has been assumed that the start of remodelling activity will not be governed by time, but will begin when there is mineralised tissue which requires maintenance or adjustment. However, this in itself is difficult to determine, as mineralised tissue may have formed both adjacent to and within the porous surface, while the repair process is still progressing. In which case repair and remodelling will exist together, and may conflict with one another. Whether these two processes will compete is difficult to say, although it does seem reasonable that they may coexist.

Ducheyne (1977), Spector (1988) and Linder (1991) point to the two possible paths of immature tissue differentiation: fibrous tissue or mineralised tissue. Their observations suggest that the tissue will progress along a particular path until tissue formation is complete. Then why is it that some porous surface regions do not achieve total bone ingrowth, even under conditions of stability? Possibly these regions were not totally infiltrated with mesenchymal tissue, or alternatively, this tissue did not differentiate into either bone or fibrous tissue. The results of Jasty and Harris (1988) have shown poor ingrowth in dogs that underwent acetabular reconstruction with an undersized reamer. Although it would appear that the implants were stable, very little bone ingrowth resulted, and the porous coating was found to be infiltrated with fibrous tissue. This study suggests that even under mechanically stable conditions, the repair process does not guarantee the formation of mineralised tissue.

Although surgeons aim to achieve a uniform press-fit when inserting a cementless implant, the broaching and reaming processes often result in gaps between the implant

and the surrounding bone. Depending on, amongst other factors, the stability of the implant, new woven bone may or may not bridge the gap and develop within the porous structure. Jasty and Harris (1988) showed that a gap adjacent to a cementless acetabular component initially showed signs of new bone formation, but in the long term only fibrous tissue existed in this region. This was in contrast to the finding of Cameron *et al.* (1976), who inserted plugs into the canine femur with a 1 and a 2mm gap, and recorded woven bone bridging the gap after two weeks. In the present model the influence of a gap adjacent to the implant has not been investigated. If the bone surrounding the implant is positioned away from the implant surface, the gap region will initially have the material properties of undifferentiated tissue, which will then mature during the repair process. This tissue may take on the properties of fibrous tissue, if the mechanical conditions are suitable.

8.3.2 Fibrous Tissue Formation

Improper repair of interface tissues can lead to bone resorption and subsequent replacement with fibrous tissue. Many research groups (Ducheyne *et al.*, 1977; Pilliar *et al.*, 1986; Søballe *et al.*, 1992; Boehler *et al.*, 1994) have experimentally demonstrated the formation of a fibrous layer adjacent to a cementless implant, following periods of large relative displacements. Although the resorption process can be caused by many factors, including wear particles at the interface, in the present work it has been assumed that excessive relative displacements will be the dominant factor, which will over-shadow any other influences. In the long term, fibrous tissue formation around a cementless implant develops as a result of gradual implant loosening. If the implant becomes debonded at one point, the resultant relative displacements may compromise the stability of the implant, causing debonding in other regions and hence more fibrous tissue formation.

The formation of fibrous tissue is, in general, associated with a degeneration of the implant-bone interface. Once a fibrous tissue layer begins to form, as a consequence of its poor mechanical properties, other areas of osseo-integration may become overloaded resulting in failure. This degeneration process can result in the entire implant surface being encapsulated by fibrous tissue. Therefore, implant stability is not guaranteed, and it is unlikely that the fibrous tissue will be replaced by bone. As a consequence of this, it is generally thought that once a fibrous layer forms it will not be replaced by mineralised bone. However, findings to the contrary were reported by Uhthoff and Germain (1978), who observed that a region of the interface categorised as having scar tissue was later re-categorised as having calcified tissue after a long period of stability. This finding suggests that interface reversibility may be possible, although this has not been widely demonstrated. In the present model, it is assumed that once the bone tissue surface has moved away from the beads, the fibrous tissue which replaces it will remain indefinitely. It may be meaningful to simulate the replacement of fibrous tissue with mineralised tissue, in the event of long term stability. However, the conditions under which this type of reversal will occur are not clear and, therefore, it is assumed once fibrous tissue formation has taken place it will remain permanently.

The optimal value of strain which is assumed to exist in mineralised bone, represents a state of remodelling equilibrium, which has not been shown to exist in fibrous tissue. Clinical observations have shown that the fibrous layer tends to reach a constant thickness in the long term. However, it is unclear as to whether this is as a result of the implant reaching a level of stability, or whether this is a biological consideration that sufficient fibrous tissue has been produced to protect the underlying bone from the harmful effects of relative displacements. The findings of Uhthoff and Germaine (1978) that, once stable with respect to loading, fibrous tissue will be replaced with mineralised tissue, suggests that fibrous tissue forms in an unstable situation, which does not reach equilibrium. In the model presented here, it is assumed that the fibrous layer will continue to form, until the relative displacements reduce to below the threshold value, so that there is no longer any stimulus aiding resorption.

Studies regarding the influence of displacement magnitude on fibrous tissue formation have shown that fibrous tissue will form when relative displacements are in the range of 150 (Ducheyne *et al.*, 1977) to 500μm (Søballe *et al.*, 1992). Although the exact relation between displacement magnitude and fibrous tissue thickness is not clear, experimental evidence points to several influencing factors. Firstly, the relative displacement magnitude needs to overcome a threshold value before mineralisation is inhibited. This has been demonstrated in experimental studies (Pilliar *et al.*, 1986), where it was found that mineralisation and osseo-integration took place in the presence of small relative displacements (up to approximately 20μm), while fibrous tissue formation resulted with displacements larger than approximately 150μm. Secondly, the rate and subsequent amount of fibrous tissue development reached a peak value, irrespective of the magnitude of the relative displacement. The experimental studies conducted by Pilliar *et al.* (1986) used dental implants to examine the influence of displacement. Whether these experimental results are relevant to other types of cementless implants is not clear.

The formulation of the numerical model for fibrous tissue formation is based on the assumption that the rate of fibrous tissue formation is a function of the cyclic relative displacement magnitude. The stiffness of mineralised interface tissue is orders of magnitude greater than that of fibrous tissue. Therefore, once slip has occurred and the mineralised interface tissue is replaced with soft tissue, the slip will be reduced as the inelastic displacements may become elastic within the fibrous tissue material. Weinans *et al.* (1993) pointed out that, as the thickness of the layer increases, for the same magnitude of relative displacement δ_t, the strain γ within the fibrous material will decrease as $\gamma = \delta_t / h$. These reasons may be explanations for the experimental evidence, which suggests that fibrous tissue tends to reach a maximum thickness, while relative displacement continues.

8.3.3 Interface Remodelling

Although early growth will be a direct result of bone regeneration, the long term maintenance of the interface is believed to be governed by the normal process of bone remodelling (Spector, 1988; Linder, 1991). However, this is a point of some controversy. Brunski *et al.* (1985) investigated the influence of load history on bone

remodelling around titanium screw shaped implants, that were inserted into the canine mandibular. After allowing a healing period of four to seven months, one group was subjected to cyclic loading, while the control group experienced no additional loading. Subsequent histological examination showed that, on average, there was no appreciable difference in the amount of intermit bone contact between the loaded and control groups. The similarity in the two interface models may be explained by the fact that the histological examinations were undertaken three days and three weeks after loading began, which may not have been sufficient time to produce a noticeable change in bone mineral content. In addition, the cyclic load which was applied may have been insufficient to induce a remodelling response. Brunski points to an additional difficulty with this, and many other studies of interface tissues, which is that it is difficult to separate the effects of stress, strain and relative displacement. As all bone tissue requires maintenance, it seems plausible that the bone adjacent to and within the porous coating should not be excluded from this process. This possibility was confirmed by Linder (1991) who showed that osteocytes were present within interface tissue. Although the manner in which loads influence the remodelling of bone tissue is not completely understood, several research groups (Cowin, 1993; Burger, 1995; Cowin, 1995) believe that osteocytes are the cells which are responsible for the sensing of strain and initiating of cellular events.

Numerous researchers have successfully predicted the remodelling response in the intact and reconstructed proximal femur using strain (Stülpner, 1995), strain energy (Huiskes *et al.*, 1987 and Van Rietbergen *et al.*, 1993) and equivalent stress measures (Carter *et al.*, 1987; Carter *et al.*, 1989) as a remodelling stimulus. However, to what extent these measures apply to the interface tissue is not clear. In cancellous or cortical bone material, the concept of an optimal strain, strain energy or stress measure may be measured or calculated based on measurement. However, the strain profile through the surface porosity varied considerably, and was found to be up to nine times the applied strain (Pedersen *et al.*, 1991; Steele, 1995). Therefore, if the interface strain is within the region of the equilibrium value then, within the beads, the material will be overloaded. This overloading may result in additional bone growth into the porous material. However, the coating has a finite thickness and, therefore, once the tissue has reached the surface of the implant substrate, it cannot advance further. This suggests that if the interface tissue is loaded to within the region of the optimal value, the tissue within the beads will not be withdrawn. And therefore, in order for tissue to be withdrawn from the porous surface, the interfacial strains need to be well below the assumed optimal value. The remodelling formulation presented assumes that the bone tissue will remodel, based on the peak strain within the tissue. Therefore, irrespective of where within the porosity the peak strain occurs, it will cause a withdrawal or an advancement of the mineralised tissue Q. In reality, a varying remodelling response through the bead thickness may be expected.

The remodelling that takes place as a result of joint reconstruction will involve both the interface region and the surrounding bone. The extent and areas of bone ingrowth will determine the manner in which load is transmitted from the implant to the surrounding bone. The subsequent strain distribution will determine the cancellous and cortical bone remodelling response. The way in which the density and structure of this bone is altered,

will determine the stresses at the implant-bone interface. Therefore, the interface and surrounding tissue responses are coupled. The present model is limited only to the interface remodelling. A possible extension of the current work would be to analyse a reconstructed joint in combination with a compatible bone remodelling algorithm. While this limitation applies to the current model, it applies equally to the many remodelling analyses of previous researchers (Huiskes *et al.*, 1987; Cheal *et al.*, 1989; Orr *et al.*, 1990; Van Rietbergen *et al.*, 1993; Weinans *et al.*, 1993), who have made an assumption regarding the extent of bonding between the implant and the bone. In most cases they have assumed perfect bonding, which would be the case when the entire porous coating is infiltrated with bone tissue - a situation which is seldom achieved (Albrektsson and Albrektsson, 1988; Harris *et al.*, 1983; Jasty and Harris, 1988).

Apart from the coupling of interfacial and global remodelling, it has been observed experimentally (Hedley *et al.*, 1982) that in unstressed areas, in addition to the withdrawal of the bone tissue from the bead surface, the mineralised tissue withdraws from the beads leaving a visible gap. In the model presented here, the mineralised tissue will only withdraw from the bead surface in the event of fibrous tissue formation. If a region experiences none, or insufficient strain, the bone tissue will withdraw to the edge of the porous surface ($Q = 0$), where it will remain unless the strain at that point increases.

The numerical model developed in this work for the simulation of the remodelling process considers strain history to be the stimulus for bone remodelling. Furthermore, it is assumed that there exists an optimal value of equivalent strain magnitude at which the bone turnover will be zero, as a result of a homeostatic equilibrium. The initial work on the prediction of the bone remodelling response (Cowin and Hegedus, 1976 and Hegedus and Cowin, 1979) considered elastic strain to be the driving force behind the remodelling response. Subsequently, strain energy density (Huiskes *et al.*, 1987) and equivalent stress measures (Carter *et al.*, 1987; Carter *et al.*, 1989; Beaupré *et al.*, 1990) have been considered. Cowin and his co-workers followed the approach put forward by Pauwels and Roux, which suggests that new bone will only be formed as a result of compressive strains and that tensile strains would result in resorption. However, it is now widely believed that both compressive and tensile strains can initiate the formation of new bone, although this is still a point of some debate. For this reason, no distinction has been drawn in the current model between tension and compression, as only magnitude is seen as determining the response. Although there is some understanding as to the influences of normal and shear strain on the repair process, their effects on remodelling are not as clear. For this reason an equivalent strain measure, which is simply the resultant strain, is used for the remodelling signal.

In its simplest form, the present model is based on the assumption that the remodelling rate (rate of movement of the mineralised tissue surface) is a function of the difference between the optimal and actual value of the equivalent strain. The remodelling *error*, which is the difference between these two values, is given by the simple tri-linear function proposed by Huiskes *et al.* (1987), which incorporates the concept of a *lazy* or *dead zone*. The remodelling formulations proposed by Cowin, formulated this error

magnitude simply as the difference between the optimal and actual strain values. More recently Stülpner (1995) proposed the use of a sigmoid function, which produces a continuous smooth function, while simultaneously incorporating the *dead zone*. The inclusion of repair and resorption in the present model necessitated a large number of evolution parameters, whose influence needed to be examined. As the tri-linear error function has been tested in several models, and represents the simplest approach, it has been used without additional testing. Based on the vast amount of data collected by Rubin and Lanyon (Lanyon and Rubin, 1984; Rubin and Lanyon,1985), the optimal equivalent strain magnitude was assumed to be 2000μstrain, with the dead zone range being 1000μstrain on either side of this value.

Issues pertaining to the stability and convergence of the remodelling algorithm, which have been addressed by Harrigan and Hamilton (1992), Harrigan and Hamilton (1993) and Weinans *et al.* (1992), have not been examined for the present model.

8.4 Memory of Cellular Events

Cellular events, such as apposition and resorption, do not respond instantaneously to load induced stimulus. During normal life, approximately 80% of the lining cells on the bone surface are inactive with regards to resorption or apposition (Parfitt, 1984), and thus strain does not induce an instant response in these cells. Martin and Burr (1989) have estimated that approximately three days are needed to start the process of cellular resorption. In addition to the lag time required to start events, once cellular processes are underway they will not simply stop when the strain, which initiated the event, ceases. Certain cells therefore "remember" past events. Subsequently, if cyclic loading is applied for a short period of time, once it ceases the cellular events will continue for some time. Skerry *et al.* (1988) showed that proteoglycan molecules remained re-orientated for approximately 48 hours after stimulus due to loading.

In the present model, a memory function has been implemented which induces a lag and a decay period. Despite the data of Skerry *et al.* (1988) and Martin and Burr (1989), an exact choice of the time constant is not clear. Levenston *et al.* (1994) implemented an exponentially decaying memory function into the remodelling formulations of several previous researches. They investigated the influence of time constants of 5, 20, 100 and 200 days. In the examples presented, time constants of 1, 4 and 7 days have been examined. While these values are lower than those used by Levenston *et al.* (1994), they are not directly comparable as the memory functions are different. From their study, they concluded that in the long term the memory function did not significantly alter the results of the models tested. However, in the short term, it was necessary to consider the memory of cellular events. The ingrowth of bone into a porous surface is both a short and a long term process. Repair activity can produce a sustainable bond within the first three weeks (Cameron *et al.*, 1973; Nilles *et al.*, 1973; Hedley *et al.*, 1982; Hedley *et al.*, 1983), while remodelling may reach equilibrium after months or years. Therefore, although the memory formulation may not be relevant for long term results, its inclusion is justified on the grounds of the importance of the bond created in the short term by the repair activity.

In addition to considering the relative influence of current and past events, the memory function serves to "smooth" the stimulus response and, subsequently, the growth rates. Without the memory function, the growth rate would be calculated based on the stimulus value produced by the activities of each day. Therefore, if on one day a greater or smaller stimulus were experienced, the growth rate would be equally effected. Biological functions, such as bone production and resorption, do not oscillate on a daily basis but are smooth over a period of days or weeks. Therefore, a sudden change in loading will produce a gradual change in the bone maintenance stimulus and resultant growth rate. In the present models, the applied loading has simply been a repetition of several commonly occurring load cases. If a more sophisticated load history were implemented, where the daily loads where not simply repeated, the memory function would be necessary to produce a more meaningful stimulus.

8.5 Example Problems

8.5.1 Wedge Between Two Blocks

The problem involving the displacement of the wedge between two blocks served to compare the present element formulation with the well accepted approach used by ABAQUS. Despite the limitation of the penalty formulation, the interface element showed remarkably similar magnitudes of normal stress when compared to the ABAQUS element, where contact was enforced explicitly. In addition, the thin element offers a higher rate of convergence than the mixed formulation used in ABAQUS. The comparison of the shear stress results, although very encouraging, cannot be made exactly, because in ABAQUS Version 5.4 the user does not have direct control of the "stiffness in stick" parameter. If the "stiffness in stick" and the shear modulus of the thin element could be made equal, similar shear stress magnitudes should result.

The example problems addressed in the previous chapter were chosen so as to examine typical applications in orthopaedic surgery. Cementless knee and hip replacements have become increasingly commonplace during the past decade and, therefore, there is an ever increasing need to improve their current designs in order to reduce the failure rate. The design of the hip, and to a lesser extent the knee, are difficult because of the high stresses that these joints experience during normal daily activity. For this reason computational methods, such as the finite element method, provide a powerful tool to aid in the design process.

8.5.2 Tibial Tray

The example of the cementless tibial tray illustrates the use of the present model in a joint replacement simulation. Apart from predicting the interface response to the cementless implant, the example serves to examine the influence of several of the evolution parameters on the tissue response. The problem was used to examine the effect of the friction coefficient, the slip threshold, and the post-operative "rest" period.

Although no convergence criteria have been included in the evolution, the model reaches equilibrium after approximately 200 days. However, it is difficult to say whether or not

further changes will take place at any points. Where a rest period has been included, no fibrous tissue was predicted. However, the long term remodelling results have predicted extensive withdrawal of bone within the bead surface, particularly beneath the lateral condyle. Following the removal of tissue and the lack of cohesion, limited inelastic displacements are predicted. However, these displacements are less than the values which were shown to produce fibrous tissue.

The greatest amount of tissue penetration occurs at the outer edges of the base of the post, where a large portion of the load is transmitted. This prediction coincides with the experimental findings of Bobyn and Engh (1988) whose findings showed the greatest degree of ingrowth and surrounding tissue densification at the base of the post. In addition, these findings are coincident with the numerical model of Hollister *et al.* (1993), who predicted ingrowth at the tip of the posts. Furthermore, they predicted that most of the load transmitted between the beads and the surrounding bone, would take place through the first row of beads, and therefore ingrowth would not necessarily penetrate further than that. This finding is consistent with the results shown along the region of the medial condyle. In this region the tissue has been removed until approximately 30% of the ingrowth remains, corresponding to the diameter of one bead.

The investigation of Shirazi-Adl *et al.* (1994) into the ability of porous coated posts to become osseo-integrated in the proximal tibia showed that the greatest pull-out strength was achieved with the plugs inserted beneath the medial condyle, followed by the lateral condyle and then by the central region. They attributed the greater pull-out strength beneath the medial condyle to the fact that the cancellous bone in this region is generally stiffer when compared to the lateral side. In the results of the first analysis, the greater bond strength on the medial side resulted from remodelling activity. However, the stiffer bone and the greater amount of osseo-integration in this region are both functions of remodelling, and therefore interfacial remodelling cannot be excluded as a reason for the higher pull-out strength.

The magnitude of the friction coefficient had little influence on the extent of ingrowth. In the early post-operative period there is no implant-bone relative displacement because of the rest period. Therefore, during this time it would be expected that the coefficient would not influence the growth results. However, in the longer term, once fracture (or lack of bonding, due to remodelling activity) has taken place, sliding is experienced. However, it was found, for all values of friction coefficient, that the magnitude of the resultant relative displacement was not sufficient to overcome the slip threshold. The reason for this is that the areas in which ingrowth is sustained have provided stability, which limits the slip in the unbonded regions.

The manner in which the shear and normal stresses are transferred to the surrounding bone are not greatly influenced by the evolutionary changes in the interface conditions. Therefore, in the knee problem, the coupling between the interface development and the remodelling of the surrounding bone, is possibly not as important as was initially thought. As most of the load is transmitted by normal rather than by shear forces, whether or not there is bone ingrowth will not dramatically alter the manner of load transmission. There is the possibility that in a hip replacement, where load is principally transmitted by

cohesion, the ingrowth pattern will have a greater influence on the nature of the stress transfer to the surrounding bone.

In the second example, where no rest period was allowed and the slip threshold value was set to zero, both bone ingrowth and fibrous tissue formation were predicted. The fibrous tissue has formed, as expected, on the vertical sides of the central post. It is in this region that the highest shear forces, and subsequent relative displacements, are experienced. The poor mechanical properties of the fibrous tissue result in a shift of the load transfer. Subsequently, a greater portion of the load is transferred through the area beneath the condyles. As a result, extensive osseo-integration is established in these regions. The finding shows that the formation of a limited amount of fibrous tissue can have a dramatic influence on the predicted growth pattern. Although this analysis was undertaken with reduced integration of the element equations, oscillations of the ingrowth pattern are evident, which were found to be more severe with fully integrated elements. However, the oscillations appear not to render the result meaningless, as the correctly predicted solution seems to lie along the midline of the oscillating pattern.

8.5.3 Reconstructed Proximal Femur

As a result of the large number of hip replacements that are undertaken annually, and the high forces experienced in this joint, the design of the femoral stem has received a considerable amount of attention. Despite the efforts of designers, maintaining long term stability of the stem still remains a substantial obstacle. The current model is intended to provide insight into the influence of the stem and porous coating design on the long term stability of the joint.

The present model has confirmed the belief that a rest period before the full load is applied, is vital to ensure that bone ingrowth is achieved, even if the implant has been initially stabilised with a press fit. Where a rest period of 14 days was simulated, the entire porous region became infiltrated with bone tissue. Furthermore, in the long term, remodelling did not cause a substantial withdrawal of the interfacial tissues, an occurrence that was seen in the example of the reconstructed tibia. Therefore, an adequate long term attachment was predicted for this case. The stress profile along the two interface surfaces has shown that the remodelling activity resulted in a more even transfer of normal and shear stress in the long term. This evolution resulted from the change in interface modulus, due to the addition or removal of bone tissue from the porous beads.

Where no rest was simulated, the full load was applied immediately. Subsequently, a limited amount of ingrowth was predicted and the solution appeared to reach an equilibrium after approximately 40 days. As the extent of the bonding was limited, the load was primarily transmitted through the smaller bonded regions. For this reason, the interface stresses on both the medial and the lateral surfaces have increased substantially. Despite the enlargement in interface stresses, the peak shear stress on the medial side in the ingrown region is well below the yield limit of the bond. The formation of fibrous tissue on the lateral surface has shown the negative effect of this tissue formation. As a result of its compliant nature, very little load is transferred through this material, which

results in a large increase in compressive stresses on either side of the material. However, with the exception of the distal end, the shear stresses over the lateral porous surface were well below the failure limit of the bond.

The large changes in interface stresses in the hip model, as a result of the different ingrowth profiles, have shown that it is not adequate to simply assume an ingrowth pattern and from that determine the interface stresses. This is in contrast to the results of the knee model, where the compressive stress distribution, and to a lesser extent the shear, was not greatly influenced by the extent of bonding. This result can most likely be attributed to the different nature of load transfer in the two joints. In the tibial tray, the transfer of stress is mainly compressive, with limited shear stress transferred through the sides of the post. However, in the femoral stem the load is transferred by shear stress because of the wedge shape of the implant. Therefore, the regions of bonding and interface stiffness will have a far greater influence on the manner of the load transfer.

Although the influence of the press-fit on subsequent implant attachment has been the focus of many experimental studies, in the current work model its effect has not been examined. In almost all cases, the results from experimental studies have shown that a press-fit is vital to ensure osseo-integration. It is, therefore, common practice in orthopaedic surgery today to press-fit cementless stems. However, the rest period and joint loading profile following surgery are not as clear. Early loading may help seat the implant and stimulate the regeneration of the damaged tissues. However, careful planning of post-operative activity is required to ensure that the loading on the stem does not harm the process of osseo-integration.

8.6 Closure

Although there are many influences on interfacial tissue development, mechanical loads are assumed to be the dominant factor. In the short term the relationship between micro-motion and the interface tissue response has been shown. However, long term remodelling of interfacial tissues, as a result of both elastic and inelastic strains, has not been widely demonstrated. Therefore additional experimental data is required to validate the current long term remodelling predictions in order to gain further understanding of the evolution of the implant-bone interface. However, the present results support the hypothesis that repair and remodelling of osseo-integrated tissues are influenced by tissue strains. This work constitutes a step towards providing an engineering basis for the understanding of the mechanisms of osseo-integration, as well as to aid in the design of porous coated implants, in order to obtain the best biological attachment.

REFERENCES

1. Albrektsson T, Albrektsson B, Implant fixation by direct bone anchorage, *Non-Cemented THA*, 87-98, Raven Press, 1988
2. Aro H T, Chao E Y S, Bone healing patterns affected by loading, fracture fragment stability, fracture types and fracture site composition, *Clin. Orthop. Rel. Res.*, **293**, 8-17, 1993
3. Ascenzi A, Biomechanics and Galileo Galilei, *J. Biomech.*, **26**, 95-100, 1993
4. Ashman R B, Rho J Y, Elastic modulus of trabecular bone material, *J. Biomech.*, **21**, 177-181, 1988
5. Askew M J, Lewis J L, Analysis of model variables and fixation post length effects on stresses around a prosthesis in the proximal tibia, *J. Biomech. Eng*, **103**, 239-245, 1981
6. Ballard W T, Callaghan J J, Sullivan P M, Johnston R C, The results of improved cementing techniques for total hip arthroplasty in patients less than fifty years old, *J. Bone Jt. Surg.*, **76A**, 959-964, 1994
7. Beaupré G S, Orr T E, Carter D R, An approach for time-dependent bone modelling and remodelling-theoretical development, *J. Orthop. Res.*, **8**, 651-661, 1990
8. Beaupré G S, Vasu R, Bony ingrowth components for the tibial plateau-a finite element analysis, *RESNA 8th Annual Conf.*, 1985
9. Beckanbaugh R D, Ilstrup D M, Total hip Arthroplasty: a review of 333 cases with long-term follow-up *J. Bone Jt. Surg.*, **60A**, 306-313, 1978
10. Beer G, An isoparametric joint/interface element for finite element analysis, *Int. J. Num. Meth. Eng.*, **21**, 585-600, 1985
11. Bobyn J D, Cameron H U, Abdulla D, Pilliar R M, Weatherly G C, Biologic fixation and bone modelling with an unconstrained canine total knee prosthesis, *Clin. Orthop. Rel. Res*, **166**, 301-312, 1982
12. Bobyn J D, Engh C A, Bone ingrowth and remodelling in canine and human porous-coated hip replacement, *Non-Cemented THA*, 49-68, Raven Press, 1988
13. Bobyn J D, Mortimer E S, Glassman A H, Engh C A, Millier, J E, Brooks C E, Producing and avoiding stress shielding, *Clin. Orthop. Rel. Res*, **274**, 79-96, 1992
14. Bobyn J D, Pilliar R M, Cameron H U, Weatherly G C, The optimum pore size for the fixation of porous-surfaced metal implants by ingrowth of bone, *Clin. Orthop. Rel. Res*, **150**, 263-270, 1980
15. Bobyn J D, Wilson G J, Effect of pore size on the peel strength of attachment of fibrous tissue to porous-surfaced implants, *J Biomed Mater Res*, **16**, 571-584, 1982

16. Boehler M, Knahr K, Plenk H, Walter A, Salzer M, Schreiber V, Long-term results of uncemented alumina acetabular implants, *J. Bone Jt. Surg.*, **76B**, 53-59, 1994

17. Bourgois R, Burny F, Measurement of the stiffness of fracture in vivo. A theoretical study, *J. Biomech.*, **5**, 85-91, 1972

18. Bourne R B, Rorabeck C H, Ghazal M E, Lee M H, Pain in the thigh following total hip replacement with a porous-coated anatomic prosthesis for osteoarthrosis, *J. Bone Jt. Surg.*, **76A**, 1464-1470, 1994

19. Brooker A F, Collier J P, Evidence of bone ingrowth into a porous-coated prosthesis, *J. Bone Jt. Surg.*, **66A**, 619-620, 1984

20. Brown T D, Pedersen D R, Gray M L, Brand R A, Rubin C T, Toward an identification of mechanical parameters initiating periosteal remodelling: A combined experimental and analytical approach, *J. Biomech.*, **23**, 893-905, 1990

21. Brunski J B, Hipp J A, Shepard M S, Modeling of the bone-implant interface in a study of interfacial bone adaptation/damage, *Adv. in Bioengineering*, ASME, 1985

22. Brunski J B, The influence of force, motion, and related quantities on the response of bone to implants, *Non-Cemented THA*, 7-21, Raven Press, 1988

23. Burger E, CISM Course: Bone Cell and Tissue Mechanics, *Udine*, July 10 - 14, 1995

24. Burr D B, Martin R B, Schaffler M B, Bone remodelling in response to in vivo fatigue microdamage, *J. Biomech.*, **18**, 189-200, 1984

25. Cameron H U, Pilliar R M, MacNab L, The effect of movement on the bonding of porous metal to bone, *J. Biomed Mater. Res.*, **7**, 301-311, 1973

26. Cameron H U, Pilliar R M, MacNab L, The rate of bone ingrowth into porous metal, *J. Biomed Mater. Res.*, **10**, 295-302, 1976

27. Carter D R, Blenman P R, Beaupré G S, Correlation's between mechanical stress history and tissue differentiation in initial fracture healing, *J. Orthop. Res.*, **6**, 736-748, 1988

28. Carter D R, Caler W E, Cycle-dependent and time-dependent bone fracture with repeated loading, *J. Biomed. Eng*, **105**, 166-170, 1983

29. Carter D R, Fyhrie D P, Whalen R T, Trabecular bone density and loading history: Regulation of connective tissue biology by mech. energy, *J. Biomech.*, **20**, 785-794, 1987

30. Carter D R, Hayes W C, The compressive behaviour of bone as a two-phase porous structure, *J. Bone Jt. Surg.*, **59A**, 954-962, 1977

31. Carter D R, Mechanical loading histories and cortical bone remodelling, *Calcif. Tissue Int.*, **36**, S19-S24, 1984

32. Carter D R, Orr T E, Fyhrie D P, Schurman D J, Influences of mechanical stress on prenatal and postnatal skeletal development, *Clin. Orthop. Rel. Res*, **219**, 237-250, 1987

33. Carter D R, Orr T E, Fyhrie D P, Relationships between loading history and femoral cancellous bone architecture, *J. Biomech.*, **22**, 231-244, 1989

34. Carter D R, The cemented acetabular component: biomechanics and skeletal adaptation, *Non-Cemented THA*, 257-276, Raven Press, 1988

35. Carter D R, Vasu R, Harris W H, Stress changes in the femoral head due to porous ingrowth surface replacement arthroplasty, *J. Biomech.*, **17**, 737-747, 1984

36. Chandler H P, Reineck F T, Wixson R L, McCarthy J C, Total hip replacement in patients younger that 30 years old, *J. Bone. and Jt. Surg.*, **72B**, 966-970, 1990

37. Cheal E J, Gerhart T N, Hayes W C, Trabeculae bone remodelling around smooth and porous coated carbon-carbon implants, *ASME Adv. BioEng.*, 293-296, 1989

38. Cheal E J, Hayes W C, White III A A, Perren S M, Stress analysis of compression plate fixation and its effects on long bone remodelling, *J. Biomech.*, **18**, 141-150, 1985

39. Chen P, Turner T M, Ronnigen H, Galante J O, Urban R, Rostoker W, A canine cementless total hip prosthesis model, *Clin. Orthop. Rel. Res*, **176**, 25-33, 1983

40. Churches A E, Howlett C R, Waldron K J, Ward G W, The response of living bone to controlled time-varying loading: methods and preliminary results, *J. Biomech.*, **12**, 35-45, 1979

41. Churches A E, Howlett C R, The response of mature cortical bone to controlled time-varying loading, *Mechanical Properties of Bone*, **AMD - Vol. 45**, 69 - 80, 1981

42. Collier J P, Bauer T W, Bloebaum R D, Bobyn J D, Cook S D, Galante J O, Harris W H, Head W C, Jasty M J, Mayor M B, Sumner D R, Whiteside L A, Results of implant retrieval from post-mortem specimens in patients with well-functioning, long-term total hip replacements, *Clin. Orthop. Rel. Res*, **274**, 97-112, 1992

43. Collier J P, Mayor M B, Chae J C, Surprenant V A, Surprenant H P, Dauphinias L A, Macroscopic and microscopic evidence of prosthetic fixation with porous-coated materials, *Clin. Orthop. Rel. Res*, **235**, 173-180, 1988

44. Cooke S D, Thomas K A, Haddad R J, Histological analysis of retrieved human porous-coated total joint components, *Clin. Orthop. Rel. Res.*, **234**, 90-101, 1988

45. Coventry M B, Lessons learned in 30 years of total hip arthroplasty, *Clin. Orthop. Rel. Res*, **274**, 22-29, 1992

46. Cowin S C, Bone remodelling III: uniqueness and stability in adaptive elasticity, *J. Elasticity*, **8**, 285-295, 1978

47. Cowin S C, Bone stress adaptation models, *J. Biomech. Eng*, **115**, 528-533, 1993

48. Cowin S C, CISM Course: Bone Cell and Tissue Mechanics, *Udine*, July 10 - 14, 1995

49. Cowin S C, Firoozbakhsh K, Bone remodelling of diaphysial surfaces under constant load: theoretical predictions, *J. Biomech.*, **7**, 471-484, 1981

50. Cowin S C, Hegedus D H, Bone remodelling I: theory of adaptive elasticity, *J. Elasticity*, **6**, 313-326, 1976

51. Cowin S C, Introduction to the symposium on the mechanical properties of bone, *Mechanical Properties of Bone*, **AMD - Vol. 45**, 1 - 12, 1981

52. Cowin S C, Mechanical modelling of the stress adaptation process in bone, *Calcif. Tissue Int.*, **36**, S98-S103, 1984

53. Cowin S C, Sadegh A M, Non-interacting modes for stress, strain and energy in anistropic hard tissue, *J. Biomech.*, **24**, 859-867, 1991

54. Cowin S C, The relationship between the elasticity tensor and the fabric tensor, *Mech. Mater*, **4**, 137-147, 1985

55. Cowin S C, Turner C H, On the relationship between the orthotropic Young's moduli and fabric, *J. Biomech.*, **25**, 1493-1494, 1992

56. Cowin S C, Van Buskirk W C, Surface bone remodelling induced by a medullary pin, *J. Biomech.*, **12**, 269-276, 1979

57. Cowin S C, Wolff's law of trabecular architecture at remodelling equilibrium, *J. Biomed. Eng*, **108**, 83-88, 1986

58. Crownshield R D, Brand R A, Johnston R C, An analysis of femoral component stem design in total hip arthroplasty, *J. Bone Joint Surg.*, **62A**, 68-78, 1980

59. Desai C S, Zaman M M, Lightner J G, Siriwardane H J, Thin-layer element for interfaces and joints, *Int. J. Num. Anal. Meth. Geomech.*, **8**, 19-43, 1984

60. DiGioia III A M, Cheal E J, Hayes W C, Three-dimensional strain fields in a uniform osteotomy gap, *J. Biomech. Eng*, **108**, 273-280, 1986

61. Ducheyne P, Aernoudt E, De Meester P, Martens M, Mulier J C, Van Leeuwen D, Factors governing the mechanical behaviour of the implant-porous coating-trabecular bone interface, *J. Biomech.*, **11**, 297-307, 1978

62. Ducheyne P, De Meester P, Aernoudt E, Martens M, Mulier J C, Influence of a functional dynamic loading on bone ingrowth into surface pores of orthopaedic implants, *J. Biomed. Mater. Res.*, **11**, 811-838, 1977

63. Duncan R, Misler S, Voltage-activated and stretch activated Ba^{2+} conducting channels in an osteoblast-like cell line, *Federation of European Biochemical societies*, **251**, 17-21, 1989

64. Engh C A, Bobyn J D, Glassman A H, Porous coated hip replacement, *J. Bone Jt. Surg.*, **69B**, 45-55, 1987

65. Engh C A, Hip arthroplasty with a Moore prosthesis with porous coating, *Clin. Orthop. Rel. Res*, **176**, 53-65, 1983

66. Firoozbakhsh K, Aleyaasin M, Moneim M S, The effect of stress concentration on bone remodelling: theoretical predictions, J. Biomed. Eng, 111, 355-360, 1989

67. Firoozbakhsh K, Cowin S C, Devolution of inhomogeneities in bone structure-predictions of adaptive elasticity theory, J. Biomech. Eng, 102, 287-293, 1980

68. Friedlander G F, Lane J M, Martin R B, The influence of various physical modalities and drugs on bone regeneration and growth, *Non-Cemented THA*, 135-142, Raven Press, 1988

69. Frost H M, The laws of bone structure, Thomas C C, Springfield, 1964

70. Fyhrie D P, Carter D R, A unifying principle relating stress to trabecular bone morphology, *J. Orthop. Res.*, **4**, 304-317, 1986

71. Fyhrie D P, Carter D R, Schurman D J, Effects of ingrowth, geometry, and material properties on stress transfer under porous-coated hip surface replacements, *J. Orthop. Res.*, **6**, 425-433, 1988

72. Fyhrie D P, Carter D R, Stress analysis of porous ingrowth hip surface replacements, *RESNA 8th Annual Conf.*, 1985

73. Galante J O, Clinical results with HGP cementless total hip prosthesis, *Non-Cemented THA*, 427-432, Raven Press, 1988

74. Galante J O, Jacobs J, Clinical performances of ingrowth surfaces, *Clin. Orthop. Rel. Res*, **276**, 41-49, 1992

75. Galante J O, Rostoker W, Lueck R, Ray R D, Sintered fibre metal composites as a basis for attachment of implants to bone, *J. Bone Jt. Surg.*, **53A**, 101-114, 1971

76. Gibson L J, The mechanical behaviour of cancellous bone, *J. Biomech.*, **18**, 317-328, 1985

77. Gluckmann A, Studies of bone structure *in vitro*. I. Influence of pressure on orientation and structure, *The Anatomic Record*, **72**, 97-113, 1938

78. Goldring S R, Schiller A L, Roelke M, The synoviallike membrane at the bone-cement interface in loose total hip replacements and its role in bone lysis, *J. Bone Joint Surg.*, **65A**, 575-584, 1983

79. Goodship A E, CISM Course: Bone Cell and Tissue Mechanics, *Udine*, July 10 - 14, 1995

80. Goodship A E, Lanyon L E, McFie H, Functional adaptation of bone to increased stress, *J. Bone Joint Surg.*, **61A**, 539-546, 1979

81. Goulet R W, Goldstein S A, Ciarelli M J, Kuhn J L, Brown M B, Feldkamp L A, The relationship between the structure and orthogonal compressive properties of trabecular bone, *J. Biomech.*, **27**, 375-389, 1994

82. Harrigan T P, Hamilton J J, An analytical and numerical study of the stability of bone remodelling theories: dependence on microstructural stimulus, *J. Biomech.*, **25**, 477-488, 1992

83. Harrigan T P, Hamilton J J, Bone strain sensation via transmembrane potential changes in surface osteoblasts: loading rate and microstructural changes, *J. Biomech.*, **26**, 183-200, 1993

84. Harrigan T P, Hamilton J J, Finite element simulation of adaptive bone remodelling: a stability criterion and a time stepping method, *Int. J. Numer. Meth. Eng.*, **36**, 837-854, 1993

85. Harrigan T P, Harris W H, A three dimensional non-linear finite element study of the effect of cement-prosthesis debonding in cemented femoral total hip components, *J. Biomech.*, **24**, 1047-1058, 1991

86. Harrigan T P, Jasty M, Mann R, Harris W H, Limitations of the continuum assumption in cancellous bone, *J. Biomech.*, **21**, 269-275, 1988

87. Harrington I J, A bioengineering analysis of the force actions on the knee in normal walking and pathalogical gait, *J. Biomed. Eng.*, **101**, 174-184, 1976

88. Harris W H, White R E, McCarthy J C, Walker P S, Weinberg E H, Bony ingrowth fixation of the acetabular component in canine hip joint arthroplasty, *Clin. Orthop. Rel. Res*, **176**, 7-11, 1983

89. Harris W H, Will stress shielding limit the longevity of cemented femoral components of total hip replacement, *Clin. Orthop. Rel. Res*, **274**, 120-123, 1992

90. Hart R T, Davy D T, Heiple K G, A computational method for stress analysis of adaptive elastic materials with a view toward applications in strain-induced bone remodelling, *J. Biomech. Eng*, **106**, 343-350, 1984

91. Hart R T, Davy D T, Heiple K G, Mathematical modelling and numerical solutions for functionally dependent bone remodelling, *Calcif. Tissue Int.*, **36**, S104-S109, 1984

92. Havelin L I, Espehaug B, Vollset S E, Engesaeter L B, Early aseptic loosening of uncemented femoral components in primary total hip replacement, *J. Bone Jt. Surg.*, **77B**, 11-17, 1995

93. Hedley A K, Clarke I C, Kozinn S C, Coster I, Gruen T, Amstutz H C, Porous fixation of the femoral component in a canine surface replacement of the hip, *Clin. Orthop. Rel. Res*, **163**, 300-311, 1982

94. Hedley A K, Kabo M, Kim W, Coster I, Amstutz H C, Bony ingrowth fixation of newly designed acetabular components in a canine model, *Clin. Orthop. Rel. Res*, **176**, 13-23, 1983

95. Hegedus D H, Cowin S C, Bone remodelling II: small strain adaptive elasticity, *J. Elasticity*, **6**, 337-352, 1976

96. Hert J, Liskova M, Landa J, Reaction of bone to mechanical stimuli. Part 1. Continuous and intermittent loading of tibia in rabbit, *Folia Morphologica*, **61**, 290-300, 1971

97. Hibbitt, Karlsson and Sorensen, Inc., *ABAQUS User's Manual*, Providence, Rhode Island, USA, 1995

98. Hollister S J, Fyhrie D P, Jepsen K J, Goldstein S A, Application of homogenization theory to the study of trabecular bone mechanics, *J. Biomech.*, **24**, 825-839, 1991

99. Hollister S J, Guldberg R E, Kuelske C L, Mosier S M, Relative effects of wound healing and mechanical stimulus on early bone adaptation to porous coated implants, *Second World Congress of Biomechanics*, **Vol II**, p 242, 1994

100. Hollister S J, Nikuchi N, Goldstein S A, Do bone ingrowth processes produce a globally optimised structure?, *J. Biomech.*, **26**, 391-407, 1993

101. Homsy C A, Cain T E, Kessler F B, Anderson M S, King J W, Porous implant systems for prosthesis stabilisation, *Clin. Orthop. Rel. Res*, **89**, 221-235, 1972

102. Hori R Y, Lewis J L, Mechanical properties of the fibrous tissue found at the bone-cement interface following total joint replacement, *J. Biomed. Mater. Res.*, **16**, 911-927, 1982

103. Howie D W, The osseous response to injury and implant fixation, *Non-Cemented THA*, 1-6, Raven Press, 1988

104. Huiskes R, Boeklagen R, Mathematical shape optimisation of hip prosthesis design, *J. Biomech.*, **22**, 793-804, 1989

105. Huiskes R, Chao E Y S, A survey of finite element analysis in orthopaedic biomechanics: The first decade, *J. Biomech.*, **16**, 385-409, 1983

106. Huiskes R, Nunamaker D, Local stress and bone adaptation around orthopaedic implants, *Calcif. Tissue Int.*, **36**, S110-S117, 1984

107. Huiskes R, Stress patterns, failure modes, and bone remodelling, *Non-Cemented THA*, 283-302, Raven Press, 1988

108. Huiskes R, Vroemen W, A standard finite element model for routine comparative evaluations of femoral hip prosthesis, *Acta Orthopaedica Belgica*, **52**, 258-261, 1986

109. Huiskes R, Weinans H, Adaptive bone remodelling applied to prosthetic design analysis, *J. Biomech.*, **20**, 1135-1150, 1987

110. Huiskes R, Weinans H, Van Rietbergen B, The relationship between stress shielding and bone resorption around total hip stems and the effects of flexible materials, *Clin. Orthop. Rel. Res*, **274**, 124-134, 1992

111. Hulbert S F, Cooke F W, Klawitter J J, Attachment of prostheses to the musculo-skeletal system by tissue ingrowth and mechanical interlocking, *J. Biomed. Res.*, **7**, 1-23, 1973

112. Hungerford D S, Kenna R V, Preliminary experience with a total knee prosthesis with porous coating used without cement, *Clin. Orthop. Rel. Res*, **176**, 95-107, 1983

113. Jasty M, Harris W H, Observations on factors controlling bony ingrowth into weight-bearing, porous, canine total hip replacements, *Non-Cemented THA*, 175-190, Raven Press, 1988

114. Jee W S S, Histology: Cell and tissue biology (Ed. Weiss L), *Urban & Schwarzenberg*, Baltimore, Munich, 1980

115. Jones H H, Priest J D, Hayes W C, Humoral hypertrophy in response to exercise, *J. Bone Joint Surg.*, **59A**, 204-208, 1977

116. Kettlekamp D D, Chao E Y, A method for quantitative analysis of medial and lateral compression forces at the knee joint during standing, *Clin. Orthop.*, **88**, 202-213, 1972

117. Ko CC, Kohn D H, Hollister S J, Micromechanics of implant/tissue interfaces, *J. Oral Implantology*, **18**, 220-230, 1992

118. Lanyon L E, Functional strain as a determinant for bone remodelling, *Calcif. Tissue Int.*, **36**, S56-S61, 1984

119. Lanyon L E, Goodhip A E, Pye C J, MacFie J H, Mechanically adaptive bone remodelling, *J. Biomech.*, **15**, 141-154, 1982

120. Lanyon L E, Hampson W G, Goodship A E, Bone deformation recorded in vivo from strain gauges attached to the human tibial shaft, *Acta. Orthop. Scanda.*, **46**, 256-268, 1975

121. Lanyon L E, Rubin C T, Static versus dynamic loads as an influence on bone remodelling, *J. Biomech.*, **17**, 897-905, 1984

122. Lappi V G, King M S, May I L, Determination of elastic constants for human femurs, *J. Biomed. Eng*, **101**, 193-197, 1979

123. Lawrence J M, Engh C A, Macalinno G E, Lauro G R, Outcome of revision arthroplasty done without cement, *J. Bone Jt. Surg.*, **76A**, 965-973, 1994

124. Levenston M E, Beaupré G S, Jacobs C R, Carter D R, The role of loading memory in bone adaptation simulation, *Bone*, **15 (2)**, 177-186, 1994

125. Lewis J L, Askew M J, Jaycox D P, A comparative evaluation of tibial component designs of total knee prostheses, *J. Bone Joint Surg.*, **64A**, 129-135, 1982

126. Lewis J, The mechanical state of bone-implant interface, *Non-Cemented THA*, 23-30, Raven Press, 1988

127. Linde F, Norgaard P, Hvid I, Odgaard A, Søballe K, Mechanical properties of trabecular bone. Dependency on strain rate., *J. Biomech.*, **24**, 803-809, 1991

128. Linder L, An overview of the histology of the principal interface types in orthopaedic surgery today, *Implant Bone Interface* (Ed: John Older), Springer-Verlag, 1991

129. Ling R S M, Observations on the fixation of implants to the bony skeleton, *Clin. Orthop. Rel. Res*, **210**, 80-97, 1986

130. Lotz J C, Gerhart T N, Hayes W C, Mechanical properties of metaphyseal bone in the proximal femur, *J. Biomech.*, **24**, 317-329, 1991

131. Mackerle J, Finite and boundary element methods in biomechanics: a bibliography (1976-1991), *Eng. Computations*, **9**, 403-435, 1992

132. Mackerle J, Finite and boundary element techniques in biomechanics - a bibliography (1991-1993), *F. E. in Analysis & Design*, **16**, 163-174, 1994

133. Maquet P G, Biomechanics of the Knee, Springer-Verlag, 1976

134. Markolff K L, Amstutz H C Hirschowitz D L, The effect of calcar contact on femoral components micro-movement. A mechanical study, *J. Bone Joint Surg.*, **62B**, 1315-1323, 1980

135. Martens M, Van Audekercke R, Delport P, De Meester P, Mulier J C, The mechanical characteristics of cancellous bone at the upper femoral region, *J. Biomech.*, **16**, 971-983, 1983

136. Martin B, A theory of fatigue damage accumulation and repair in cortical bone, *J. Orthop. Res.*, **10**, 818-825, 1992

137. Martin R B, Burr D B, Structure, Function, and Adaptation of Compact Bone, Raven Press, 1989

138. Martin R B, Determinants of the mechanical properties of bone, *J. Biomech.*, **24**, 79-88, 1991

139. Meade J B, Cowin S C, Klawitter J J, Van Buskirk W C, Skinner H B, Bone remodelling due to continuously applied loads, *Calcif. Tissue Int.*, **36**, S25-S30, 1984

140. Meroi E A, Natali A N, A numerical approach to the biomechanical analysis of bone fracture healing, *J. Biomed. Eng*, **11**, 390-397, 1989

141. Morrison J B, The mechanics of the knee joint in relation to normal walking, *J. Biomech.*, **3**, 51-61, 1970

142. Murase K, Crownshield R D, Pedersen D R, An analysis of tibial component design in total knee arthroplasty, *J. Biomech.*, **16**, 13-22, 1983

143. Muschler G F, Lane J M, Martin R B, Bone Ingrowth fixation in abnormal bone, *Non-Cemented THA*, 119-134, Raven Press, 1988

144. Neuman W F, Neuman M W, The chemical dynamics of bone, *University of Chicargo Press*, Chicargo, 1958

145. Nilles J L, Coletti J R, Wilson C, Biomechanical evaluation of bone-porous material interfaces, *J. Biomed Mater. Res.*, **7**, 231-251, 1973

146. Numamaker D M, Perren S M, A radiological and histological analysis of fracture healing using prebending of compression plates, *Clin. Orthop. Rel. Res*, **138**, 167-174, 1979

147. O'Connor J A, Lanyon L E, MacFie H The influence of strain rate on adaptive bone remodelling, *J. Biomech.*, **15**, 767-781, 1982

148. Oishi C S, Walker R H, Colwell C W, Jolla L A, The femoral component in total hip arthroplasty, *J. Bone Jt. Surg.*, **76A**, 1130-1136, 1994

149. Orr T E, Beaupre G S, Carter D R, Schurman D J, Computer predictions of bone remodelling around porous-coated implants, *J. Arthroplasty*, **5**, 191-200, 1990

150. Orr T E, Carter D R, Finite element analysis of porous ingrowth components for the humerus, *RESNA 8th Annual Conf.*, 296-298, 1985

151. Parfitt A M, The cellular basis of bone remodelling: The quantum concept re-examined in the light of recent advances in cell biology of bone, *Calcif. Tissue Int.*, **36**, S37-S45, 1984

152. Paul J P, Loading on the normal hip and knee joint replacements, *Adv. Artificial Hip and Knee Joint Technology*, Springer-Verlag, 1976

153. Pauwels Biomechanics of the locomotor apparatus, Springer-Verlag, 1980

154. Pedersen D R, Brown T D, Brand R A, Interstitial bone stress distributions accompanying ingrowth of screen-like prosthesis anchorage layer, *J. Biomech.*, **24**, 1131-1142, 1991

155. Perren S M, Physical and biological aspects of fracture healing with special reference to internal fixation, *Clin. Orthop. Rel. Res*, **138**, 175-196, 1979

156. Pilliar R M, Cameron H U, Welsh R P, Binnington A G, Radiographic and morphologic studies of load-bearing porous-surfaced structured implants, *Clin. Orthop. Rel. Res*, **156**, 249-257, 1981

157. Pilliar R M, Lee J M, Maniatopoulos C, Observations of the effect of movement on bone ingrowth into porous-surfaced implants, *Clin. Orthop. Rel. Res*, **208**, 109-113, 1986

158. Pilliar R M, Powder metal-made orthopaedic implants with porous surface for fixation by bone tissue, *Clin. Orthop. Rel. Res*, **176**, 43-51, 1983

159. Prendergast P J, Taylor D, Prediction of bone adaptation using damage accumulation, *J. Biomech.*, **27**, 1067-1076, 1994

160. Rancourt D, Friction properties of the interface between porous-surfaced metals and tibial cancellous bone, *J. Biomed. Mater. Res.*, **24**, 1503-1519, 1990

161. Raut V V, Siney P D, Wroblewki B M, Revision for aseptic loosening using the cemented Charnley prosthesis, *J. Bone Jt. Surg.*, **77B**, 23-27, 1995

162. Reilly D T, Burstein A H, The elastic and ultimate properties of compact bone tissue, *J. Biomech.*, **8**, 393-405, 1975

163. Rice J C, Cowin S C, Bowman J A, On the dependence of the elasticity and strength of cancellous bone on apparent density, *J. Biomech.*, **21**, 155-168, 1988

164. Roberts W E, Mozsary P G, Morey E R, Suppression of osteoblast differentiation during weightlessness, *The Physiologist*, **24**, S75-S76, 1981

165. Røhl L, Larsen E, Linde F, Odgaard A, Jorgensen J, Tensile and compressive properties of cancellous bone, *J. Biomech.*, **24**, 1143-1149, 1991

166. Rohlmann A, Cheal E J, Hayes W C, Bergmann G, A nonlinear finite element analysis of interface conditions in porous coated hip endoprostheses, *J. Biomech.*, **21**, 605-611, 1988

167. Rohlmann A, Mossner U, Bergmann G, Finite element analysis and experimental investigation in a femur with hip endoprosthesis, *J. Biomech.*, **16**, 727-742, 1983

168. Rubin C T, Lanyon L E, Regulation of bone formation by applied dynamic loads, *J. Bone Jt. Surg.*, **66A**, 397-402, 1984

169. Rubin C T, Skeletal strain and the functional significance of bone architecture, *Calcif. Tissue. Int.*, **36**, S11-S18, 1984

170. Rubin C T, Lanyon L E, Regulation of bone mass by mechanical strain magnitude, *Calcif. Tissue. Int.*, **37**, 411-417, 1985

171. Rubin C T, McLoed K J, Functional strains and cortical bone adaptation: Epigenetic assurance of skeletal integrity, *J. Biomech.*, **23**, 43-54, 1990

172. Rubin C T, The benefits and consequences of structural adaptation in bone, *Non-Cemented THA*, 41-48, Raven Press, 1988

173. Rydell I V W, Forces acting on the femoral head prosthesis, *Acta. Orthop. Scanda.*, Suppl., **88**, 1966

174. Sadegh A M, Luo G M, Cowin S C, Bone ingrowth: an application of the boundary element method to bone remodelling at the implant interface, *J. Biomech.*, **26**, 167-182, 1993

175. Samiento A, Natarajan V, Barden L S, Marks K E, Radiographic performance of two different total hip cemented arthroplasties, *Orthop. Clin. North. Am.*, **19**, 605, 1988

176. Shirazi-Adl A, Dammak M, Zukor D J, Fixation pull-out response measurement of bone screws and porous surface posts, *J. Biomech.*, **27**, 1249-1258, 1994

177. Shrivastava S C, Ahmed A M, Shirazi-Adl A, Effect of cement-bone composite layer and prosthesis geometry on stresses in a prosthetically reconstructed tibia, *J. Biomed. Mater. Res.* **16**, 929-949, 1992

178. Skerry T M, Bitensky L, Chayen J, Loading-related reorientation of bone proteoglycan in vivo. Strain memory in bone tissue, *J. Orthop. Res.*, **6**, 547-551, 1988

179. Snyman M F, Bird W W, Martin J B, A simple formulation of a dilatant joint element governed by coulomb friction, *Engineering Computations*, **8**, 215-229, 1990

180. Søballe K, Hansen E S, Rasmussen H B, Jørgensen P H, Bünger C, Tissue ingrowth into titanium and hydroxyapatite-coated implants during stable and unstable mechanical conditions, *J. Orthop. Res.*, **10**, 285-299, 1992

181. Spector M, Current Concepts of bone ingrowth and remodelling, *Non-Cemented THA*, 69-85, Raven Press, 1988

182. Spector M, Davis R J, Lunceford E M, Harmon, Porous polysulfone coatings for fixation of femoral stems by bony ingrowth, *Clin. Orthop. Rel. Res*, **176**, 35-41, 1983

183. Spector M, Michno M J, Smarook W H, Kwiatowski G T, A high-modulus polymer for porous orthopaedic implants: biomechanical compatibility of porous implants, *J. Biomed. Mater. Res.*, **12**, 665-677, 1978

184. Stauffer R N, Ten year follow-up study of total hip replacement with particular reference to reontgenographic loosening of components, *J Bone & Joint Surg.*, **64A**, 983-990, 1982

185. Steele M A study of the stress distribution throughout the porous layer of a cementless prosthesis, B.Sc. Thesis Project, Dept. Mechanical Engineering, University of Cape Town, 1995

186. Stone J L, Beaupre G S, Hayes W C, Multiaxial strength characteristics of trabecular bone, *J. Biomech.*, **16**, 743-752, 1983

187. Stülpner M Various continuum bone remodelling algorithms applied to the proximal femur in two and three dimensions, M.Sc. Thesis Project, Dept. Mechanical Engineering, University of Cape Town, 1995

188. Sumner D R, Turner T M, Urban R M, Galante J O , Remodelling and ingrowth of bone at two years in a canine cementless total hip-arthroplasty model, *J Bone & Joint Surg.*, **74-A (2)**, 239-250, 1992

189. Sutherland C J, Wilde A H, Barden L S, Marks K E, A ten year follow-up of one hundred consecutive Muller curved stem total hip arthroplasties, *J. Bone & Joint Surg.*, **60A**, 970-982, 1982

190. Tensi H M, Gese H, Ascherl R, Non-linear three dimensional finite element analysis of a cementless hip endoprosthesis, *J. Eng. Med.*, **203**, 203-222, 1990

191. Thompson D W, On growth and form, *Cambridge University Press*, Cambridge, England, 1917

192. Torzilli P A, Takebe K, Burnstein A H, Heiple K G, Structural properties of immature canine bone, *J. Biomech. Eng*, **103**, 233-238, 1981

193. Turner C H, Cowin S C, Rho J Y, Ashman R B, Rice J C, The fabric dependence of the orthotropic elastic constants of cancellous bone, *J. Biomech.*, **23**, 549-561, 1990

194. Turner C H, On Wolff's law of trabecular architecture, *J. Biomech.*, **25**, 1-9, 1992

195. Turner C H, Yield behaviour of bovine cancellous bone, *J. Biomech. Eng*, **111**, 256-260, 1989

196. Turner T M, Sumner D R, Urban R M, Rivero D P, Galante J O, A comparative study of porous coatings in a weight-bearing total hip arthroplasty model, *J. Bone Jt. Surg.*, **68A**, 1396-1409, 1986

197. Uhthoff H K, Germain J P, The reversal of tissue differentiation around screws, *Clin. Orthop. Rel. Res*, **123**, 248-252, 1977

198. Van Rietbergen B, Huiskes R, Weinans H, Sumner D R, Turner T M, Galante J O, The mechanism of bone remodelling and resorption around press-fitted THA stems, *J. Biomech.*, **26**, 369-382, 1993

199. Vasu R, Carter D R, Schurman D J, Beaupré G S, Epiphyseal-based designs for tibial plateau components-I. Stress analysis in the frontal plane, *J. Biomech.*, **8**, 647-662, 1986

200. Vichnin H H, Batterman S C, Stress analysis and failure prediction in the proximal femur before and after total hip replacement, *J. Biomech. Eng*, **108**, 33-41, 1986

201. Weinans H, Huiskes H, Grootenboer H J, Quantitative analysis of bone reactions to relative motions at implant-bone interfaces, *J. Biomech.*, **26**, 1271-1281, 1993

202. Weinans H, Huiskes R, van Rietbergen B, Sumner D R, Turner T M, Galante J O, Adaptive bone remodelling around bonded noncemented total hip arthroplasty: A comparison between animal experiments and computer simulation, *J. Orthop. Res.*, **11**, 500-513, 1993

203. Weinans H, Huiskes R, Grootenboer H J, The behaviour of adaptive bone remodelling simulation models, *J. Biomech.*, **25**, 1425-1441, 1992

204. Weinans H, Huiskes R, Trends of mechanical consequences and modelling of fibrous membrane around femoral hip prostheses, *J. Biomech.*, **23**, 991-1000, 1990

205. Weinbaum S, Cowin S C, Zeng Y, A model for the excitation of osteocytes by mechanical loading-induced bone fluid shear stresses, *J. Biomech.*, **27**, 339-360, 1994

206. White A A III, Panjabi M M, Southwick W O, The four stages of fracture repair, *J. Bone Jt. Surg.*, **59A**, 188-192, 1977

207. Whitehouse W J, Dyson E D, Scanning electron microscope studies of trabecular bone in the proximal end of the human femur, *J. Anat*, **118**, 417-444, 1974

208. Whiteside L A, The effect of stem fit on bone hypertrophy and pain relief in cementless total hip arthroplasty, *Clin. Orthop. Rel. Res*, **247**, 138-147, 1989

209. Williams J L, Lewis J L, Properties and an anisotropic model of cancellous bone from the proximal tibial epiphysis, *J. Biomech. Eng.*, **104**, 51-56, 1982

210. Wolff J, The law of bone remodelling, Springer-Verlag, 1986